



Norwegian University of
Science and Technology

Drilling Fluid Volume Change due to Hydrate Formation and its Impact on Well Control

Michaela Gunhildrud
Bendik Helgestad

Petroleum Geoscience and Engineering

Submission date: June 2017

Supervisor: Sigbjørn Sangesland, IGP

Co-supervisor: Roar Larsen, IGP

Norwegian University of Science and Technology
Department of Geoscience and Petroleum

Summary

Natural gas hydrates are crystal structures of water containing gas inside cavities. Hydrates can form if gas and water are present in a system with high pressure and low temperature conditions. Hydrate formation is considered a well control issue, and should be prevented.

Maintaining well control is crucial during drilling operations, and at least two barriers against the reservoir pressure are required. The drilling fluid column act as the primary barrier. A gas kick is a term used for the critical well control situation where a volume of gas enters the well. In case of a kick, the well should be shut-in and the kick circulated out. The kick is often detected by observing the mud level rising in the mud pit.

Hydrate formation inside the well after a gas kick will make the mud level reduce, as the hydrate volume in general is less than the separate volume of gas and water. Determining whether the change in mud level is a result of hydrate formation or loss of circulation can be challenging. The volume change due to hydrate formation is defined as the volume the mud column reduces with when gas and water form hydrates. If a kick with a volume of 4m^3 enters the well, and all the gas are converted, the volume change will be 3.03m^3 at a system pressure of 181 bar. This volume change will decrease the height of the mud column by 114m, if drilling is performed with a 5" drillpipe where a 9 5/8" casing is used in the previous section.

20 hydrate formation experiments were performed at NTNU, where the objective was to observe which additives had an impact on hydrate formation, and the significance of the volume change and reduction when hydrates form. Tap water, Nidelv water, Fjord water, barite, bentonite, KCHOO, NaCl and CaCl_2 was the different compounds used in the aqueous solution. The gas composition used was a mixture of 90% methane and 10% propane. The pressure cell was pressurized up to 24 bar and placed inside a refrigerator at 5°C , for a period of approximately 24 hours.

Additionally, a hydrate formation experiment was conducted at the SINFEF multiphase flow

laboratory at Tiller. A flow loop was filled with water and gas to observe hydrate formation, and the associated volume reduction in a high pressure system. The gas had a similar composition as a reservoir gas retrieved from the Barents Sea. In SINTEF Test 2 the system was initially pressurized to 181bar, before cooling the system to 12°C. The heating of the system started, when the system reached steady state at 104 bar after approximately 70 hours.

Hydrates were detected both visually and by pressure observations in both the NTNU experiments and SINTEF Test2. Analysis of the effect of the additives and water types in the NTNU experiment suggests that NaCl is the most efficient hydrate inhibitor. Furthermore, the analysis showed that both the amount of surface area available in the aqueous solution and an increase in viscosity seems to act favourable in terms of hydrate formation speed, and that an increase in viscosity might impact the hydrate growth rate. Hydrate formation stops before reaching hydrate equilibrium in most of the NTNU experiments and in SINTEF Test 2, at a pressure of approximately 18 bar and 104 bar respectively. The hydrate formation possibly stopped because the hydrates created a physical boundary between the gas and aqueous phase, which prevented further growth.

The volume reduction for the NTNU experiments is in the range between 92.7% and 96.3%, when 95% of the large and 50% of the small cavities are assumed to be filled in the hydrate crystal structure. In the SINTEF Test 2, the volume reduction is 76.1% when considering the same number of filled cavities. When the system pressure increases, the volume reduction reduces.

Finally, the temperatures after shut-in in a well located in the Barents Sea has been considered in order to find the well interval where hydrates can form at various times after shut-in. The amount of inhibitor needed to prevent hydrate formation has also been calculated. Depending on the mud density, hydrate formation could start between 900m to 1250m below the seabed in the Barents Sea well. To inhibit hydrate formation in such a scenario, between 14.2wt% and 18.0wt% NaCl or 16.7wt% and 22.0wt% CaCl₂ have to be added to the water phase of the aqueous solution.

Sammendrag

Gass hydrater er en krystallstruktur av vann hvor gassmolekyler er fanget inne i strukturen. Hydrater krever et system hvor gass og vann er tilgjengelig under høyt trykk og lav temperatur for å kunne dannes. Hydratdannelse i brønnen er ansett som et brønnskrollproblem og burde forhindres.

Opprettholdelse av brønnskroll er helt nødvendig, derfor må minst to barrierer eksistere for å kontrollere reservoartrykket. Den hydrostatiske kolonnen av borevæske regnes som den primære barrieren. Et kick er en ukontrollert innstrømning av reservoarfluider inn i brønnen, og regnes som et brønnskrollproblem. Brønnen må da stenges og kicket må sirkuleres ut. Et kick blir ofte detektert ved at man observerer en økning i borefluidnivået i borevæsketanken.

Hydratdannelse i brønnen etter et kick vil gjøre at borefluidnivået reduseres, som et resultat av at hydratvolumet generelt er mindre enn volumet av gass og vann som forbrukes i dannelsesprosessen. Det kan være vanskelig å avgjøre om reduksjonen i volum skyldes hydratvekst eller tap av borefluid til formasjonen. Volumendringen grunnet hydratvekst er definert som reduksjonen i borefluidvolum når vann og gass danner hydrater. Dersom et kick med volum 4m^3 strømmer inn i brønnen, vil volumendringen være 3.03m^3 dersom trykket er 181 bar. Dette vil resultere i et 114m fall i borefluidkolonnen, dersom man borer med en 5" borestreng hvor et 9 5/8" fôringsrør er satt i forrige seksjon.

20 ulike eksperimenter ble utført ved NTNU for å se hvordan ulike kjemiske tilsetningsstoffer i borefluidet påvirker hydratvekst, og hvor stor volumreduksjon som vil oppstå ved hydratdannelse. Vann fra springen, vann fra Nidelva, vann fra Snillsfjord, baritt, bentonitt, KCHOO, NaCl og CaCl_2 var de ulike komponentene som ble tilsatt i vannfasen. Gasskomposisjonen som ble brukt bestod av 90% metan og 10% propan. Denne gassen ble trykksatt til 24 bar og plassert inn i et kjøleskap med en temperatur på 5°C i cirka 24 timer.

Enda et hydratforsøk ble utført på SINTEFs flerfaselaboratorie på Tiller. Her ble en strømnings-

løyfe fylt med vann og gass, hvor målet var å danne hydrater. Fokuset var å evaluere hydratdannelse med tanke på hvor stort hydratvolum som ble dannet og hvor stor volumreduksjon dette utgjorde i et høytrykksystem. Gassen hadde en tilsvarende komposisjon som en reservoargass funnet i Barentshavet. Systemet ble trykksatt til 181 bar før det ble nedkjølt til 12°C. Systemet ble varmet opp etter 70 timer, når likevekt var nådd ved 104 bar.

Hydratdannelse ble bevist både visuelt og gjennom analyse av trykkendringer som oppstod gjennom forsøkene, både ved SINTEF og NTNU. Analyser av de ulike tilsetningsstoffene og vanntypene i NTNU-eksperimentene viser at NaCl er den mest effektive hydratinhibitoren. Andre interessante funn var at mengden av tilgjengelig overflateareal i vannfasen påvirker hastigheten av hydratvekst, samt at en økning i viskositet muligens påvirker hastigheten til hydratvekst. Hydratveksten stoppet før den oppnådde termodynamisk likevekt i de fleste forsøkene gjort på NTNU, hvor trykket stoppet rundt 18 bar. Det samme ble observert på SINTEF-forsøket, hvor trykket stabiliserte seg på 104 bar. En mulig årsak til at dette skjedde er at hydratene dannet en fysisk barriere mellom gas- og vannfasen i systemet, noe som hindret videre hydratvekst.

I NTNU-eksperimentene varierer volumreduksjonen fra 92.7% til 96.3%, når 95% av de store og 50% av de små hulrommene er antatt å være fylt av et gassmolekyl i hydratstrukturen. I SINTEF Test 2 var volumreduksjonen på 76.1% når likt antall hulrom var fylt. Når trykket i systemet øker reduseres volumreduksjonen.

Til slutt har temperaturen etter at brønnen er blitt stengt blitt vurdert for å finne brønnintervallet hvor hydrater kan dannes. Dette gjelder for en brønn lokalisert i Barentshavet. Det har også blitt gjort beregninger på mengden av inhibitorer som trengs for å hindre at hydrater dannes. Avhengig av tettheten på borefluidet kan hydratdannelse skje mellom 900m og 1250m under havbunnen for denne brønnen. For å inhibere hydratdannelse i dette tilfellet må det tilsettes mellom 14.2vekt% og 18.0vekt% NaCl eller 16.7vekt% og 22.0vekt% CaCl₂ i vannfasen til borefluidet.

Preface

This is a master thesis written at NTNU as a part of the study program Petroleum Technology, written during the spring semester of 2017.

The report is written in such a way that it will be understandable for readers with technical background but without topic expertise.

Trondheim, 2017-06-11

.....

Bendik Helgestad and Michaela Gunhildrud

Acknowledgment

First of all, we would like to thank our supervisors, Professor Sigbjørn Sangesland and Professor Roar Larsen, for their help and guidance throughout the work of this master thesis. We would also like to thank them for their support and providing us with feedback throughout the semester. A big thank you for sharing your knowledge and valuable experience with us, as it has been essential for the outcome of this work.

We would also like to thank PhD student Dag Vavik for including us in the SINTEF experiment, PhD student Lucas Cantinelli Sevillano for his temperature model and the staff at the PTS mechanical workshop for helping us with the design of the pressure cell and the experimental setup.

Additionally, we are thankful towards Hanne Schøld Sæterdal and Eric Bohlin for proof reading this thesis.

A warm and special thanks to all our classmates who have made our years in Trondheim unforgettable. Lastly, we would like to thank our families for their love and support throughout our time at NTNU.

B.H. and M.G.

Contents

Summary	i
Summary	iii
Preface	v
Acknowledgment	vii
Nomenclature	xxiv
1 Introduction	1
2 Theory	3
2.1 Natural Gas Hydrates	3
2.1.1 Water Molecule and Hydrogen Bonds	5
2.1.2 Gas Hydrate Crystal Structure	5
2.1.3 Hydrate Nucleation	12
2.1.4 Hydrate Growth	19
2.1.5 Hydrate Prevention Theory	23
2.1.6 Hydrate Dissociation	27
2.2 Well Control	28
2.2.1 Drilling Fluid	29
2.2.2 Kick - A Critical Issue During Drilling Operations	32
2.2.3 Causes of Kicks and How to Manage it	33
2.3 Natural Gas Hydrates as a Drilling Hazard	36
2.3.1 Drilling Challenges in Deepwater and Arctic regions	36
2.3.2 Drilling Hazards Related to Hydrate Formation During Shut-in Periods	39

2.3.3	Drilling Fluid Volume Change and Gas Volume Reduction	43
2.3.4	Hydrate Prevention in Drilling Operations	48
2.3.5	Hydrate Remedial Methods	50
2.4	Temperature Model of a Barents Sea Well	51
3	Laboratory Experiment and Equipment	55
3.1	NTNU Experiments	55
3.1.1	Experimental Apparatus	56
3.1.2	NTNU Experimental Procedure	60
3.1.3	The Various Fluid Compositions Tested	61
3.1.4	Gas Solubility in Experiment Fluids	63
3.2	SINTEF Test	65
3.2.1	Experimental Apparatus	66
3.2.2	SINTEF Experimental Procedure	68
3.2.3	Gas solubility in the SINTEF Test	69
4	Results and Discussion	71
4.1	NTNU Experiments	71
4.1.1	Initial and Final System Conditions	71
4.1.2	Evidence of Hydrate Growth	73
4.1.3	Start of Hydrate Growth	74
4.1.4	Temperature Fluctuation and Apparatus Temperature Discrepancy	76
4.1.5	Comparison of Hydrate Pressure Drop to Real Gas Law Pressure Drop	78
4.1.6	Comparison of PVT and Systems Without Hydrate Growth	80
4.1.7	Time Until System Equilibrium	81
4.1.8	Shape of the Pressure Profile	82
4.1.9	Comparison of the NTNU Experiments	84
4.1.10	Hydrate Formation in Theory	94
4.1.11	Volume Reduction and Total Hydrate Volume	95
4.1.12	Experimental Errors	108

4.2	SINTEF Test	117
4.2.1	Filling of the Wheel Flow Loop	117
4.2.2	Evidence of Hydrate Growth	118
4.2.3	Volume Reduction and Hydrate Volume Calculations	122
4.2.4	Experimental Errors	125
4.3	Comparison of the Volume Reduction in the NTNU Experiments and the SINTEF Test 2	128
4.4	Hydrate Formation in a Barents Sea Well	130
5	Conclusion	135
6	Further Work	139
6.1	Further Work - NTNU Experiments	139
6.2	Further Work - SINTEF Test	141
6.3	Further Work - Temperature Model	141
A	Figures	143
B	Calculations	157
B.1	Aqueous Solution Weight Fraction Calculations	157
B.2	Determining the Apparatus Volume	158
B.3	Hydrate Volume and Volume Change Calculations	160
B.4	Conversion of Hydrate Equilibrium Pressure into Depth	166
C	Procedures	169
C.1	Shut-in Procedure	169
C.2	Well Control Methods	171
D	Risk Assessment	173
E	Tables and Lists	179
E.1	Technical Description of Equipment Used in the NTNU Experiments	179

E.2	Van't Hoff Factor and Molar Mass for NaCl, CaCl ₂ and KCHOO	180
E.3	Effect of MEG, MeOH and NaCl as Hydrate Inhibitors	180
E.4	Hydrate Equilibrium Pressure and Temperature	181
E.5	General Information About the Different Experiments	
	Performed at NTNU	183
E.5.1	Notes From the NTNU Experiments	183
E.5.2	Composition and Initial Volume of the Aqueous Phase	185
E.5.3	Volume Change and Amount of Hydrate Volume Formed	187
	Bibliography	190

List of Figures

2.1	Hydrate equilibrium curve for a water and gas system. The gas phase consists of 90% methane (C_1) and 10% propane (C_3), while the liquid phase is pure water. The area left of the curve is defined as the hydrate area. Obtained from Aspen HYSYS software.	4
2.2	Structure of the water molecule and how water molecules are connected via hydrogen bonds (David L. Nelson, 2012).	6
2.3	The three cavities which create sI and sII (Sloan and Koh, 2007).	6
2.4	Hydrate crystal unit structures and the number and types of cavities used to form sI and sII (modified from Sloan and Koh (2007) and Heriot-WattUniversity (2016)).	8
2.5	Comparison of the volume excess free energy (ΔG_v) and surface excess free energy (ΔG_s). The black curve represents the sum of the two (modified from Sloan and Koh (2007)).	12
2.6	Hydrate formation time line and the total gas consumption in various phases of the hydrate formation (modified from Sloan and Koh (2007)).	14
2.7	Schematic model of labile cluster growth (modified from Sloan and Koh (2007)).	16
2.8	Schematic model of nucleation at the interface hypothesis which shows adsorption of gas molecules onto labile hydrate cavities at gas-water interface (Sloan and Koh, 2007).	16
2.9	Snapshots of clathrate clusters at given times [ns] (Sloan and Koh, 2007).	17
2.10	Photograph of single hydrate crystals of (a) ethylene oxide (sI) and (b) tetrahydrofuran (sII) (modified from Sloan and Koh (2007)).	20

2.11 Schematic step by step visualization of the hydrate growth (Sloan and Koh, 2007). . .	22
2.12 Hydrate formation from a water droplet (modified from Sloan and Koh (2007)). . .	23
2.13 Hydrate equilibrium curve for a 10% methane and 90% propane gas-water system. The hydrate curves for 5wt% and 20wt% NaCl in the aqueous solution are corrected with ΔT by using Equation 2.9 and Equation 2.12.	27
2.14 Example and description of one possible solution for defining and illustrating well barrier envelopes for drilling, coring and tripping with shearable string (modified from NORSOK (2013)).	29
2.15 Volume reduction of the synthetic natural gas mixture given in Table 3.2 at 6°C for three different hydration numbers.	44
2.16 Example of the volume change when a gas influx of 4 m ³ enters the well and converts into hydrates at a pressure of 181 bar (Helgestad, B., 2017).	45
2.17 Well sketch illustrating how the mud level changes when a gas influx of volume V_G convert into hydrates. V_1 is the well volume change due to hydrate formation. V_2 is the gas volume reduction (Helgestad, B., 2017).	46
2.18 Well sketch illustrating how the mud level changes when a gas influx creates a fracture and mud leaks from the wellbore into the formation. V_3 is the well volume change due to the leakage. If $V_4 \approx V_2$ the two scenarios may be difficult to distinguish (Helgestad, B., 2017).	47
2.19 The figure shows how the hydrate equilibrium curve changes when various salts are added to the water phase. The black curve illustrates an uninhibited system, while the other curves illustrates 10wt% of NaCl, CaCl ₂ and KHCOO dissolved in the water phase.	49
2.20 Temperature in the annulus at different time after shut-in. The temperature model is created by Lucas Cantinelli Sevillano, as a part of his PhD thesis. Initial mud temperature, lithology, cement and casing thermal conductivity, formation and water temperature gradient, friction, including several other factors are taken into consideration in this well temperature model (Sevillano, 2017).	52

3.1	Picture of the experimental apparatus inside the refrigerator. The various components present inside the refrigerator when running the experiment are numbered from one to eight. 1: Relief valve, 2: 3-way-valve, 3: Temperature sensor, 4: Pressure sensor, 5: Steel cap, 6: Steel cylinder, 7: Magnetic stirrer, 8: External temperature sensor placed in water filled Erlenmeyer flask (Helgestad, B., 2017)	57
3.2	Sketch of the steel cap and steel cylinder. The dimensions are marked on the sketch. The two parts were made in the PTS mechanical workshop (Vedvik, 2017).	58
3.3	The various components contributing to the total volume inside the pressure cell when running the experiments, numbered from one to seven. 1: Temperature sleeve, 2: Inlet temperature sensor, 3: Inlet 3-way valve, 4: Relief valve (only considered the volume to the outlet), 5: Inlet pressure sensor, 6: Inside of steel cylinder, 7: Magnetic stir bar (Gunhildrud, M., 2017, modified from Vedvik (2017)). . . .	59
3.4	(a) Methane solubility in pure water and (b) Methane solubility in aqueous NaCl solution (modified from Duan and Mao (2006)).	63
3.5	Picture of the Wheel Flow Loop inside the climate chamber (Helgestad, B., 2017) . .	65
3.6	Sketch of the wheel flow loop and motor. The rotational direction is clockwise when observed from the point of the motor (Fossen, 2017a)	66
3.7	A sketch of the Wheel Flow Loop. The placement of the pressure sensor, temperature sensors, camera and gas filling points are marked with arrows. The placement of the equipment on the sketch is aligned with Figure 3.5. The approximate water level is illustrated, as well as the gas flow inside the wheel (Helgestad, B., 2017) . .	67
3.8	Methane solubility in pure water at 25°C for various pressures (modified from Duan and Mao (2006)).	69
4.1	Comparison of the pressure declination in experiment 3 (Nidelv water), 4 (Fjord water), 11(Tap water and 5wt% bentonite) and 13 (Tap water and 10wt% CaCl ₂). Time=0 is defined as the time where the experiment temperature is 21.5°C , thus not the start of the experiments.	75

4.2	Temperature curve for experiment 8, showing the temperature fluctuations. This is a typical example of the temperature fluctuations observed in all the experiments.	76
4.3	Pressure change as a function of temperature according to real gas law. Since the Z-factor is assumed constant, the relationship between pressure and temperature becomes linear.	78
4.4	Comparison of the pressure curve obtained from experiment 4 and the theoretical pressure drop in an equivalent system according to real gas law.	79
4.5	Comparison of pressure drop in systems with no hydrate growth, and pressure drop in equivalent systems according to real gas law. The yellow curve represents the theoretical pressure drop when gas dissolving into the aqueous solution is accounted for.	81
4.6	Visual representation of the main shapes of pressure curve with and without hydrate formation. The red arrows indicate the point where hydrates start to grow (Helgestad, B., 2017).	83
4.7	A comparison of experiment 3 (Nidelv water), 5 (3.5wt% NaCl in Fjord water), 9 (20wt% NaCl in Nidelv water) and 20 (tap water). The blue arrow indicates the final pressure in experiment 20, reached at Time = 65hrs. The red arrows indicate the collection of pressure and temperature curves.	85
4.8	A comparison of experiment 3 (Nidelv water), 6 (10wt% barite in Nidelv water) and 11 (5wt% bentonite in tap-water). The red arrows indicate the collection of pressure and temperature curves.	87
4.9	A comparison of experiment 3 (Nidelv water), 8 (10wt% NaCl in tap water), 13 (10wt% CaCl ₂ in tap water) and 17 (10wt% KHCOO in tap water). The red arrows indicate the collection of pressure and temperature curves.	88

4.10 The hydrate equilibrium curves for various salts in solution are plotted and compared to the final conditions of the experiments performed with the same type of water base in the aqueous solution. The actual final conditions are marked with a circle coloured with the same colour as the related hydrate equilibrium curve. The final temperature of experiment 13 and 8 have been corrected by -1°C , marked as triangles.	90
4.11 Hydrates observed by visual inspection in experiment 11. The bentonite slurry makes it difficult to see the hydrates inside the cell, but when picked up and moved to a beaker, the size and shape of the hydrate chunks can be observed. The glass beaker has a diameter of approximately 70mm (Gunhildrud, M., 2017).	92
4.12 Hydrates observed by visual inspection in experiment 20. Several hydrate chunks, surrounded by a hydrate slurry were observed. The biggest lumps were removed from the cell and placed in a glass beaker. The glass beaker has a diameter of approximately 90mm (Helgestad, B., 2017).	93
4.13 Hydrates observed in experiment 4 (a) and in experiment 17 (b). The hydrates were in the shape of a thick slurry in both of the experiments (Helgestad, B., 2017).	93
4.14 Volume reduction extrapolation for the NTNU gas at 6°C . The volume reduction for three different hydration numbers is considered.	100
4.15 Hydrate equilibrium curves for different wt% NaCl for the NTNU gas.	103
4.16 Hydrate equilibrium curve for 10wt% NaCl.	104
4.17 Visual inspection of hydrate occurrence in the SINTEF Test, observed through the sapphire glass section of the wheel (Fossen, 2017b).	119
4.18 Hydrate equilibrium curve for the gas used in the SINTEF Test.	121
4.19 Pressure and temperature changes in Test 2, SINTEF Test.	122
4.20 Volume reduction extrapolation for the SINTEF gas at 6°C . The volume reduction for three different hydration numbers is considered.	125
4.21 Volume reduction extrapolation for the NTNU and SINTEF gas (in-between case).	129

4.22	The hydrate equilibrium curve as a function of dept, and the well temperature model. A fluid density of 1000 kg/m^3 is used to convert the hydrate equilibrium pressures into depth. The arrows shows the depth, where the well conditions enters the hydrate formation area.	131
4.23	The well temperature model and the hydrate equilibrium curve for SINTEF gas, at various drilling fluid densities. The yellow curve represents a fully inhibited water phase. The arrows shows the depth, where the well conditions enters the hydrate formation area.	133
A.1	Pressure and temperature changes in Experiment 1. This experiment was aborted after 3.4 hours because a leakage was believed to have occurred. The pressure cell was cooled down inside the refrigerator before starting to log the temperature and pressure. The leakage was not verified visually and the pressure decrease could have occurred because of hydrate formation.	143
A.2	Pressure and temperature changes in Experiment 2.	144
A.3	Pressure and temperature changes in Experiment 3.	144
A.4	Pressure and temperature changes in Experiment 4.	145
A.5	Pressure and temperature changes in Experiment 5.	145
A.6	Pressure and temperature changes in Experiment 6.	146
A.7	Pressure and temperature changes in Experiment 7.	146
A.8	Pressure and temperature changes in Experiment 8.	147
A.9	Pressure and temperature changes in Experiment 9.	147
A.10	Pressure and temperature changes in Experiment 10. Leakage verified.	148
A.11	Pressure and temperature changes in Experiment 11.	148
A.12	Pressure and temperature changes in Experiment 12.	149
A.13	Pressure and temperature changes in Experiment 13.	149
A.14	Pressure and temperature changes in Experiment 14.	150
A.15	Pressure and temperature changes in Experiment 15.	150
A.16	Pressure and temperature changes in Experiment 16. Leakage verified.	151
A.17	Pressure and temperature changes in Experiment 17.	151

A.18 Pressure and temperature changes in Experiment 18. 152

A.19 Pressure and temperature changes in Experiment 19. 152

A.20 Pressure and temperature changes in Experiment 20. 153

A.21 Pressure and temperature changes in Experiment 2.2, dissociation of hydrates. . . 153

A.22 Pressure and temperature changes in Experiment 3.2, dissociation of hydrates. . . 154

A.23 Pressure and temperature changes in Experiment 12.2, dissociation of hydrates. . 154

A.24 Pressure and temperature changes in Experiment 14.2, dissociation of hydrates. . 155

A.25 Standing and Katz chart (DrillingFormulas.com, 2016) 156

List of Tables

2.1	The temperature depression effect on the freezing point of various salts. The values are calculated based on Equation 2.12.	26
3.1	List of experiments performed at the NTNU laboratory with corresponding mud composition, date performed and an explanation of which action was taken after the end of an experiment.	62
3.2	Synthetic natural gas composition used in the SINTEF Test.	68
4.1	Initial and final pressure and temperature in the pressure cell for each experiment. The pressure and temperature change from start to finish are also calculated. Experiments where dissociation of hydrates occurred is marked as Experiment X.2.	72
4.2	Hydrate volume and volume reduction in each experiment performed at NTNU. Three scenarios are showed, an in-between case, best case and worst case.	96
4.3	volume reduction of the experiments performed at the NTNU laboratory in a decreasing order, organized from greatest to smallest (in-between case).	97
4.4	The effect NaCl has on volume reduction.	98
4.5	Comparison of the effect of 10wt% NaCl, CaCl ₂ , Barite and KHCOO on volume reduction.	99
4.6	The effect NaCl has on hydrate growth.	101
4.7	Hydrate volume organized from greatest to smallest value, in the experiments conducted at the NTNU laboratory. The in-between case is considered.	102

4.8	Comparison of 10wt% NaCl, CaCl ₂ , Barite and KHCOO.	105
4.9	Hydrate volume in solutions with 5wt% bentonite, 10wt% KHCOO and the combination of the two.	105
4.10	Hydrate volume obtained from calculations when methane dissolved into the aqueous solution has been considered and not.	107
4.11	Experiments performed at NTNU showing the volume reduction and hydrate volume formed listed in a decreasing order.	108
4.12	volume reduction for Test 2, performed at SINTEF laboratory with the synthetic natural gas mixture given in Table 3.2.	123
4.13	Comparison of hydrate volume formed at Test 2, SINTEF Test	124
C.1	Example procedure for shut-in while drilling (retrieved from Robinson (2015)). . .	169
C.2	Well control procedure for the first circulation in Driller's Method (Brechan (2015); WildWellControl (2016); Welltrain (2008)).	171
C.3	Well control procedure for the second circulation in Driller's Method (WildWellControl (2016); Welltrain (2008); Samuel (2010)).	171
C.4	Well control procedure for the Wait & Weight Method (WildWellControl (2016); Welltrain (2008)).	172
E.1	Technical description of the equipment used in the NTNU experiments.	179
E.2	Van't Hoff factor and molar mass for various solutes used in used in Equation 2.12.	180
E.3	The temperature depressing effect of different inhibitors, in various concentrations, on the hydrate equilibrium. Calculated using Equations in (KAMATH and PATIL, 1994).	180
E.4	Hydrate equilibrium pressures at various temperatures, for different gas compositions. Data obtained from AspenHYSYS simulations.	181
E.5	Input values retrieved for the hydrate equilibrium curve for the SINTEF gas using Aspen HYSYS software.	182
E.6	Composition of the aqueous phase in each experiment.	185
E.7	Initial volume of the aqueous phase in each experiment.	186

E.8 Total amount of hydrates formed and the volume reduction obtained in the experiments conducted at the NTNU laboratory with the NTNU gas (in-between case). 187

E.9 Total amount of hydrates formed and the volume reduction obtained in the experiments conducted at the NTNU laboratory with the NTNU gas (best case). 188

E.10 Total amount of hydrates formed and the volume reduction obtained in the experiments conducted at the NTNU laboratory with the NTNU gas (worst case). 189

Nomenclature

BHP = Bottomhole Pressure

BOP = Blowout Preventer

CDPP = Circulating Drillpipe Pressure

COF = Coefficient of Friction

ECD = Equivalent Circulating Density

HEN = Heterogeneous nucleation

HON = Homogeneous nucleation

HSE = Health, Safety, Environment

ID = Internal Diameter

LOC = Loss of Circulation

MPD = Managed Pressure Drilling

MWT = Measurement While Tripping

NORSOK= Norsk sokkels konkuransesposisjon

NPT = Non-Productive Time

OBM = Oil Based Mud

OD = Outer Diameter

RKB = Rotary kelly bushing

sH = Structure H unit cell

sI = Structure I unit cell

SICP = Shut-in Casing pressure

sII = Structure II unit cell

UBD = Underbalanced Drilling

WBE = Well Barrier Element

WBM = Water Based Mud

wt% = Weight percentage

ΔG_{crit} = Critical energy required to grow hydrates

ΔG_s = Surface excess free energy

ΔG_v = Volume excess free energy

ΔG = Gibb's free energy

$\Delta P_{(T)}$ = Pressure resuction due to temperature decrease

$\Delta P_{Dissolve}$ = Pressure reduction due to gas dissolving in the aqueous solution

ΔP_H = Pressure reduction due to hydrate formation

Δt = Time until system Equilibrium

ΔT_f = Change in freezing point

ρ_a = Density of additive i

ρ_{final} = Final gas density

ρ_{gas} = Gas density

ρ_{hyd} = Hydrate density

ρ_w = Water density

ρ = Density

θ_{iJ} = Fractional occupation of cavity i by component J

$5^{12}6^2$ = Tetrakaidecahedron

$5^{12}6^4$ = Hexakaidecanhedron

ν_i = Number of type i cavities per water molecule in unit cell

x_a = Weight fraction of additive a

$X_{Large\ cavities}$ = Total number of large cavities in the structure cell

$X_{Small\ cavities}$ = Total number of small cavities in the structure cell

136 = Mole water per unit cell

16 = Number of small cavities in sII unit cell

5^{12} = Pentagonal dodecahedra

- 8 = Number of large cavities in sII unit cell
- b = Molality C_1 = Methane
- C_3 = Propane
- $D_{Cylinder_6}$ = Diameter of steel cylinder
- D_{Pres_5} = Diameter of inlet hole for the pressure sensor
- D_{Temp_1} = Diameter of temperature sleeve
- D_{Temp_2} = Diameter of inlet hole for the temperature sleeve
- D_{Valve_3} = Diameter of inlet hole for 3-way valve
- D_{Valve_4} = Diameter of inlet for the safety valve
- E = Edges of a polyhedra
- F = Faces
- G = Guest molecule
- $h_{Cylinder_6}$ = Height of steel cylinder
- h_{Pres_5} = Height of inlet hole for the pressure sensor
- h_{Temp_1} = Height/ length of temperature sleeve
- h_{Temp_2} = Height of inlet hole for the temperature sleeve
- h_{Valve_3} = Height of inlet hole for 3-way valve
- h_{Valve_4} = Length of inlet for the safety valve
- i = van't Hoff factor ID = Inner diameter of the wheel
- K_f = Freezing point depression constant
- L = Length of the wheel
- M = Molecular weight
- m = Mass
- m_{a_i} = Mass of additive i
- $m_{drained\ water}$ = Mass of the drained water
- $m_{gas,used}$ = Mass of gas used to form hydrate
- M_{gas} = Molecular weight of the gas
- M_{hyd} = Molecular weight of hydrate
- M_i = Molecular weight of gas component i

$m_{\text{pycnometer w/ water}}$ = Mass of pycnometer filled with water

$m_{\text{pycnometer}}$ = Mass of pycnometer

m_{tot} = Total mass

m_w = Mass of water

$m_{\text{water inside wheel}}$ = Mass of water inside the wheel

$m_{\text{water,used}}$ = Mass of water used to form hydrate

M_{water} = Molecular weight of water

$m_{\text{wheel w/ water}}$ = Mass of wheel filled with water

m_{wheel} = Mass of wheel

$m_{\text{wheel drained}}$ = Mass of wheel when water has been drained

MW_J = Molecular weight of component J

N = Hydration number

n = Mole

N_{Ava} = Avogadro's number, $6.023 \cdot 10^{23}$ molecules/mole

$n_{\text{gas,initial}}$ = Mole gas initially in place in the pressure cell/wheel

$n_{\text{gas,used}}$ = Mole gas used to form hydrate

$n_{\text{water,used}}$ = Mole water used to form hydrate

N_w = Number of water molecules per unit

p_{ci} = Critical pressure of gas component i

p_{final} = Final pressure

p_{initial} = Pressure initially in place in the pressure cell/wheel

p_{pc} = Pseudocritical pressure

p_{pr} = Pseudoreduced pressure

R = Gas constant

T_{ci} = Critical temperature of gas component i

T_{final} = Final temperature

T_{initial} = Temperature initially in place in the pressure cell/wheel

T_{pc} = Pseudocritical temperature

T_{pr} = Pseudoreduced temperature

V = Vertices of a polyhedra

V = Volume

V_{a_i} = Volume of additive i

V_{cell} = Volume of pressure cell

$V_{Cylinder_6}$ = Volume of steel cylinder

$V_{drained\ water}$ = Volume of the drained water

$V_{gas,initial}$ = Volume of gas initially in place in the pressure cell/wheel

$V_{gas,left}$ = Volume of gas left in the cell/ wheel after hydrate formation

$V_{gas,used}$ = Volume of gas used to form hydrates

$V_{gas\ in\ wheel}$ = Volume of gas inside the wheel after drainage of water

V_{hyd} = Hydrate volume

V_{magnet_7} = Volume of magnetic bar stirrer

V_{Pres_5} = Volume of inlet hole for the pressure sensor

$V_{pycnometer}$ = Volume of pycnometer

V_{Temp_1} = Volume of of temperature sleeve

V_{Temp_2} = Volume of inlet hole for the temperature sleeve

V_{tot} = Total volume

V_{tot} = Total volume of pressure cell

V_{Valve_3} = Volume of inlet hole for 3-way valve

V_{Valve_4} = Volume of inlet for the safety valve

V_w = Volume of water

$V_{water,initial}$ = Volume of water initially in place in the pressure cell/wheel

$V_{water,left}$ = Volume of water left in the cell/ wheel after hydrate formation

$V_{water,used}$ = Volume water used to form hydrate

$V_{water\ inside\ wheel}$ = Volume of water inside the wheel after drainage

V_{wheel_1} = Volume of wheel calculated using ID and L

V_{wheel} = Volume of wheel determined by weight

V_{cell} = Volume unit cell

X = Percentage of large cavities occupied by a guest molecule

Y = Percentage of Small cavities occupied by a guest molecule

X_a = wt% of solute added

Z = Compressibility factor

Z_{final} = Compressibility factor at final pressure and temperature conditions

Chapter 1

Introduction

The past three decades, exploration drilling has expanded into deepwater and ultra-deepwater areas ([Nimblett, 2005](#)). From 2005 to 2015, the offshore oil production in deep- and ultra-deepwater environments increased by 25%, implying that production and exploration in these environments will continue ([Manning, 2016](#)). Another region of interest is the Arctic areas, as the United States Geological Survey has concluded that approximately 13% of the world's undiscovered oil and 30% of the world's undiscovered gas might be found in the area north of the Arctic Circle ([Gautier et al., 2009](#)).

New drilling challenges arise as exploration drilling expands into deeper water and higher latitudes ([Yakushev, 1992](#)). One major drilling hazard in these areas is hydrate formation due to the low seabed temperature and high pressure. Even though gas hydrates represent a significant hazard to drilling operations, only a few actual problems have been documented. It is important to make the industry aware of the danger hydrates represent in order to recover and produce hydrocarbons in these areas in a safe manner. By identifying where and how hydrates form in the well, solutions to prevent hydrate formation can be found. Thus, the drilling hazards related to hydrate formation can be minimized or eliminated.

Clathrate hydrate(s) of natural gas, referred to as natural gas hydrates in this thesis, are an ice-like crystal structure consisting of water and gas ([Sloan and Koh, 2007](#)). Under favourable pres-

sure and temperature conditions, guest molecules are trapped inside hydrogen-bonded cavities created by water molecules (Yakushev, 1992). In a well control situation, the well temperature and the hydrostatic pressure of the drilling fluid column provide suitable conditions for hydrate formation (Østergaard et al., 2000).

The main objective of this master thesis is to acquire valuable information about hydrate formation in drilling fluid and how it affects well control. A phenomenon occurring when hydrates are formed is that the hydrate volume has a less volume than the total volume of water and gas used to form the hydrates. A hypothesis is that this volume change can be misinterpreted with loss of circulation in a well control situation. Laboratory experiments have been performed at the NTNU laboratory with focus on hydrate formation in drilling fluid. The goal was to observe how different drilling fluid additives affect hydrate formation in the drilling fluid, and how significant the volume reduction is, when these additives are present. Another experiment was conducted by SINTEF research center for Future Well Control AS, where the aim was to determine possible volume reduction when gas hydrates form (Fossen, 2017a). In this experiment, a more realistic pressure and gas composition was used, compared to the NTNU experiments.

The following sections in Chapter 2 are based on the project reports written by Michaela Gunhildrud and Bendik Helgestad, fall of 2016 at NTNU (Helgestad, 2016; Gunhildrud, 2016);

Section 2.1 (except 2.1.5.1 and 2.1.6),

Section 2.2 (except 2.2.1.2),

Section 2.3 (except 2.3.1, most parts of 2.3.3 and 2.3.4).

It should also be mentioned that most of the hydrate theory is retrieved and modified from Sloan and Koh (2007).

Chapter 2

Theory

This chapter consists of three main parts. The first part gives an introduction to natural gas hydrates, the second part to well control, while the third part ties these two together and describes natural gas hydrates as a drilling hazard. Finally, a well temperature model is presented to show the well interval where hydrates can form.

These topics form the theoretical framework required for understanding the experimental analysis, and how hydrate formation impacts well control.

2.1 Natural Gas Hydrates

Natural gas hydrates are ice-like crystal structures, consisting of water and gas. The water molecules create a cavity where a gas molecule is trapped. Hydrates exist naturally subsurface, but can form in petroleum equipment if the required temperature and pressure conditions are met. In the petroleum industry today, hydrates are considered as a major problem ([Sloan and Koh, 2007](#)).

The factors which are required to form hydrates are; (1) high pressure, (2) low temperature, (3) water and (4) a guest molecule. If one of the four factors are removed, hydrates cannot form.

This fact forms the basis for all hydrate prevention and remedial methods (Sloan and Koh, 2007).

The general in-situ temperature range for hydrates found in marine settings are between 2°C and 20°C, depending on the in-situ pressure (Lasse Amundsen and Reichel, 2013). The higher the pressure, the higher the subsurface temperature can be without the hydrates dissociating.

Figure 2.1 shows the *hydrate equilibrium curve* for a water-gas system consisting of 90% methane and 10% propane, i.e. the conditions where hydrate, gas and liquid water are in equilibrium. The area left of the curve will be referred to as the *hydrate area*. When the system conditions are within this area, hydrate formation may occur. Right of the curve, hydrate formation is impossible for the considered fluid composition. Hydrate formation do not need to occur, even if the in-situ conditions are within the hydrate area. The reason behind this is further discussed in Section 2.1.3.

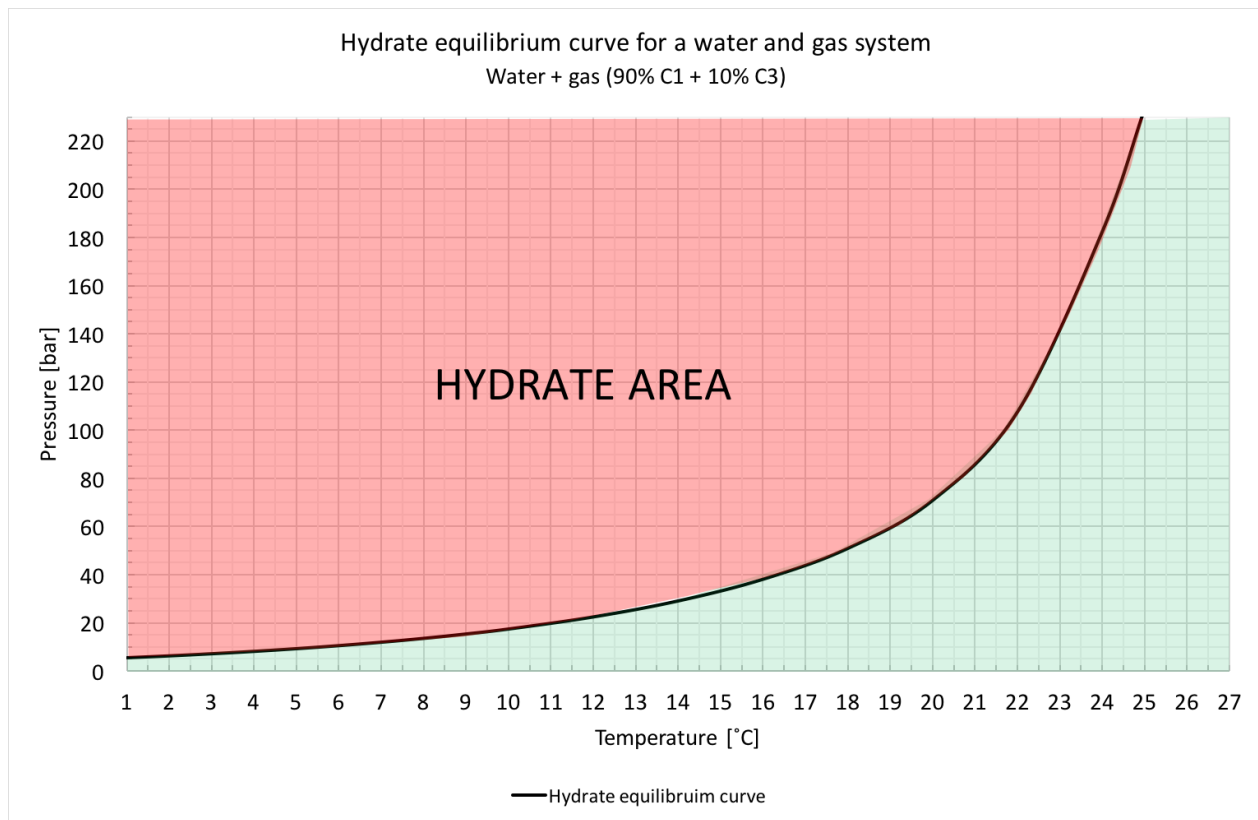


Figure 2.1: Hydrate equilibrium curve for a water and gas system. The gas phase consists of 90% methane (C₁) and 10% propane (C₃), while the liquid phase is pure water. The area left of the curve is defined as the hydrate area. Obtained from Aspen HYSYS software.

This section will give the theoretical basis needed to understand hydrate formation. The water properties affect the hydrate properties, thus some insight into the structure of the water molecule will be provided first.

2.1.1 Water Molecule and Hydrogen Bonds

Water is the main component in hydrates. Understanding the structure and properties of the water molecule is therefore necessary in order to understand hydrate formation. The water molecule consists of one oxygen atom connected to two hydrogen atoms by polar covalent bonds (Fjellvåg, 2009). This structure makes the water molecule polar due to a higher electron density at the oxygen side. The polarity causes the molecule to have a bond angle of 104.5° .

The water molecule has four charges; two positive and two negative. The different charges create four points where the water molecule can connect to other molecules, as can be observed from Figure 2.2. Because of the polarity, the negative pole of one molecule will bond to the positive pole of another molecule. This leads to a structure in solid water where each water molecule is bonded to four other water molecules via hydrogen bonds. In liquid water, the hydrogen bonds are created and broken continuously. When water crystallizes into ice or hydrates, these bonds become permanent. (Sloan and Koh, 2007).

2.1.2 Gas Hydrate Crystal Structure

The crystal structure of hydrates differs from the one observed in ice. In ice, water is bonded together in hexagonal crystal structures, whereas the hydrate structure consists of pentagonal and hexagonal rings created by water molecules. The rings gather around a molecule of specific size, called *guest molecule*, to create cage-like structures called *cavities*. The most common gas hydrate structures are the cubic structure I (sI) and cubic structure II (sII). In addition, hexagonal structure (sH) exists, but will not be described in this thesis (Sloan and Koh, 2007).

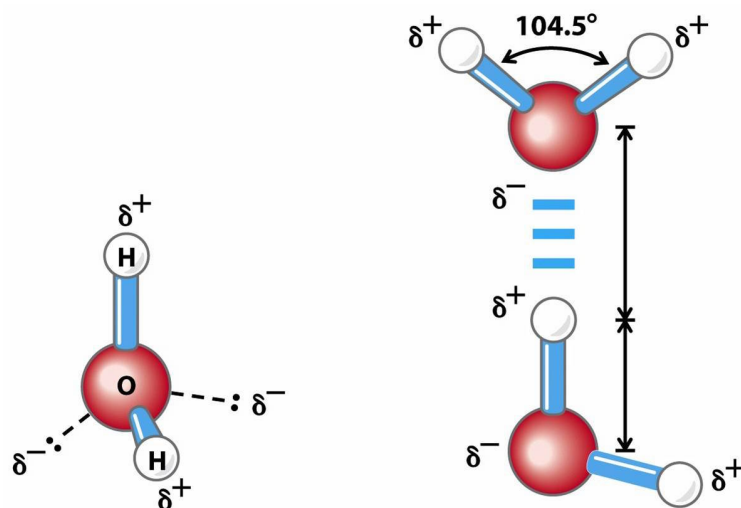


Figure 2.2: Structure of the water molecule and how water molecules are connected via hydrogen bonds (David L. Nelson, 2012).

2.1.2.1 Cavities in Gas Hydrates

The building blocks of a hydrate structure are the cavities containing a gas molecule. The three most commonly observed cavities, creating sI and sII are; pentagonal dodecahedra, tetrakaidecahedron and hexakaidecanhedron. Depending on the size of the guest molecule, the different cavities are created (Sloan and Koh, 2007).

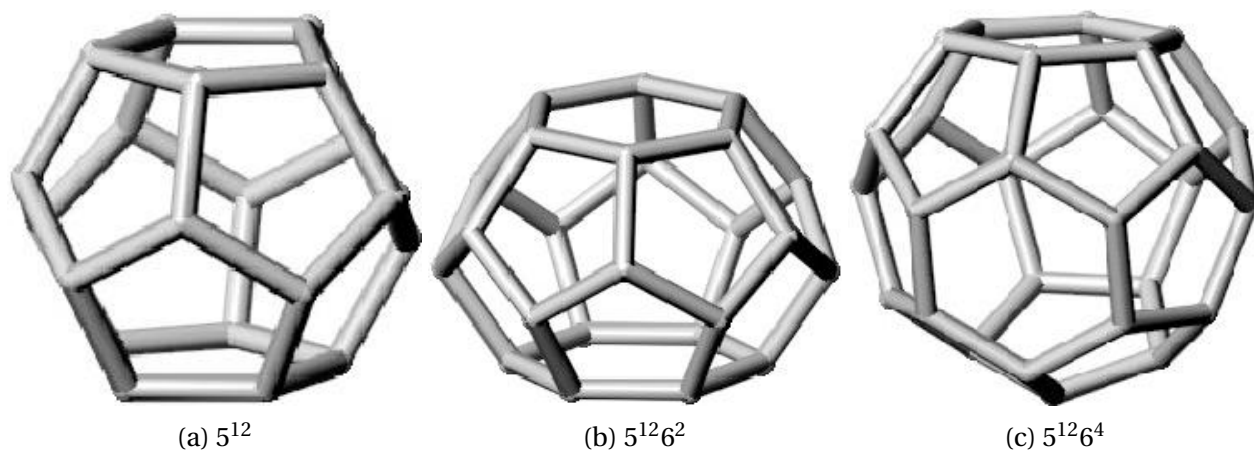


Figure 2.3: The three cavities which create sI and sII (Sloan and Koh, 2007).

The cavities will be labeled by the nomenclature $n_i^{m_i}$ in this report. Here, n_i is the number of edges in face type "i", and m_i is the number of faces with n_i edges. The cavities can contain maximum one guest molecule. The exception is at very high pressures [GPa]. The guest molecule is held within the cage by dispersion forces. They prevent the hydrate cavities from collapsing since they act as a repulsive force, either in a large percentage of the neighboring cavities or in the cavities itself (Sloan and Koh, 2007). *Euler's Theorem*, concerning polyhedra composed of pentagons and hexagons, is useful when looking at the hydrate crystal structure (Watkins, 2016). The theorem states that if F is the faces, V is the vertices and E is the edges of a polyhedra, the relationship in Equation 2.1 is valid. The exception is for cavities containing square faces (Sloan and Koh, 2007).

$$F + V = E + 2 \quad (2.1)$$

The most basic cavity is called *Pentagonal Dodecahedra* and labeled by the nomenclature as 5^{12} . This is the smallest cavity and acts a building block in most natural gas hydrates. The 5^{12} cavity consists of 12 pentagonal water rings connected together as a cage, as shown in Figure 2.3a. 60 water molecules are needed to create 12 separate pentagonal rings. When the rings are bonded together to form a cavity, the water molecules are shared. Thus, only 20 water molecules are required to create a Pentagonal Dodecahedra (Sloan and Koh, 2007).

Tetrakaidecahedron is a cavity consisting of twelve pentagonal rings and two hexagonal rings connected together, labeled as $5^{12}6^2$. This is the second smallest cavity present in hydrate structures. It only contains small guest molecules. Figure 2.3b shows the geometry of the Tetrakaidecahedron cavity. This structure follows Euler's theorem with 14 faces and 24 vertices, which yield 36 edges (Sloan and Koh, 2007).

Hexakaidecanhedron consists of twelve pentagonal and four hexagonal rings, labeled as $5^{12}6^4$. Its geometry is shown in Figure 2.3c. The radius of the cavity does not vary more than 1.7%, thus the hexakaidecanhedron is the most spherical of all cavities. Its internal diameter allows guest

molecules with a diameter up to 6.6\AA , that is $6.6 \cdot 10^{-10} m$, to fit inside and stabilize the cavity. Propane and iso-butane fit inside this cavity. Euler's theorem is fulfilled by this structure as well, having 16 faces, 28 vertices and 42 edges (Sloan and Koh, 2007).

2.1.2.2 Structure I and II

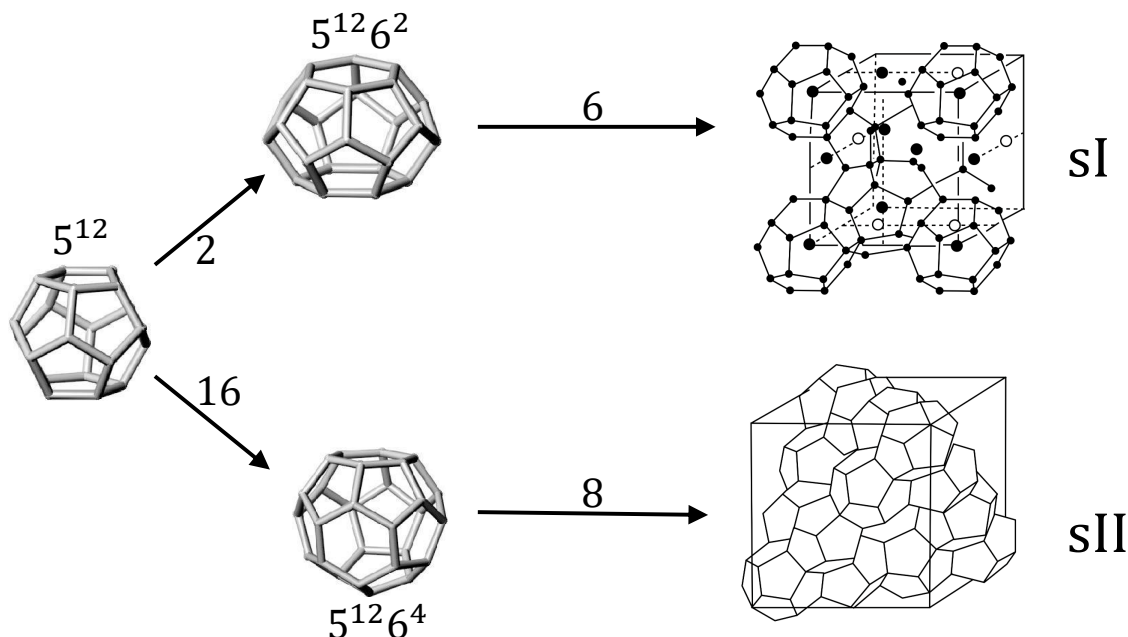


Figure 2.4: Hydrate crystal unit structures and the number and types of cavities used to form sI and sII (modified from Sloan and Koh (2007) and Heriot-WattUniversity (2016)).

Figure 2.4 gives a visual representation of the difference between sI and sII. sI consists of 5^{12} and $5^{12}6^2$ cavities, while sII is made up of 5^{12} and $5^{12}6^4$ cavities. Fourfold hydrogen bonds are obtained by linking the basic cavity in two different ways; (1) by linking the vertices of dodecahedra and (2) by sharing common faces of adjacent dodecahedra. This represents the contrast of sI and sII structures. Fourfold hydrogen bonds in sI are obtained by vertex-linking of the cavities in three dimensions, whereas sII is obtained by face-sharing (Sloan and Koh, 2007).

This structural difference affects the hydrate formation pressure. In order to form sI, a greater pressure is required than for sII at the same temperature. This is because the large cavities in

sII are more stable and remains stable at a lower pressure, compared to the smaller cavities in sI (Sloan and Koh, 2007).

Due to smaller cavities in sI, this structure nucleates when the hydrocarbon fluid composition only contains small amounts of large molecules like propane or iso-butane. If such molecules are present in the gas phase with a concentration greater than 1%, sII unit cell forms. This is because they stabilize the large cavities. Consequently, the majority of the hydrates forming in petroleum industry equipment are categorized as sII, as most hydrocarbon gas mixtures contain more than 1% of propane and iso-butane (Sloan and Koh, 2007).

2.1.2.3 The Guest Molecule

The guest molecule is stabilizing the cavity by the *Van der Waal forces* that acts between the guest molecule and the cavity. The characteristics of guest molecules can be used as a second classification of hydrates. It is a function of two factors; (1) the chemical nature of the guest molecule and (2) the size and shape of the guest molecule. The size is in most cases directly related to the hydration number and to its non-stoichiometric value (Sloan and Koh, 2007).

The guest molecules can be categorized in one of the following four groups:

1. Hydrophobic Compounds
2. Water-soluble acid gases
3. Water-soluble polar compounds
4. Water-soluble ternary or quaternary alkylammonium salts.

Since most of the common components of natural gas are hydrophobic, i.e. non-polar molecules that do not combine with water, they fall within the first category (Williams, 2017).

2.1.2.4 The Size and Shape of Guest Molecules

Only a limited number of hydrates can be created due to the space limitations inside the cavity. Consequently, only molecules with a diameter between 3.5Å and 7.5Å can fit into sI and sII. The restrictions of chemical nature of guest molecules stated above must be obeyed if all molecules between the size of 3.8 Å (argon) to 6.5 Å (cyclobutanone) shall be able to form sI and sII. It is mainly the size of the guest molecule that affects the structure and properties of sI and sII. The shape only plays a minor role (Sloan and Koh, 2007).

The free energy change is affected by changes in the lattice parameter with guest size and unit cell volume. Because of the size difference of guest molecules, the forces acting on the cavity varies. The lattice parameter, hence the average cavity diameter is a function of pressure, temperature and guest composition. Small changes in the lattice parameter may cause significant changes to the hydrate formation pressure. Simulations have shown that a change of 0.5% in the lattice size may result in a 15% change in formation pressure (Sloan and Koh, 2007).

When determining the upper and lower limits to guest size, the diameter ratios of the guest molecule to each cavity for simple hydrate formers should be considered. The lower bound of the size ratio is often set to 0.76. Below this value, the molecular attractive forces contribute less to cavity stability. The upper bound ratio was found to be 1.0. At higher values, the guest molecules cannot fit into a cavity without distortion (Sloan and Koh, 2007).

Distortion of the cavities have a significant effect on the hydrate formation pressure. If simple hydrate species are capable of occupying a cavity of either sI or sII, it will also enter the large cavities of the structures. Methane, ethane, carbon dioxide and hydrogen sulfide are the natural gas components that form sI as simple hydrates. Nitrogen, propane and iso-butane are known to form sII (Sloan and Koh, 2007).

2.1.2.5 Hydration Number

The hydration number illustrates the water-to-guest ratio in the hydrate structure. It varies, depending on how many cavities are filled with guest molecules. Note that it is impossible for guest molecules to occupy all cavities and that all cavities do not need to be filled in order to create a stable hydrate structure. Thus, simple hydrates consist of more water molecules than the ideal composition. For sI, the ideal water-to-guest ratio is $G \cdot 5\frac{2}{3}H_2O$. The ideal water-to-guest ratio in sII, where all cavities are occupied by a guest molecule is $G \cdot 17H_2O$.

The occupancy of large cavities is typically greater than 95%. The small cavities are more dependent on the guest composition, temperature and pressure, making it difficult to estimate how many of the small cavities are occupied. Typical fractional occupancies of the smaller cavities are 0.3-0.9, based on size restrictions. This variation causes the hydrates to be nonstoichiometric (E. Dendy Sloan, 2008).

Variations in the filling grade of the cavities affect the amount of gas trapped inside the hydrates. In practice, the amount of gas trapped in natural occurring hydrates are often in the range between 140 to 160 standard volume units of gas per volume unit of hydrates, while hydrates with an ideal water-to-guest ratio would contain approximately 180 standard volume units of gas per volume unit of hydrates (Sloan and Koh, 2007).

A realistic estimate of the hydration number can be performed by assuming that 95% of the large cavities and 50% of the small cavities are filled with a guest molecule. The number of gas molecules per sII unit cell are then calculated using Equation 2.2. Since 136 water molecules are needed to create one unit cell of hydrate, the hydration number in such a case can be calculated using Equation 2.3 (Sloan and Koh, 2007).

$$\begin{aligned}
 G &= 0.95X_{Large\ cavities} + 0.5X_{Small\ cavities} \\
 &= 0.9 \cdot 8 + 0.5 \cdot 16 = 15.6
 \end{aligned}
 \tag{2.2}$$

$$N = \frac{n_{water}}{G} = \frac{136}{15.6} = 8.72
 \tag{2.3}$$

2.1.3 Hydrate Nucleation

Hydrate nucleation is defined as the process where small clusters of water and gas try to grow together past a *critical size*. Critical size is defined as the size of a cluster where the spontaneous growth starts. It is important to understand the stochastic nature of hydrate nucleation. This is especially apparent in systems with low *driving forces*, i.e. the system conditions are close to the hydrate equilibrium curve. In systems with low driving forces, the nucleation is more stochastic and thereby the distribution range is broader, making the predictability limited. Consequently, a gas-water system can be placed in an environment where hydrates should be occurring, without any hydrate formation. This is due to the energy potential known as *Gibbs free energy* (Sloan and Koh, 2007).

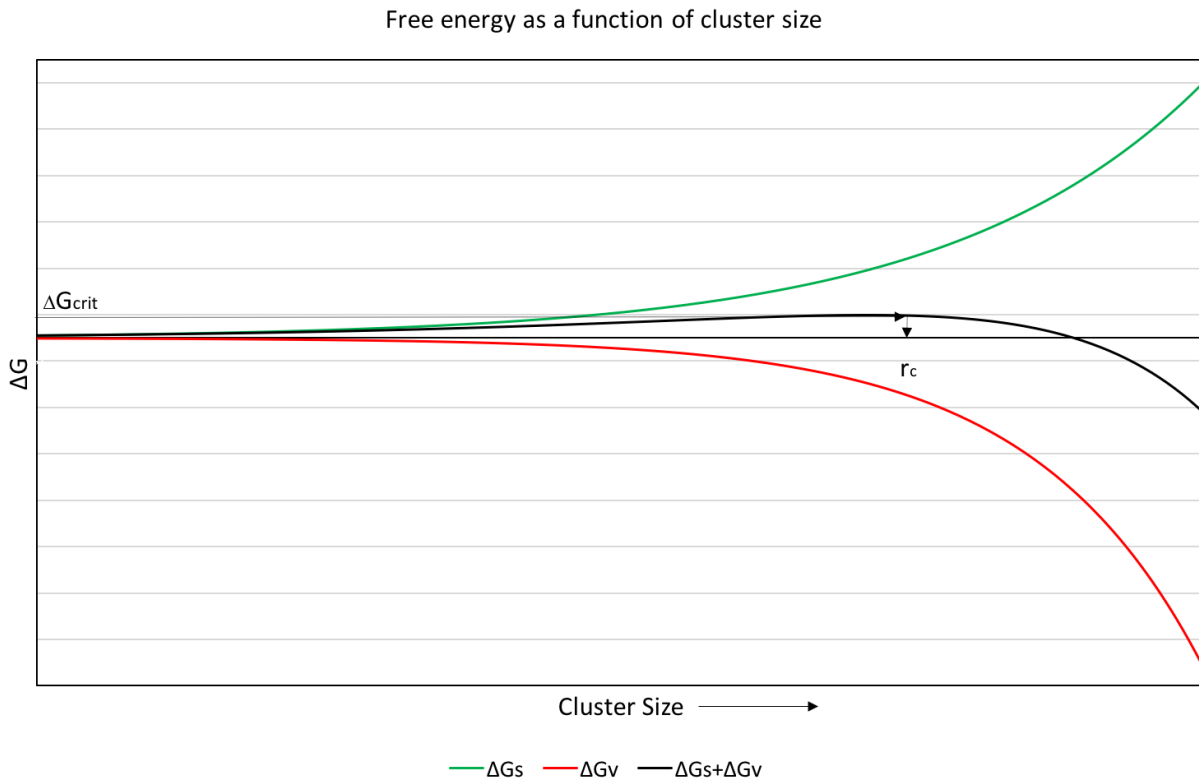


Figure 2.5: Comparison of the volume excess free energy (ΔG_v) and surface excess free energy (ΔG_s). The black curve represents the sum of the two (modified from Sloan and Koh (2007)).

Figure 2.5 shows how Gibbs free energy, ΔG , changes with the cluster size. The spontaneous growth starts when the sum of ΔG_v , volume excess free energy, and ΔG_s , surface excess free energy, is equal to ΔG_{crit} i.e. when ΔG has its maximum value. ΔG_s and ΔG_v are expressed in Equation 2.4 and Equation 2.5.

$$\Delta G_s = 4\pi r^2 \sigma \quad (2.4)$$

$$\Delta G_v = \frac{4}{3}\pi r^3 \Delta g_v \quad (2.5)$$

Thus, the total excess Gibbs free energy can be expressed as

$$\Delta G = \Delta G_s + \Delta G_v = 4\pi r^2 \sigma + \frac{4}{3}\pi r^3 \Delta g_v \quad (2.6)$$

As can be observed from Equation 2.7, the change in Gibbs free energy is a function of the radius of the cluster. When the clusters are small, $\Delta G > 0$ due to a greater initial increase in ΔG_s than ΔG_v . By differentiating Equation 2.7 and set the result equal to zero, the maximum value of ΔG and the critical cluster radius is obtained in Equation 2.8.

$$\Delta G_{crit} = \frac{\delta}{\delta r}(\Delta G) = 0 \quad (2.7)$$

$$\Delta G_{crit} = 4\pi \sigma r_c^2 / 3 \quad (2.8)$$

ΔG_{crit} is important. If the critical energy required to grow hydrates is too big, hydrates may never form, even if the the in-situ conditions are inside the hydrate area. The time taken until achieving critical cluster size is called *nucleation time*. Since the clusters are still small when reaching the critical size, the nucleation time can be difficult to determine. Therefore, *induction time* is a frequently used term of the early times of hydrate formation (Sloan and Koh, 2007).

2.1.3.1 Induction Time and Hydrate Formation Timeline

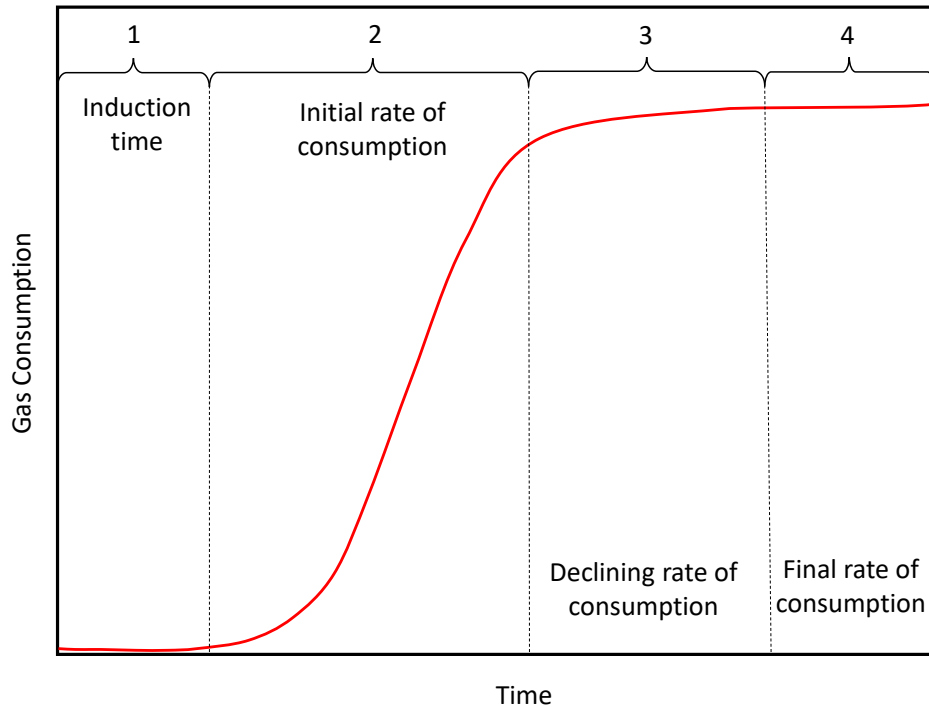


Figure 2.6: Hydrate formation time line and the total gas consumption in various phases of the hydrate formation (modified from [Sloan and Koh \(2007\)](#)).

The induction time is defined as the time taken for a detectable crystal structure to form, which means that nucleation and some growth have occurred. During this period, the pressure and temperature must be inside the hydrate stable region. The induction time is marked as phase one in Figure 2.6. Since limited growth has to occur before detection of clusters is possible, the gas consumption in the induction time is small ([Sloan and Koh, 2007](#)).

Phase two in Figure 2.6 represents the beginning of the growth phase. In this period, large amounts of gas are consumed and trapped inside the hydrates. In phase three, the rate of gas consumption declines. This is because the driving forces are weaker, or less water and gas are available compared to phase two. In phase four the gas consumption rate is constant or zero,

i.e. the hydrate is growing constantly or not growing at all (Sloan and Koh, 2007).

It is concluded that induction time may be applied under very restricted conditions. There are three reasons for that. First, hydrate nucleation and growth is a stochastic phenomenon and therefore difficult to predict. The induction times are very scattered, particularly at low driving forces. Second, induction times appear to be dependent on the apparatus used. Third, time-dependent variables such as the gas composition, history of water and the presence of foreign particles affect the induction time. These findings explain the difficulty of measuring and correlate hydrate formation processes (Sloan and Koh, 2007).

2.1.3.2 Hydrate Nucleation Theory at Molecular Level

No single hydrate nucleation theory at a molecular level is recognized as the correct one. Instead, three different models could possibly describe the hydrate nucleation at a molecular level. These three are presented below. Note that parts of each model have been criticized, thus experimental validation is required to verify which of the nucleation hypothesis most accurately represent hydrate nucleation (Sloan and Koh, 2007).

Labile cluster nucleation hypothesis: Figure 2.7 shows a schematic model of the labile cluster nucleation hypothesis. A description of the different steps is given below.

1. Initial condition: No gas molecules are dissolved in the water, only pressure and temperature conditions required for hydrate formation
2. Labile clusters: Labile clusters form immediately when gas dissolves in water
3. Agglomeration: By sharing faces, the labile clusters agglomerate. An increase in disorder occur
4. Primary nucleation and growth: Growth begins as soon as the size of agglomeration reaches a critical value

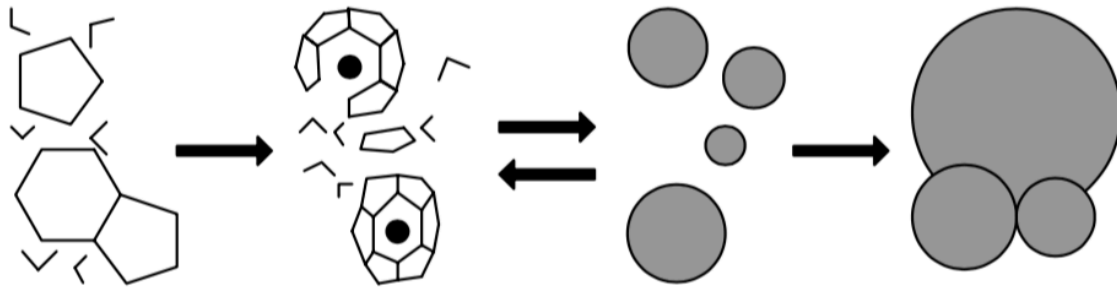


Figure 2.7: Schematic model of labile cluster growth (modified from Sloan and Koh (2007)).

Nucleation at the interface hypothesis: The different steps of the nucleation at the interface hypothesis is described below and showed in Figure 2.8. It is important to understand that clusters can both grow and shrink. The hypothesis should not be viewed as an orderly progression from small water clusters to large hydrate masses (Sloan and Koh, 2007).

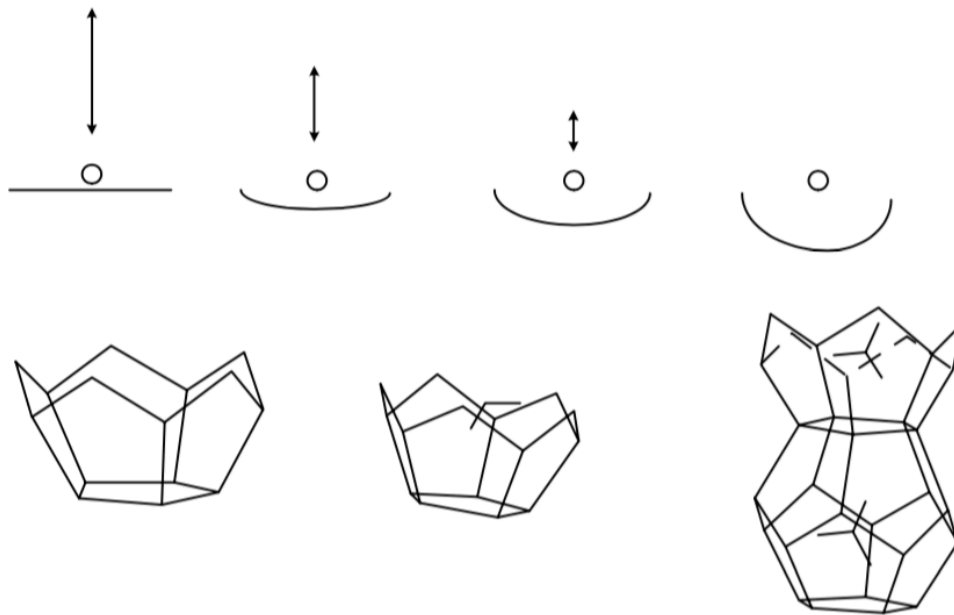


Figure 2.8: Schematic model of nucleation at the interface hypothesis which shows adsorption of gas molecules onto labile hydrate cavities at gas-water interface (Sloan and Koh, 2007).

1. Transportation of gas molecules to the interface.
2. Gas adsorbs on the aqueous surface.
3. Gas molecules migrate to a location that is suitable for adsorption through surface diffu-

sion. The water molecules form first partial cages around the adsorbed gas, then complete cages.

4. At the vapor side of the surface is where labile clusters join and grow until a critical size is achieved.

Local structuring nucleation hypothesis: Local structuring nucleation hypothesis is demonstrated in Figure 2.9, which shows snapshots of clathrate clusters at different times. A description of the nucleation hypothesis is given below.

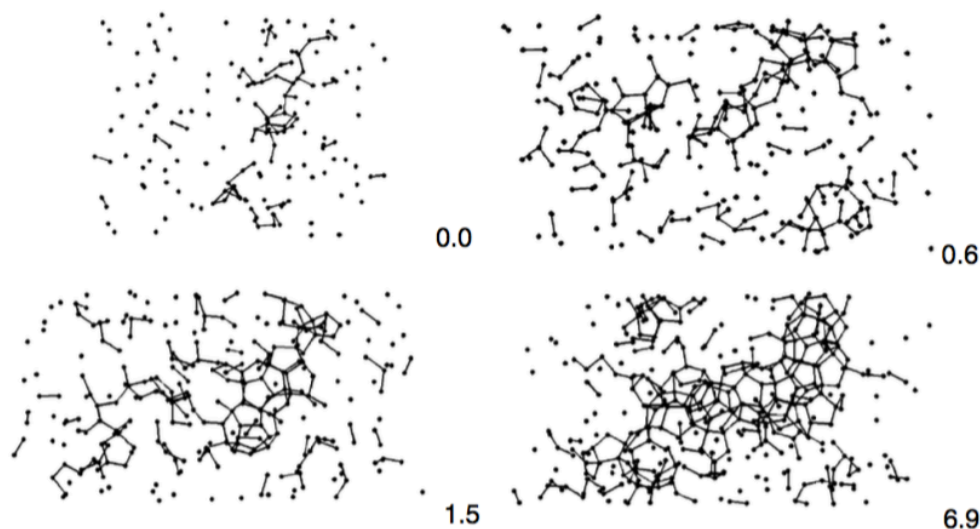


Figure 2.9: Snapshots of clathrate clusters at given times [ns] (Sloan and Koh, 2007).

1. A group of guest molecules are arranged in a configuration similar to that in the clathrate hydrate phase due to thermal fluctuations. The finite temperature of the system makes the structure of water molecules around the locally ordered guest molecules perturbed. This process is stochastic.
2. The critical nucleus is exceeded by number of guest molecules in a locally ordered arrangement. Guest-guest and host-host order parameters take on values that are very close to the clathrate hydrate phase. Formation of critical nucleus is the result.

2.1.3.3 Homogeneous and Heterogeneous Nucleation

There are two types of hydrate nucleation; homogeneous and heterogeneous nucleation. *Homogeneous nucleation* (HON) occurs when the nucleation is not influenced by impurities, thus happening away from a surface. Such nucleation is unlikely to observe naturally, and difficult to achieve in a controlled environment. Due to the lack of surface area to nucleate on, the nucleation must occur in three dimensions, without any surface lowering the energy barrier, ΔG (Sloan and Koh, 2007).

Heterogeneous nucleation occurs when a surface is available in the fluid as a nucleation site. The surface could be in the form of a foreign body inside the fluid or a pipe wall. Since there is a surface available, HEN occurs in two dimensions instead of three. Thus, less free energy is required for HEN, and the probability of nucleation is higher. ΔG_{crit} is lowered to a new critical free energy $\Delta G'_{crit}$, because of the contact angle θ between the hydrate crystal and surface. In general, θ is less than 180° , but if the surface is completely non-wetting $\theta = 180^\circ$, $\Delta G'_{crit} = \Delta G_{crit}$, i.e. the same critical energy is required for HEN as HON. This means that the smaller the wetting angle, the smaller will $\Delta G'_{crit}$ be, and thus r_c . In other words, the smaller the wetting angle, the bigger the probability of getting heterogeneous nucleation (Sloan and Koh, 2007).

At the vapour-liquid interface, Gibbs free energy of nucleation is lowered. The interface is also the location where there exists high concentrations of host and guest molecules. This combination makes the vapour-liquid interface the perfect place for hydrate formation to occur. Researchers have also confirmed that subsequent growth and nucleation occurs at the water-hydrocarbon interface (Sloan and Koh, 2007).

2.1.3.4 Memory Effect

Hydrate researchers have observed a phenomenon called the *memory effect*. When hydrates form from gas and water obtained from dissociated hydrates, hydrates form more easily and faster (Sowa and Maeda, 2015). They retain a memory of their structure when melted at mod-

erate temperatures. The memory effect is not applicable if freshwater with no hydrate history form new hydrates. It should be noted that the memory effect is not observed if the system is heated to temperatures greater than 28°C, or after several hours of heating (Sloan and Koh, 2007).

The memory effect has been explained by three hypotheses: (1) Residual hydrate structures exist in the aqueous phase. (2) Diffusion of guest molecules are retarded in the water formed after gas hydrate dissociation, leading to supersaturation of the guest molecules in the aqueous phase. (3) Impurities or container walls are conditioned after the first gas hydrate formation, which results in a more potent heterogeneous nucleation sites for the second and subsequent hydrate formation. Studies have shown that the memory effect exists, but that non of the existing hypothesis could account for all the observed aspects of the memory effect (Sowa and Maeda, 2015).

2.1.4 Hydrate Growth

During the hydrate growth phase, factors like mass transport and heat transfer become important. Hydrate growth is exothermic, i.e. the hydrate growth process releases heat. If the heat is not removed from the system, the hydrate cannot continue to grow because the temperature will increase beyond the temperature of hydrate formation. Mass transfer is also important because gas needs to be transported to the hydrate surface for continued growth (Sloan and Koh, 2007).

The hydrate growth can be divided into four different processes, where (1) and (2) are further described below (Sloan and Koh, 2007).

1. Single crystal growth
2. Hydrate film/ shell growth at the interface between water and hydrocarbon
3. Multiple crystal growth in an agitated system.
4. Growth of metastable phases

2.1.4.1 Single Crystal Growth

Single crystals can grow in a water-hydrocarbon solution under low driving force conditions. A single hydrate crystal of sI and sII is showed in Figure 2.10. They are grown from stoichiometric solutions of ethylene oxide and tetrahydrofuran. It is important to realize that the rapidly growing single crystal planes disappear, which means that it is only the slowest-growing planes that are observed (Sloan and Koh, 2007).

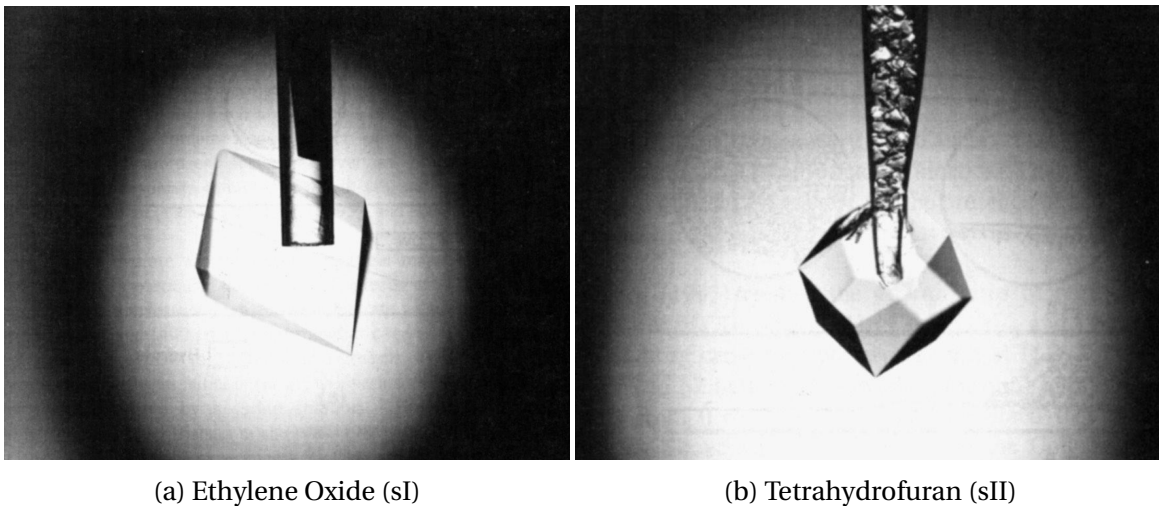


Figure 2.10: Photograph of single hydrate crystals of (a) ethylene oxide (sI) and (b) tetrahydrofuran (sII) (modified from Sloan and Koh (2007)).

2.1.4.2 Hydrate Film/ Shell Growth at the Interface Between Water and Hydrocarbon

As described in Section 2.1.3.3, hydrate formation occurs at the water-hydrocarbon interface. It has been suggested that the supersaturation, or driving force, affects the morphology. Hydrates might nucleate and grow at different locations at high driving forces. Many nucleation sites will be present with faster nucleation kinetics. This can explain why a more random crystal growth and a rougher surface appear at higher driving forces. If the driving force is low, hydrates can form in a more regular manner and location. The droplet surface is smooth and has a shiny texture at low driving forces compared to needle-like crystals on the droplet surface at high driving forces (Sloan and Koh, 2007)

When water is converted to hydrate, parts of the droplet collapses and the internal droplet volume decreases. A decrease in internal droplet volume will also occur if water diffuse to the outer shell surface from the interior droplet and then react with hydrate former (Sloan and Koh, 2007).

It has been observed that an analogous feature exists between growth behavior at the surface of a liquid droplet and at a water–hydrate former planar interface. At a planar interface, growth studies imply that the hydrate film grows laterally across the entire interface. The hydrate film thickens over time and the final thickness depends on the degree of subcooling. With increasing subcooling, an increase in thickness will occur. The hydrate film will thicken into the water phase (Sloan and Koh, 2007).

2.1.4.3 Growth Process on a Microscopic Scale

Hydrate growth on a microscopic scale is often described in six simplified steps, shown in Figure 2.11. These steps describe the phenomenon where a guest molecule in a cluster attaches to an existing hydrate surface. This is the assumed process after nucleation, which will continue until a limiting factor stops further growth.

- (i) A cluster is transported towards the hydrate surface. Because of a lower ΔG , the cluster is attracted to the surface
- (ii) The cluster is absorbed to the hydrate surface. When it is absorbed, some of the excess water molecules detach from the cluster
- (iii) The cluster only moves on the hydrate surface, i.e. in two dimensions
- (iv) After moving on the surface, the cluster is absorbed by a crystal step. When locked in two dimensions the energy potential is even lower
- (v) The cluster can only move in one dimension
- (vi) The cluster is totally absorbed on a kink site, making it immovable

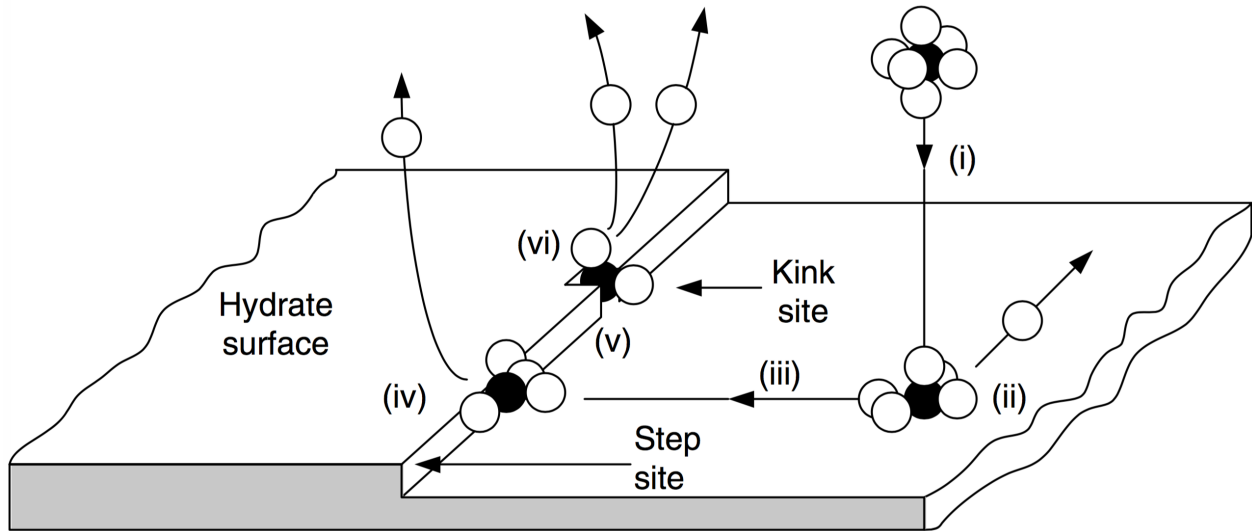


Figure 2.11: Schematic step by step visualization of the hydrate growth (Sloan and Koh, 2007).

For every step where the cluster is further absorbed into the hydrate surface, excess water molecules are detached and transported back into the water phase. This is only a conceptual view of hydrate growth and has not been confirmed extensively, but it gives an understanding of the growth process (Sloan and Koh, 2007).

2.1.4.4 Growth on a Macroscopic Scale

When a water droplet is in contact with hydrocarbons, the hydrate growth occurs on the water-hydrocarbon interface. Figure 2.12 shows how a water droplet surrounded by hydrocarbons crystallizes into a hydrate sphere. Figure 2.12a shows the suspended water droplet prior to any hydrate growth. In Figure 2.12b, a thin and porous hydrate shell starts to grow. Then, in Figure 2.12c, the whole droplet is covered in a thin hydrate shell. After a period, the hydrate shell starts to thicken, as can be observed in Figure 2.12d. Figure 2.12e shows the final step where the whole droplet is converted into hydrate (Sloan and Koh, 2007).

There are some doubts whether this is how the growth occurs because the theory does not explain how the inside of the droplet is converted to hydrate after the hydrate shell is covering the surface. Gas needs to be transported through the solid surface to convert the inside, which the

theory does not explain. Hydrate nucleation and growth are associated with large uncertainties, where a range of theories explain the same phenomenon in different ways (Sloan and Koh, 2007).

If particles are distributed in the water phase, several small hydrate droplets may be formed separately. In a system with a lot of small hydrate particles, the hydrates could be in the shape of a slurry. Alternatively, if no or few surfaces are present, the hydrates may form into a single plug or chunk. This happens because it is easier for the new hydrate mass to form on an existing surface than nucleate homogeneous in the water phase, as described in Section 2.1.3.3 (Larsen, 2017).

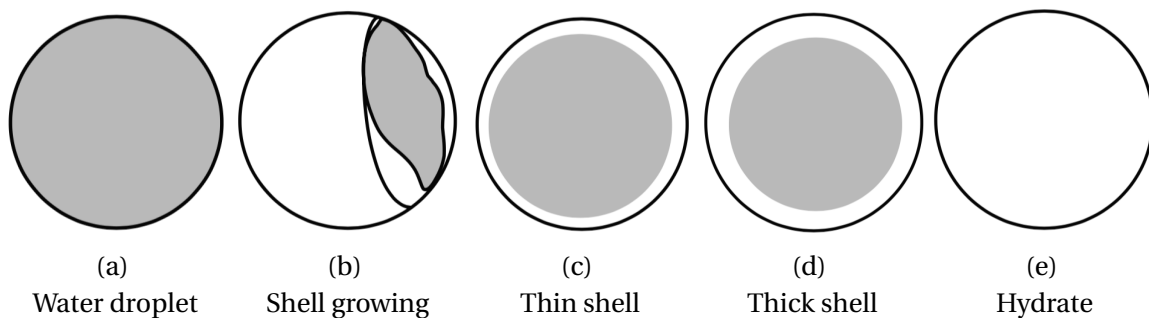


Figure 2.12: Hydrate formation from a water droplet (modified from Sloan and Koh (2007)).

2.1.5 Hydrate Prevention Theory

Hydrates are in most systems reckoned as a problem and should be avoided. Therefore, prevention of hydrates are important and often less expensive than hydrate remedial methods (Barker and Gomez, 1989a). Two general principles are used to prevent hydrate formation, either ensure that the system conditions are outside the hydrate formation area or ensure that gas or water is not present in the system. Limiting the available water phase in a fluid mixture is a common way to prevent hydrate formation, but if the removal of gas or water is not an option, hydrate formation can be prevented by adding a *hydrate inhibitor* to the water phase (Botrel, 2001).

Hydrate inhibitors is a term used for chemicals that have the ability to lower the hydrate formation temperature at a given pressure. Hydrate inhibitors changes the water properties, making

the hydrate equilibrium curve shift to less favorable pressure and temperature conditions regarding hydrate formation. Experimental data has shown that the effectiveness of the hydrate inhibitor is closely related to the chemicals ability to lower the freezing point of water (KAMATH and PATIL, 1994).

Further hydrate growth can be limited if the the hydrates create a physical boundary between the gas and the water phase. If a hydrate layer covers the entire gas-water interface, the hydrate growth could stop, even if the system conditions are within the hydrate area and the driving forces are large. The equivalent phenomenon can happen in systems where another fluid or physical barrier separates the gas and the water phase (Larsen, 2017).

By ensuring that the system is outside the hydrate area, hydrate formation is prevented. Heating or depressurization of the system is a possible solution in some systems, while in others the use of inhibitors are the best solution. In the petroleum industry, inhibitors are commonly used. Methanol, glycol and salts are used in various systems. In drilling applications, salts are often preferred as hydrate inhibitor due to the drilling fluid chemistry (Sloan and Koh, 2007). The effectiveness of three different salts are presented in Section 2.1.5.1.

2.1.5.1 Salts as Hydrate Inhibitors

The thermal properties of the aqueous solution changes when salt is added to the water phase. NaCl has proven to be the most efficient thermodynamic inhibitor on a weight basis (Ebeltoft et al., 1997). Experimental analysis have shown that Equation 2.9 describes the hydrate temperature depression when $X_{wt\%}$ of NaCl is added to the water phase (Larsen, 2015). The temperature depression of the hydrate equilibrium, ΔT_h , is defined as $\Delta T_h = T_{(h, after)} - T_{(h, before)}$. Here $T_{h, before}$ is the hydrate equilibrium temperature in the solution before adding inhibitor and $T_{h, after}$ is the hydrate equilibrium temperature in the solution after adding inhibitor at a given pressure.

$$\Delta T_{h,NaCl} = -0.42X_{NaCl} - 0.0202X_{NaCl}^2 \quad (2.9)$$

Other salts like CaCl_2 and KHCOO also act as inhibitors when dissolved in water. Little research has been performed on the effectiveness of these salts acting as hydrate inhibitor, thus an equation describing the temperature depression on the hydrate equilibrium, such as for NaCl , do not exist. Nevertheless, a viable approximation is to assume that the hydrate equilibrium temperature depression is equivalent to the freezing point depression of water when adding salt to an aqueous solution (Larsen, 2017).

The change in freezing point of a solvent in a solution from the pure solvent, is directly proportional to the molal concentration of the solute, i.e. the moles of solute per kg of solvent (Puredue, 2017). This relationship is described by Equation 2.10, where ΔT_f is the change in freezing point of the solvent, i is the van't Hoff factor, b is the molality and K_f is the freezing point depression constant.

$$\Delta T_f = K_f i b \quad (2.10)$$

The molality can be expressed as a function of mass of water, as well as mass and molar mass of the additive by using the relationship in Equation 2.11a.

$$b = \frac{n_a}{m_w} = \frac{m_a / M_a}{m_w} = \frac{m_a}{M_a m_w} \quad (2.11a)$$

Thus, by using Equation B.3 and B.4, the molality in terms of the wt% of solute added (X_a) to the water phase can be expressed as Equation 2.11b.

$$b = \frac{X_a}{100 M_a (1 - X_a / 100)} \quad (2.11b)$$

Finally, the temperature depression as a function of wt% solute is obtained from Equation 2.12.

$$\Delta T_f = K_f i \frac{X_a}{100 M_a (1 - X_a / 100)} \quad (2.12)$$

The values are calculated using the van't Hoffs factor and molar mass found in Appendix E, Table E.2. The K_f for water is $-1.853 \text{ K} \cdot \text{kg}/\text{mole}$ (Puredue, 2017). Table 2.1 shows how the freezing point of the solution changes with increasing weight fraction of the various solutes.

Table 2.1: The temperature depression effect on the freezing point of various salts. The values are calculated based on Equation 2.12.

Salt in solution [wt%]	NaCl	CaCl ₂	KHCOO
	ΔT_f [°C]		
2.5	-1.63	-1.28	-1.13
5	-3.34	-2.64	-2.32
7.5	-5.14	-4.06	-3.57
10	-7.05	-5.57	-4.90
12.5	-9.06	-7.16	-6.29
15	-11.19	-8.84	-7.77
20	-15.85	-12.52	-11.01
25	-21.14	-16.70	-14.69
30	-27.18	-21.47	-18.88

When comparing the results of ΔT_f for NaCl in Table 2.1 with ΔT_h of NaCl in Table E.3, similar results are observed. Figure 2.13 shows the temperature depression discrepancy between Equation 2.9 and Equation 2.12. The discrepancy is marked with red arrows when 5wt% and 20wt% of NaCl is added to the water phase of aqueous solution. Notice that the ΔT_h represents the conservative temperature depression at 5wt% NaCl, while ΔT_f represent the conservative temperature depression at a concentration of 20wt% NaCl in the water phase. The discrepancy increases as the weight fraction increases beyond 20wt%.

It is reasonable to believe that the discrepancy between the temperature depression on the freezing point, and the hydrate equilibrium, act similar for all salts. Consequently, it is assumed that the temperature depression on the freezing point is similar to the temperature depression of the hydrate equilibrium. This assumption seems reasonable when the salt concentration is in the range of 5wt% and 20wt%.

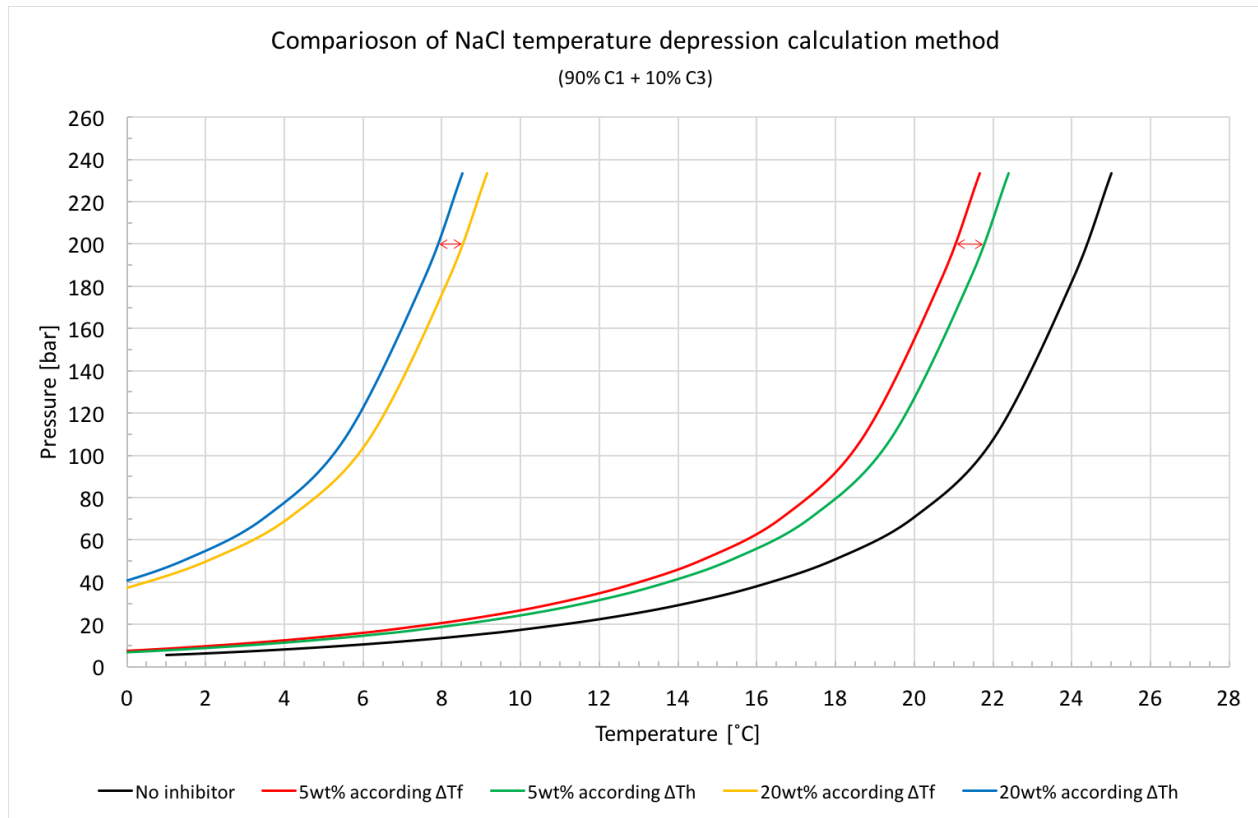


Figure 2.13: Hydrate equilibrium curve for a 10% methane and 90% propane gas-water system. The hydrate curves for 5wt% and 20wt% NaCl in the aqueous solution are corrected with ΔT by using Equation 2.9 and Equation 2.12.

2.1.6 Hydrate Dissociation

The dissociation of hydrates is an endothermic process. To break the hydrogen bonds between water molecules, heat must be supplied externally. The heat will also break the van der Waals interaction forces between the guest and water molecules of the hydrate lattice. This process will decompose the hydrate into water and gas. All hydrate dissociation methods involve moving the in-situ conditions out of the hydrate area (Sloan and Koh, 2007).

Because hydrate dissociation is endothermic, the surrounding area are temporarily cooled. Depending on the thermal conductivity of the nearby media, and the size of the hydrates, the time until the hydrates are completely dissociated can vary (Larsen, 2017).

2.2 Well Control

According to NORSOK Standard D-010 “Well integrity in drilling and well operations” rev 4. 2013, the definition of well control is (NORSOK, 2013):

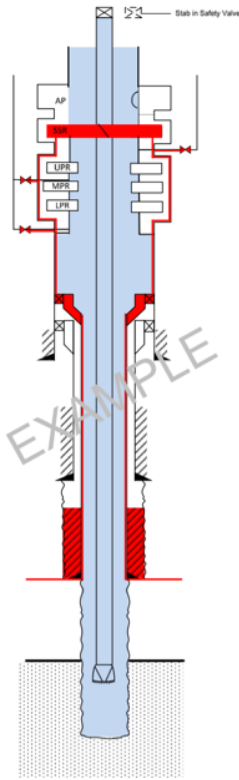
“Collective expression for all measures that can be applied to prevent uncontrolled release of well-bore fluids to the external environment or uncontrolled underground flow”.

In order to maintain *well control* it is important that all phases of the drilling operations are involved. That includes operations related to the initial planning, completion and abandonment. The goal of well control is to prevent blowout and other critical situations from occurring. This is obtained by accurately predicting the pore -and fracture pressure, good design and use of equipment, as well as proper kick detection system and killing procedures (Schubert et al., 2003).

A primary and secondary well barrier is required to have sufficient well control. *“The well barriers shall be defined prior to commencement of an activity or operation by identifying the required WBE to be in place, their specific acceptance criteria and monitoring method”*, according to NORSOK Standards. The function of well barriers is to prevent inflow of formation fluid into the well (NORSOK, 2013). An example of a wellbore sketch is showed in Figure 2.14.

This section will describe the function of drilling fluid as a primary well barrier. It will also describe kick as a critical issues which can arise when drilling, what causes a kick to occur, as well as different well control and kick detection methods in conventional drilling.

Well control in conventional drilling is maintained by keeping the bottomhole pressure in the operation between the pore and fracture pressure to avoid influx into the well or fluid loss to the formation (Veisene, 2014). This is obtained when drilling with a sufficient mud weight with a suitable composition. If a well control situation arises, the well is shut-in to prevent gas migrating up the riser and develop into a blowout.



Well barrier elements	EAC table	Verification/monitoring
Primary well barrier		
Fluid column	1	
Secondary well barrier		
In-situ formation	51	
Casing cement	22	
Casing	2	
Wellhead	5	
High pressure riser	26	
Drilling BOP	4	

Figure 2.14: Example and description of one possible solution for defining and illustrating well barrier envelopes for drilling, coring and tripping with shearable string (modified from [NORSOK \(2013\)](#)).

2.2.1 Drilling Fluid

Drilling fluid, also known as mud, is a liquid medium having several functions during drilling operations. The drilling fluid transports the cuttings out of the wellbore, lubricate and cools down the drilling bit and provide information about the wellbore. Nevertheless, the most important property is to act as the primary well barrier with the ability to maintain well control ([PetroWiki, 2015](#)).

The drilling fluid is a complex mixture of chemicals with a variety of functions. The mud mixture needs to be tailored to the individual drilling operation. The selection of drilling fluid is essential to achieve a successful and safe drilling operation ([Bleier, 1990](#)). Cost, technical performance and the impact it has on the environment are three factors that should be taken into consider-

ation when deciding which drilling mud to use. WBM is often the preferred choice since it is cheaper, more environmental friendly and makes cutting disposal easier (SPE, 2015).

2.2.1.1 Drilling Fluid Types

Various types of drilling fluid exist. They are categorized both by their composition and their usage. This thesis will focus on *water based mud* (WBM) because it is the one most relevant regarding the experiments conducted, discussed in Chapter 3 and 4. Note that other drilling fluids such as oil based mud, synthetic based drilling fluid, drill-in fluids, all-oil fluids and pneumatic drilling fluids exist (SPEinternational, 2015a).

The main component in WBM is water. In general, WBM consists of above 75% water. It can be based on fresh water, brine, seawater, saturated brine or formate brine. The remaining 25% are additives like barite, salts and bentonite (Neff, 2005). WBM is the most common drilling fluid type, and it is used at approximately 80% of all wells drilled. The water based mud is categorized either as a non-dispersed or dispersed system (SPEinternational, 2015a).

A disadvantage with WBM is how it interacts with clay particles, and make them swell. This can cause hole stability problems and possible stuck pipe incidents. When drilling in deepwater and Arctic regions, hydrate formation may occur in the drilling fluid if gas enters the well. Critical issues related to hydrate formation in the drilling fluid are described in Section 2.3.

2.2.1.2 Drilling Fluid Additives

A variety of chemical compounds can be added to the drilling fluid to alter the mud properties. These chemicals are referred to as *additives*. It is important to carefully choose an appropriate combination of additives to achieve a successful drilling operation. There are different additives that serve the same purpose, but one can be preferred based on the well conditions and the compatibility with other additives. Additives can work as weighting agents, where the main purpose is to make the drilling fluid more dense. They can be thinners and dispersants, which

decreases the viscosity, or they can be suspending agents, which increase the share viscosity. Additives can also act as fluid loss control agents preventing fluid loss ([SPEinternational, 2015a](#)). In cases where the need for preventing further leakage of mud into the formation, lost circulation material can be added to the mud. Some additives work as lubricants, reducing the COF between the surfaces and the drilling fluid. An important function of additives in deepwater and Arctic regions is to act as hydrate inhibitors to prevent hydrate formation ([Chemtotal, 2012](#)).

Below is a presentation of some common drilling fluid additives. These additives have been experimentally tested at the NTNU laboratory to observe their effect on hydrate formation in a closed system. The results are given in Section [3.1](#).

2.2.1.2.1 Barite

Barium sulfate (BaSO_4), also known as barite, is a dense mineral used as a weighting agent in drilling fluids, that can be added to all types of drilling mud. If the barite has been contaminated from cement, gypsum or anhydrite, it can cause problems in certain mud systems. It is therefore important to conduct a thorough quality check of the drilling mud and different additives before use ([SchlumbergerOilfieldGlossary, a](#)).

2.2.1.2.2 Bentonite

Bentonite is a clay mineral widely used for viscosity and filtration control in drilling mud. When added to the drilling fluid it starts to swell over time, which results in a more viscous mud. Note that factors like hardness ions in the water, mechanical shear-degradation, bacterial attack and high temperature when in use at the rig affect the effectivity of the bentonite additive and can make it ineffective ([SchlumbergerOilfieldGlossary, b](#)).

2.2.1.2.3 Salts

Different kind of salts are added to the drilling fluid. It is often added to the drilling fluid as a hydrate inhibitor, because it shifts the hydrate equilibrium curve, as described in Section 2.1.5.1.

Sodium chloride (NaCl) is the salt most responsible for the salinity of seawater, having a density of 2160kg/m³ (?). NaCl is among the most commonly used salts in drilling fluid (Ebeltoft et al., 1997).

Calcium chloride (CaCl₂) is a highly soluble salt, which is used to design brines or drilling and workover fluids with a density ranging from 998kg/m³ to 1390kg/m³ (Schlumberger, 2017a). CaCl₂ is often preferred in OBMs because it offers the best inhibition properties for most shales (SPEinternational, 2015a). CaCl₂ is in some cases used in preference over NaCl because of the greater water phase salinity, higher activity and higher density (GeoDF, 2010).

Potassium formate (KHCOO) is an organic salt frequently used to form clear brines. Potassium formate has a maximum solubility in water of 75% at ambient temperatures, and a density of 1910kg/m³ (Weatherford, 2010). Consequently, potassium formate brines are often used in completion and workover operations which require a fluid density ranging from 1007 to 1570kg/m³ (Schlumberger, 2017b). Potassium formate has several advantages in drilling applications. It provides high-density, solid-free brines which have a low formation damage quotient when used as drill-in fluid, as well as being environmentally benign and extends polymer thermal stability (Weatherford, 2010).

2.2.2 Kick - A Critical Issue During Drilling Operations

When drilling a well, critical and unwanted issues can occur. Some are minor failures, which does not cause any damage, while others can have major implications.

Kick is one of the most dominating problems regarding well control. When there is a pressure difference between the formation fluid and the fluid in the borehole, fluid is forced from the

high-pressure regime to the low-pressure regime. The influx of reservoir fluid is called a kick. Three important factors that affect the severity of a kick is the permeability, porosity and the pressure difference between the formation fluid and the mud hydrostatic pressure. A kick may develop into a blowout if the influx is uncontrolled. When the influx is controlled, the kick is considered killed ([Lake and Mitchell, 2006](#)).

2.2.3 Causes of Kicks and How to Manage it

2.2.3.1 Causes of Kicks

A kick can be caused by several factors, including insufficient mud weight, lost circulation, improper hole fill-up during trips, swabbing and gas cut. This thesis will focus on how insufficient mud weight and lost circulation can cause a kick.

Insufficient mud weight is the predominant cause of kicks. As previously described, a kick may occur when the formation pressure exceeds the wellbore pressure. In conventional drilling, the hydrostatic mud pressure should always be greater than the formation pressure to prevent an influx of formation fluids ([Lake and Mitchell, 2006](#)). Also, the hydrostatic pressure should not be larger than the formation fracture pressure at any depth in the well in order to avoid fracturing the formation. Fracturing of the formation can lead to lost circulation, which may induce a kick. The pressure regime between the pore pressure and the fracture pressure is often called the *safe mud weight window*.

Abnormal pressures in the formation are pressures greater than the pressure expected under normal conditions. It is one of the greatest concerns regarding well control situations and are often associated with causes of kicks. If an abnormal pressure zone is encountered, the mud weight might be too low, resulting in an influx of formation fluid. The factors described in Section [2.2.2](#) will determine if a kick will develop or not. Kicks caused by insufficient mud weight can be prevented by using existing methods to estimate formation pressure and detect abnormal pressure zones ([Lake and Mitchell, 2006](#)).

2.2.3.2 Kick Detection

Early kick detection is very important. Indications and warning signs that the well is taking a kick is observed at the surface in conventional drilling. All signs do not positively identify that the well is taking a kick, but they are a warning of a potential kick situation. The kick detection methods discussed are; increase in flow rate, pit volume increase and flowing well with pumps off.

One important kick indicator is when the flow rate out of the well increases when pumping at a constant rate. When the formation contributes to move the fluid up the annulus, the flow rate will increase (Lake and Mitchell, 2006).

If the pit volume increases it is a primary indicator of a kick. This is a result of influx of formation fluids into the wellbore. When the kick fluid enters the hole, it displaces an equal volume of mud at the flowline, which results in pit gain (Lake and Mitchell, 2006). When traveling towards surface, the gas will expand, contributing to an even further increase in pit level. It is important to have in mind that environmental effects such as pitch, roll and heave motions can impact the pit level and mud return detection methods significantly on offshore rigs (Robinson, 2015).

The mud pumps need to be turned off and the well must stabilize to positively identify a kick. It is a strong indication that a kick is in progress if the well flows when no liquid is being pumped. If this is observed, a flow check is performed (Robinson, 2015). If the mud in the drill pipe is considerably heavier than in the annulus it can cause the well to flow when the pumps are off. This does not mean that a kick is in progress, but can indicate that a slug is present (Lake and Mitchell, 2006).

2.2.3.3 Well Control Procedures

If a kick is observed, the well needs to be closed to avoid further influx according to standard procedures (Carlsen, 2008). This will allow the pressure to reach equilibrium sufficient to balance formation pressures. Variables such as permeability, porosity, rock type and the original

amount of pressure change affect the required shut-in time. The shut-in time can vary from a few minutes to several hours (SPEinternational, 2015b).

Shut-in procedures depend on the type of rig and drilling operation (Lake and Mitchell, 2006). An example of a well control procedure during shut-in for drilling operations is given in Table C.1 (Robinson, 2015).

2.2.3.4 Well Control Methods

Traditional well control techniques such as the *Driller's Method* and *Wait & Weight Method* are based on circulating an influx out of the hole. They are referred to as "constant bottomhole" methods. Their function is to keep the BHP equal to, or slightly above the formation pressure to prevent further influx (WildWellControl, 2016). This thesis will look into the well control procedures for the Driller's Method and the Wait & Weight Method.

Driller's Method requires two complete circulations to kill the well. During the first circulation, the kick fluid is circulated out by using the existing mud weight, which holds the drill pipe pressure constant (Robinson, 2015). The first circulation removes the kick from the well, whereas the second circulation kills the well (WildWellControl, 2016). For the second circulation, kill mud is weighted up and pumped to the bit while following a drill pipe pressure schedule. Then, it is circulated to surface (Robinson, 2015). The procedure for the first and second circulation is given in Table C.2 and C.3.

This technique is perhaps the most common well control method used today. The method is preferred if the kick fluid has a high migration rate, which can result in shut-in problems or swabbing (WildWellControl, 2016). The advantages of Driller's Method are that circulation can start more quickly compared to other methods. This reduces the probability for hydrate formation. It also allows circulation to start even if no weighting material is immediately available. The disadvantages are that it is more time consuming to kill the well, compared to other methods. This can cause higher pressure in the annulus (Robinson, 2015; WildWellControl, 2016).

The Weight & Wait Method requires only one single circulation. Kill mud is weighted up and pumped down the drill pipe to the bit while following a drill pipe pressure schedule. When the kill mud enters the annulus and is circulated to surface, the CDPP is held constant (Robinson, 2015). Table C.4 shows the different steps needed to kill a well with the Weight & Wait Method.

The advantages of using the Weight & Wait Method are that the well is killed faster and it keeps the wellbore and surface pressure lower compared to other methods. The disadvantages are that a full crew and more supervision is required, as well as a good mixing facility (Robinson, 2015; WildWellControl, 2016).

2.3 Natural Gas Hydrates as a Drilling Hazard

Deepwater and Arctic regions are favorable for hydrate growth due to the low temperature and high pressure. In these environments, the pressure and temperature conditions are especially suitable to form and keep natural gas hydrates stable after a kick has been taken (Nimblett, 2005). This section will discuss drilling hazards related to hydrate formation during shut-in periods, and how to prevent hydrate growth.

2.3.1 Drilling Challenges in Deepwater and Arctic regions

2.3.1.1 Narrow Drilling Window

A narrow drilling window is often encountered in deepwater drilling, which could make conventional drilling troublesome. It dictates that multiple and frequent casing strings have to be set when drilling with a conventional marine riser system, which is time consuming and expensive (Fossil and Sangesland, 2004).

In some cases, the drilling window is so tight that fluctuations in the bottomhole pressure caused by mud pump operations threatens wellbore integrity (Hilts, 2013). A kick-loss scenario is a

common issue encountered in deepwater wells due to a narrow drilling window ([Hannegan, 2005](#)).

The first danger when a kick occurs is the possibility of it traveling all the way up to the surface facilities, developing into a blowout as described in Section 2.2.2. Another problem occurring when gas is present in the well during shut-in is hydrate formation inside the well.

2.3.1.2 Ballooning

Ballooning occurs when fluids are lost to the surrounding rock during over-pressured operations, which then flows back into the well when the pressure is reduced ([PetroWiki, 2013](#)). This is the case when the mud pumps are turned on before they are turned off. When the pumps are on, the ECD might exceed the formation fracture and create micro fractures. Mud loss can appear, but the micro fracture will not cause severe or total losses. The ECD will then reduce when the pumps are turned off as the annular pressure loss becomes zero. The induced micro fractures will then close, and the drilling fluid will flow back into the wellbore ([DrillingFormulas.com, 2011](#)). Ballooning can be misinterpreted as a kick ([PetroWiki, 2013](#)), which can implement well control procedures.

2.3.1.3 Loss of Circulation

Loss of Circulation is a term used when mud is flowing from the well into the formation. To avoid lost circulation it is important to estimate the rock strength of the formation, defined as the pressure the formation rock can withstand without inducing a fracture ([Lake and Mitchell, 2006](#)). If induced fracturing occurs, drilling fluid may flow from the well and into the fractures, leading to fluid loss. This is detected by more mud being pumped into the well than flowing back to the mud pit, resulting in a decreasing mud pit level ([Onan and Brake, 1996](#)).

Loss of circulation is a common problem encountered in deepwater areas, especially when drilling in highly fractured, faulted or through depleted formations ([Fossil and Sangesland, 2004](#)).

This is often related to the narrow drilling window and the difficulty in choosing an appropriate drilling mud. Certain areas of the Norwegian Barents Sea consist of weathered and naturally fractured carbonate formations, which might incorporate open karsts. If drilling into such formations, there is a great possibility that total loss can occur, resulting in a rapid decrease of the mud level (Bysveen et al., 2017). Influx of formation fluid and borehole collapse may occur if the rig crew is not able to refill the mud level in the riser (Onan and Brake, 1996).

2.3.1.4 Hydrate Formation

There is a possibility that hydrate formation will occur if gas is introduced to a well, as the pressure and temperature condition in parts of the well might be within the hydrate area of the reservoir gas. Hydrate plugs can cause severe well control challenges (Fossil and Sangesland, 2004). This is discussed in Section 2.3.2.

2.3.1.5 Shallow Hazards

Drilling of the top hole section in the wellbore is critical and one should take precautions. Hazards such as shallow gas, shallow water and in-situ hydrates in the marine sediments can be encountered. These scenarios can lead to kick and may threaten the safety of the rig crew and the environment (Brandee A Elieff, 2006). When drilling through a hydrate bearing zone, the pressure and temperature in the sediments may change and cause hydrates to destabilize and dissociate (Khabibullin et al., 2011). Hydrate dissociation in a hydrate bearing zone can lead to uncontrolled gas release (Ji et al., 2013; V. Løvø, 1990). Shallow hazards are therefore important to take into consideration prior to drilling.

2.3.1.6 Managed Pressure Drilling - A Possible Solution in Deepwater and Arctic Regions

A well control situation in deepwater and Arctic areas are more critical regarding hydrate formation compared to other drilling environments. One way to prevent hydrate formation is by

limiting the amount of gas introduced to the well. One drilling technique that might reduce the occurrences of kick is *Managed Pressure Drilling* (MPD).

In comparison to conventional drilling techniques, the wellbore pressure profile is more precisely controlled using MPD methods. In conventional drilling, where the mud weight is controlled to change the bottomhole pressure, 0.1 ppg or approximately 7 bar, is the smallest practical downhole pressure change that is typically made. With some MPD systems, it is possible to reliably control the surface backpressure in increments of about 0.7 bar. This increases the precision of control by an order of magnitude compared to conventional drilling, which is beneficial in environments where narrow drilling windows are present (Weems et al., 2016).

Early kick detection can be obtained by continuously monitoring and comparing deviations from flow in and flow out. Through a data acquisition system, trends can be monitored and alarms set. Coriolis type flow meter is the most common flow meter used in MPD operations for early kick detection (Vieira et al., 2009).

The use of MPD equipment can in many cases enhance the drilling safety. One of the reasons is that it can minimize the size of an influx that has become a kick (Gabaldon et al., 2014).

Three MPD techniques exist; (1) constant bottomhole pressure, (2) mud cap drilling and (3) gradient drilling. The application of the different methods depend on the formation and project specific requirements (Vieira et al., 2009).

2.3.2 Drilling Hazards Related to Hydrate Formation During Shut-in Periods

Hydrates can form during a shut-in period if gas is available in the well. Deepwater and Arctic environments are especially exposed because of the favorable pressure and temperature conditions. The main drilling problems related to hydrate formation are hydrates forming in the drilling fluid, hydrates plugging the choke- and kill lines, hydrate formation in the BOP stack and formation in the locking mechanism of the wellhead-to-BOP stack connector (Robinson,

2015; Barker and Gomez, 1989b). Since the BOPs and choke- and kill lines are exposed to seawater there is a high probability that hydrates will form in these areas (Yousif, 1997). Misinterpretation of a decrease in mud return after a kick is observed is a suggested consequence of hydrate formation. Another problem regarding hydrate formation in the well is immobilization of the drillstring (Østergaard et al., 2000).

2.3.2.1 Choke- and Kill Line Plugging

A hydrate plug can start to form in areas where there are little or no circulation. Areas such as choke- and kill lines, and inside the BOP stack are at risk for hydrate formation. The hydrate growth rate can be rapid once hydrate formation starts, and hydrates can spread to other parts of the system (Kotkoskie et al., 1992).

The choke line is a pipe filled with fluids connected from the BOP to the back-pressure choke at surface. The identical fluid is often present both in the choke-line and in the well. This is because during a well control operation, the well fluid will flow through the choke line to the choke manifold, which reduces the pressure. The kill line is a high-pressure line connecting the mud pumps to the BOP. The kill line allows fluid to be pumped into the well while the BOP is closed during well control operations (Bybee, 2001).

Both the choke- and kill lines are used to circulate a kick out of the wellbore, and therefore have a high risk of being plugged by hydrates. The friction loss in these lines are high due to the small pipe diameter making circulation rate low and the systems cool rapidly. This increases the probability of hydrate formation (Bybee, 2001).

Plugging of both the choke- and kill lines is considered a critical issue, and should be resolved immediately. Otherwise, safety situations can occur in case of a well control event. If there is a risk of hydrate growth in the choke- or kill lines, hydrate inhibitors such as methanol or glycol can be injected.

2.3.2.2 Hydrates Plugging the BOP Stack

Close to the wellhead, the well temperature could be equivalent to the ocean temperature. Therefore, the wellhead often falls within the hydrate area. If gas enters the well, and the in-situ condition for hydrate formation is in place, hydrate growth may occur. As a large part of the equipment is located at the wellhead, the surface area is relatively large, and the mud may be more stationary than in the rest of the well (Bybee, 2001).

Valves and constrictions are generally areas where hydrates tend to nucleate. Thus, the probability of hydrate growth may be higher in the equipment near the wellhead compared to a uniform surface, such as the casing. Hydrates that form deeper in the wellbore can migrate up to the BOP, because they have a lower density than the mud (Bybee, 2001).

Accumulation of gas in the space between the closed BOP and the outlet used for circulation is called *trapped gas*. It is possible for gas to be trapped in multiple locations in the BOP stack due to leakage in the pipe ram, or if the annular was initially closed and later swapped to a pipe ram (Robinson, 2015).

Water depth influence the effect of the trapped gas. Deeper water causes the hydrostatic pressure to increase at a given depth below the seabed. Gas is a compressible fluid, and under higher pressure, it makes the gas more dense. When gas migrates to the surface, it expands due to lower pressure regimes higher up in the riser. Gas from a depth of 457.3 m with a pressure of 65.5 bar, having an original volume of 0.8 m³ can expand to more than 47.7 m³ when reaching the surface, i.e. 60 times larger than it originally was (Robinson, 2015).

If water is introduced to the trapped gas during a well control situation, the consequences may be fatal if hydrates form. It can prevent well pressure monitoring below the BOP's, immobilize drillstring movement and prevent the BOP's to fully open or close (Barker and Gomez, 1989b). The consequences of not be able to close and open the BOP rams are severe. If the rams do not close, gas can migrate up in the riser. If not diverted successfully, the kick can escalate into a blowout.

2.3.2.3 Hydrate Formation In Drilling Fluid

In general, natural gas contains between 1% and 4% propane and iso-butane. Consequently, the majority of the hydrate structures observed in drilling processes are sII. Both water based mud and oil based mud consist of water, meaning that water is available in the well at all times during drilling. In the case of a kick, gas flows into the well and mix with the drilling fluid. If the water is not sufficiently inhibited, all four criteria for hydrate formation, as mentioned in Section 2.1, can be present in parts of the well. The hydrates can either form in a non-inhibited drilling mud or together with the formation water (Soghondikolaee, 2014).

In WBM there are two severe problems that can occur if hydrates are formed. Hydrates can form a plug within the wellbore, blocking equipment, or result in a change in the mud properties (Kotkoskie et al., 1992).

Hydrates consist of more than 85% water, dependent on the hydration number. This water can be extracted from the drilling mud, causing the flow properties to change severely. Solids may also start to settle out, and thereby change the drilling fluid density. In extreme situations, little or no fluid may remain in the well after solids removal (Kotkoskie et al., 1992).

Some oil based muds consist of as much as 30-vol% water, and it has been proved that hydrates can form in OBM as well. Experimental analysis have shown that OBM, with oil as a continuous phase, acts as an inhibitor to hydrate formation, but does not prevent it. OBM suppress the hydrate equilibrium curve with 2.7-5.5°C at pressures in the range of 35-315 bar. When hydrate formation is initiated in the OBM, the formation rate is greater than in WBM (Grigg and Lynes, 1992).

Another aspect of hydrate formation in the well which should be considered is the volume change and volume reduction of the drilling fluid column when gas becomes trapped inside hydrates. This volume change has a similar well response as fluid loss, and therefore it can be difficult to distinguish between the two different scenarios. The volume change and reduction phenomenon is described in Section 2.3.3.

2.3.3 Drilling Fluid Volume Change and Gas Volume Reduction

One volume unit of hydrates has a smaller volume than the volume occupied by a gas and water, containing the same number of molecules as in the hydrate volume unit (Behseresht and Bryant, 2012). In other words, the total original volume decreases when gas and water turn into hydrates. The extent of volume reduction is dependent on the hydration number, N , described in Section 2.1.2.5. The hydration number changes with variation in hydrate cage occupancy, which is a function of gas composition, pressure and temperature (Behseresht and Bryant, 2012).

Figure 2.15 shows the gas volume reduction extrapolation from the SINTEF gas. The gas mixture used, is a modification of a real natural gas found in the Barents Sea. The gas composition is given in Table 3.2. Figure 2.15 illustrates how the gas volume reduction varies with the hydration number. The gas volume reduction will be referred to as the volume reduction in this thesis. A lower hydration number yields a larger volume reduction at the identical pressure, compared to hydrates with a higher hydration number. Observe that at higher pressures, the volume reduction is less than at lower pressures. This is because the gas phase is more dense when the pressure is high, making the volume reduce less in a high-pressure system than in a low-pressure system.

The gas volume reduction is found using Equation 2.13.

$$\text{Gas volume reduction} = \frac{V_{gas, used} - V_{hyd} + V_{w, used}}{V_{gas, used}} = \frac{V_1}{V_{gas, used}} \quad (2.13)$$

The volume reduction will cause the volume of the drilling fluid to change. In order to understand how substantial this volume change of the drilling fluid is in reality, it is interesting to scale the gas volume up to a volume similar to one observed in a kick. By multiplying the volume of gas used in the SINTEF Test 2 by a factor of 1783, one yield a realistic gas kick volume of 4.00 m³. Figure 2.16 shows the volume of water needed to capture all of the gas inside the hydrates, the resulting hydrate volume and the volume change.

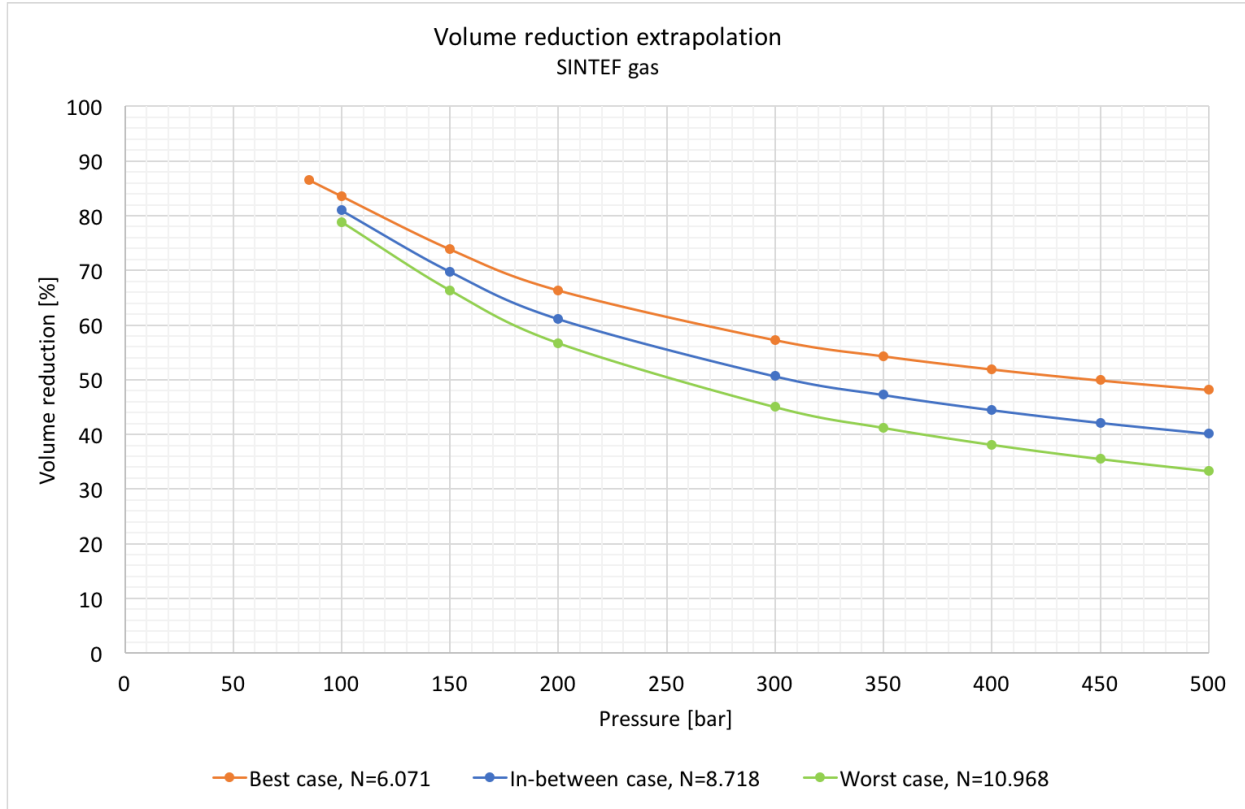


Figure 2.15: Volume reduction of the synthetic natural gas mixture given in Table 3.2 at 6°C for three different hydration numbers.

Notice that V_1 , V_2 and V_G in Figure 2.17 and 2.16 are representing the same volume. The drilling fluid volume in the well decreases with 3.04 m³ if all gas are converted to hydrates, i.e. the drilling fluid volume change. The drilling fluid volume change is described by Equation 2.14.

$$\text{Drilling fluid volume change} = V_{gas, used} + V_{w, used} - V_{hyd} = V_1 \quad (2.14)$$

When the formation is fractured and drilling fluid is lost into the formation, the drilling fluid volume inside the well reduces. It can be challenging to determine whether the fluid volume in the well was reduced because of hydrate formation, or because drilling fluid is lost to the formation.

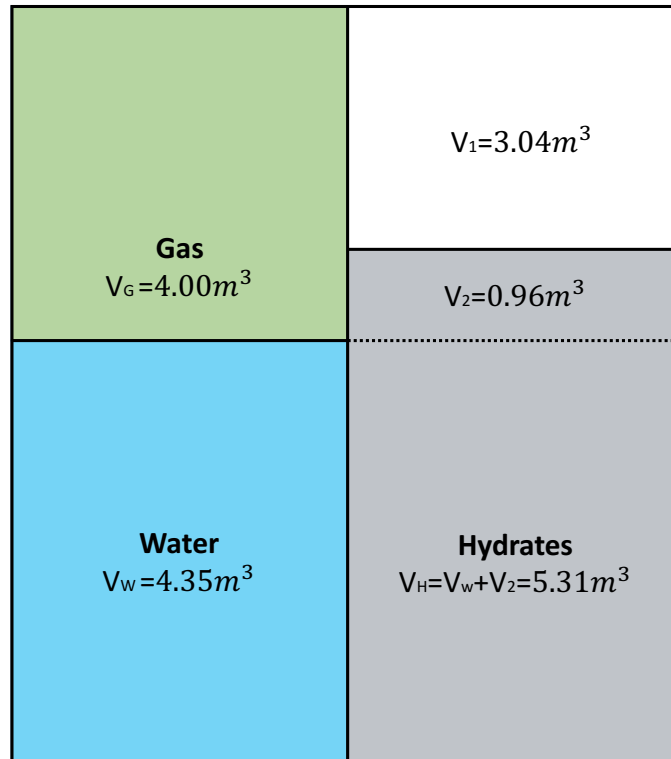


Figure 2.16: Example of the volume change when a gas influx of $4 m^3$ enters the well and converts into hydrates at a pressure of 181 bar (Helgestad, B., 2017).

Figure 2.17 and 2.18 illustrate the different scenarios; hydrate formation and loss of circulation due to a fracture near the casing shoe where the mud level behave similar over time.

Stage A in Figure 2.17 shows the mud level prior to a influx of gas. When gas enters the well, the mud level raises immediately. This new mud level after the well has taken a gas kick is marked as mud level 1 in stage B. When the kick is noticed, the well is shut-in and the SICP increases.

If hydrate formation is initiated, the mud level will decrease. When or if, all the gas is converted to hydrates, the mud level will reduce substantially. At stage D, all the gas are converted to hydrates. The final mud level is equal to the initial mud level plus the volume of hydrates, minus the volume of the water used in the hydrates, i.e. Final level = Start level + V_2 .

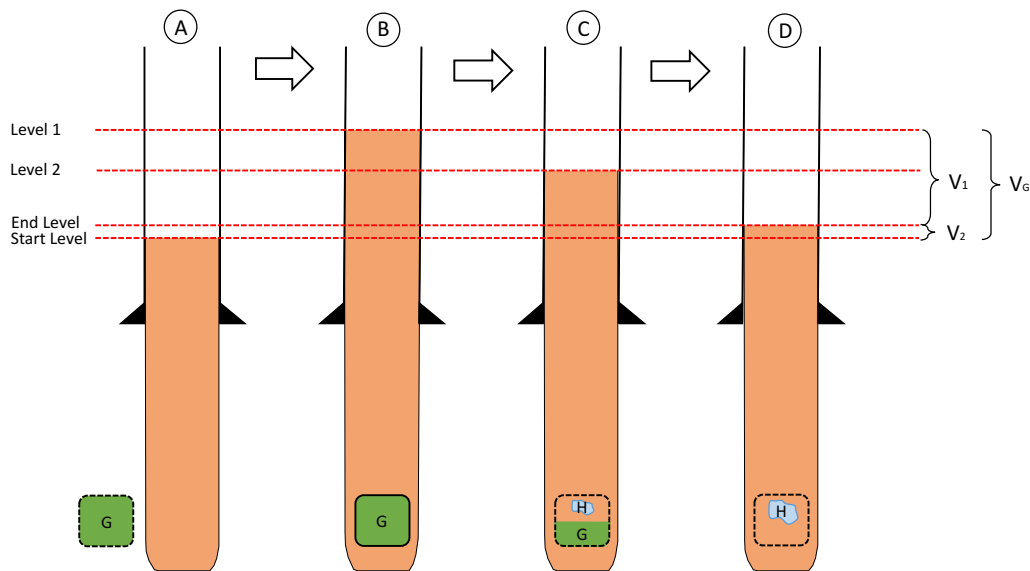


Figure 2.17: Well sketch illustrating how the mud level changes when a gas influx of volume V_G convert into hydrates. V_1 is the well volume change due to hydrate formation. V_2 is the gas volume reduction (Helgestad, B., 2017).

If the formation is fractured when a kick enters the well, a similar mud level response could be observed. This is visualized in step E in Figure 2.18, where drilling fluid is lost into the formation until the mud column is in balance.

It might be challenging to distinguish between the two scenarios because the mud level and the well pressure response is similar. If loss of circulation is handled in the same way as hydrate formation, it could be problematic and lead to further gas influx. By knowing the magnitude of the volume change in various mud compositions, it may be easier distinguishing between the two scenarios, which may impact well control.

To better understand the impact the volume change has on the mud level, a calculation of the volume change expressed as a change in mud column height is shown below. If the trip tank is empty, and no mud is pumped back into the well after a kick is taken, the volume change will result in a drop in the mud column height. If a 4.00 m^3 kick enters the well and converts into hydrates, the volume will reduce by 3.03 m^3 as illustrated in Figure 2.16. By considering a 9 5/8"

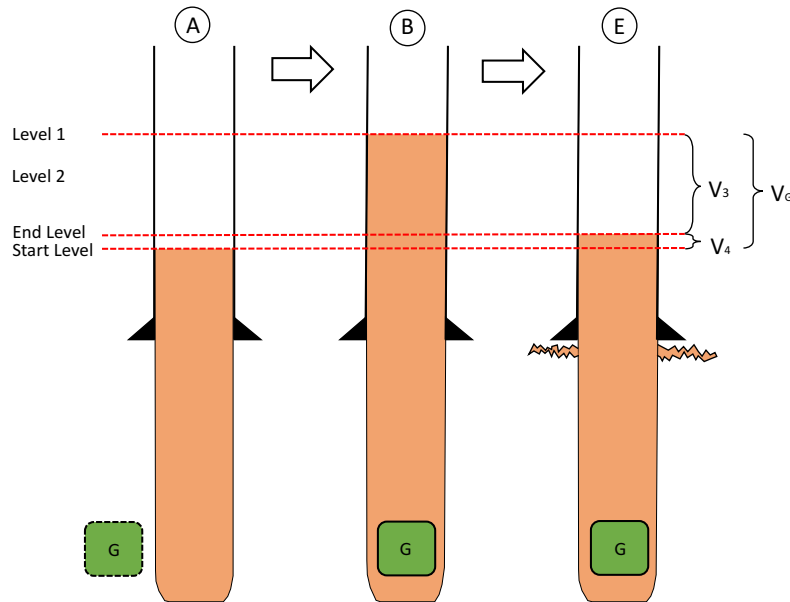


Figure 2.18: Well sketch illustrating how the mud level changes when a gas influx creates a fracture and mud leaks from the wellbore into the formation. V_3 is the well volume change due to the leakage. If $V_4 \approx V_2$ the two scenarios may be difficult to distinguish (Helgestad, B., 2017).

casing with an ID of 8.8" (0.2235 m) and a drillpipe with an OD of 5" (0.1270 m), the annulus cross section area can be calculated using Equation 2.15.

$$A_{cross\ section} = \frac{\pi}{4}(ID_{casing}^2 - OD_{drillpipe}^2) = \frac{\pi}{4}(0.2235^2 - 0.1270^2) = 0.0266m^2 \quad (2.15)$$

Thus, the decrease is calculated using Equation 2.16.

$$h = \frac{V_{change}}{A_{cross\ section}} = \frac{3.03m^3}{0.0266m^2} = 114.06m \quad (2.16)$$

A 114.06m mud column will reduce the BHP with more than 11 bar depending on the drilling fluid density, which is a pressure reduction large enough to initiate another kick. Therefore, it is very important to monitor the mud level and ensure that the trip tank can handle a volume change of this size to avoid further well control issues.

2.3.4 Hydrate Prevention in Drilling Operations

Prevention of hydrates are preferred over remedial actions, because of the safety issues associated with the removal of hydrates. Hydrate removal is a costly and time-consuming operation, requiring severe resources. As described in Section 2.1.5, hydrate formation is prevented by removing one of the physical conditions necessary for hydrate formation to take place (E. Dendy Sloan, 2008).

When drilling, fully removing the water phase is difficult, as both OBM and WBM consist of enough water to form hydrates. 100% water free drilling fluids exist, however they do not protect against gas and water influx. By heating the mud, it is possible to keep the annulus temperature outside the hydrate area when circulating, but in case of an extended shut-in period, the mud will cool down and hydrates could form in part of the well. Thermal insulation is another option, but this is expensive (Botrel, 2001). Therefore, the most common way to prevent hydrate formation is by adding hydrate inhibitors to the water phase of the drilling fluid.

Methanol, glycol and various salts can all be used as inhibitors, as discussed in Section 2.1.5. Methanol and glycol may interfere with other components of the drilling fluid, thus affect the mud properties. Salts are therefore the preferred hydrate inhibition additive in most drilling fluids.

The main types of salt used to inhibit the water phase of the drilling fluid is NH_4Cl , CsCl , CsBr , NaCl , NaBr , KCl , KBr , HCOONa , KHCOO , CaCl_2 , CaBr_2 and ZnBr_2 . Other salts may be more effective inhibitors, but they can react unfavorably in contact with chemicals in the mud. Depending on the concentration of the salt, the brines mixed into the drilling fluid can have a density varying from 1010kg/m^3 to 2500kg/m^3 (Pakulski et al., 2005).

The amount of inhibitor required in the water phase of the drilling fluid, in order to prevent hydrate formation, can be determined using Equation 2.12. Figure 2.19 illustrates the inhibiting effect when 10wt% of NaCl , CaCl and KHCOO is added to the water phase.

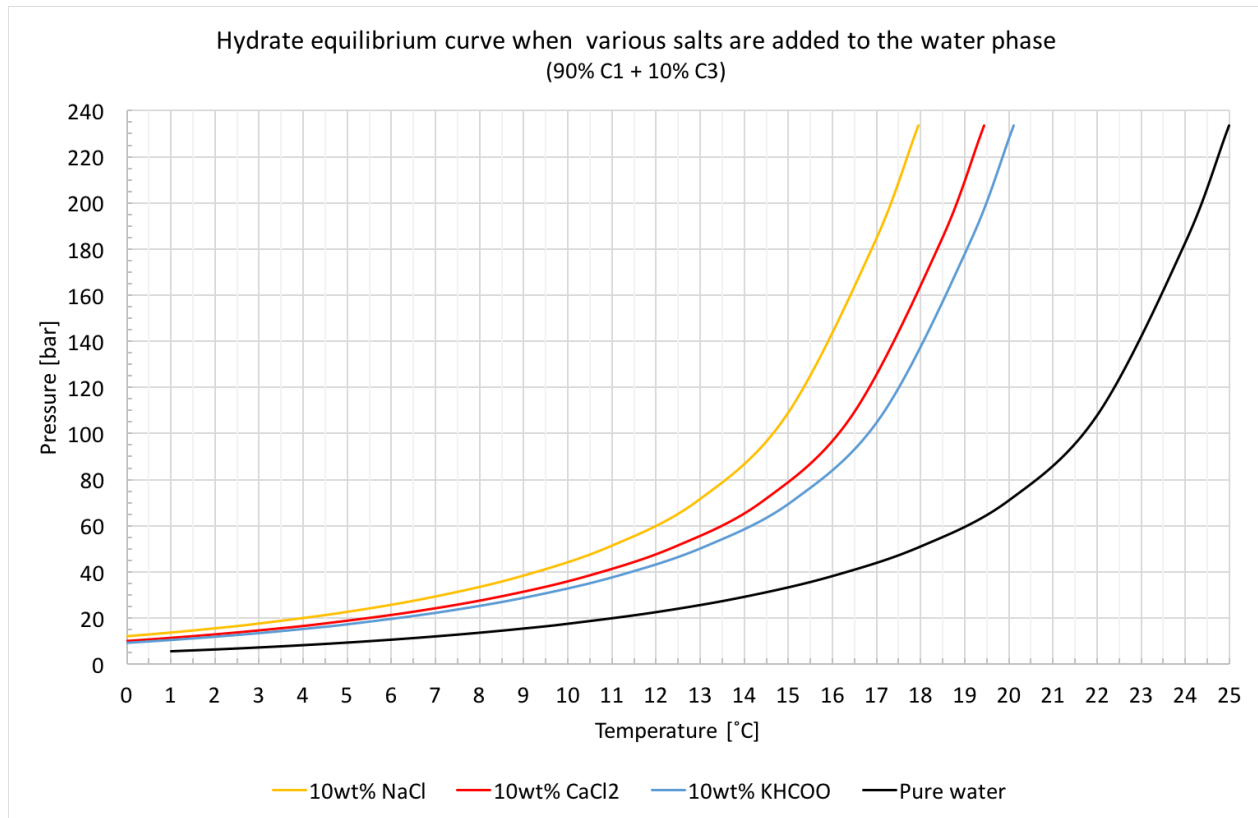


Figure 2.19: The figure shows how the hydrate equilibrium curve changes when various salts are added to the water phase. The black curve illustrates an uninhibited system, while the other curves illustrate 10wt% of NaCl, CaCl₂ and KHCOO dissolved in the water phase.

NaCl is the most commonly used inhibitor in drilling applications because of its inhibiting effect, low cost and compatibility with other additives. The inhibiting effect of NaCl increases with saturation. Adding 20wt% NaCl to the drilling fluid is common when drilling deepwater wells in order to avoid hydrate formation. If the drilling fluid contains 20wt% NaCl and 50wt% water, the wt% of NaCl present in the water phase is 28.57wt%. This means that the NaCl concentration in the water phase of the drilling fluid usually ends up close to the saturation concentration of 359g/l (Pinho and Macedo, 2005; Lai and Dzialowski, 1989).

The drilling fluid is often chemically complex. Knowing which chemical compound that contributes to the suppression of hydrate formation is therefore not always clear. Synergy effects can be observed, i.e. the combination of chemicals can be more effective than the sum of each compound, making it difficult to predict the inhibiting effect of drilling fluids without perform-

ing experimental analysis. Thus, most drilling fluids need additional inhibitors in the water phase in order to prevent hydrate formation at different circumstances.

2.3.5 Hydrate Remedial Methods

Remedial methods are the techniques used to remove hydrates which has formed in the system. Common remedial methods used to remove hydrates from the well are described below.

Depressuriazation: Removal by depressurization is often the preferred remedial action when hydrates have occurred. In many cases, the mud level cannot be reduced sufficiently while well control is still maintained. Thus, if hydrates form in the well, low enough pressure to dissociate the hydrates can be difficult to achieve.

Heating of the mud: If circulation is maintained, heating the mud prior to pumping it into the drillstring can make the hydrates dissociate. By increasing the temperature, the conditions in the well can be shifted outside the hydrate area. The flow rate needs to be high enough to ensure that the mud has a high temperature when it reaches the hydrates ([Barker and Gomez, 1989a](#)).

Chemical injection: Methanol has successfully been used to remove hydrates blocking the well-head connector. A problem that arises when using methanol is the safety issues of storing large quantities of methanol aboard an offshore drilling platform ([Botrel, 2001](#)). Glycol is therefore often preferred. Dissociation of hydrates by chemical injection is often very time consuming, thus considered a costly method.

Direct heating: Internal heating systems can be used to remove hydrates, and considered less risky than external heating. Electric-element tools combined with methanol injection has successfully removed hydrate plugs in choke- and kill-lines. This is a highly efficient and low-cost way to remove plugs if the plug is accessible ([Botrel, 2001](#)).

Mechanical removal: Mechanical removal can in some cases be the fastest and safest way to remove a hydrate plug. Drilling or jetting tools are lowered into the well in order to break the

hydrates into small pieces which can be transported out of the well. Coiled tubing with a nozzle has been used to safely remove hydrates blocking the kill-line (Botrel, 2001).

2.4 Temperature Model of a Barents Sea Well

In order to determine the well interval where hydrates may form, the temperature at various depths needs to be calculated. In the case of a kick, the gas migrates up through annulus. By comparing the drilling fluid temperature in annulus to the hydrate equilibrium curve, the part of the well where hydrates might form can be determined.

Because the formation temperature increases with increased depths, hydrates in general do not form in sediments at great depths below the seabed. Inside the well however, hydrates are able to occur at deeper depths than what naturally occur in the sediments. Hydrate formation inside the well relies on the ocean temperature, formation temperature, initial mud temperature, mud density, friction between the mud and borehole wall among other factors. The well pressure can be very high if the drilling fluid must suppress a high formation pressure, since a high-density mud must be used. The increased pressure will impact the hydrate formation at various depths (Sloan and Koh, 2007).

Figure 2.20 shows the annulus drilling fluid temperature at various times after shut-in, calculated based on input values from a well drilled in the Barents Sea. The model uses the initial drilling fluid temperature, ocean and formation temperature, casing and cement thermal conductivity, annulus area, friction, sea current profile and temperature, drilling fluid type and lithology, to estimate the drilling fluid temperature in annulus at different times after shut-in (Sevillano, 2017).

The model simulates the well temperature when mud is flowing at a constant rate until the temperature reaches equilibrium, i.e. $\frac{\delta T}{\delta t} = 0$. The temperature at time=0 is the temperature at shut-in, equivalent to the drilling fluid temperature in annulus when the temperature has reached equilibrium. When the time after shut-in increases, the mud temperature converges towards

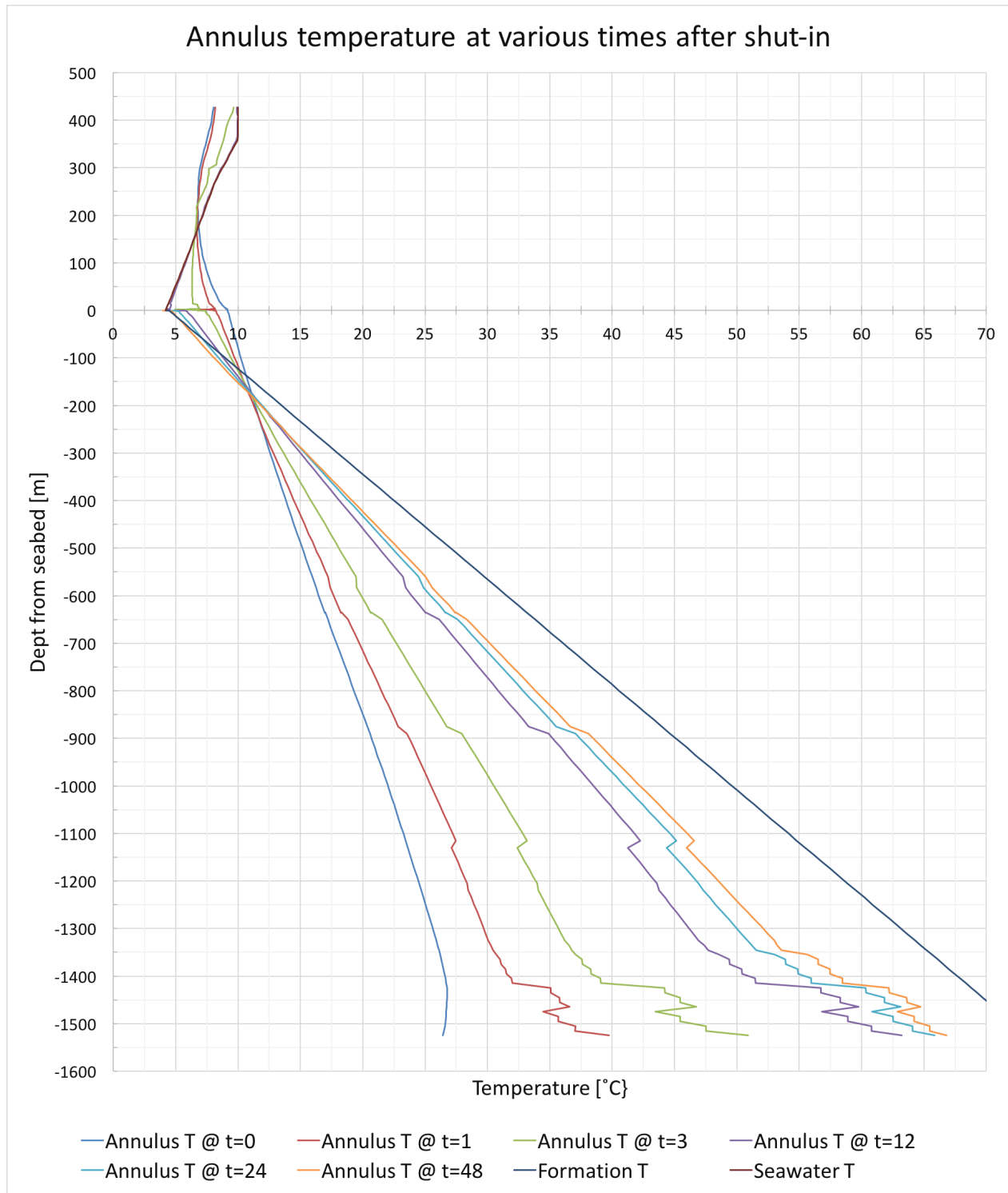


Figure 2.20: Temperature in the annulus at different time after shut-in. The temperature model is created by Lucas Cantinelli Sevillano, as a part of his PhD thesis. Initial mud temperature, lithology, cement and casing thermal conductivity, formation and water temperature gradient, friction, including several other factors are taken into consideration in this well temperature model (Sevillano, 2017).

the formation temperature. The temperature fluctuates at various depths of the well due to the variation in the conductivity of the lithologies, which impacts the drilling fluid temperature.

This model is compared to the hydrate equilibrium curve for a reservoir gas in Section [4.4](#) in order to find the well interval where hydrates may form.

Chapter 3

Laboratory Experiment and Equipment

The laboratory experiments conducted at NTNU and the SINTEF Test are described in this chapter. The apparatus and procedure are described in such a way that they should be possible to recreate.

3.1 NTNU Experiments

Knowledge concerning hydrate formation in drilling fluid and the effect various chemicals have on hydrate growth can be used to improve well control. Since hydrate formation is a topic with large uncertainties, experimental analysis are often more useful than analytically derived models. The NTNU experiments were performed to better understand how common drilling fluid additives affect hydrate formation. They can also provide valuable information about the hydrate volume, which can be used to estimate the volume reduction due to hydrate formation in low-pressure areas of the well.

It was necessary to design and create a new pressure cell before the experiments could take place. A sketch of the pressure cell, together with the components needed, was provided to the NTNU workshop in November 2016. The gas mixture of 90% methane and 10% propane was ordered from AGA the 16th of November, with a delivery time of approximately four weeks. In

December 2016, the final drawings and blueprints of the pressure cell were provided. Experiment start-up was initially estimated to late January or early February 2017. The pressure cell was finished by the 31st of January, however, the pressure and temperature sensors had not yet been ordered. The temperature sensor had four weeks delivery time, but did not arrive until the 3rd of March. At this point, it was discovered that a safety valve had not been mounted onto the pressure cell cap and a new one had to be ordered. On the 13th of March, the pressure cell, together with all other components, was ready for use.

After installation of LabView, the first experiment was initiated on the 20th of March. A large leakage occurred, and the experiment had to be stopped. Large leakages accompanied with smaller ones continued to occur for three days. Action was taken, and thread sealing tape was applied. Unfortunately, this did not prevent further leakage from occurring. A new design of the pressure valve had to be initiated to prevent future leakages from occurring. On the 23rd of March, the first experiment was conducted with the new pressure cell design. Due to different obstacles and factors described above, the experimental start-up was delayed for almost two months.

3.1.1 Experimental Apparatus

In order to simulate the pressure and temperature conditions one may observe in the upper part of the well, an experimental apparatus where hydrates could form was created. The apparatus can withstand a pressure of 50 bar in combination with low temperatures. Figure 3.1 shows the apparatus, with all components connected, placed inside the refrigerator. The sealed pressurized steel container is referred to as the *pressure cell* in this thesis.

The pressure cell consists of three main parts. The bottom part is a steel cylinder with 24.8mm of threads on the outside of the upper section. The middle part is a steel cap with 23mm of threads on the inside of the lower section, which can be screwed together with the steel cylinder. Figure 3.2 shows the steel cylinder and the steel cap. A toric joint is placed between the two steel parts, in order to ensure that the pressure cell is sealed.



Figure 3.1: Picture of the experimental apparatus inside the refrigerator. The various components present inside the refrigerator when running the experiment are numbered from one to eight. 1: Relief valve, 2: 3-way-valve, 3: Temperature sensor, 4: Pressure sensor, 5: Steel cap, 6: Steel cylinder, 7: Magnetic stirrer, 8: External temperature sensor placed in water filled Erlenmeyer flask (Helgestad, B., 2017)

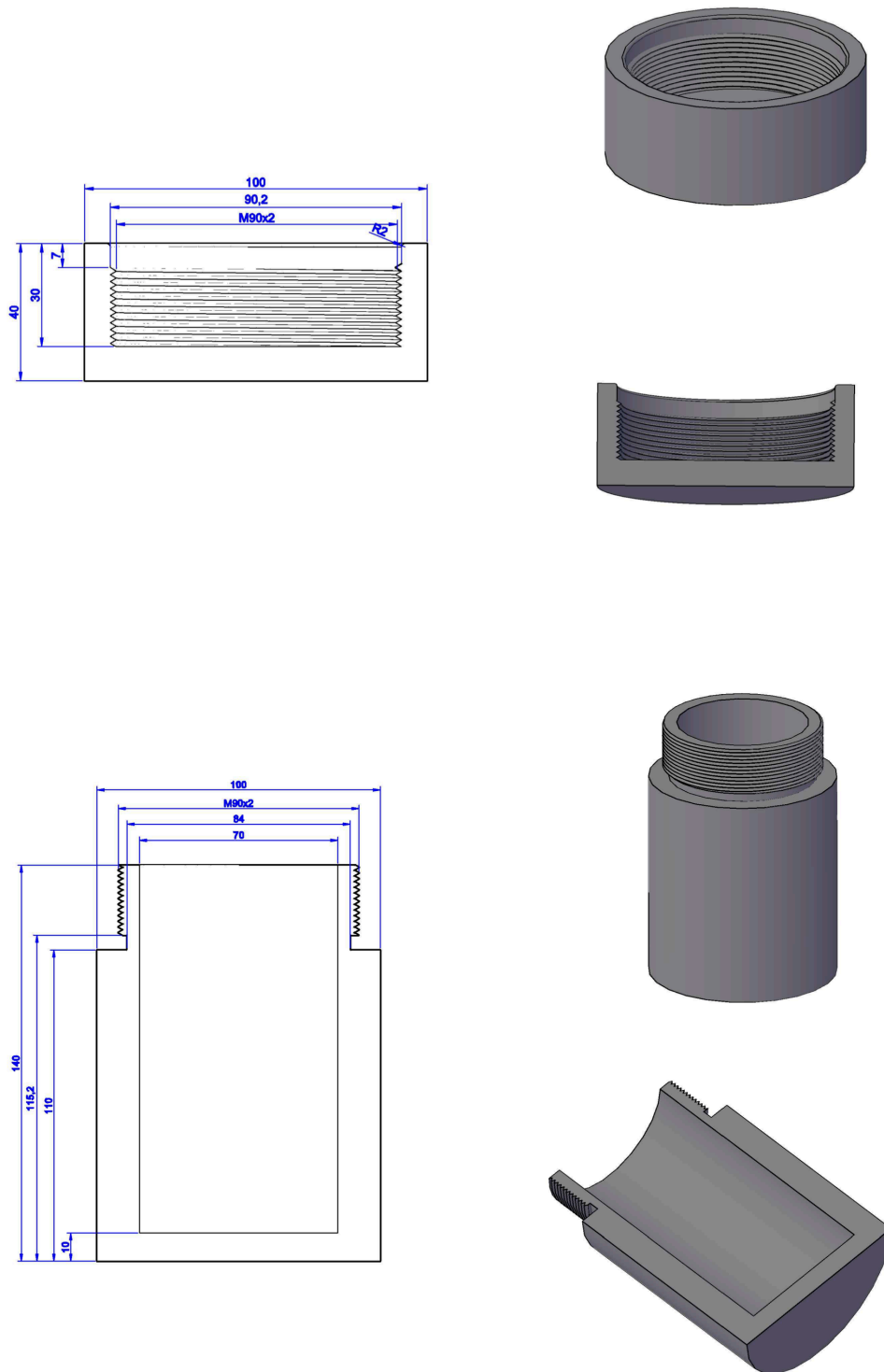


Figure 3.2: Sketch of the steel cap and steel cylinder. The dimensions are marked on the sketch. The two parts were made in the PTS mechanical workshop (Vedvik, 2017).

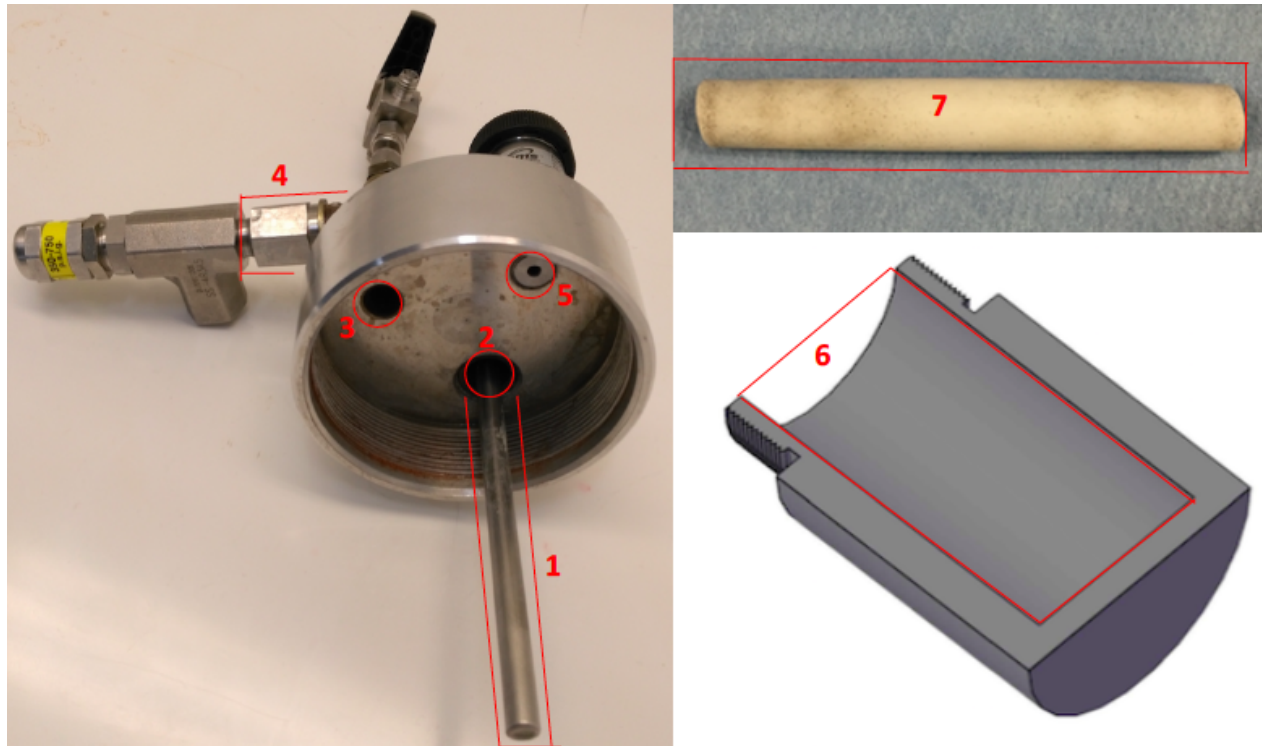


Figure 3.3: The various components contributing to the total volume inside the pressure cell when running the experiments, numbered from one to seven. 1: Temperature sleeve, 2: Inlet temperature sensor, 3: Inlet 3-way valve, 4: Relief valve (only considered the volume to the outlet), 5: Inlet pressure sensor, 6: Inside of steel cylinder, 7: Magnetic stir bar (Gunhildrud, M., 2017, modified from [Vedvik \(2017\)](#)).

A third part is connected to the top of the cell, called the *filling and measure assembly*. This consists of three parts; a pressure gauge, a temperature gauge and piping connecting the three-way ball valve and safety valve to the system. Threads were drilled on the top of the cap, and the 3-way valve, pressure and temperature gauge are screwed into these holes. A technical description of each part can be found in [Table E.1](#).

The gas used in the NTNU experiments was mixed by AGA, and consisted of 90% CH_4 and 10% C_3H_8 on a mole basis. This gas will be referred to as the NTNU gas. The methane-propane gas mixture used was filled on a 50 L pressure cylinder. Because of the dew point of the gas mixture, the pressure cylinder delivered a maximum pressure of approximately 30 bar. The pressure was regulated by a *Linde REDLINE C300* pressure regulator.

3.1.1.1 Determining the Apparatus Volume

Determining the apparatus volume is crucial to estimate the total amount of hydrates generated. The volume can be calculated based on the dimensions given in Figure 3.2. There are three holes in the steel cap where the pressure sensor, the temperature sensor and the piping are connected, which can increase the total volume slightly. The temperature sensor is connected to the steel cap, and a temperature steel sleeve is passing through the inside of the pressure cylinder. The volume of the outside of the steel sleeve should be subtracted in order to determine the total internal volume.

Figure 3.3 shows the different components contributing to the total volume inside of the pressure cell. The procedure used to determine the apparatus volume is shown in Section B.2.

3.1.2 NTNU Experimental Procedure

The experimental procedure can be divided into two main parts. The first part consists of measuring and mixing of the aqueous fluid phase, and the second part of the procedure is the filling and running of the experiment.

Mixing of Aqueous Fluid Phase Procedure

1. Determine the total weight of the fluid and calculate the wt% of each compound
2. Use a scale with a maximum error of ± 0.01 g, and measure the weight of the fluid and additive in separate beakers
3. Add the additive to the fluid. Use a magnetic stirrer and a magnetic stir bar to mix the phases together. For barite and bentonite solutions, use a mud mixer
4. Calculate the mass of the aqueous fluid which yield a volume of 150 mL, by using Equation B.1 - B.5 in Appendix B.1
5. Transfer the exact calculated mass to a clean beaker, ready to be filled in the steel cylinder

Filling and Running Experiment Procedure

1. Clean and dry the inside of the steel cylinder and the steel cap. Place the magnetic stir bar in the steel cylinder and fill with the exact mass of the aqueous fluid phase
2. Screw the steel cap on the steel cylinder. Connect the high-pressure gas flask to the 3-way valve. Open the 3-way valve
3. Fill gas until reaching approximately 3 bar. Disconnect and open 3-way valve to equalize the pressure, and to minimize the amount of air inside the container
4. Reconnect and fill to approximately 24 bar. Close 3-way valve and disconnect
5. Connect the pressure and temperature connectors and place the pressure cell inside the refrigerator with an internal temperature of approximately 5°C
6. Start logging of pressure and temperature versus time. Use a logging frequency of 0.25Hz

3.1.3 The Various Fluid Compositions Tested

The three various water types used in these experiments were tap water, Nidelv water and Fjord water. The Nidelv water was collected from the Nidelva river in Trondheim, while the Fjord water was collected from Krokstad in Snillfjord. Both water types were filtered prior to the experiment in order to remove the macroscopic particles.

The Nidelv- and Fjord water were initially preferred instead of tap water due to the microscopic impurities, which makes hydrate nucleation easier because they can act as nucleation sites. Relatively few particles exist in tap water, which means that few nucleation sites exist in the aqueous solution. Tap water was used later in order to remove the effect of the water impurities, thereby fully observe how the chemical compounds affect the nucleation.

Barite, Bentonite, NaCl, CaCl₂ and KHCOO was added to the water phase in various concentrations, in order to observe both their individual and combined effect on hydrate formation.

These are common additives in drilling fluid, and their impact on hydrate formation should be of interest when choosing drilling fluid composition. The composition of the aqueous phase used in the experiments is listed in Table E.6. Table 3.1 shows which date the experiments were conducted, the aqueous phase composition and whether the pressure cell was opened, leaking or heated after stopping the main experiment.

Table 3.1: List of experiments performed at the NTNU laboratory with corresponding mud composition, date performed and an explanation of which action was taken after the end of an experiment.

Experiment	Date	Mud composition	Leakage/melting/ opened
1	23.03.17	Nidelv water	Leakage
2	24.03.17	Nidelv water	
2.2	27.03.17	Nidelv water	Melting
3	28.03.17	Nidelv water	
3.2	29.03.17	Nidelv water	Melting
4	29.03.17	Fjord water	Opened
5	30.03.17	Fjord water, 3.5wt% NaCl	Opened
6	18.04.17	Nidelv water, 10wt% Barite	Opened
7	19.04.17	Nidelv water, 30wt% Barite	
8	20.04.17	Nidelv water, 10wt% NaCl	
9	24.04.17	Nidelv water, 20wt% NaCl	
10	25.04.17	Tap water, 5wt% Bentonite	Leakage
11	26.04.17	Tap water, 5wt% Bentonite	Opened
12	27.04.17	Tap water, 5wt% Bentonite, 20wt% CaCl ₂	
12.2	01.05.17	Tap water, 5wt% Bentonite, 20wt% CaCl ₂	Melting
13	01.05.17	Tap water, 10wt% CaCl ₂	
14	02.05.17	Taper water, 5wt% Bentonite 10wt% CaCl ₂ , 10wt% Barite	
14.2	03.05.17	Taper water, 5wt% Bentonite 10wt% CaCl ₂ , 10wt% Barite	Melting
15	03.05.17	Tap water, 5wt% Bentonite, 20wt% CaCl ₂	Opened
16	04.05.17	Tap water, 10wt% Bentonite	Leakage
17.1	05.05.17	Tap water, 10wt% KHCOO	Leakage
17.1.2	05.05.17	Tap water, 10wt% KHCOO	Opened
18	08.05.17	Tap water, 30wt% KHCOO	Opened
19	09.05.17	Tap water, 5wt% Bentonite, 10wt% KHCOO	Opened
20	10.05.17	Tap water	Opened

3.1.4 Gas Solubility in Experiment Fluids

Methane solubility in an aqueous NaCl solution decreases as the NaCl concentration increases. Figure 3.4b shows that by adding 10wt% NaCl to the aqueous phase at 24.1 bar, the methane solubility is almost halved from 0.0325 mole/kg to 0.019mole/kg (Duan and Mao, 2006). This pressure is similar to the one used in the NTNU experiments. A higher methane concentration dissolved in the aqueous phase, will be increasingly favorable for hydrate formation (Sloan, 1991).

Furthermore, the methane solubility increases with increasing pressure. Figure 3.4a shows that for a system with a temperature of 2°C, the methane solubility at 24 bar is approximately 0.055 mole/kg (Duan and Mao, 2006).

The NTNU gas mixture consists of 90% methane and 10% propane. Propane has a water solubility of 0.624 g/kg, i.e 0.0141 mole/kg at 1atm and 25°C, which means that propane is less soluble than methane. As a worst case scenario, the solubility of a 100% methane gas will be considered at the point where methane solubility has its highest value (HMDB, 2017).

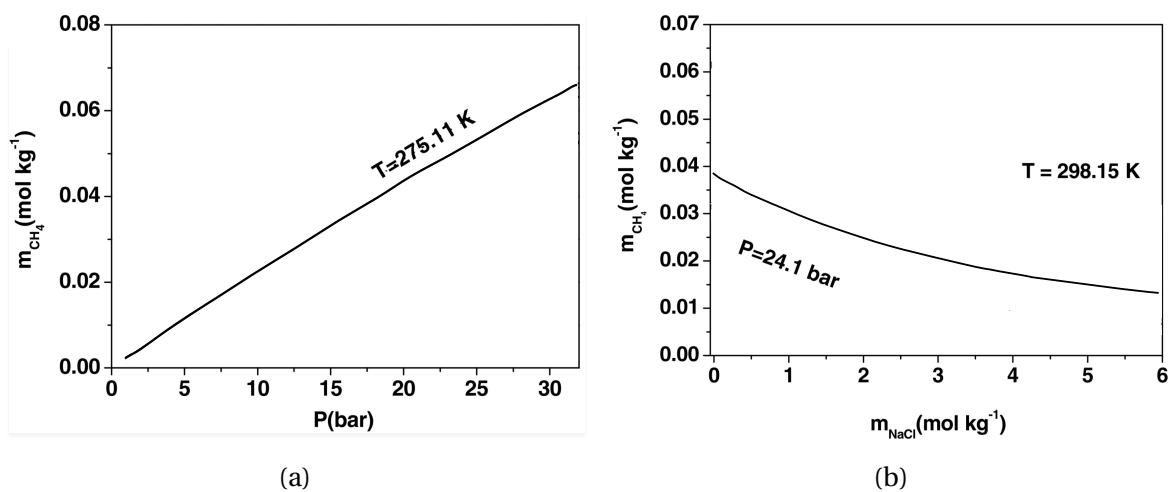


Figure 3.4: (a) Methane solubility in pure water and (b) Methane solubility in aqueous NaCl solution (modified from Duan and Mao (2006)).

Methane solubility in an aqueous CaCl_2 solution is lower compared to a NaCl solution at the same pressure and temperature. At 25°C and 24.1 bar, the solubility of methane is 0.02 mole/kg in a 1.0 mole/kg CaCl_2 solution, compared to the methane solubility of 0.025 mole/kg in a NaCl solution at equivalent conditions (Duan and Mao, 2006).

Based on this observation, the highest gas solubility possibly obtained in the NTNU experiments would be approximately 0.050 mole/kg at 5°C and 25 bar where the aqueous phase consists of pure water and the gas phase is assumed to be pure methane (Duan and Mao, 2006).

When running the NTNU experiments with 100% tap water, the weight is 150g. Thus, the amount of methane gas which could dissolve in the water phase is 0.0075 mole. This is a worst case scenario since the gas used in the experiments contain 10% propane, thus less gas will be dissolved.

When the cell is pressurized to 24.61 bar at 27.54°C , 0.3717 moles of the methane-propane mixture is present in the gas phase. When this amount of gas is cooled down to 5°C , the pressure is 22.77 bar. If 0.0075 moles are removed from the gas phase and dissolved into the aqueous phase, the pressure reduction can be calculated using the real gas law. The calculation shows that the system pressure will reduce by 0.46 bar, which result in an equilibrium pressure of 22.31 bar. This reduction in pressure is significant and should not be neglected.

3.2 SINTEF Test

This section is written on the basis of knowledge and observations done during the experiments performed the 14th and 16th of March 2017, as well as the SINTEF Report of Future Well Control "Hydrate formation in wheel flow loop" (Fossen, 2017a). Two tests were conducted, but this thesis focus on SINTEF Test 2.

Controlling the volume of the active drilling fluid is used to identify influx of reservoir fluids into the wellbore, as well as identifying loss of drilling fluid into the formation. This experiment was conducted by SINTEF for Future Well Control AS to determine the volume reduction of gas in annulus when gas hydrates form in a high-pressure system (Fossen, 2017a).



Figure 3.5: Picture of the Wheel Flow Loop inside the climate chamber (Helgestad, B., 2017) .

3.2.1 Experimental Apparatus

An experimental apparatus made at SINTEF's multiphase flow laboratory, called the *Wheel Flow Loop*, was used to simulate hydrate flow in the wellbore. The apparatus is a steel pipe shaped like a wheel, connected to the axle by steel beams. Figure 3.5 and 3.6 show a picture and a schematic sketch of the wheel flow loop.

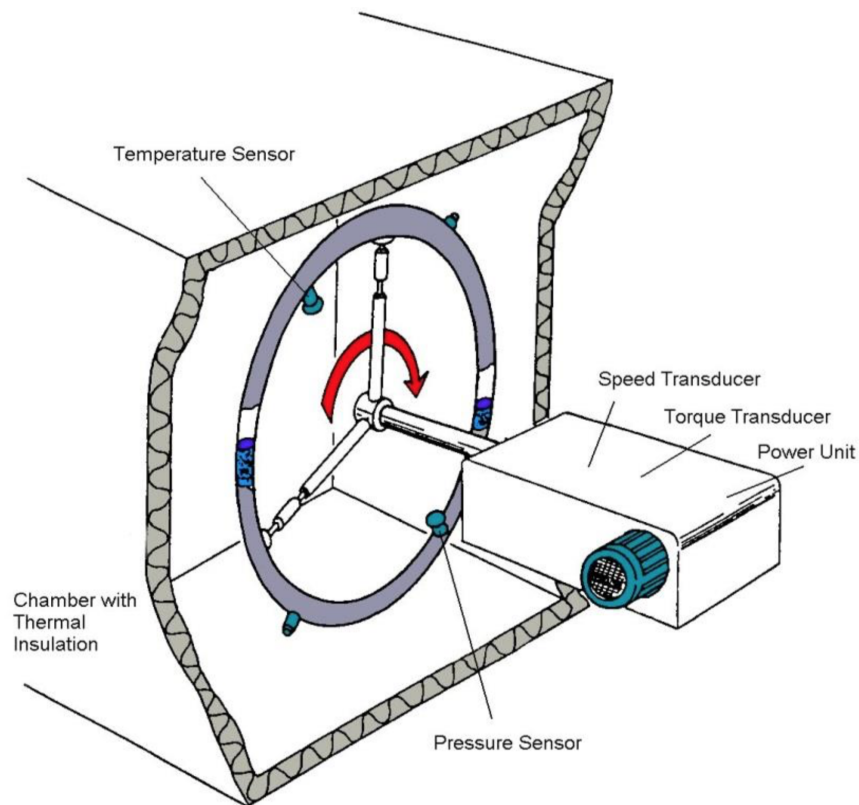


Figure 3.6: Sketch of the wheel flow loop and motor. The rotational direction is clockwise when observed from the point of the motor (Fossen, 2017a) .

The wheel has a diameter of 2.0 m, an internal pipe diameter of 52.4 mm and a wall thickness of 3.91 mm. This makes the internal volume of the wheel flow loop 13.6 L. A camera is mounted onto the wheel to film the inside of the pipe through a sapphire glass section of the pipe. The wheel is placed inside a climate chamber, which makes it possible to regulate the temperature between 60°C and -10°C. The chamber is also acting as a safety barrier, which is required since the wheel can sustain pressures up to 250 bar.

The scale measuring the weight of the wheel has an error margin of ± 5 g. Calculations were performed to determine the expansion of the wheel due to the internal pressure. They concluded that the volume can be neglected because the calculations showed that the volume increase would be within the error margin.

Two temperature sensors were mounted on the outside of the wheel flow loop in order to observe the heat transfer due to hydrate formation. The placement of the pressure and temperature sensors, as well as the inflow gas valve, can be observed in Figure 3.7.

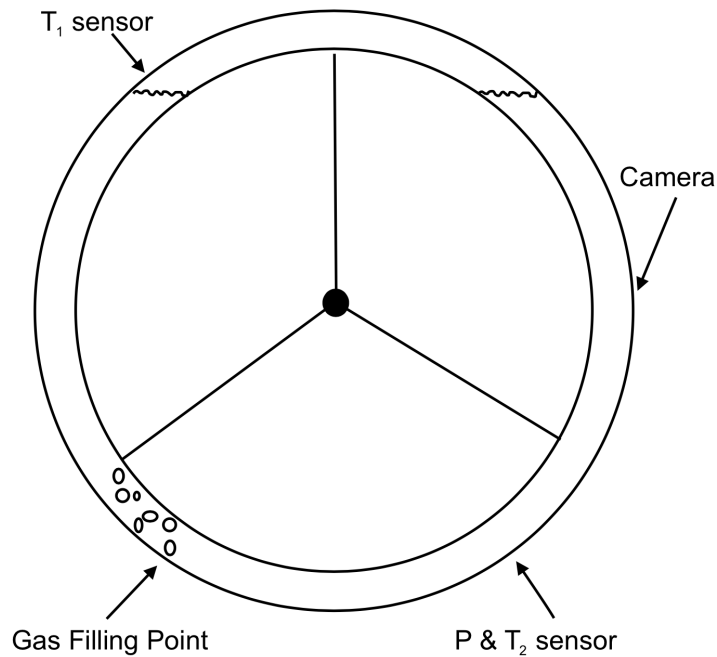


Figure 3.7: A sketch of the Wheel Flow Loop. The placement of the pressure sensor, temperature sensors, camera and gas filling points are marked with arrows. The placement of the equipment on the sketch is aligned with Figure 3.5. The approximate water level is illustrated, as well as the gas flow inside the wheel (Helgestad, B., 2017) .

The wheel flow loop is controlled by the software LabView from a separate control-room, where the wheel rotational speed and chamber temperature can be controlled. The wheel has a maximum working pressure of 250 bar and a maximum velocity of 5 m/s. The gas composition used in the SINTEF Tests are given in Table 3.2, and is referred to as the SINTEF gas in this thesis.

Table 3.2: Synthetic natural gas composition used in the SINTEF Test.

Gas component	mole %	MW [g/mole]	Weight [g]	wt%
N ₂	6.79	14.0067	95.13	5.37
CO ₂	0.50	44.01	21.83	1.23
C ₁	84.17	16.04	1350.06	76.16
C ₂	5.49	30.07	165.04	9.31
C ₃	2.63	44.1	116.00	6.54
iC ₄	0.42	58.12	24.70	1.39
SUM	100		1772.76	100.00

3.2.2 SINTEF Experimental Procedure

The experimental procedure in the wheel flow loop experiments is described below. The procedure is based on the observations done by the authors and the procedure description given in the SINTEF report ([Fossen, 2017a](#)).

1. Fill the wheel with sea water containing 3.5wt% NaCl to verify the volume
2. Drain 3.0 L of water from the wheel. Replace the water with methane gas
3. Pressurize the system by injecting a natural gas mixture through the inflow gas valve. The target amount of gas is 560 g
4. The temperature of the seawater should be 10°C, and the chamber temperature should be 4°C or lower. Consequently, the seawater temperature will not be constant, but start to cool down
5. Fill the wheel with the predetermined amount of the SINTEF gas, and rotate the wheel to identify hydrates
6. If hydrates occur, heat and melt before performing a second test. In the second test, let the wheel spin at a constant velocity while cooled down to 12°C. Let the system go to steady state

3.2.3 Gas solubility in the SINTEF Test

Figure 3.8 shows the effect of increasing pressure on methane solubility at a temperature of 25°C. As described in Section 3.1.4, the methane solubility increases with increasing pressure.

The SINTEF gas contains 84.17% methane on a mole basis, but the gas composition inside the wheel flow loop contains even more methane. This is because methane was injected initially in order to drain the water, and methane was injected after the SINTEF gas flask was empty as discussed in Section 4.2.1. Thus, the gas solubility in the SINTEF test is probably close to the methane solubility in Figure 3.8 at similar pressures.

Figure 4.19 shows that the system pressure was approximately 160 bar when the temperature was 25°C, making the methane solubility 0.14 mole/kg. The mass of seawater inside the wheel flow loop was approximately 10 kg, meaning that 1.4 moles of gas dissolve into the aqueous solution in Test 2. Calculations show that by removing 1.4 moles from the gas phase in Test 2, the system pressure will reduce with approximately 10 bar.

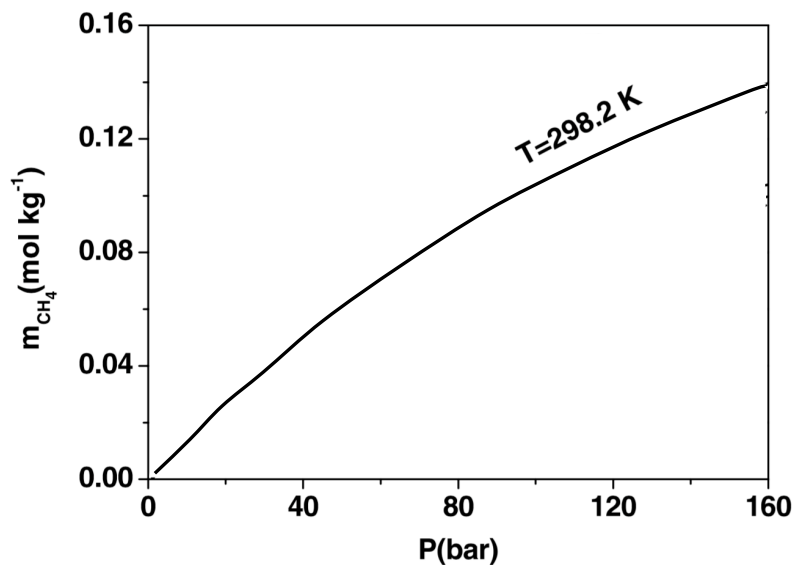


Figure 3.8: Methane solubility in pure water at 25°C for various pressures (modified from [Duan and Mao \(2006\)](#)).

Chapter 4

Results and Discussion

4.1 NTNU Experiments

In this section will the results obtained from the experiments performed at the NTNU laboratory be presented and discussed. Some descriptive pressure and temperature plots obtained will be shown and compared in this section, while the other pressure and temperature plots can be observed separately in [Appendix A](#).

Note that the results obtained and presented in this chapter are analyzed and interpreted based on the writers' knowledge of the hydrate behaviour and the experimental setup. Hydrate formation is a difficult and stochastic field of study where unexpected results can occur. Being too conclusive based on a relatively small sample size could therefore be problematic.

4.1.1 Initial and Final System Conditions

Table [4.1](#) shows the initial and final system conditions, as well as the pressure and temperature decrease observed in the NTNU experiments. The aim was to achieve an initial system pressure of 24 bar in each experiment, but this was difficult due to the low resolution on the pressure regulator display.

Table 4.1: Initial and final pressure and temperature in the pressure cell for each experiment. The pressure and temperature change from start to finish are also calculated. Experiments where dissociation of hydrates occurred is marked as Experiment X.2.

Experiment	$P_{Initial}$ [bar]	P_{Final} [bar]	$T_{Initial}$ [°C]	T_{Final} [°C]	ΔP [bar]	ΔT [°C]
1*	23.75	20.79	7.06	6.94	-2.96	-0.12
2	24.21	18.55	19.36	6.69	-5.66	-12.67
2.2	18.83	24.42	7.22	22.40	5.59	15.18
3	24.42	18.71	22.40	6.95	-5.71	-15.45
3.2	18.71	24.30	6.95	21.40	5.59	14.45
4	24.44	18.75	19.72	6.73	-5.69	-12.99
5	24.11	19.48	13.31	6.72	-4.63	-6.589
6	23.81	18.04	15.78	6.40	-5.77	-9.38
7	23.76	18.30	15.42	6.34	-5.46	-9.08
8	23.83	19.93	20.12	6.63	-3.90	-13.49
9	24.84	22.34	28.80	6.25	-2.50	-22.55
10*	24.56	14.50	22.03	6.02	-10.06	-16.01
11	24.83	18.07	27.52	6.33	-6.76	-21.19
12	22.06	19.58	29.50	6.70	-2.48	-22.80
12.2	19.58	22.31	6.70	21.81	2.73	15.11
13	24.28	17.79	27.45	6.62	-6.49	-20.83
14	22.50	16.39	23.70	6.98	-6.11	-16.72
14.2	16.40	22.87	6.93	23.74	6.47	16.81
15	24.61	22.14	27.54	7.05	-2.47	-20.49
16*	22.12	10.36	26.83	18.78	-11.76	-8.05
17	24.00	18.98	21.22	5.68	-5.02	-15.54
18	24.15	21.79	23.63	5.86	-2.36	-17.78
19	21.08	17.19	26.49	5.61	-3.90	-20.88
20	24.85	18.03	24.70	5.98	-6.82	-18.72

*Leakage

In experiment 1, 2 and 3, the pressure cell was cooled down inside the refrigerator before injecting gas. This was not done in the latter experiments because observing the pressure profile as the system enters the hydrate area may give valuable information about hydrate formation. Therefore, the initial temperature in most of the experiments was above 20°C

4.1.2 Evidence of Hydrate Growth

There is no window into the pressure cell which makes it impossible to observe hydrate formation while the experiments are running. Verification of hydrate formation is therefore based upon the pressure and temperature logs, and visual observations after depressurization and opening of the pressure cell. Note that no hydrates observed by visual inspection does not disprove hydrate formation, because the hydrates may dissociate during depressurization. On the other hand, if they are observed during the visual inspection, they verify that hydrates have formed in the current experiment.

In some of the experiments, an excess pressure drop was observed which cannot be explained solely by a change in temperature. Experiment 3 is one experiment where this was observed. The ΔP from start to finish in experiment 3 is -5.71 bar. The pressure could be lowered due to a leakage, but this is unlikely because the pressure remains stable during the last 15 hours of the experiment. This suggests that hydrates have caused the pressure to decrease in experiment 3.

A method used to determine if a leakage had occurred was to heat the pressure cell after the main experiment was stopped. If the pressure increased to the initial pressure of the main experiment, when heated to the initial temperature, the mass inside the system is unchanged, i.e. no leakage. This method was used on experiment 2, 3, 12 and 14. The pressure plots for dissociation of hydrates in these experiments can be observed in Figure [A.21](#), [A.22](#), [A.23](#) and [A.24](#). Table [4.1](#) shows that the pressure increased to a similar pressure as the initial pressure in all of the dissociation experiments.

To confirm hydrate formation visually, the pressure cell was opened for several of the experiments. The pressure cell was quickly disconnected from the pressure and temperature sensor, then depressurized to atmospheric pressure and opened. The pressure cell was opened in experiment 4, 11, 17 and 20, and the visual inspection confirmed hydrate formation in all four experiments.

4.1.3 Start of Hydrate Growth

Determining when the hydrate growth starts during the experiment can be done by visual inspection, identify the time temperature change or pressure change. Visual inspection is not an option in the current experimental apparatus since there is no window into the pressure cell. Hydrate growth is exothermic, thus a temperature change can be observed near the growth site. The temperature change was difficult to observe, most likely because the temperature sensor was located inside the aqueous solution and not in the gas-water interface where hydrates tend to form. The pressure on the other hand has changed its declination rate in several of the experiments performed. The discontinuity where the pressure starts to decline more rapid will be called the *break-point* of the curve. Due to the sudden pressure decrease, it is reason to believe that this could be the point where hydrate formation started.

Figure 4.1 shows the pressure and temperature measurement of the first few hours of experiment 3, 4, 11 and 13. The break-points are marked with arrows down to the time axis. For experiment 3, 4 and 11, the break-point seem to occur when the system temperature reaches 10°C to 11°C, after approximately one hour. Note that the temperature at $t=0$ for all the experiments in Figure 4.1 are 20°C. This means that the temperature has been corrected from the initial temperature in each experiment to yield the same start temperature for all the experiments in the plot. This is done in order to better compare the different experiments.

In experiment 3,4 and 11, only small amounts of salt is present in the water phase, and the water contains impurities. This could make hydrate formation happen soon after the pressure and temperature conditions are within the hydrate area. The equilibrium pressure and temperature conditions for the NTNU gas are shown in Table E.4. At a pressure equal to 22.5 bar, the equilibrium temperature is 12°C. This means that the break-points for experiment 3, 4 and 11 are located approximately 2°C to the left of the hydrate equilibrium curve, i.e. the system is subcooled with 2°C.

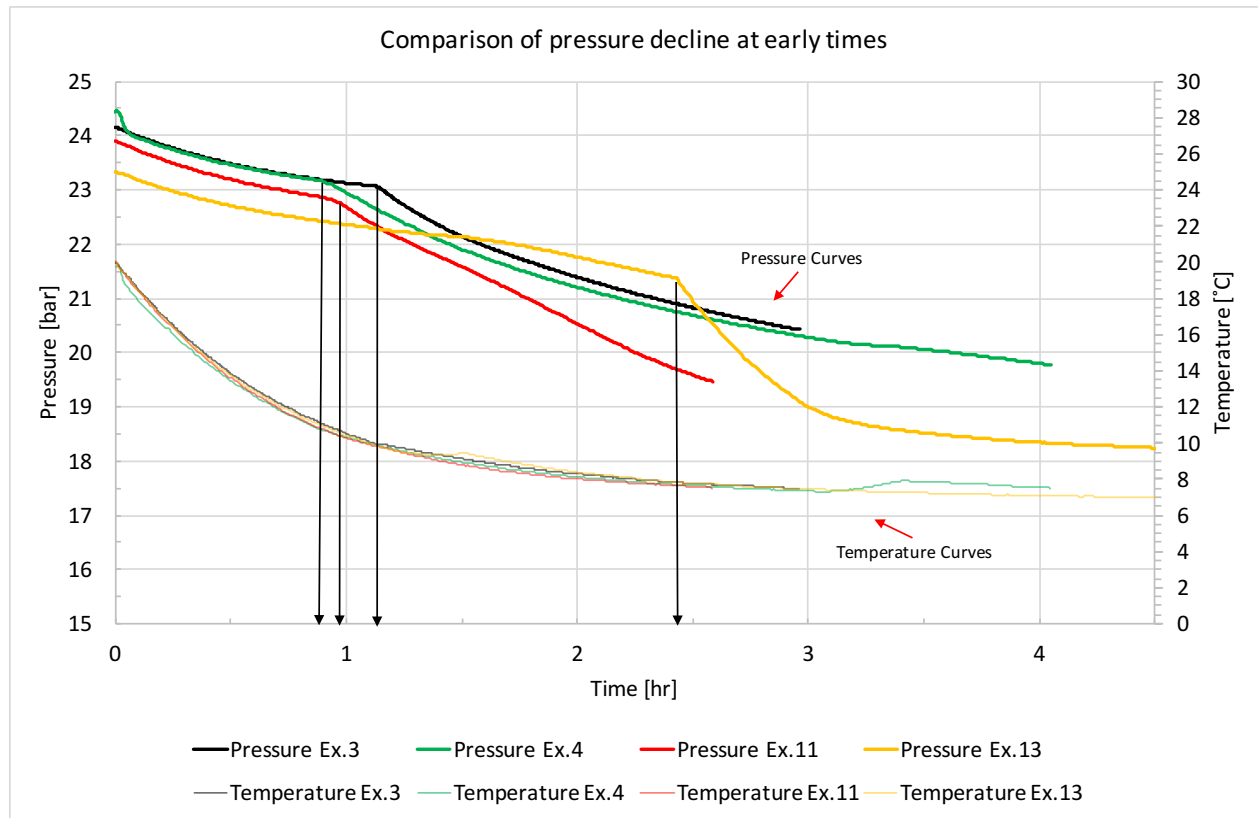


Figure 4.1: Comparison of the pressure declination in experiment 3 (Nidelv water), 4 (Fjord water), 11 (Tap water and 5wt% bentonite) and 13 (Tap water and 10wt% CaCl_2). Time=0 is defined as the time where the experiment temperature is 21.5°C , thus not the start of the experiments.

The break-point for experiment 13 is occurring after approximately 2.5 hours. At this point, the system temperature is much lower, close to 8°C . The lower hydrate formation temperature in experiment 13 is as expected as CaCl_2 works as an inhibitor. The red curve in Figure 4.10 shows that the hydrate equilibrium temperature is 5.5°C for the 10wt% CaCl_2 solution at 21.5 bar. This suggests that experiment 13 had not entered the hydrate area when the break-point occurred. Consequently, the break-point was caused by another factor, if the hydrate equilibrium curve is correct.

It is worth noticing that the declination occurring after the break-point is steepest in experiment 13, compared to the other experiments. One explanation might be the lack of impurities in tap water, which can prevent hydrate growth at low subcooling (Sloan, 1991). Consequently, when hydrates form, the driving forces are large and hydrates will initially grow very fast. When the

system pressure is lowered, the driving force is lowered, and the hydrate growth follows a similar pattern as in experiment 3, 4 and 11.

A distinct break-point is not observed in several of the experiments, but it does not disprove hydrate formation. If the growth rate is low, the pressure is slowly reduced, thus a rapid declination is not observed. Another factor affecting the visibility of the break-point can be that the pressure change due to hydrate growth is camouflaged by the PVT pressure change in the gas phase. This would lead to a continuous slope of the pressure curve, and not a sharp break-point.

4.1.4 Temperature Fluctuation and Apparatus Temperature Discrepancy

It is difficult to maintain a steady temperature over time. The pressure cell is located inside the refrigerator when running the experiments, without the refrigerator door being opened at any point. Nevertheless, the temperature fluctuated throughout the course of the experiments.

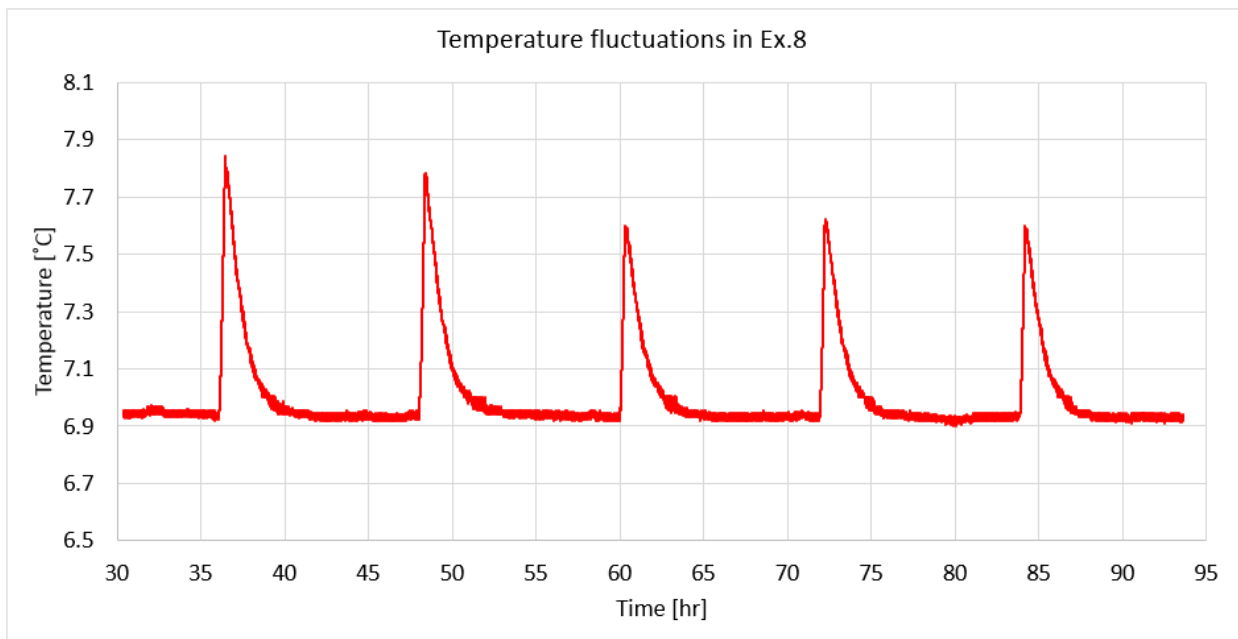


Figure 4.2: Temperature curve for experiment 8, showing the temperature fluctuations. This is a typical example of the temperature fluctuations observed in all the experiments.

The temperature fluctuations are observed in all the temperature logs, and seems to increase the system temperature by approximately 0.75°C . Every experiment follows a similar pattern, where the temperature suddenly increases, before the temperature decreases exponentially until reaching the equivalent temperature as prior to the sudden increase. These fluctuations probably occurred because the refrigerator compressor followed a programmed deicing cycle, which temporarily increased the temperature inside the refrigerator.

Figure 4.2 shows the temperature curve for the last 45 hours of experiment 8. The temperature is steady in the period between these major temperature fluctuations. The average period between the five spikes was calculated to be 11.946 hours, varying from 11.925 hours between spike 1 and 2, up to 11.987 hours from spike 2 to 3. These temperature fluctuations have affected the pressure curves for a limited time, but when experiments are analyzed, these pressure changes have been neglected.

Throughout all the experiments, there has been a discrepancy between the temperature measurement done by the temperature sensor integrated into the apparatus and the temperature sensor placed in the water filled Erlenmeyer flask next to the apparatus. Thus, one or both temperature sensors are displaying a wrong temperature.

In order to cope with this discrepancy, a test was conducted with the purpose of showing what temperature the sensors displayed when the measured fluid had a known temperature. A simple way to create a system where the temperature is constant over time is by measuring a system where a phase transition is occurring. In this test, melting of ice was used to achieve a constant temperature of 0°C .

Cold water and ice were mixed in a beaker and placed into a refrigerator. After one hour, the system was assumed to be in equilibrium since both ice and water were still present. Both temperature sensors were placed into the beaker while the system remained inside the refrigerator. The temperature was logged frequently on both devices. The actual temperature sensor is believed to be placed in the bottom of both devices, thus the bottom part of each temperature sensor was placed in the zone of the beaker where ice was floating. The temperature sensor

used in the Erlenmeyer flask showed 0.0°C when the sensor was inside the ice zone, whereas the lowest recorded temperature from the experimental temperature sensor was 0.3°C . The discrepancy in this test was not as large as when running the experiments, where the discrepancy varied between 0.5 and 1°C , which could indicate that the discrepancy increases with temperature. Therefore, the logged data should probably be corrected by subtracting at least 0.3°C from the logged temperature.

4.1.5 Comparison of Hydrate Pressure Drop to Real Gas Law Pressure Drop

The real gas law is an equation of state for real gasses, described by Equation 4.1 (LeTran, 2017).

$$PV = nRTZ \quad (4.1)$$

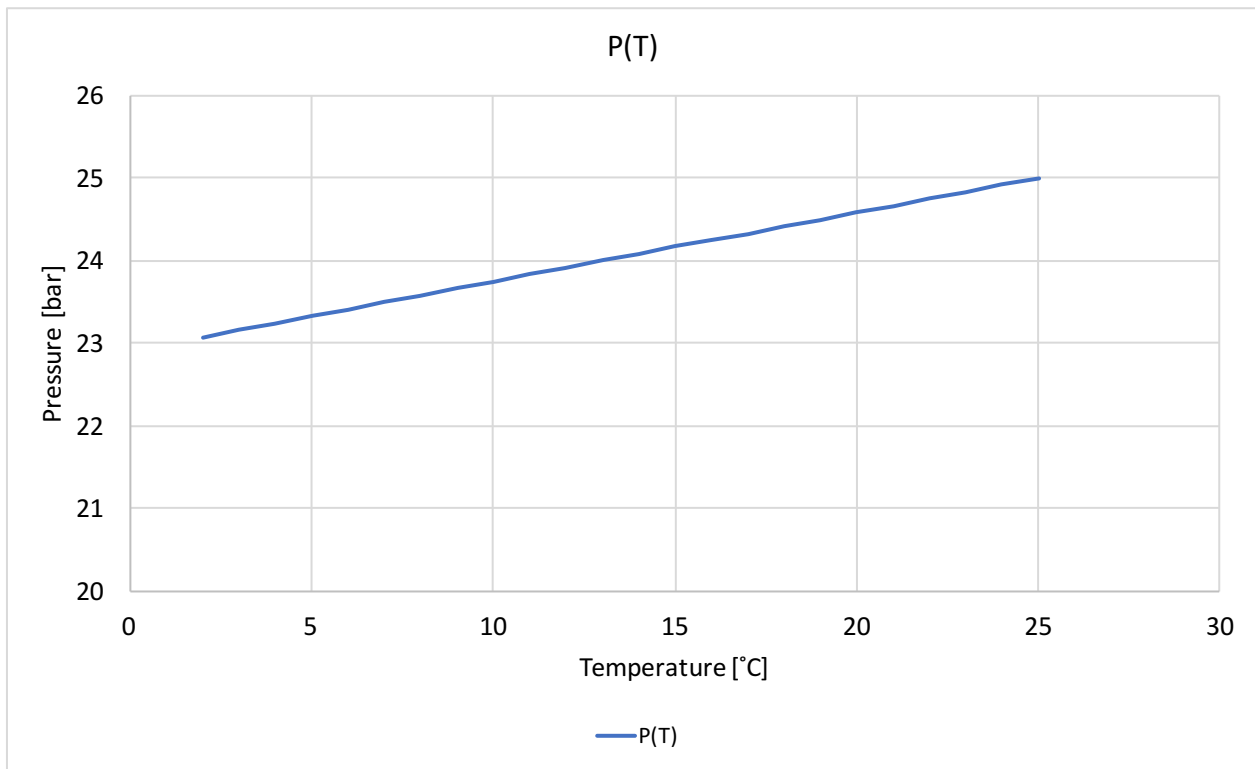


Figure 4.3: Pressure change as a function of temperature according to real gas law. Since the Z-factor is assumed constant, the relationship between pressure and temperature becomes linear.

The pressure in the pressure cell generally varies between 25 bar and 18 bar. The Z-factor for the methane-propane gas mixture is almost identical at these two pressures, when considering the start and end temperature. Therefore, when applying the real gas law to estimate the pressure drop due to temperature change in the system, it is reasonable to assume that initial and final Z-factor is equal to each other. The pressure drop inside the pressure cell can be calculated using Equation 4.2.

$$P_2 = \frac{P_1 \cdot T_2}{T_1} \quad (4.2)$$

Figure 4.3 shows how the pressure decreases with decreasing temperature. At 25°C, the pressure is 25 bar. If the temperature decreases with 20°C, a new pressure of 23.3 bar will be obtained i.e. the pressure will drop 1.7 bar due to a change in temperature.

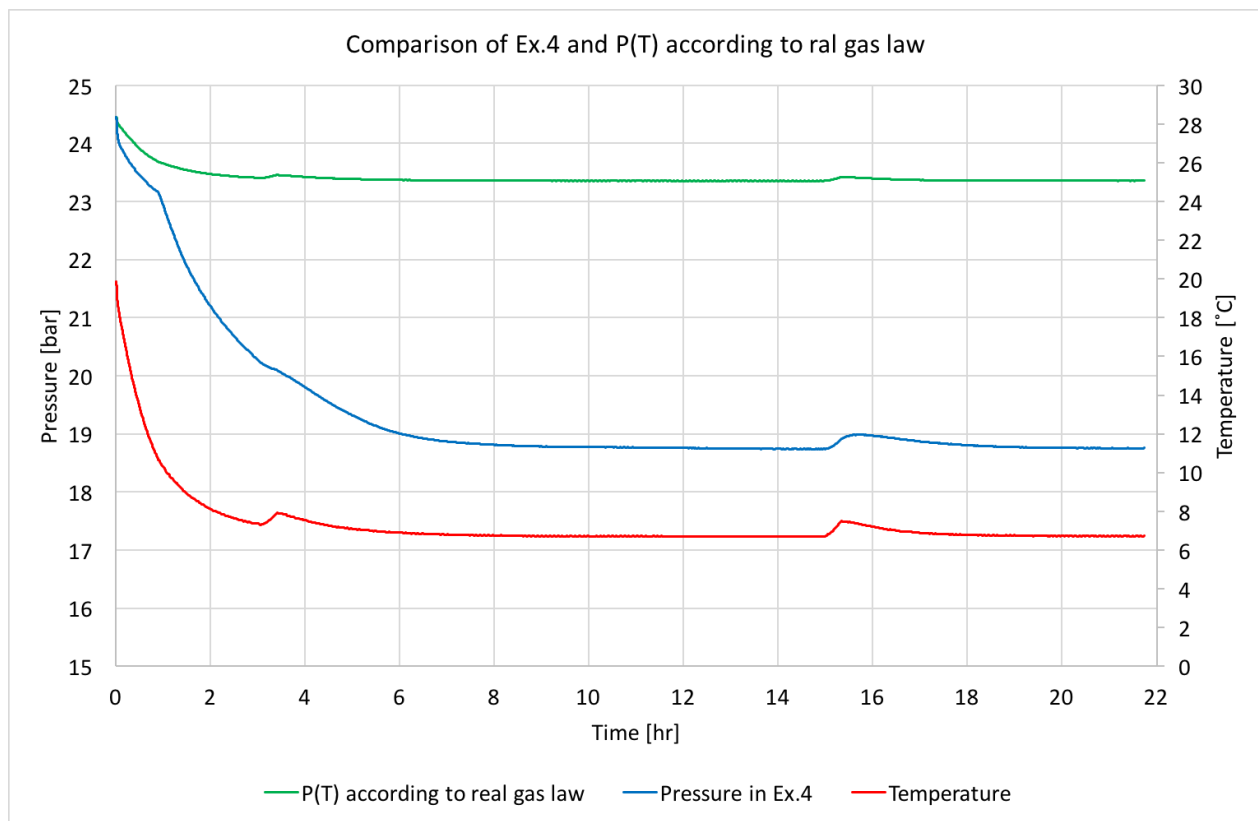


Figure 4.4: Comparison of the pressure curve obtained from experiment 4 and the theoretical pressure drop in an equivalent system according to real gas law.

To distinguish the pressure drop due to decreasing temperature from the pressure drop caused by hydrate formation, it is necessary to plot the temperature pressure drop as a function of the system temperature over the course of an experiment. The green line in Figure 4.4 represents the pressure drop according to the real gas law, whereas the blue curve is the pressure in experiment 4. When the system has reached steady state after 20 hours, the pressure difference between the two curves are 4.60 bar. This observation is a strong evidence of hydrate formation.

4.1.6 Comparison of PVT and Systems Without Hydrate Growth

Experiment 9 was conducted using 20wt% NaCl solution. Table E.3 shows how NaCl affects the hydrate equilibrium curve when added to the water phase. By adding 20wt%, the hydrate equilibrium temperature at a given pressure is shifted to the left by 16.48 °C, resulting in a smaller hydrate area. When looking at the hydrate equilibrium curve, the temperature at a pressure of 29.19 bar shows that the formation temperature at this pressure is 14°C. Since 20wt% NaCl depresses the temperature by 16.48°C, the temperature needed to form hydrates at this pressure is subzero, thus hydrates will never form in the system if 20wt% NaCl is added to the water phase. Therefore, the pressure in experiment 9 should only be affected by the temperature decrease according to real gas law. Figure 4.5 compares the recorded pressure in experiment 9 with the expected pressure obtained by using real gas law. It is observed that these graphs do not align. The most likely reason is that some of the gas has dissolved in the aqueous solution. According to Section 3.1.4, a methane-saturated water phase can result in a pressure reduction of 0.46 bar at 5°C and 23 bar. When correcting for the theoretical pressure drop for methane solubility, the curves nearly match, as observed from the yellow and blue curves in Figure 4.5. The actual pressure is still slightly lower than the calculated pressure. This discrepancy might occur because Z_1 is not equal to Z_2 , as assumed in Section 4.1.5.

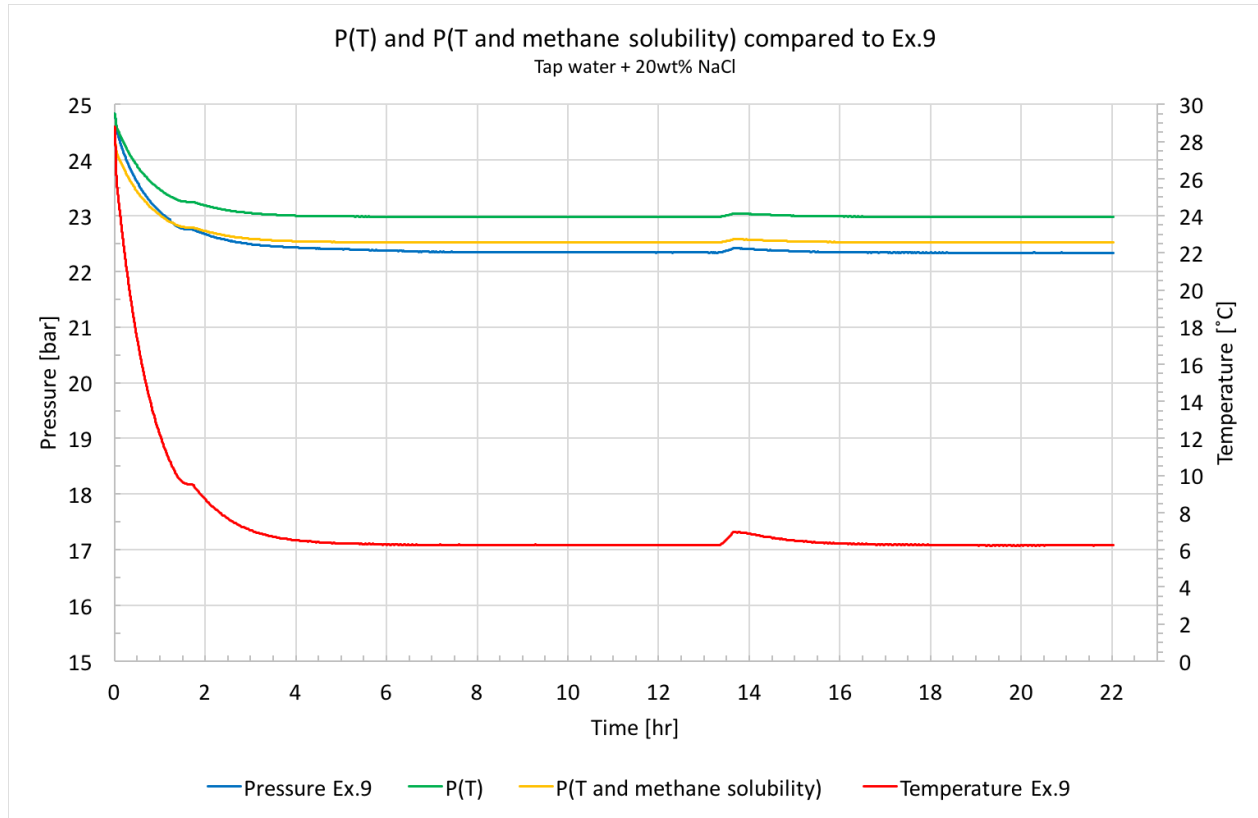


Figure 4.5: Comparison of pressure drop in systems with no hydrate growth, and pressure drop in equivalent systems according to real gas law. The yellow curve represents the theoretical pressure drop when gas dissolving into the aqueous solution is accounted for.

4.1.7 Time Until System Equilibrium

When comparing the pressure and temperature logs retrieved from the NTNU experiments there is a variation in pressure curve decline before stabilizing. This period is referred to as the *time until equilibrium*, Δt_{equ} . The system is assumed to be in equilibrium when the pressure curve has flattened out, i.e. $\frac{\delta P}{\delta t} = 0$. An illustration of the time until equilibrium is showed in Figure 4.6, where time until equilibrium is marked as Δt_1 and Δt_2 .

The time until equilibrium varies throughout the experiments. In experiment 11, Δt_{equ} is less than 8 hours, whereas in experiment 20 the time until equilibrium is more than 60 hours. In Figure A.8, it looks like experiment 8 reached equilibrium after 28 hours, but an additional pressure decrease of 0.5 bar is observed after 93 hours. This could be an indication of a leakage, or that

Experiment 8 has a large Δt_{equ} . For most other experiments, equilibrium was reached after 10 to 15 hours.

The most apparent factors affecting the time until equilibrium, are the hydrate growth rate and the final hydrate mass. If the surface area where hydrates can grow is large and the driving forces are strong, the growth rate is high. Thus, the system will reach steady state faster, and Δt_{equ} will be smaller. If the system allows for large amount of hydrates to grow, it will make Δt_{equ} larger, because more hydrate formation form before system equilibrium is reached. The red curve in Figure 4.6 represents a typical curve where the hydrate growth rate is high, while the blue curve represent a slower growth rate, resulting in a greater Δt_{equ} .

4.1.8 Shape of the Pressure Profile

The shape of the pressure profile can give valuable information about the process inside the pressure cell. A steep pressure slope is expected in the beginning of the experiment, due to the rapid temperature decrease that occurs when the pressure cell is placed inside the refrigerator. The temperature curve will decrease exponentially, which makes the pressure curve decrease exponentially, due to the linear relationship between pressure and temperature discussed in Section 4.1.5. The pressure curves from the NTNU experiments can be divided into three main categories; no hydrate growth, fast hydrate growth and slow hydrate growth, marked as A, B and C in Figure 4.6

The green curve in Figure 4.6 represents a typical pressure reduction in a system where the temperature decreases, no gas dissolves into the aqueous solution and no hydrate formation occurs. The pressure reduces by $\Delta P_{(T)}$. If gas dissolves into the aqueous solution as the temperature decreases, without hydrates forming, the pressure curve will look more like the black curves in Figure 4.6. The black curves are similar to the one observed in experiment 9 where no hydrate formation occurred. The pressure is further reduced by $\Delta P_{Dissolve}$, making the total pressure drop equal to $\Delta P_{(T)} + \Delta P_{Dissolve}$. The shape of the pressure curve might be similar to either profile B or C in Figure 4.6 if the system conditions allow for hydrate formation.

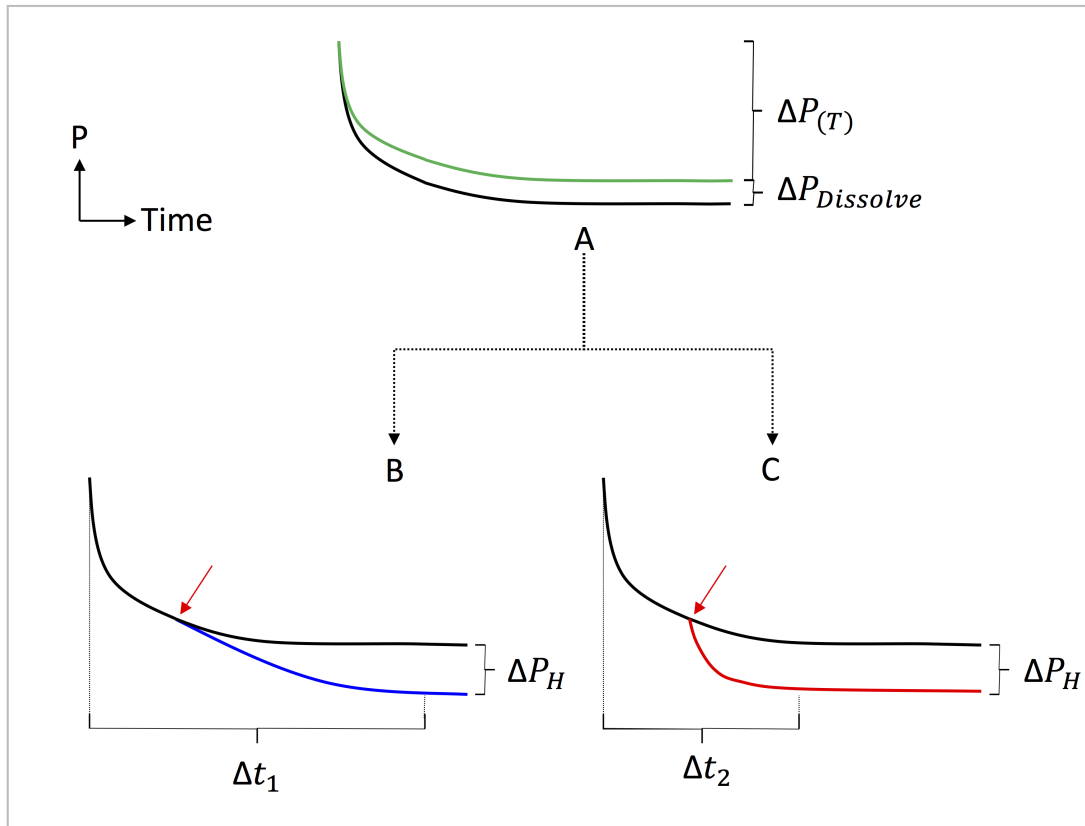


Figure 4.6: Visual representation of the main shapes of pressure curve with and without hydrate formation. The red arrows indicate the point where hydrates start to grow (Helgestad, B., 2017).

The pressure initially decrease similarly in profile B as in profile A, but when the system conditions enters the hydrate area, marked with a red arrow, the pressure continues to decrease slowly. The blue line in Figure 4.6 represents a slow growth rate, making the pressure decline linear. Since the growth rate is low, the time until equilibrium is large, marked as Δt_1 . Experiment 20 is an example of a pressure curve which looks like profile B.

The other main shape of the pressure curve is visualized in Figure 4.6 as profile C. In profile C, the pressure rapidly decreases when hydrates form, creating a break-point in the pressure curve. The pressure profile might look like profile C if the hydrate growth is fast. This results in a small time until equilibrium. Experiment 11 is an example of a pressure curve which looks like profile C.

Note that even though the dissolved gas is not removed from the gas phase and into hydrates initially, the dissolved gas probably gets converted to hydrates when the system conditions enters the hydrate formation area. This means that the total amount of gas trapped inside the hydrates at equilibrium is equivalent to the moles of gas which reduce the system pressure by $\Delta P_{Dissolve} + \Delta P_H$.

Not all pressure curves obtained from the NTNU experiments fit into these profiles, and the majority of the pressure curves from the NTNU experiments are somewhere in between profile B and C.

4.1.9 Comparison of the NTNU Experiments

Twenty hydrate formation and four hydrate dissociation experiments were conducted during the spring of 2017. Several interesting results have been obtained and analyzed. This section will compare some of the experiments and discuss the differences and the similarities observed.

Note that the curves are shifted in such a way that the time shown are not from the beginning of the experiment, but from the time when the experiment's temperature surpassed a certain level. This is implemented to make the comparison of the experiments easier.

4.1.9.1 Comparison of Pressure Curves from experiment 3, 5, 9 and 20

Figure 4.7 compares the low salinity experiments without other additives in the aqueous solution, to the high salinity solution in experiment 9. There is a difference between the four pressure curves, both in terms of ΔP_H and shape of pressure curve.

Experiment 3 has the largest pressure drop within the first 24 hours. The pressure drops with almost one bar more compared to experiment 5, where 3.5wt% NaCl is dissolved into the water phase, suggesting that by adding 3.5wt% NaCl, the hydrate equilibrium is shifted approximately

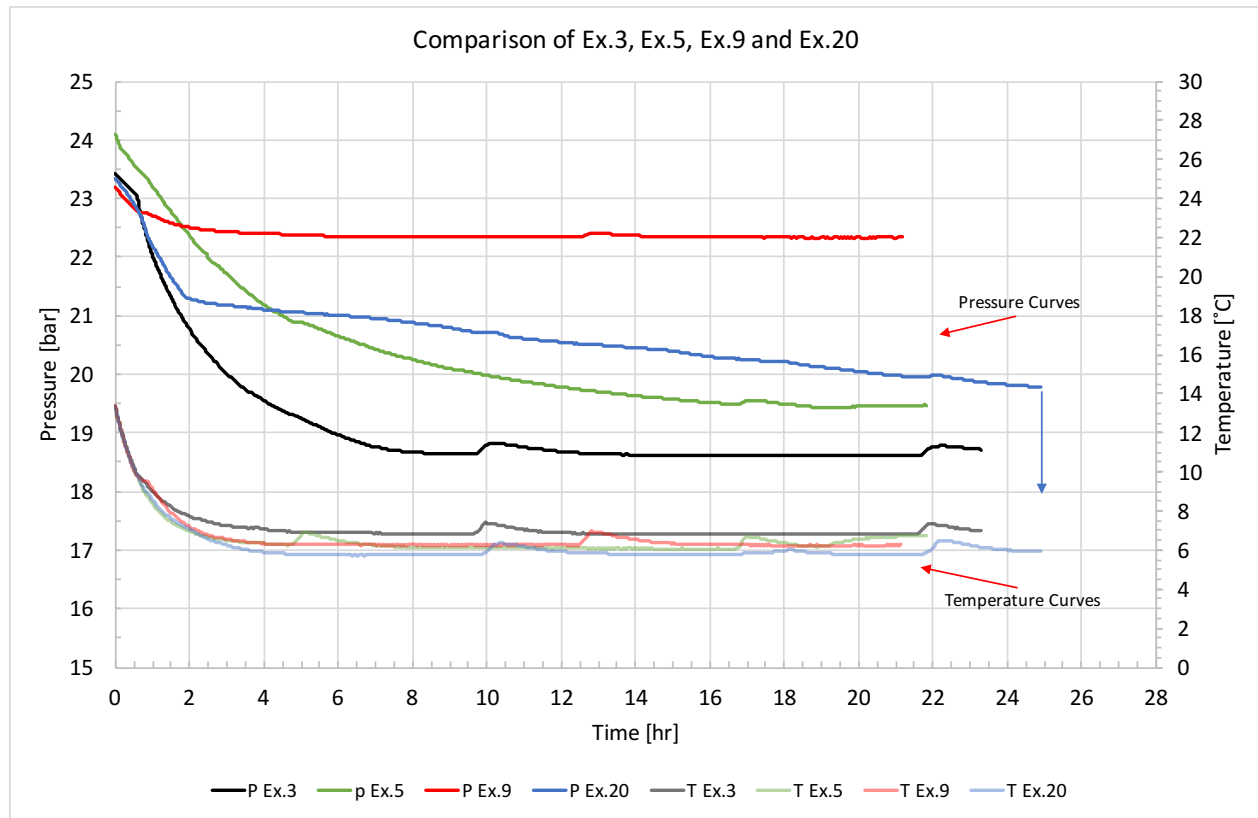


Figure 4.7: A comparison of experiment 3 (Nidelv water), 5 (3.5wt% NaCl in Fjord water), 9 (20wt% NaCl in Nidelv water) and 20 (tap water). The blue arrow indicates the final pressure in experiment 20, reached at Time = 65hrs. The red arrows indicate the collection of pressure and temperature curves.

one bar. By adding 3.5wt% to the water phase, the equilibrium is shifted -1.72°C , making the hydrate equilibrium pressure at 6.5°C equal to 14.0 bar. Thus, both experiment 3 and 5 are within the hydrate area when the system reaches steady state, and the 3.5wt% NaCl cannot explain the pressure difference between experiment 3 and 5.

The shape of the pressure curve in experiment 3 and 5 are similar to each other, suggesting a fast hydrate growth rate, following the pattern of profile B in Figure 4.6. The pressure curve in experiment 20 is almost linear, having a much slower growth rate compared to experiment 3 and 5. No hydrate growth occurs in experiment 9 due to the high concentration of NaCl. As shown in Figure 4.5, the pressure curve in experiment 9 follows the expected pressure drop due to temperature change and gas dissolving in water.

Since experiment 3, 5 and 20 have a similar salinity, the main factor affecting the hydrate formation is the water phase. Experiment 3 and 5 contain Nidelv water and experiment 20 tap water, thus the most likely explanation of the big difference in growth rate, is the amount of impurities. It seems like the impurities have a huge effect on the Δt_{equ} , but no effect on the total amount of hydrate growth, since the pressure in experiment 20 eventually reduces the most. The fact that all of these experiments reach steady state while the system conditions still are within the hydrate area suggests that there is a factor limiting further growth.

4.1.9.2 Comparison of Pressure Curves from Experiment 3, 6, and 11

Figure 4.8 compares experiment 3, containing no additives, with experiment 6 and 11, which contain additives. These are compared to observe the individual effect of two commonly used additives in drilling fluids. The three experiments have a very similar pressure profile.

At first glance, the barite seems to have little or no effect on hydrate growth other than acting as impurities, increasing the surface area, which can increase the growth rate. It would have been interesting to test barite and tap water to see if the barite acts similarly as the impurities in Nidelv water.

Experiment 11 differs from the two other experiments in terms of pressure decline after the break-point. The pressure declines faster in the 5wt% bentonite experiment, thus reaching equilibrium much faster. Most likely, the fast hydrate growth occurs because the bentonite particles act as hydrate nucleation and growth sites.

Experiment 6 and 3 have a similar pressure profile, but since experiment 6 contains barite particles, the barite affects hydrate formation in one of two ways. Either the barite particles do not act as nucleation sites, making the particles from the Nidelv water the only hydrate formation sites, or that the Nidelv water has enough particles present, thus the addition of more particles will not make the growth happen faster.

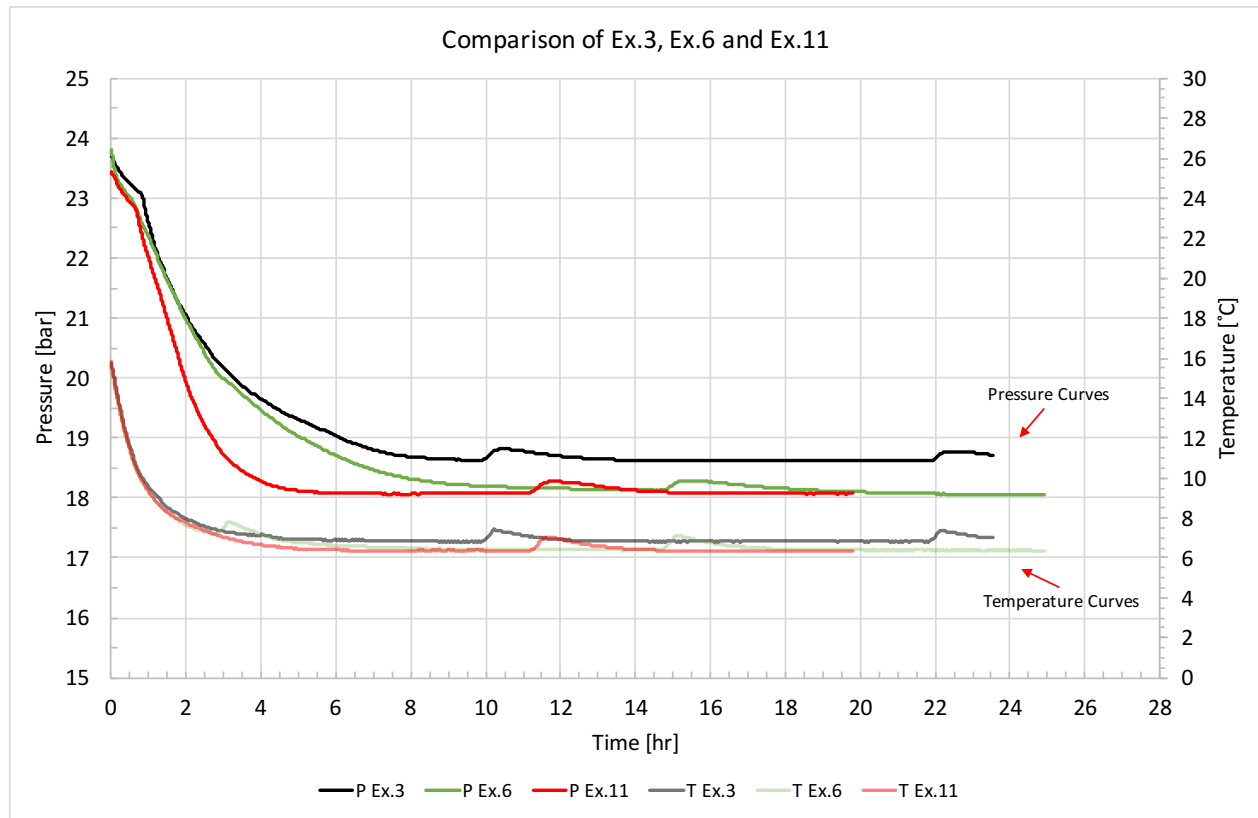


Figure 4.8: A comparison of experiment 3 (Nidelv water), 6 (10wt% barite in Nidelv water) and 11 (5wt% bentonite in tap-water). The red arrows indicate the collection of pressure and temperature curves.

When comparing the curves, it seems like there are factors which allow for faster hydrate formation in the bentonite solution in experiment 11. It could be the viscosity, which can lead to better mixing inside the pressure cell. Better mixing could increase the hydrate formation rate. On the other hand, an increase in viscosity might make hydrate formation more difficult since the water becomes less accessible. Another possibility is that the surface of the bentonite particles acts as very good nucleation sites, making fast hydrate formation possible. A combination of these factors could also be an explanation.

The equilibrium pressure is equivalent in both experiment 6 and 11, slightly below the final pressure in experiment 3. Corrected for the varying initial temperature, the total pressure drop in the three experiments are very similar. Based on this there is reason to believe that similar amounts of hydrates are generated in the three experiments.

4.1.9.3 Comparison of Pressure Curves from Experiment 3, 8, 13 and 17

Figure 4.9 compares experiment 8, 13 and 17, containing 10wt% of salt and tap water, with experiment 3, containing Nidelv water in the aqueous solution. There is a big difference in both steepness and equilibrium pressure in the different experiments. Figure 4.10 compares the final pressure and temperature in experiment 3, 8, 13 and 17 with their respective hydrate equilibrium curve. These curves are made by using the hydrate equilibrium curve for the NTNU gas mixture, and corrected for the temperature depression by using Equation 2.12.

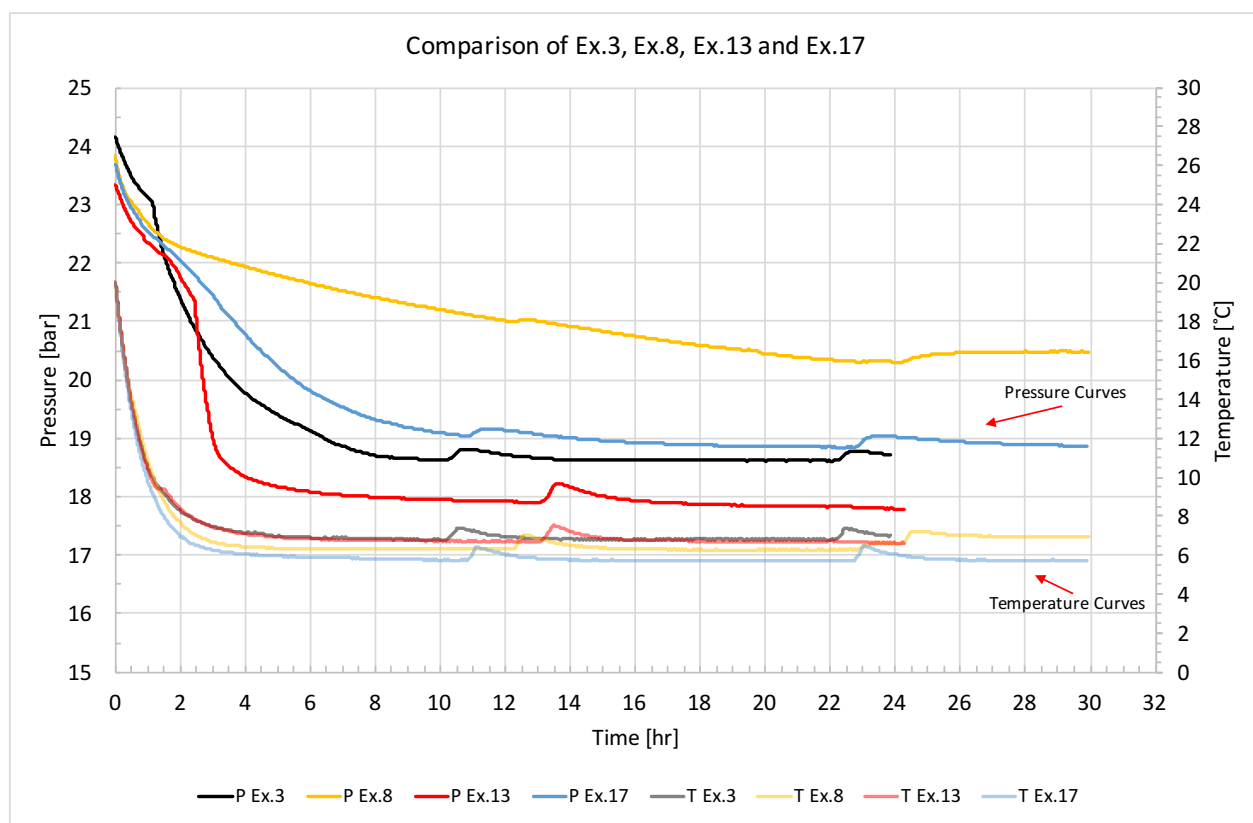


Figure 4.9: A comparison of experiment 3 (Nidelv water), 8 (10wt% NaCl in tap water), 13 (10wt% CaCl₂ in tap water) and 17 (10wt% KHCOO in tap water). The red arrows indicate the collection of pressure and temperature curves.

The final pressure and temperature in experiment 3 and 17 are within the hydrate area, whereas experiment 8 and 13 are outside the hydrate region. Since there are doubts about whether the temperature measurements are correct, as discussed in Section 4.1.4, the final conditions in

experiment 8 and 13 are corrected by -1°C . The corrected temperatures are plotted as triangles in Figure 4.10. Even if the temperature is corrected, the final conditions in experiment 8 and 13 are outside the hydrate area.

The pressure curve for experiment 13 looks strange, both in terms of steepness and ΔP_H . According to Table 2.1, CaCl_2 is a better hydrate inhibitor than KHCOO , contrary to the results observed in Figure 4.9. Thus the system pressure should have been higher, supported by the red hydrate equilibrium curve in Figure 4.10.

The steepness of the pressure curve in experiment 13 suggests that the hydrate growth rate was very fast, even faster than the growth in experiment 11. The pressure profile can be explained by a major leakage, but the fact that the pressure seems to stabilize after about seven hours, contradicts this hypothesis. Nevertheless, a leakage which is big at high pressures and becomes smaller as the pressure decreases, could explain the rapid pressure decline. A slight decrease in pressure is observed from six hours until the end of the experiment.

The system pressure is outside of the hydrate region most of the time in experiment 13. If hydrate formation occurred in the beginning of experiment 13, the dissociation process would begin after three hours, when the pressure reaches 20 bar. There is a possibility that hydrate formation and a leakage in the beginning of experiment 13 made the pressure drop very fast, until the system conditions moved outside the hydrate area. The hydrates then started to dissociate, which compensated for the pressure decrease due to the leakage. This way, the leakage was camouflaged by the hydrate dissociation. This theory could explain what occurred in experiment 13.

The pressure in experiment 17 behaves as expected theoretically. The final system pressure in experiment 17 is equivalent to the theoretical hydrate equilibrium pressure for the 10wt% KHCOO solution. This suggests that the hydrate formation stopped because the hydrate equilibrium was reached, and not because of some other factors, such as lack of communication between the gas and aqueous phase. This is supported by the ΔP_H , which is smaller in experi-

ment 17 than in experiment 3. This can indicate that the hydrate layer is thicker in experiment 3 compared to experiment 17, where it seems like communication was obtained throughout the entire experiment.

Experiment 8 is difficult to interpret because the system conditions are mainly outside the hydrate area. The pressure declines the first 24 hours before reaching steady state. A small leakage may have occurred which stopped after 24 hours. After 24 hours, the temperature fluctuations have a peak, which can explain why the pressure do not decrease for a period.

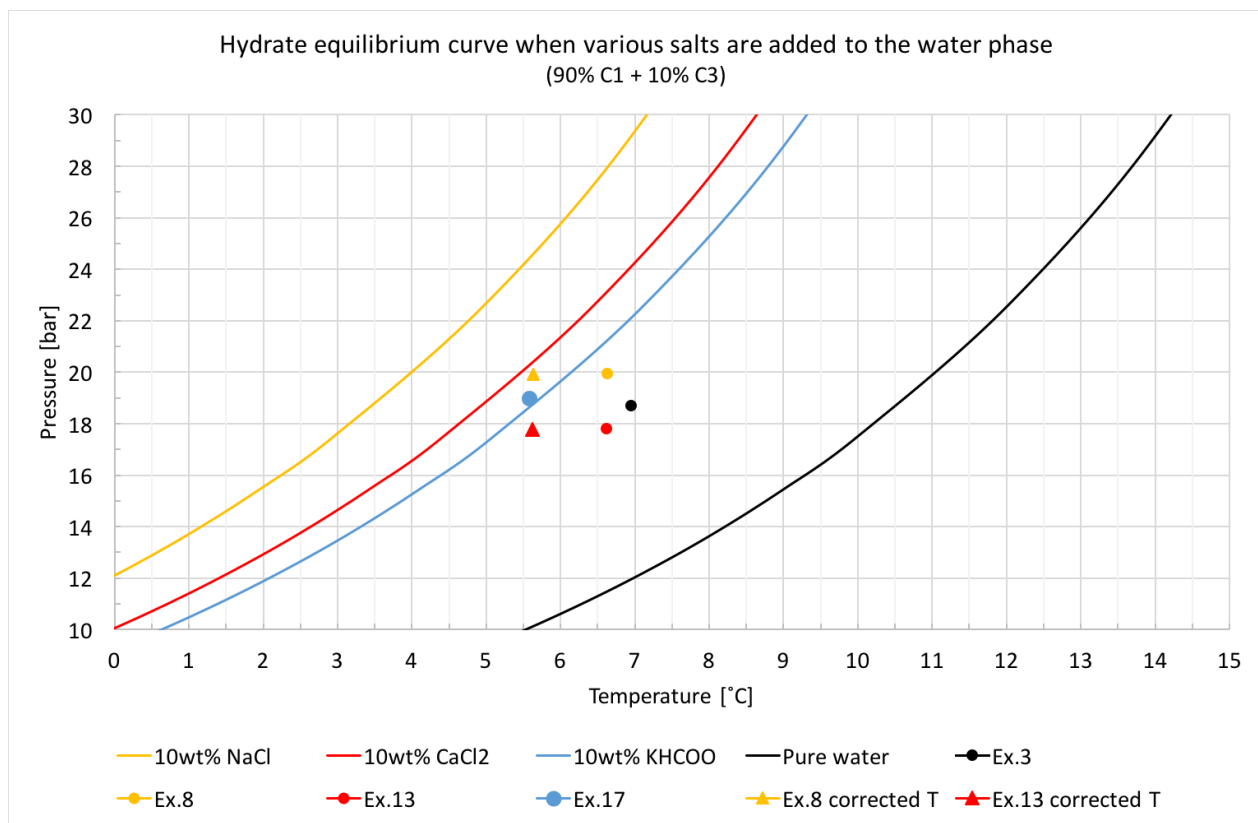


Figure 4.10: The hydrate equilibrium curves for various salts in solution are plotted and compared to the final conditions of the experiments performed with the same type of water base in the aqueous solution. The actual final conditions are marked with a circle coloured with the same colour as the related hydrate equilibrium curve. The final temperature of experiment 13 and 8 have been corrected by -1°C , marked as triangles.

4.1.9.4 Comparison of the Various Types of Hydrates Observed by Visual Inspection

Experiment 4, 5, 6, 11, 17 and 20 were opened in an attempt to observe hydrates after the experiments were stopped. Dissociation of hydrates where gas was released from the hydrate surface was observed in these experiments. To ensure that as much of the hydrates were present when opening the pressure cell, the pressure sensor and temperature sensor was disconnected inside the refrigerator, prior to depressurization. Then the pressure cell was moved into a fume hood and fully depressurized, before unscrewing the steel cap.

The pictures in Figure 4.11a, 4.12a, 4.13a and 4.13b were taken immediately after the removal of the steel cap. They show the hydrates observed in experiment 4, 11, 17 and 20 respectively. There is a notable difference in the type of hydrates observed in the pictures. While the hydrates are in the shape of a slurry in experiment 4 and 17, shown in Figure 4.13, where Fjord water and an aqueous 10wt% KHCOO solution were tested, solid hydrate chunks were observed when opening experiment 11 and 20. As shown in Table 3.1, the aqueous solution consisted of tap water and 5wt% bentonite in experiment 11, and tap water in experiment 20.

When looking at experiment 11 and 20, there is a possibility that the chunks were formed in these two experiments because of the increased viscosity in experiment 11, and the lack of impurities in the aqueous solution in experiment 20. By adding bentonite, the aqueous solution becomes more viscous. Even a small increase in the bentonite concentration will increase the viscosity. When hydrates form in the bentonite solution, the viscosity will further increase, as the bentonite concentration in the water phase increases as water transfers from the aqueous solution into the hydrates. The increased viscosity could make it more difficult for gas to come in contact with the water phase in the aqueous solution (Larsen, 2017). Consequently, it may be easier for hydrates to grow on existing hydrate surfaces rather than nucleating on other impurities present in the aqueous solution.

Another possibility is that the bentonite particles act as nucleation sites, contributing to fast hydrate formation onto bentonite particles. This theory is supported by the red pressure curve

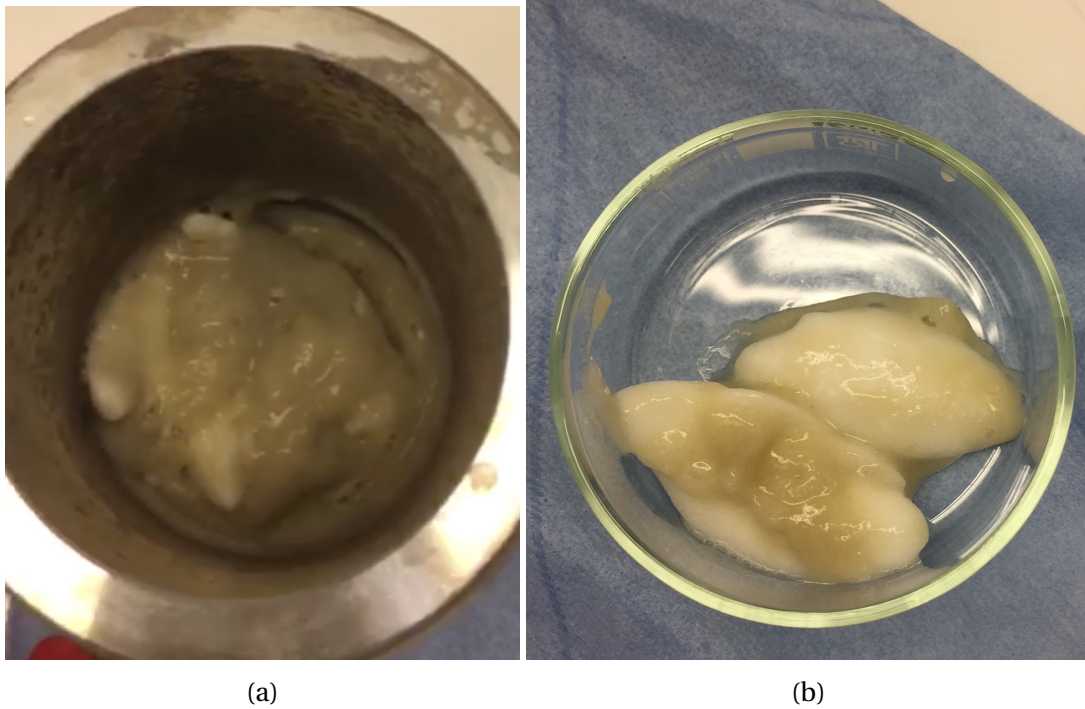


Figure 4.11: Hydrates observed by visual inspection in experiment 11. The bentonite slurry makes it difficult to see the hydrates inside the cell, but when picked up and moved to a beaker, the size and shape of the hydrate chunks can be observed. The glass beaker has a diameter of approximately 70mm (Gunhildrud, M., 2017).

for experiment 11 showed in Figure 4.8. The pressure curve decreases rapidly after entering the hydrate area, suggesting a fast hydrate growth. The fast growth implies many nucleation sites, which probably would generate hydrates in the form of a slurry. When the hydrates were inspected visually, one observed the chunks showed in Figure 4.11b. Thus, the hydrate particles may have grouped together over time to form uniform and oval chunks due to the high viscosity. When comparing these hydrate chunks with the one obtained in experiment 20, which has a more random distorted shape, it is reason to believe that different processes have occurred.

The lack of impurities in experiment 20 may be the reason why hydrate chunks were formed. When hydrates first form, only a limited number of particles start to grow. Further growth would then most likely occur on the surface of an already existing hydrate chunk instead of in the water phase because of the lower Gibbs free energy, as shown in Section 2.1.3 (Larsen, 2017).

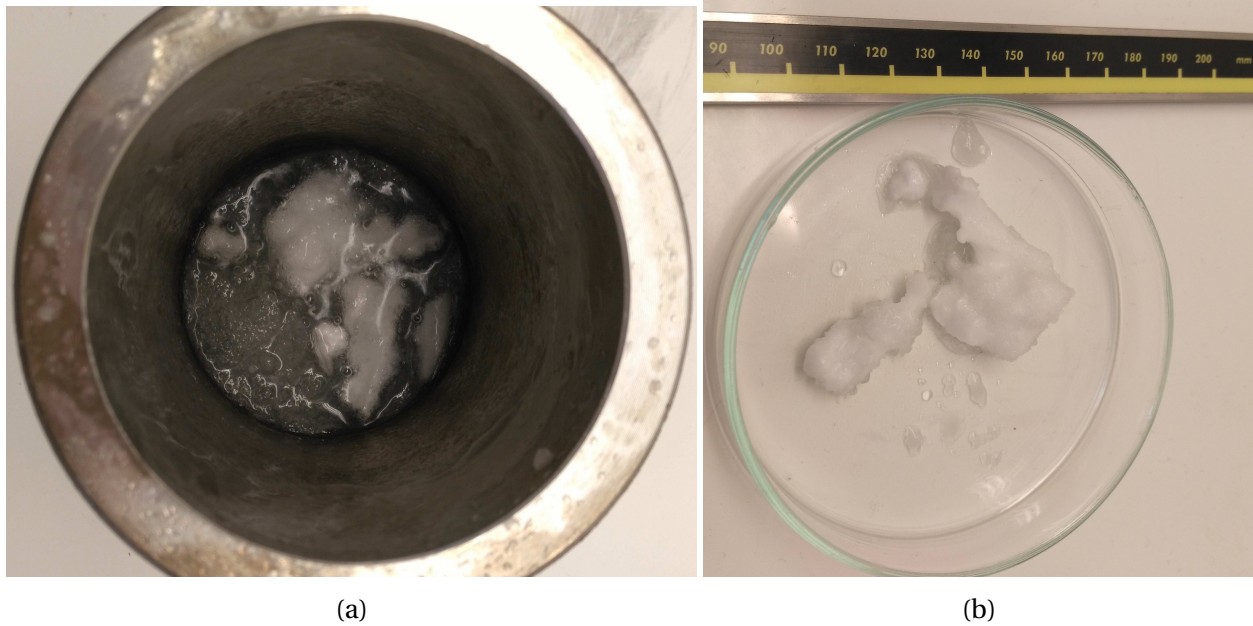


Figure 4.12: Hydrates observed by visual inspection in experiment 20. Several hydrate chunks, surrounded by a hydrate slurry were observed. The biggest lumps were removed from the cell and placed in a glass beaker. The glass beaker has a diameter of approximately 90mm (Helgestad, B., 2017).

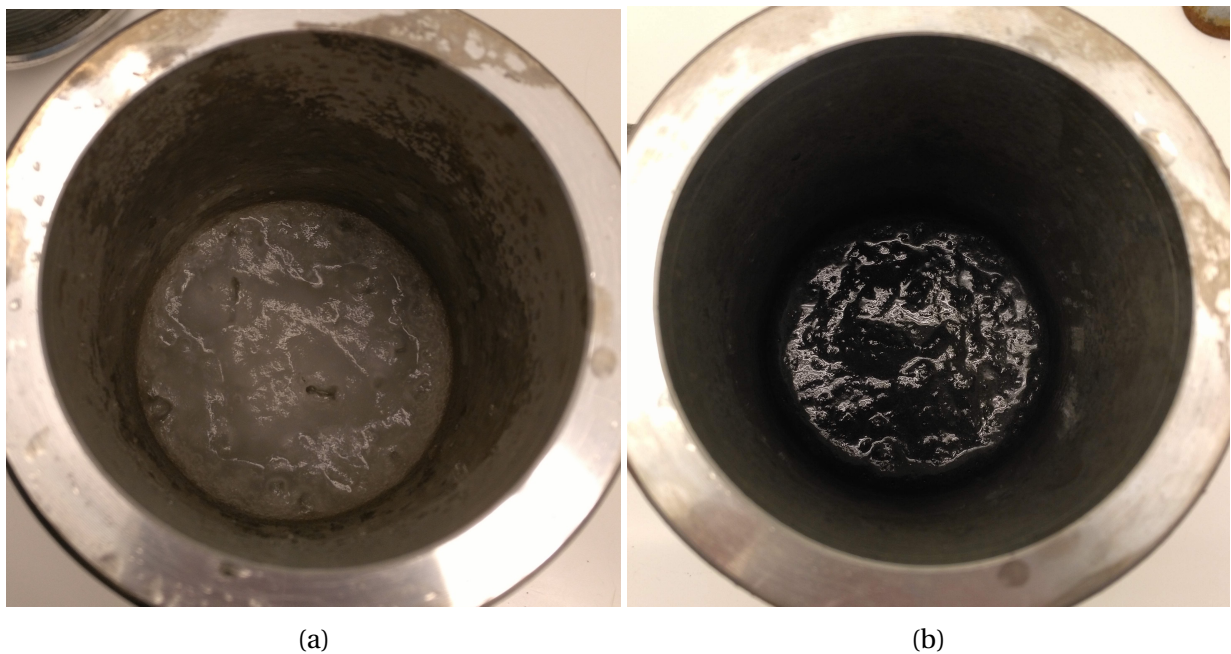


Figure 4.13: Hydrates observed in experiment 4 (a) and in experiment 17 (b). The hydrates were in the shape of a thick slurry in both of the experiments (Helgestad, B., 2017).

Experiment 20 has a different pressure curve than the other experiments. The pressure reduction is linear during the whole hydrate growth period, before it flattens out when the system reaches steady state, as discussed in Section 4.1.9.1. The pressure decline in most of the other experiments are exponentially shaped. The exponential decrease is natural because as the pressure decreases, the driving force becomes weaker, resulting in a slower growth. When the hydrate layer above the aqueous solution becomes thicker, less of the aqueous solution is exposed to the gas, thus exponential decrease is expected.

In experiment 20, several factors may balance each other, resulting in a linear pressure decrease. As the hydrate chunk increases in size, the surface area becomes larger. The increase in area suggest that the hydrate growth rate should increase. On the other hand, since the pressure reduces in the pressure cell as the hydrates grow, the driving force for growth slowly diminishes. These two mechanisms are believed to act against each other, making the growth rate constant.

As mentioned, the hydrate formation in experiment 4 and 17, observed in Figure 4.13, are of a significantly different character than in experiment 11 and 20. Here, the hydrates formed are in the shape of a slurry, and not solid chunks. Some type of slurry was also observed in experiment 20, in the water surrounding the solid chunks. The hydrate slurry most likely formed because hydrate formation occurred on several separate sites in the aqueous solution. Thus, a continuous liquid hydrate phase is created on the top of the aqueous solution. A continuous hydrate slurry on top of the water phase could limit further growth of hydrates, which is discussed in Section 4.1.10.

4.1.10 Hydrate Formation in Theory

When looking at the hydrate equilibrium curve for the gas mixture used in the NTNU experiments, at a temperature of 6°C, the hydrate equilibrium pressure is 10.63 bar. Experiment 20 was the experiment among the NTNU experiments with the biggest pressure reduction. Here the pressure stopped decreasing at 18.03 bar.

In theory, hydrate growth could and should continue until the pressure inside the pressure cell was reduced by another 7.40 bar, if enough water and gas are available. If one of these factors are limited, the growth will stop. The hydrate formation might have stopped at approximately 18 bar, due to lack of communication between the aqueous solution and the gas phase. In the experiments containing no inhibitor in the water phase, hydrates most likely occurred. When several cm³ of hydrate have formed inside the pressure cell, a hydrate layer is formed on top of the aqueous solution. The internal cross section area of the pressure cell is 38.48 cm², thus a 3 mm thick hydrate layer has accumulated when 11.55 mL of hydrates have formed.

This layer may be thick enough to prevent the stirring mechanism from creating contact between the water and gas phase. If no gas is in contact with the aqueous solution, the hydrate formation will stop. A continuous hydrate layer is most likely the main limiting factor for the NTNU experiments where no inhibitors are added to the water phase. This theory might explain why experiments such as 3, 4 and 17 reached steady state, while the system conditions still were inside the hydrate area.

4.1.11 Volume Reduction and Total Hydrate Volume

A calculation method was created in Microsoft Excel to find the volume of hydrates and volume reduction, based on the excess pressure drop observed, i.e. the difference between the final pressure and the expected pressure according to the real gas law. The model iterates the hydrate volume until the pressure, calculated based on the moles of gas left in the pressure cell, equals the final pressure of the experiment. The step by step description of the calculation method is given in Appendix B.3.

The results obtained from the NTNU experiments regarding volume reduction and hydrate volume formed are demonstrated in Table E.8 - E.10. Three different cases have been reviewed based on the percentage of occupied cavities that could occur in sII unit cells (Sloan and Koh, 2007). The cases are labeled as the *best case*, *worst case* and *in-between case*. In the best case, 100% of the large cavities and 90% of the small cavities are occupied. This yield a hydration

Table 4.2: Hydrate volume and volume reduction in each experiment performed at NTNU. Three scenarios are showed, an in-between case, best case and worst case.

Experiment	In-between case		Best case		Worst case	
	V_{hyd} [mL]	Volume reduction [%]	V_{hyd} [mL]	Volume reduction [%]	V_{hyd} [mL]	Volume reduction [%]
1*						
2	15.09	96.3	10.95	96.8	18.64	95.8
3	14.90	96.2	10.80	96.8	18.40	95.8
4	15.32	96.1	11.10	96.7	19.64	95.7
5	14.36	95.8	10.40	96.5	17.76	95.3
6	17.33	95.2	12.53	96.0	21.47	94.4
7	16.86	92.8	12.11	94.4	21.02	91.4
8	8.92	95.4	6.45	96.1	11.05	94.7
9	0.01	94.2	0.01	95.3	0.02	93.2
10*						
11	16.48	95.9	11.94	96.6	20.37	95.4
12	0.56	94.5	0.41	95.6	0.70	93.6
13	15.80	95.7	11.44	96.4	19.55	95.1
14	16.41	94.5	11.84	95.7	20.37	93.6
15	0.05	93.8	0.03	95.0	0.06	92.8
16*						
17	12.03	95.6	8.71	96.3	14.89	95.0
18	0.23	93.8	0.17	95.0	0.29	92.7
19	10.44	95.7	7.56	96.4	12.93	95.0
20	18.59	96.3	13.49	96.8	22.96	95.9

* Leakage

number of $N = 6.071$. In the worst case, 95% of the large cavities and 30% of the small cavities are occupied, which gives a hydration number of $N = 10.968$. 95% of the large cavities and 50% of the small cavities are occupied in the in-between case. This gives a hydration number of $N=8.716$. Table 4.2 shows the calculated hydrate volume and volume reduction for the three different cases. The volume reduction is calculated based on Equation 2.14.

In order to analyze and discuss these results, two additional tables were created. Table 4.3 focus on the volume reduction observed, while Table 4.7 focus on total hydrate volume formed. The in-between case is used for discussion. Both tables are organized from greatest to lowest amount

of hydrates/volume reduction. Based on these tables, the effect the additives have on hydrate formation and volume reduction has been analyzed.

4.1.11.1 Volume Reduction, NTNU Experiments

Table 4.3: volume reduction of the experiments performed at the NTNU laboratory in a decreasing order, organized from greatest to smallest (in-between case).

Experiment	Mud composition	$n_{gas, used}$ [mole]	Volume reduction [%]
20	Tap water	0.09508	96.3
2	Nidelv water	0.07718	96.3
3	Nidelv water	0.07619	96.2
4	Fjord water	0.07832	96.1
11	Tap water, 5wt% Bentonite	0.08428	95.9
5	3.5wt% NaCl	0.07344	95.8
13	Tap water, 10wt% CaCl ₂	0.08083	95.7
19	Tap water, 5wt% Bentonite, 10wt% KHCOO	0.05342	95.7
17	Tap water, 10 wt% KHCOO	0.06154	95.6
8	10wt% NaCl	0.04563	95.4
6	Nidelv water, 10wt% Barite	0.08865	95.2
14	Tap water, 10wt% CaCl ₂ , 5wt% Bentonite, 10wt% Barite	0.08395	94.5
12**	Tap water, 20wt% CaCl ₂ , 5wt% Bentonite	0.00288	94.5
9**	20wt% NaCl	7.706E-05	94.2
15**	Tap water, 20wt% CaCl ₂ , 5wt% Bentonite	0.00024	93.8
18**	Tap water, 30wt% KHCOO	0.00118	93.8
7	Nidelv water, 30wt% Barite	0.08626	92.8

** Assumed not possible to form hydrates in this system at the given pressure and temperature conditions.

The volume reduction in the in-between case ranges from 92.8 for 30wt% barite to 96.3 % for tap water, which is presented in Table 4.3. Observe that the volume reduction is not directly affected by how many moles gas have been used to form hydrates.

The effect NaCl has on volume reduction

Table 4.4 illustrates that only a minor difference in volume reduction exist in the different experiments. Experiment 9 is not included in this analysis because the system conditions are outside the hydrate region, thus hydrate formation is impossible. The biggest volume reduction is observed in 100% tap water, while the smallest volume reduction is in the system with 10wt% NaCl. The volume reduction is in a descending order with increasing weight percentage NaCl added to the water phase.

Table 4.4: The effect NaCl has on volume reduction.

Experiment	Mud composition	$n_{gas,used}$ [mole]	P_{final} [bar]	Volume reduction [%]
20	Tap water	0.09508	18.03	96.3
2	Nidelv water	0.07718	18.55	96.3
3	Nidelv water	0.07619	18.71	96.22
4	Fjord water	0.07833	18.75	96.1
5	Fjord water, 3.5wt% NaCl	0.07344	19.48	95.8
8	Tap water, 10wt%NaCl	0.04563	19.93	95.4
9**	Nidelv water, 20wt% NaCl	7.706E-05	22.34	94.2

** Assumed not possible to form hydrates in this system at the given pressure and temperature conditions.

Table 4.4 shows that less NaCl added to the water phase, gives a lower final pressure. A lower pressure in the pressure cell might indicate that more moles of gas have been used to form hydrates, which in turn indicate more hydrate formation. Based on this observation, it is reasonable to think that the volume reduction should increase with decreasing final pressure. This theory seems to apply for systems where only NaCl is added to the water phase. For systems with different compounds added to the aqueous solution, the amount of hydrates formed does not solely determine the volume reduction. This is because all parameters used to calculate the volume reduction in Equation 2.14 are dependant on each other, thus the ratio determines the volume reduction. This explains why all experiments have a similar volume reduction independent of total moles gas used.

Comparison of the effect NaCl, CaCl₂, Barite and KHCOO on the volume reduction.

The difference in volume reduction caused by the different additives in Table 4.5 is barely recognizable, only a difference of approximately 0.5% is observed. As described above, the ratio of the variables in Equation 2.14 determines the volume reduction.

Note that the volume reduction for the salts increase with decreasing final pressure. This trend was also found in the comparison of various amounts of NaCl added to the aqueous solution. More research and experiments must be conducted in order to verify the trend.

Table 4.5: Comparison of the effect of 10wt% NaCl, CaCl₂, Barite and KHCOO on volume reduction.

Experiment	Mud composition	$n_{gas,used}$ [mole]	P_{final} [bar]	Volume reduction [%]
13	Tap water, 10wt%CaCl ₂	0.08083	17.79	95.7
17	Tap water, 10 wt% KHCOO	0.06154	18.98	95.6
8	Nidelv water, 10wt% NaCl	0.04563	19.93	95.4
6	Nidelv water, 10wt% Barite	0.08865	18.04	95.2

General observations regarding volume reduction

Figure 4.14 illustrates the volume reduction extrapolation for the NTNU gas. It shows that the volume reduction decreases with increasing pressure, and that a smaller hydration number yields a greater volume reduction.

The volume reduction in the experiments conducted at NTNU does not differ much because the parameters used to calculate the volume reduction are related, as shown in Equation 2.14. The moles of gas used to form hydrates does not have a direct impact on the volume reduction. Therefore, a larger system with equivalent conditions would experience the equivalent volume reduction. Since the system pressure in the NTNU experiments is relative low, the volume reduction for the three different cases are very similar.

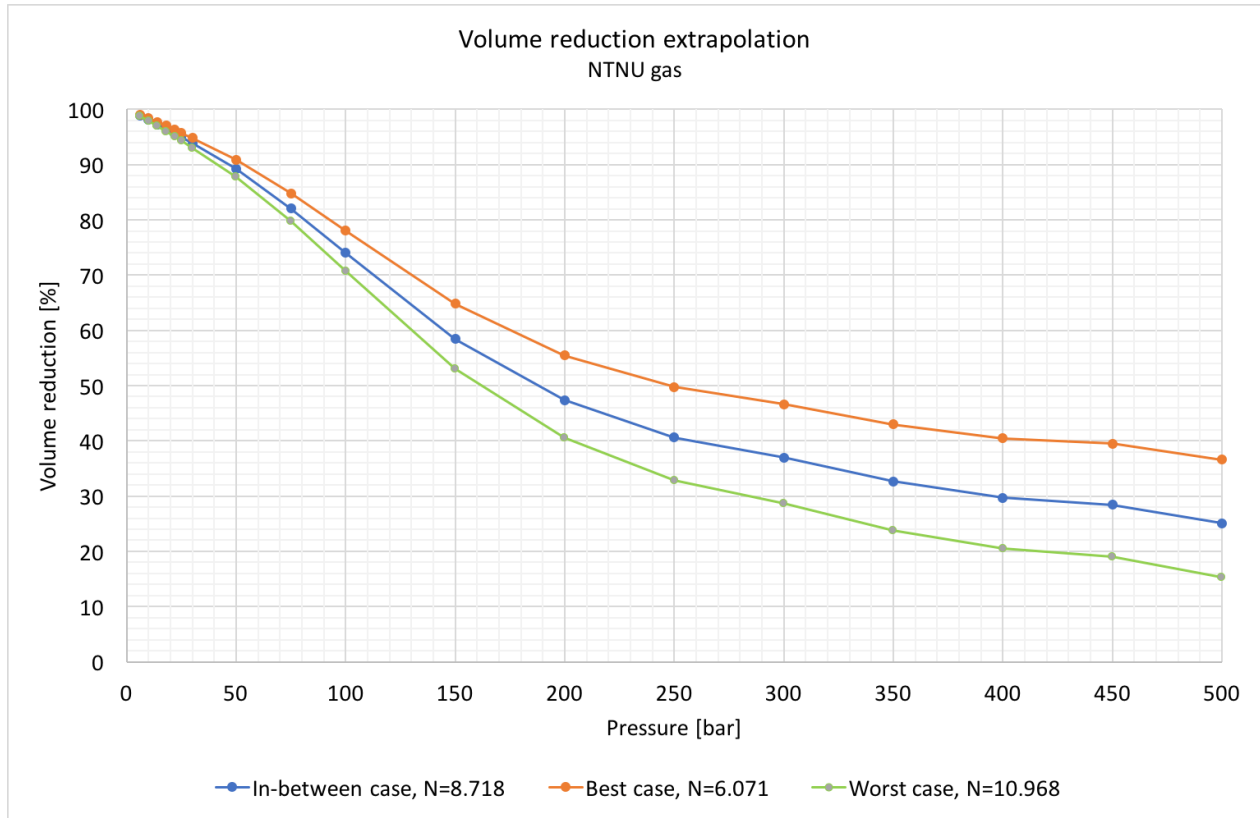


Figure 4.14: Volume reduction extrapolation for the NTNU gas at 6 °C. The volume reduction for three different hydration numbers is considered.

4.1.11.2 Total Hydrate Volume

Table 4.7 demonstrates that total hydrate volume is directly related to the moles of gas used. An increase in gas used will result in an increase in hydrate volume. Therefore, it is reasonable to assume that total volume of gas used would yield a similar effect. It follows the same trend, but with one exception. Experiment 14 has the second largest volume of gas used, but only the fifth highest hydrate volume. This might be due to the low final system pressure at 16.36 bar.

The effect of NaCl on the total hydrate volume

Table 4.6 shows the hydrate volume in the various experiments containing different amounts of NaCl. Less NaCl yields a greater volume of hydrates, except in the Fjord water experiment. It is

assumed to contain more NaCl than the Nidelv water experiments, due to a higher density. An explanation might be that experiment 3 and 4 were stopped while hydrates still were forming. This is based on the observation that it took approximately 60 hours for tap water in experiment 20 to stabilize, whereas experiment 3 and 4 were stopped after 21 hours and 23 hours. On the other hand, experiment 2 ran for almost 70 hours, where the pressure stabilized after approximately 20 hours.

Table 4.6: The effect NaCl has on hydrate growth.

Experiment	Mud composition	P_{final} [bar]	$n_{gas, used}$ [mole]	$V_{gas, used}$ [mL]	V_{hyd} [mL]
20	Tap water	18.03	0.09508	99.40	18.59
4	Fjord water	18.754	0.07832	81.22	15.31
2	Nidelv water	18.548	0.07718	80.93	15.09
3	Nidelv water	18.71	0.076198	79.46	14.89
5	3.5wt% NaCl	19.48	0.073440	74.28	14.36
8	10wt% NaCl	19.93	0.045626	46.65	8.92
9**	20wt% NaCl	22.34	7.706E-05	0.073*	0.02*

* Methane solubility in the water phase has been taken into account.

** Assumed not possible to form hydrates in this system at the given pressure and temperature conditions.

If more impurities exist in the Fjord water than in the Nidelv water, more surface areas where hydrates can form exist in the Fjord water. The hydrate formation speed is dependant on the surface areas available in the aqueous solution (Larsen, 2017). This theory can be supported by looking at Figure A.2, A.3 and A.4. These plots show that experiment 4 has a shorter time until equilibrium is reached compared to experiment 2 and 3. This might indicate that more particles have been available for hydrates to form.

Since the difference in hydrate volume is quite small in experiment 2, 3 and 4, another possible explanation is that the initial volume gas used to calculate the volume of hydrates formed is incorrect. This has to do with the fact that the volume of water filled into the pressure cell was determined by a beaker and not by weight, which gives a greater error in exact volume. An increase in mud volume yields a decrease in hydrate volume. Experiment 2, 3 and 4 reached

Table 4.7: Hydrate volume organized from greatest to smallest value, in the experiments conducted at the NTNU laboratory. The in-between case is considered.

Experiment	Mud composition	$n_{gas, used}$ [mole]	$V_{gas, used}$ [mL]	V_{hyd} [mL]
20	Tap water	0.09508	99.40	18.59
6	Nidelv water, 10wt% Barite	0.08865	93.73	17.33
7	Nidelv water, 30wt% Barite	0.08626	90.19	16.86
11	Tap water, 5wt% Bentonite	0.08428	89.47	16.48
14	Tap water, 10wt% CaCl ₂ , 5wt% Bentonite, 10wt% Barite	0.08395	98.00	16.41
13	Tap water, 10wt% CaCl ₂	0.08083	87.52	15.80
4	Fjord water	0.07832	81.22	15.31
2	Nidelv water	0.07718	80.93	15.09
3	Nidelv water	0.07619	79.46	14.89
5	3.5wt% NaCl	0.07344	74.28	14.36
17	Tap water, 10 wt% KHCOO	0.06154	64.07	12.03
19	Tap water, 5wt% Bentonite, 10wt% KHCOO	0.05342	62.34	10.44
8	10wt% NaCl	0.04563	46.65	8.92
12**	Tap water, 20wt% CaCl ₂ , 5wt% Bentonite	0.00288	3.16*	2.37
18**	Tap water, 30wt% KHCOO	0.00118	1.15*	2.22
15**	Tap water, 20wt% CaCl ₂ , 5wt% Bentonite	0.00024	0.23*	1.86
9**	20wt% NaCl	7.706E-05	0.07*	1.77

* Methane solubility in the water phase is considered.

** Assumed not possible to form hydrates in this system at the given pressure and temperature conditions.

equilibrium in the system, while still being inside the hydrate area. This suggests that another factor limited further growth. A hydrate layer on the gas-water interface could separate the two phases, preventing the hydrate formation.

These experiments support the idea that NaCl acts as an inhibitor in the drilling fluid, preventing hydrate formation. This is because the hydrate equilibrium curve is shifted to the left, which is less favourable for hydrate formation. Figure 4.15 shows how the equilibrium curve is moved to the left with greater weight percentage of NaCl. The coloured dots show the points where the different experiments reached steady state. Observe that the final conditions in both experiment 8 and 9 are right of their respective hydrate equilibrium curve, thus no hydrates should form.

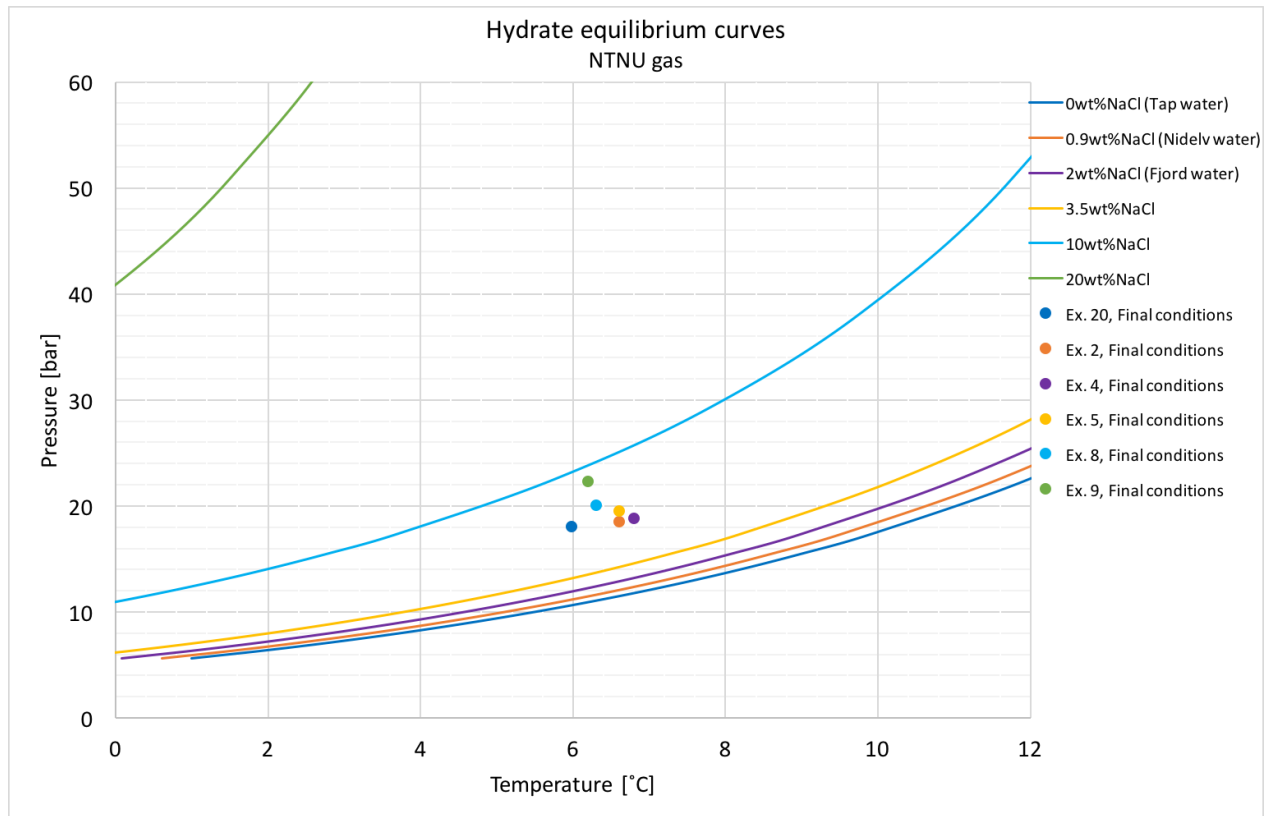


Figure 4.15: Hydrate equilibrium curves for different wt% NaCl for the NTNU gas.

Experiment 8, containing 10wt% NaCl, is close to the hydrate equilibrium curve. Figure 4.15 shows that the final pressure and temperature conditions are outside of the hydrate region, whereas Figure 4.16 demonstrates that it is inside the hydrate zone during the experiment.

The coloured dots in Figure 4.15 represent the final conditions, whereas Figure 4.16 shows both the final condition, as a red triangle, and the point where the temperature started to stabilize around 6°C, as a green triangle. Initially, the pressure and temperature conditions are inside the hydrate region according to Figure 4.16, and hydrate formation should be possible. If hydrate formation occurred in this experiment, either the temperature sensor showed an incorrect temperature or the hydrate equilibrium curve obtained from HYSYS software was calculated incorrectly. Note that the temperature was corrected with -1°C based on findings discussed in Section 4.1.4.

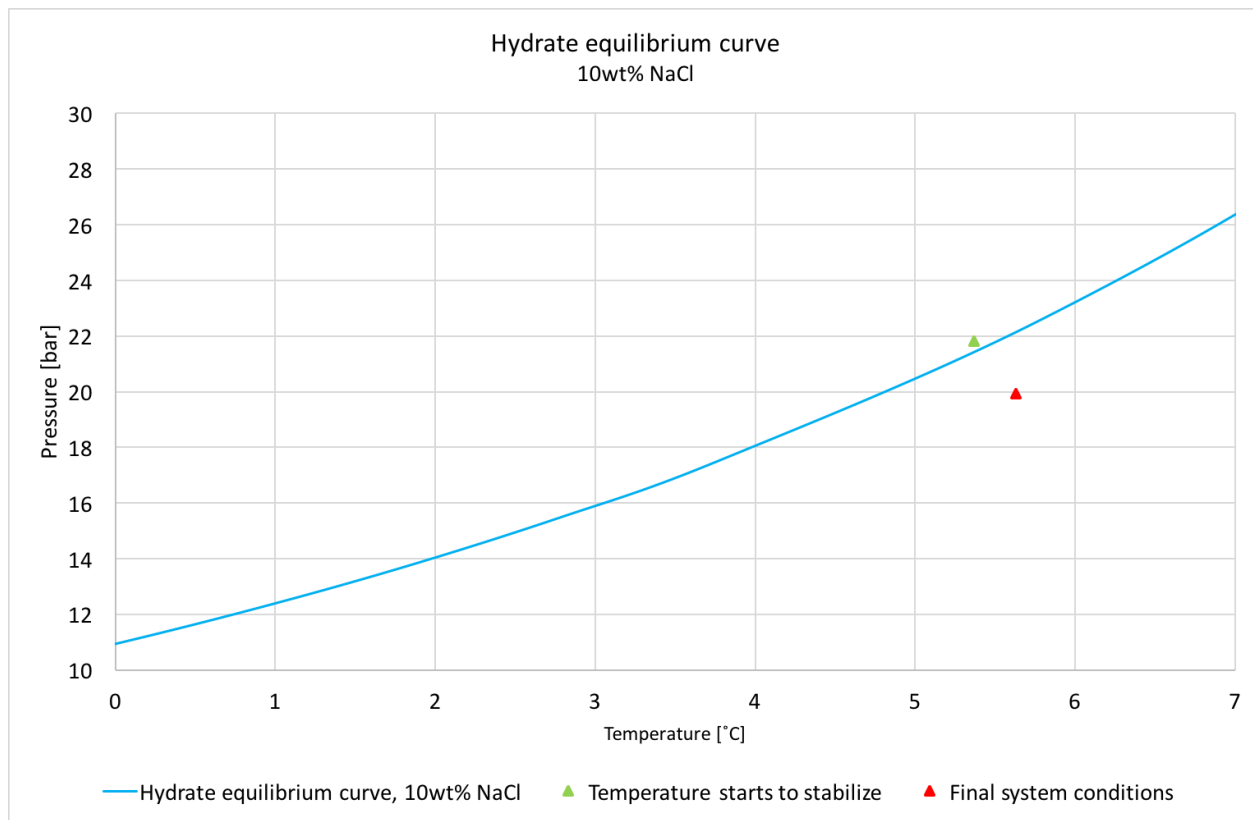


Figure 4.16: Hydrate equilibrium curve for 10wt% NaCl.

The pressure drop observed in Figure A.8 might be a result of a small leakage. The first 25 hours, the pressure drop is more distinct compared to the next 70 hours. One explanation can be that impurities such as salt or barite became stuck in the O-ring, which cause the gas to leak from the pressure cell at high pressures. When the pressure is lowered, the leakage may reduce. The pressure curve in Figure A.8, does not seem fully stabilized when the experiment was ended. Another possible explanation is that the 3-way valve was not completely closed, making gas escape from the pressure cell.

Calculations based on the final pressure and temperature in experiment 9 indicated that a small amount of hydrates had formed. This should not be possible according to the hydrate equilibrium curve. The gas might be dissolved into the aqueous solution as discussed in Section 3.1.4 and 4.1.6, instead of forming hydrates. When taking the methane solubility into account, the hydrate volume is almost reduced to zero, as shown in Table 4.10.

Comparison of the effect NaCl, CaCl₂, Barite and KHCOO have on hydrate formationTable 4.8: Comparison of 10wt% NaCl, CaCl₂, Barite and KHCOO.

Experiment	Mud composition	P_{final} [bar]	$n_{gas, used}$ [mole]	$V_{gas, used}$ [mL]	V_{hyd} [mL]
6	Nidelv water, 10wt% Barite	18.04	0.08865	93.73	17.33
13	Tap water, 10wt%CaCl ₂	17.79	0.08083	87.52	15.80
17	Tap water, 10 wt% KHCOO	18.98	0.06154	64.07	12.03
8	Nidelv water, 10wt% NaCl	19.93	0.04563	46.65	8.92

Based on the final pressure and temperature in the experiments shown in Table 4.8, it is observed that NaCl acts as the best hydrate inhibitor of the additives tested, whereas barite has no inhibiting effect. The table is organized from highest to lowest hydrate volume value, showing which additives inhibit the least and which inhibit the most among the tested additives. These findings contradicts with the results observed in Table 2.1, which shows that CaCl₂ is a more efficient inhibitor than KHCOO.

Experiment 16, containing 10wt% bentonite, leaked and is therefore not included in the comparison. It would have been interesting to see how 10wt% bentonite affects hydrate formation as 5wt% bentonite initiated hydrate chunks.

The inhibiting effect of KHCOO when bentonite is present.

Table 4.9: Hydrate volume in solutions with 5wt% bentonite, 10wt% KHCOO and the combination of the two.

Experiment	Mud composition	P_{final} [bar]	$n_{gas,used}$ [mole]	V_{hyd} [mL]
11	Tap water, 5wt% Bentonite	18.07	0.08428	16.48
17	Tap water, 10 wt% KHCOO	18.98	0.06154	12.03
19	Tap water, 5wt% Bentonite, 10wt%KHCOO	17.19	0.05342	10.44

Table 4.9 demonstrates that less hydrates form when both bentonite and KHCOO exist in the aqueous solution. An explanation might be that the KHCOO reacts with the impurities in the

bentonite, making them less available for hydrate nucleation. At the same time, the hydrate equilibrium curve is shifted due to the KHCO_3 , making the hydrate region smaller. The viscosity increase could have made it more difficult to form hydrates, since the water is less accessible in the aqueous solution.

General observations regarding hydrate volume formed

Table 4.7 shows that the moles of gas used to create hydrates is directly related to the total volume of gas hydrates formed. This conclusion can also be made based on Equation B.17, used to calculate hydrate volume. Experiment 14 is the only exception, which has the second highest amount of gas volume used, but only the fifth highest amount of hydrate volume formed. When looking at the pressure-temperature plot for experiment 14, a sudden drop in the pressure after 9 hours is observed, as shown in Figure A.14. This pressure drop might have occurred due to a hydrate plug that formed on, or nearby, the pressure sensor and suddenly loosened. This plug might isolate a gas zone, making it lose the communication with the rest of the pressure cell volume. Thus, a different pressure was measured by the sensor, than the actual pressure in the system (Fossen, 2017a).

It is reasonable to believe that no hydrate formation occurred in the NTNU experiments containing salt concentrations greater than 20wt%. Even if the final pressure and temperature suggests hydrate formation in some of these experiments, it is more likely that there is another explanation for the additional pressure drop. As stated previously, some of the methane could dissolve in the aqueous solution. Table 4.10 shows the "new" hydrate volume formed, $V_{hyd,modified}$, when assuming a molality of 0.05 mol/kg (Duan and Mao, 2006).

Barite seems to induce hydrate formation rather than inhibit it. In experiment 6 with Nidelv water and 10wt% barite, a greater amount of hydrates were formed compared to experiment 2 and 3 where only Nidelv water was used. The surface of barite particles might be more "dirty" than particles from the other additives, which makes it easier for hydrates to start forming, as more surface area is available. It might also lead to an increase in hydrate growth rate. This

Table 4.10: Hydrate volume obtained from calculations when methane dissolved into the aqueous solution has been considered and not.

Experiment	$V_{hyd,experiment}$ [mL]	$V_{hyd,modified}$ [mL]
9	1.765	0.015
12	2.367	0.563
15	1.863	0.046
18	2.218	0.230

finding is of particular interest as barite is a commonly used additive in the drilling mud. More experiments are required in order to verify if this observation yields for other systems.

Table 4.7 shows that 10wt% CaCl_2 , tested in experiment 13, has a greater inhibiting effect alone, than in combination with barite and bentonite, tested in experiment 14. When looking at the hydrate volume, there are almost no difference between experiment 11, containing 5wt% bentonite and experiment 14, containing tap water, 10wt% CaCl_2 , 10wt% barite and 5wt% bentonite. This suggests that either the barite and the CaCl_2 cancel each other out or that both the bentonite and barite particles are more dominated than the CaCl_2 , thus inducing instead of preventing hydrate formation.

4.1.11.3 The Relationship Between Volume Reduction and Total Hydrate Volume in NTNU Experiments

There is no apparent relationship between which experiments have formed much hydrates and how that affects the volume reduction. For instance, experiment 6, which has the second largest hydrate volume value, has only the eleventh highest volume reduction, while experiment 20 has both the largest hydrate volume and the greatest volume reduction. This is shown in Table 4.11. As discussed above, the volume reduction is determined by a ratio where all parameters are related. The volume reduction is therefore not directly affected by the moles of gas used, whereas the hydrate volume is directly related to moles of gas used. The pressure affects the volume reduction.

Table 4.11: Experiments performed at NTNU showing the volume reduction and hydrate volume formed listed in a decreasing order.

Experiment	Volume reduction [%]	Experiment	V_{hyd} [mL]
20	96.3	20	18.59
2	96.3	6	17.33
3	96.2	7	16.86
4	96.1	11	16.48
11	95.9	14	16.41
5	95.8	13	15.80
13	95.7	4	15.31
19	95.7	2	15.09
17	95.6	3	14.89
8	95.4	5	14.36
6	95.2	17	12.03
14	94.5	19	10.44
12**	94.5*	8	8.92
9**	94.2*	12**	0.56*
15**	93.8*	18**	0.23*
18**	93.8*	15**	0.05*
7	92.8	9**	0.02*

* Methane solubility in the aqueous solution has been considered.

** Assumed not physically possible to form hydrates in this system at the given pressure and temperature conditions.

4.1.12 Experimental Errors

4.1.12.1 Pressure Measurement Error

Abnormal and unexpected results were observed in experiment 12 due to surprising changes in the pressure log. The total running time for the experiment was 94.5 hours. The first 17 hours followed the same pressure and temperature pattern as most of the other experiments. It seemed like the system was in steady state, in the period between 5 and 17 hours. The pressure dropped suddenly after 17.8 hours from 19.6 bar to 18.2 bar over a period of five hours. After this, three sudden pressure peaks were observed. The peaks happened after 33.1 hours, 49.8 hours and 84.4 hours. The pressure remained steady after this. A similar pressure behavior was

observed in experiment 14.

The most plausible explanation for the abnormal and unexpected results is that the pressure sensor was not recording the actual system pressure during parts of experiment 12 and 14. This could occur as a result of hydrate formation on the pressure sensor, or damage to the sensor itself. The pressure at the end of the experiment is approximately the same as the pressure in the period prior to the sudden pressure drop. Thus, the first 17 hours of the experiment may show the correct pressure and temperature. Since the sensor is recording the correct pressure in later experiments, hydrate formation near the sensor is a more likely explanation.

4.1.12.2 Temperature Measurement Errors

Except from a few temperature data points in experiment 1, no outliers were removed from the pressure or temperature data. The temperature points removed from experiment 1 measured a temperature of 80°C over a period of a few seconds. Five of these outliers were removed from experiment 1. Comparing this to the millions of temperature data points logged, the pressure and temperature measurements are consistently precise.

It might be an error in the logging of the temperature, as discussed in Section 4.1.4, where the logged temperature showed a higher temperature than the actual system temperature. It has also been observed that the constant, stabilized temperature in all experiments vary. For instance, the average constant temperature in experiment 3 is logged to be 6.8°C while the average constant temperature for experiment 20 is 6.0°C. These temperature measurements were done in exactly the same refrigerator on the same temperature settings. Whether this discrepancy is due to error on the refrigerator or the temperature sensor is unknown.

In experiment 8, the temperature was constant for 20 hours before suddenly increasing by 0.7°C. The experiment continued to stay at this higher temperature for the next 70 hours. These observations may suggest that the temperature gauge is accurate, but is not tuned to the right temperature.

4.1.12.3 Varying Initial Pressure and Temperature

The system temperature and pressure should ideally have been equivalent in all the experiments. This would have made the various experiments more comparable, and made the analysis easier. When comparing the different experiments, this has been accounted for.

4.1.12.4 Errors in Volume Calculation of the Pressure Cell

The length and diameter of the temperature sleeve were determined using a sliding caliper. It has an accuracy of ± 0.1 mm. The diameter differed with 2 mm between the thickest and thinnest area of the sensor, thus an average thickness was used. To determine the volume of the hole where the temperature sleeve was located, the same sliding caliper was used for both the height and diameter. A greater error than ± 0.1 mm should be used to determine the hole diameter, because it was not possible to use the inside small jaws, due to the height of the steel cap. Therefore, the outside large jaws were used. When using the large outside jaws, there was no "wall" to stop the jaws from opening, so the authors had to decide the stop position of the jaws.

The sliding caliper was used to determine the diameter and height of the hole where the 3-way valve is positioned. The same uncertainties and errors yield for the determination of the height and diameter as for the temperature sleeve inlet hole. There are many uncertainties related to the volume of the relief valve, marked as number 4 in Figure 3.3. It is not known how far into the relief valve gas can migrate because there were no provided drawings or sketches of the new design, thus the length of the relief outlet was assumed to be just before the outlet of the relief valve (see red line in Figure 3.3, number 4). The inner diameter could not be measured and no drawings of the design have been provided. The inner diameter is assumed to be equal to the diameter of the 3-way valve hole.

The inlet hole for the pressure sensor was narrow, shown in Figure 3.3, making it impossible to use the sliding caliper directly to determine the height of the hole. Instead, a tiny plastic pipe

was inserted into the hole and a pen was used to mark the top of the hole. Then, the sliding caliper was used to determine the length. In order to determine the diameter of the hole, the same method was used as stated above with the outside large jaws.

The height and diameter of the steel cylinder was provided by Noralf Vedvik at the NTNU mechanical workshop. It is assumed that the steel cap is screwed onto the steel cylinder in a way that no excess air gap is created between the height of the steel cylinder and the steel cap.

The shape of the magnetic stir bar changed over time, and decreased during the running time of all the experiments performed. The volume used for the stir bar is the final volume after all experiments had been conducted. This means that the total volume in the pressure cell was smaller for the first experiments due to a greater volume of the magnetic stir bar. The volume was measured using a 10 mL glass test tube. The glass test tube has an accuracy of ± 0.2 mL.

4.1.12.5 Errors in Calculation Method of Hydrate Volume and volume reduction

Volume of pressure cell

The uncertainties related to the volume of the pressure cell affect the hydrate volume. By increasing the pressure cell volume, the amount of initial moles of gas increase. This will lead to an increase in gas and water moles used to form hydrates, which increases the hydrate volume. The volume reduction will stay unchanged in the conducted experiment.

Aqueous solution volume

The volume of the aqueous solution was determined using a syringe in the first 5 experiments. The syringe had an accuracy of ± 1 mL. The volume for the other experiments were determined by weight. To more easily compare the results obtained from the different experiments, a pre-determined volume of 150 mL was set for the aqueous phase. By following the steps showed in Appendix B.1, the total weight of the mud mixture in order to obtain a volume of 150 mL can be

calculated. The scale used had an accuracy of ± 0.001 g. A calculation error of the total weight needed in experiment 17 and 18 resulted in a greater volume of the initial aqueous solution. This is showed in Table E.7.

The uncertainty related to the initial volume of mud in the pressure cell impacts the error margin of total hydrate volume. When the aqueous solution volume increase, the initial gas volume decrease, which means that less gas is injected into the pressure cell. Less gas initially in place will result in fewer gas and water molecules being consumed by hydrates. Therefore, the hydrate volume decreases with an increase in aqueous solution volume. The volume reduction remains unchanged in the conducted experiment.

Z-factor

Both the initial Z-factor and the Z-factor obtained after hydrate formation is found from the Standing-Katz chart, shown in Figure A.25. The uncertainty lies in the rounding errors related to the critical temperature and pressure for methane and propane, when calculating the pseudo-critical pressure and temperature, as well as when calculating the pseudoreduced pressure and temperature. Another uncertainty is the readings of the pseudoreduced pressure and temperature on the Standing-Katz chart, which gives the Z-factor. A higher initial Z-factor value results in less moles of gas initially in place. Thus, not acquiring a correct value can affect the hydrate volume and volume reduction calculations.

Number of occupied cavities

The number of cavities occupied is determined by the volume of hydrates formed. In this calculation method, the hydrate volume is determined by a fixed hydration number. Otherwise, it would be difficult to obtain a hydrate volume. Three different cases have been considered. It is reason to believe that the amount of cavities occupied lies somewhere in between the "best case" and the "in-between case" (Larsen, 2017). The "best" and "worst" cases represent the

two extremes, when it comes to the number of occupied cavities. For a better determination of how many small and how many large cavities that are occupied is a software such as CSMGEM required (Sloan and Koh, 2007). The authors did not have access to such software.

Hydrate density

The hydrate density used in all three cases is 0.9 g/cm^3 . This density is obtained if all cavities are occupied in a methane clathrate (Chernov et al., 2017). This value is incorrect for the experiments performed at the NTNU laboratory, giving a significant error in the calculations. The main reason why this value is incorrect is that the gas composition is different, and that it is impossible for all the cavities to be occupied. Equation 4.3 enables the hydrate density to be calculated (Sloan and Koh, 2007). The fraction of methane and propane occupying the small and large cavities are two factors affecting the density. This can be determined using a software, which the authors did not have access to.

The fact that the identical hydrate density has been used for all the three cases is another calculation error. The hydrate density should be greater when more cavities are filled. When the hydrate density increases, more cavities are occupied, resulting in a smaller hydration number and less hydrate volume.

$$\rho = \frac{N_w MW_{H_2O} + \sum_{j=1}^C \sum_{i=1}^N \theta_{ij} v_i MW_j}{N_{Ava} V_{Cell}} \quad (4.3)$$

Gas density used to form hydrates

The gas phase density inside the pressure cell will change during hydrate growth, since both the amount of moles left in the cell and the volume reduction over time. An average of the initial and final gas density was used. The hydrate growth is faster initially and slows down when it is close

to reaching equilibrium. This means that most of the hydrates are formed in the early times of the hydrate formation process where the pressure is high. Thus, at the time when the most gas is consumed, the density are higher than the average density, making the average density used too low.

Moles of gas used to form hydrates

The moles of gas used to form hydrates is dependant on all the factors described above, and difficult to determine correctly. In this method, the excess pressure drop observed in the experiments which are not fully inhibited is assumed to occur as a result of hydrate formation. Parts of the pressure drop could be explained by a leakage or gas entering the aqueous solution.

Pressure and temperature conditions

The initial pressure and temperature regime affects the moles of gas initially in place, which affects the hydrate volume. If the initial temperature is high, less gas can be injected before reaching a pressure of 24 bar. This affects the hydrate volume, since the pressure in the system is lower when the system enters the hydrate area, resulting in a lower driving force.

Gas composition

The composition of the gas phase is assumed to stay constant during the entire experiment. In reality, the composition changes because the heavy molecules will create hydrates first, which makes the propane content in the NTNU gas phase decrease. Furthermore, the heavy compounds will go into the structure first, which makes it more difficult to form hydrates after a while.

4.1.12.6 Fluid Composition and Fluid Measurement Errors

When mixing the aqueous fluid phase, errors in both measurements and calculations may have occurred. An example of error in calculation is observed in experiment 17 and 18 where the density calculations of the fluid was slightly off, leading to a larger aqueous solution volume in these experiments compared to the other experiments. Other errors when measuring the weight of additives could have occurred, but none was detected when the numbers was back-calculated after the experiments were conducted.

When adding inhibitor to the aqueous solution, it is the relative amount of inhibitor to the water phase that decide the inhibiting effect. In experiments where several additives were added to the water phase, including salt, the inhibiting effect was larger than estimated. For instance, in experiment 14, where 20wt% CaCl₂, 10wt% barite and 5wt% were added to the water phase, the actual wt% of salt relative to the water was 11.76wt% and not 10wt%. In further experiments, the wt% of inhibitor should be calculated based on the mass of water and not the total mass of the aqueous solution. This error in inhibitor calculation was done in experiment 12, 14, 15 and 19.

4.1.12.7 Leakage

Minor leakages could have occurred in several of the experiments. Experiment 8 is an example where a minor leakage probably occurred without being verified visually by using leakage spray. In this experiment, the pressure was reduced by 0.4 bar during a period of 45 hours. A leakage affects the results, indicating that more moles of gas have been consumed by hydrates.

Small leakages which is difficult to verify visually are challenging to detect, unless heating the system back to initial temperature is performed. This is because low hydrate formation rate could affect the pressure in a similar way. Experiment 13 and 19 are examples where either a minor leakage, or slow hydrate formation occurred.

A major leakage was observed in experiment 10, 16 and possibly in experiment 1. It was believed that the pressure decline in experiment 1 indicated a leakage, however, it could have been hydrate formation, as the system temperature was inside the hydrate area from the start of the experiment. The leakage in experiment 1 was not verified by heating or leakage spray. In experiment 10 and 16 a leakage was observed visually, and confirmed by the pressure curve, which declined with a constant rate to a pressure outside the hydrate equilibrium curve. Thus, experiment 10 and 16 were not considered or analyzed further.

Gas Solubility

As given in Section 3.1.4, the solubility of methane in water can result in a 0.45 bar pressure decrease at the conditions of the NTNU experiments. The gas solubility varies with the gas composition and the aqueous fluid phase composition. Therefore, it is difficult to determine how much of the gas has dissolved into the aqueous solution in each experiment, i.e. the pressure drop due to dissolving gas. A worst-case estimate is 0.45, as the gas and fluid composition used in the experiment would result in a lower gas solubility.

In the hydrate volume calculations for the experiments where hydrate formation is believed to have occurred, all gas dissolved in the aqueous solution are assumed to be converted to hydrates. This is a reasonable assumption because the dissolved gas will be in contact with water when the system is inside the hydrate area, and probably be converted into hydrates (Larsen, 2017). Since it is unknown whether this is the case, it could lead to an overestimation of the hydrate volume in the NTNU experiments.

Air Contamination of the Gas Phase

Before pressurizing the pressure cell, air was flushed out of the system by injecting gas until 3 bar was reached, before releasing the pressure. This should remove most of the air, but some air will still be inside the pressure cell when conducting the experiment. Ideally, the system should have been flushed several times to remove all of the air in the system.

4.2 SINTEF Test

SINTEF Petroleum AS carried out two tests in the wheel flow loop on behalf of Future Well Control AS. The authors had no active part in the planning and conduction of the experiments, but were invited to observe the experiments. All data recorded and the first revision of the report were shared with the authors for analysis and calculation purposes regarding hydrate volume and volume reduction.

This section presents and discuss the results obtained from Test 2 performed in SINTEF's wheel flow loop. The focus is on the hydrate volume formed, and the significance of the volume reduction due to hydrate formation. The results obtained and presented in this section are analyzed and interpreted based on the writers' knowledge of the hydrate behaviour and the experimental setup.

4.2.1 Filling of the Wheel Flow Loop

The water used in the SINTEF Tests, was filtered and prepared in advance. Seawater from Krokstad in Snillfjord was filtered and mixed with additional salt to achieve a weight percentage of 3.5wt% salt. The final density was measured to 1.02659 g/c^3 , by using a pycnometer.

The wheel flow loop was initially filled with water to determine the internal volume. In total, 13.573 kg of seawater was filled into the wheel. Then, some of the water was displaced by injecting methane gas. After draining 3.03 L of seawater, the pressure in the methane gas cap was 0.7 barg.

The SINTEF gas was injected until the pressure reached approximately 122 bar. The SINTEF gas flask was then empty, thus methane gas was injected to increase the pressure. The injection of methane gas stopped when the total weight of the injected gas reached 541 g. The internal pressure was 140 bar and the temperature was 2°C after all the gas was injected. The tests were conducted as described in Section [3.2.2](#)

4.2.2 Evidence of Hydrate Growth

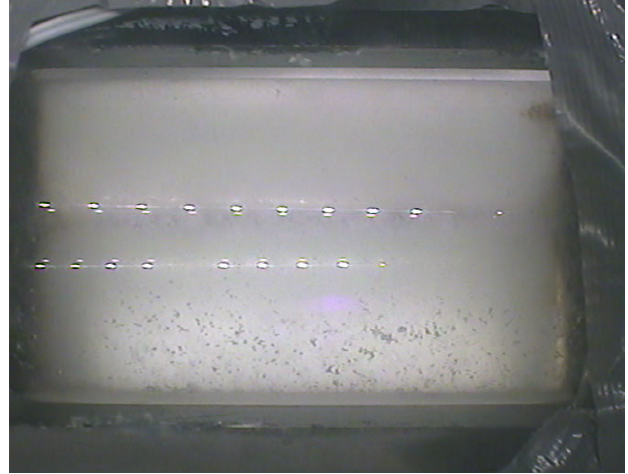
Hydrates clearly formed in the SINTEF Test, confirmed by both visual inspection and the pressure and temperature logs. A sapphire glass section of the pipe made it possible to observe the hydrate growth visually during the experiment. A slurry of hydrates was observed when watching the video, obtained from the camera mounted on the wheel. The camera was recording through the sapphire glass section of the pipe during the entire experiment. Figure 4.17 shows four pictures taken through the sapphire glass section of the wheel flow loop. Hydrates are observed in Figure 4.17b, 4.17c and 4.17d.

The recorded pressure and temperature logs can give an indication of hydrate formation. If the pressure drop in the wheel is greater than the one expected from the decreasing temperature, according to real gas law, it can indicate hydrate formation. The excess pressure drop can also be a result of a leakage. One way to disprove a leakage, is by melting the hydrates, as done in some of the NTNU experiments. Determining if hydrate formed in the system can be done by checking the hydrate equilibrium curve. If the pressure and temperature are inside the hydrate area, hydrates may have formed. If the pressure and temperature conditions lies on the outside of the hydrate region, hydrates cannot form, and the excess pressure drop must be due to a leakage.

Figure 4.19 illustrates the pressure curve obtained from the experiment and the pressure curve expected from PVT-calculations without hydrate growth. The pressure curve given by the real gas law stabilizes at a greater pressure than the one obtained from the experiment. This is in agreement with the visual observation that hydrates have formed during the experiment. The assumptions are identical to the ones given in Subsection 4.1.5 for Equation 4.2. $Z_1 \approx Z_2$ do not yield for a pressure reduction of 10 bar, meaning that the Z-factor should have been accounted for. The methane solubility should also have been taken into consideration in order to achieve a more correct pressure. Based on this, the green curve in Figure 4.19 has most likely stabilized at a greater pressure than what it should have. However, it is a good illustration of the excess pressure drop, which is most likely due to hydrate formation.



(a) There is no hydrates observed through the sapphire optical section at this stage in the experiment (time: 13:05).



(b) A small amount of hydrates is observed as the small particles floating close to the bottom through the sapphire optical section (time: 14:26).



(c) Hydrate slurry observed in the lower, left corner (darker area) through the sapphire optical section in the wheel 15:16.



(d) A hydrates slurry is observed along the lower part through the sapphire optical section in the wheel (time: 15:18).

Figure 4.17: Visual inspection of hydrate occurrence in the SINTEF Test, observed through the sapphire glass section of the wheel (Fossen, 2017b).

The equilibrium curve given in Figure 4.18 shows that the pressure-temperature conditions lies within the hydrate region. The purple arrows indicate that the experiment reached equilibrium at 104 bar and 12°C. Observe that the experiment reached steady state before intersecting the hydrate equilibrium curve. In theory, hydrate growth could continue until the pressure in the wheel was reduced by another 64 bar. This is only possible if there is enough water and gas available, and if there is communication between the two phases in the system, for continuous growth as described in Section 4.1.10.

Even by continuous rotation of the wheel, the gas might have been isolated between hydrate plugs, which stopped the hydrate formation. This would prevent the system from reaching the hydrate equilibrium curve.

A reason might be that when hydrates are formed, the salt concentration in the remaining water becomes higher, which moves the hydrate equilibrium curve to the left, as shown in Figure 4.15. Another factor might be that the heavy components of the gas phase form hydrates first can make continued hydrate formation more difficult, as a higher methane content in the gas phase shifts the hydrate equilibrium to the left.

In the SINTEF Test, the latter reason is most likely, because the water volume removed from the water phase was probably not large enough to drastically change the salinity of the aqueous solution.

4.2.2.1 Start of Hydrate Growth

Hydrate formation was initiated after approximately 12.7 hours at 11.5°C and 145 bar (Fossen, 2017a). This is in agreement with what is observed in Figure 4.19. Immediately after the temperature reached its minimum at 11.5°, the temperature started to increase to around 12°. The small increase in temperature is most likely a result of hydrate formation. This is supported by the pressure curve having a sharp break-point at the same time.

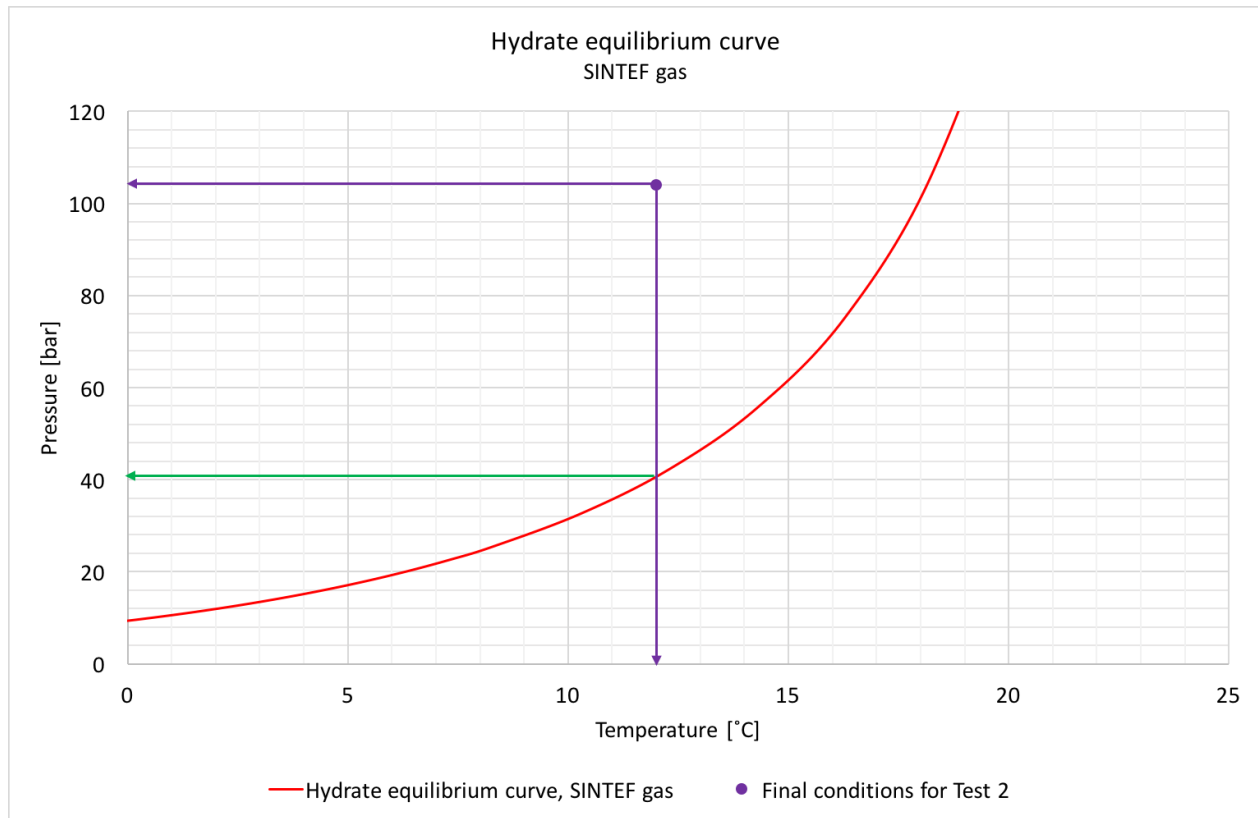


Figure 4.18: Hydrate equilibrium curve for the gas used in the SINTEF Test.

The pressure rapidly decreases after the break-point, which indicates hydrate formation. The steep pressure decline lasted for approximately four hours, where the pressure decreased from 145 bar to 112 bar. One explanation to this rapid hydrate growth is the many impurities in the Fjord water. As described in Section 2.1.3.3, impurities work as nucleation sites for hydrate growth. More nucleation sites could yield faster hydrate growth. This theory is strengthened by the fact that the hydrates visually observed was a slurry. The large driving forces caused by the pressure decrease, when hydrate formation is initiated, contribute to a fast hydrate formation.

After 17 hours, the hydrate formation seems to slow down, probably due to a lower driving force or less contact between water and gas. The test stopped after 72 hours. At this stage, the pressure decline was so low that for practical purposes it was stopped. Even if the system equilibrium might not have been fully reached, it is assumed that the system was very close to steady state.

It is therefore concluded that the steady state pressure and temperature were reached at 104 bar and 12°C.

According to Figure 4.19, the pressure at 12°C should be equal to 165 bar if no hydrate formation or leakage occurs. Instead, the pressure has dropped further, to 104 bar. Most likely, the majority of the excess pressure drop, is caused by hydrate formation.

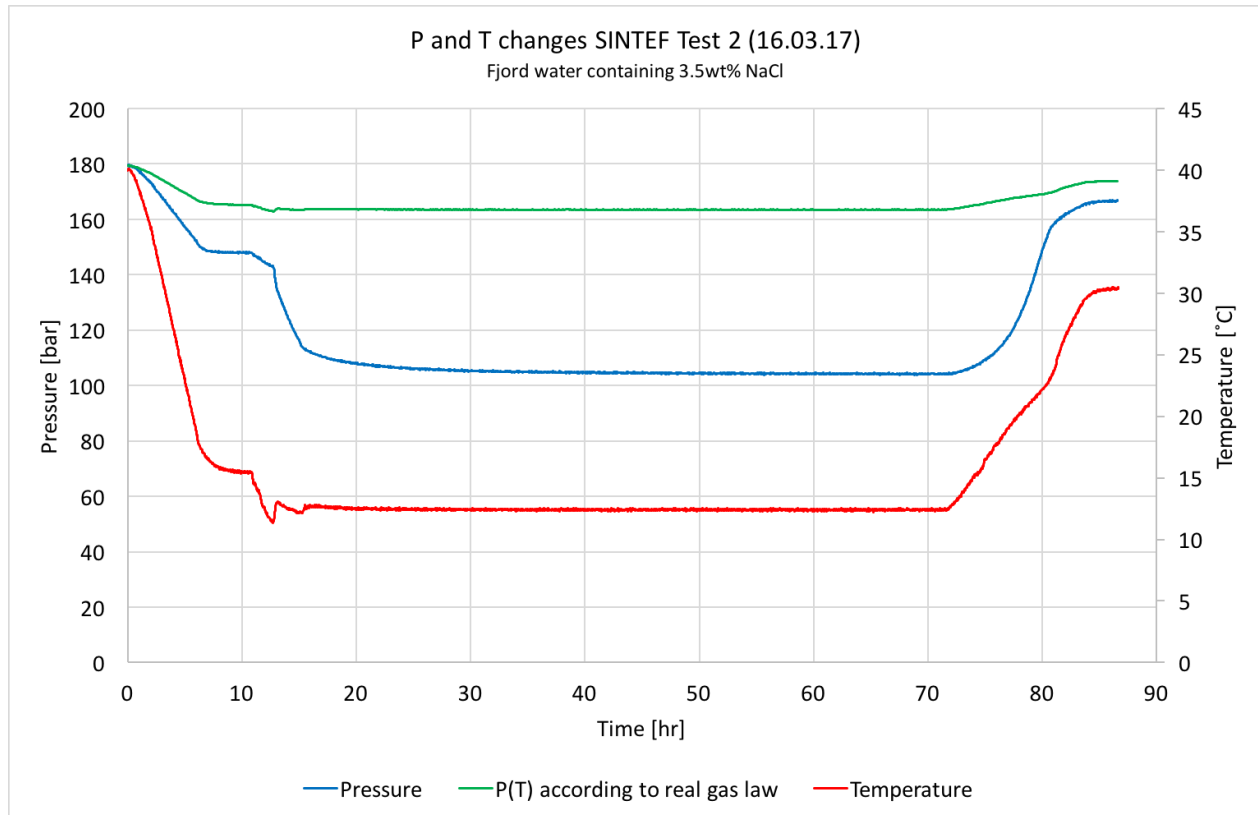


Figure 4.19: Pressure and temperature changes in Test 2, SINTEF Test.

4.2.3 Volume Reduction and Hydrate Volume Calculations

A step by step overview of all the calculations performed in order to find the volume reduction and the hydrate volume formed in the SINTEF Test is provided in Appendix B.3.

The results shown in Table 4.12 for Test 2, is based on calculations performed in Microsoft Excel. The calculation method used is created by Bendik Helgestad and Michaela Gunhildrud.

Table 4.12: volume reduction for Test 2, performed at SINTEF laboratory with the synthetic natural gas mixture given in Table 3.2.

	Test 2				
	$V_{gas, used}$ [mL]	$V_{water, used}$ [mL]	$V_{tot, used}$ [mL]	V_{hyd} [mL]	Volume reduction [%]
In-between case	2.24	2.44	4.68	2.97	76.1
Best case	2.18	1.65	3.83	2.10	79.3
Worst case	2.30	3.14	5.44	3.75	73.4

These results are not in agreement with the results obtained by SINTEF. Table 4.13 demonstrates the difference in obtained result. Further investigation is necessary to conclude which calculation model is correct, or if any of them are. The results calculated by Helgestad and Gunhildrud is assumed to be more reliable, thus used for further discussion in this thesis. The three main reasons why, are discussed below.

1. The change in gas volume left in the wheel after hydrate formation is considered in Helgestad and Gunhildrud's calculation model. When hydrates form, a smaller gas volume than the initial gas volume will occur in the wheel. In SINTEF's calculations, this has not been taken into consideration. A greater gas volume after hydrate formation means that less moles of gas has been used in the hydrate formation process. This can explain why Helgestad and Gunhildrud have concluded that more moles of gas have been consumed by hydrates.

2. The gas density used to calculate the hydrate volume in Helgestad and Gunhildrud's case is an average of the initial gas density and the final gas density. This has been done as the gas density changes during the hydrate formation process. The calculations performed at SINTEF have used the final gas density after the total volume of hydrates have been formed. A smaller final gas density implies more moles of gas used to form hydrates. This means that if the same gas density had been used in both calculation models, the difference would increase even more.

3. Some of the calculated numbers in the SINTEF report is considered to have little credibility.

First, the moles of gas used to form hydrates differs throughout the report. One place it states that 7.1 moles of gas are used, while in the final results, as showed in Table 4.13, 7.8 moles of gas are assumed to have been captured inside the hydrates. In a plot showing the moles of gas used, the peak is located at approximately 6.2 moles. The authors do not know how these calculations are performed. According to the SINTEF report, the gas volume used is 0.14 L. If calculating the moles of gas used, using this value together with the given gas density and molecular weight of the gas, the amount of gas is 0.72 moles. These observations are the basis for why the report has little credibility.

Table 4.13: Comparison of hydrate volume formed at Test 2, SINTEF Test

Performed by	In-between case				
	$n_{gas,used}$ [mole]	$V_{gas,used}$ [L]	$n_{water,used}$ [mole]	$V_{water,used}$ [L]	V_{hyd} [L]
Helgestad and Gunhildrud	15.9	2.24	138.7	2.44	2.97
SINTEF	7.8	0.14	61.7	1.12	1.33

Figure 4.20 shows the estimated volume reduction at various pressures for the SINTEF gas. It is assumed that the moles of gas used to form hydrates are the same as the one calculated using Helgestad and Gunhildrud's calculation method for Test 2.

A similar trend is observed in Figure 4.20, as in the volume reduction observed in the NTNU gas, shown in 4.14. It shows that the volume reduction reduces with increasing pressure, and that a smaller hydration number gives a larger volume reduction.

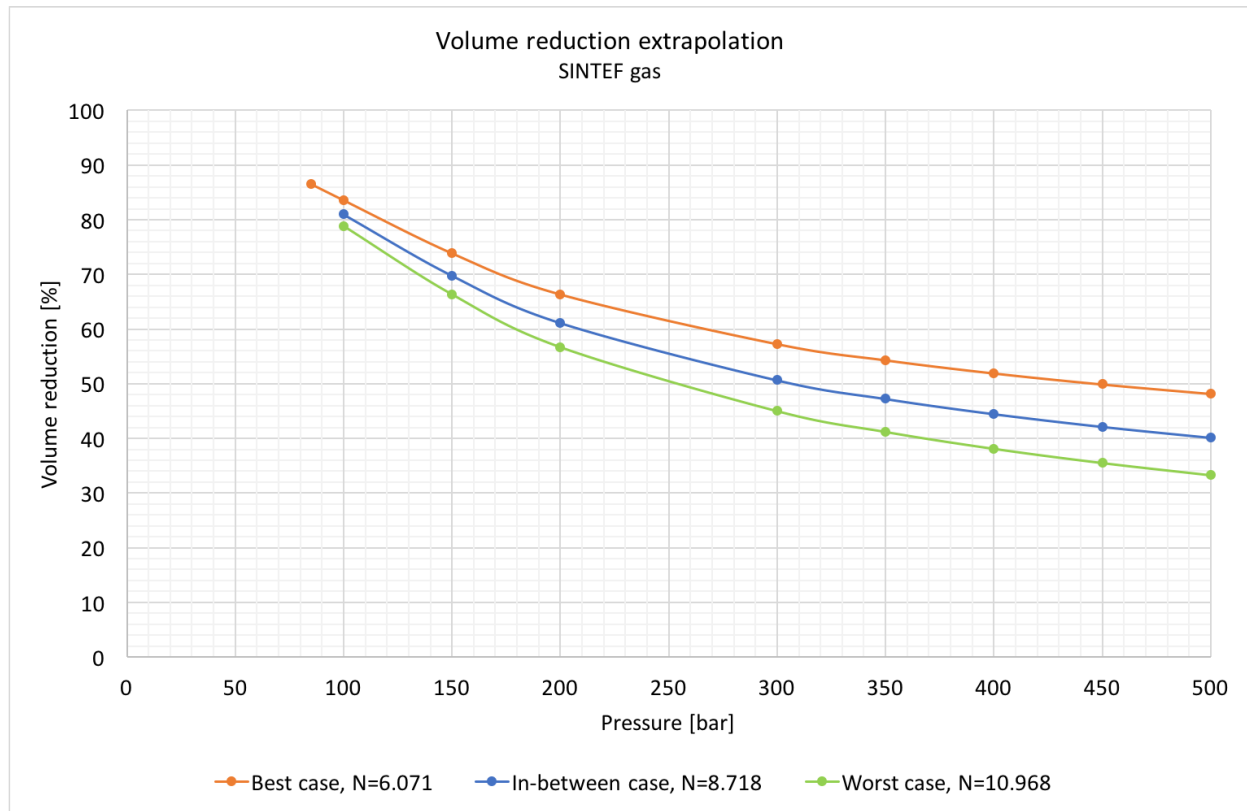


Figure 4.20: Volume reduction extrapolation for the SINTEF gas at 6 °C. The volume reduction for three different hydration numbers is considered.

4.2.4 Experimental Errors

4.2.4.1 Moles of Gas Injected

The major uncertainty in the SINTEF Test is the moles of gas injected into the wheel. This impacts the calculated volume of hydrates formed, and the corresponding volume reduction. Three different methods were used to determine the moles of gas. All three methods gave different values.

The SRK equation of state was used to perform PVT simulations (Fossen, 2017a). The flash calculations were conducted at 155 bar and 20.7°C. This was done by Martin Fossen at SINTEF. The calculated amount of gas filled using this method was 527 g (Fossen, 2017a). This corresponds to 30.05 moles of gas, assuming the molecular weight is 17.54 g/mole, as given in the SINTEF

report (Fossen, 2017a).

According to the measured weight, the amount of gas injected was 541 g. This corresponds to 30.84 moles of gas used. The scale used to determine the weight have an accuracy of ± 5 g.

Test 2 had an initial temperature of 40°C and a pressure of 180 bar (Fossen, 2017a). This is outside of the hydrate region, as can be seen from Table E.5. This means that all gas that had been consumed by hydrates in Test 1 have melted. If no gas has been released from the wheel, the moles of gas should be equal to the moles of gas initially injected. If not, a leak might have occurred. If back calculating using the real gas law with a Z-factor equal to 0.83, the calculated amount of gas is 28.43 moles (Unitrove, 2017).

The reason for the deviation might be the uncertainty and inaccuracy in the weight process, together with rounding errors in the calculation process, or gas entering the aqueous solution. Some inaccuracies may be present in the equation of state used in the PVT simulations. It should also be noted that the PVT simulations were performed at a greater pressure and temperature than the initial conditions in Test 1 when all gas were injected. The biggest uncertainty related to the back-calculation method, is the Z-factor.

4.2.4.2 Moles of Gas Consumed by Hydrates

Another big uncertainty is related to the moles of gas consumed by hydrates. This is dependant on the initially moles of gas in place, the pressure and temperature conditions, the mixing of gas and water, the communication between the gas and water phase, how the gas composition changes during hydrate formation, how the salinity in the aqueous solution changes when hydrates form and the calculation method used to determine moles of gas consumed by hydrates.

PVT simulations have been used to calculate the mole of gas used to form hydrates in the SINTEF method. In the report provided by SINTEF, there are many contradictions and inconsistencies. Also, some of the values originally given have been changed and corrected more than once, excused as human errors. As mentioned, the value for the calculated moles of gas used to form

hydrates are different through the SINTEF report.

Helgestad and Gunhildrud's calculation model is another method used to find the moles of gas consumed by hydrates. Uncertainties in this model is stated in Section 4.1.12.5. It is assumed that the gas composition is the same both before and after hydrate formation, also the water salinity is assumed to be constant. All of these factors will play a role on how much hydrates will form.

The pressure sensor was only located in one place. If a hydrate plug formed, it could hold a gas phase that did not have communication with the rest of the wheel volume, resulting in a different pressure than where the pressure sensor was measuring (Fossen, 2017a).

4.2.4.3 Gas Composition

The pre-mixed synthetic gas mixture ran out after approximately three hours, thus methane gas was used to increase the pressure to the initial pressure. This means that the gas composition changed from the one originally planned, as shown in Table 3.2, to one with a greater methane content. A larger amount of methane will change the the gas composition, thus change the hydrate equilibrium conditions. A higher methane content will shift the hydrate equilibrium curve to the left, making the hydrate area smaller, and hydrate formation more difficult. The reason for the shortage of the pre-mixed synthetic gas was that the 15 meter pipe section with a 10mm diameter leading up to the wheel had not been considered. It is assumed that most of the gas present in the wheel was the pre-mixed gas.

The initial pressure condition before the synthetic gas mixture was injected into the wheel was a slightly pressurized atmosphere of methane at approximately 0.7 barg. This will also contribute to a greater amount of methane in the gas composition.

4.2.4.4 Error in Apparatus Volume Calculations

The volume of the wheel was determined based on calculations using the inner diameter of the wheel and the length of the wheel provided by SINTEF. The significance of this error is not stated in the SINTEF report.

The scale used to determine the weight of the water have an accuracy of $\pm 5\text{g}$, which affect the volume calculations. It will not only affect the volume of the wheel, but also the remaining water volume after drainage and the gas volume.

4.2.4.5 Error in Gas Hydrate Volume Calculations

Since the hydrate volume is dependant on the factors listed above, the errors related to those factors increase the uncertainties of the calculated hydrate volume. The solubility of methane gas has not been taken into account and could affect the hydrate volume. An explanation of this phenomenon is described in Subsection [3.1.4](#).

4.3 Comparison of the Volume Reduction in the NTNU Experiments and the SINTEF Test 2

In experiment 5 performed at the NTNU laboratory and the experiment performed at SINTEF, the equivalent aqueous phase composition containing 3.5wt% NaCl is used.

Many of the experiments where hydrate formation has been visually confirmed shows the same trend on the pressure curve, where a breaking-point indicates the start of hydrate formation. This yield both for the NTNU experiments and the SINTEF Test. This observation can be used as an argument that hydrates most likely occurred in the experiments where visual proof was not obtained, but had the same trend on the pressure curve and lies within the hydrate region.

4.3. COMPARISON OF THE VOLUME REDUCTION IN THE NTNU EXPERIMENTS AND THE SINTEF TEST 212

In the experiment performed at SINTEF, the natural gas composition used, was modified from a real gas found in the Barents Sea. This makes the results obtained from this test more applicable to real life scenarios, regarding volume reduction and hydrate formation volume. The NTNU experiments on the other hand, used a gas mixture of 90% methane and 10% propane. The high amount of propane was chosen in order to form hydrates more easily. The red and green curve in Figure 4.21 demonstrates the volume reduction extrapolations for the NTNU and SINTEF gas. It is observed that the volume reduction retrieved by extrapolation for the NTNU gas is less than the one obtained for the SINTEF gas. At 200 bar, the volume reduction for the in-between case is 47.4% for the NTNU gas and 60.1% for the SINTEF gas. One explanation to the difference in volume reduction is that two different gas compositions are used.

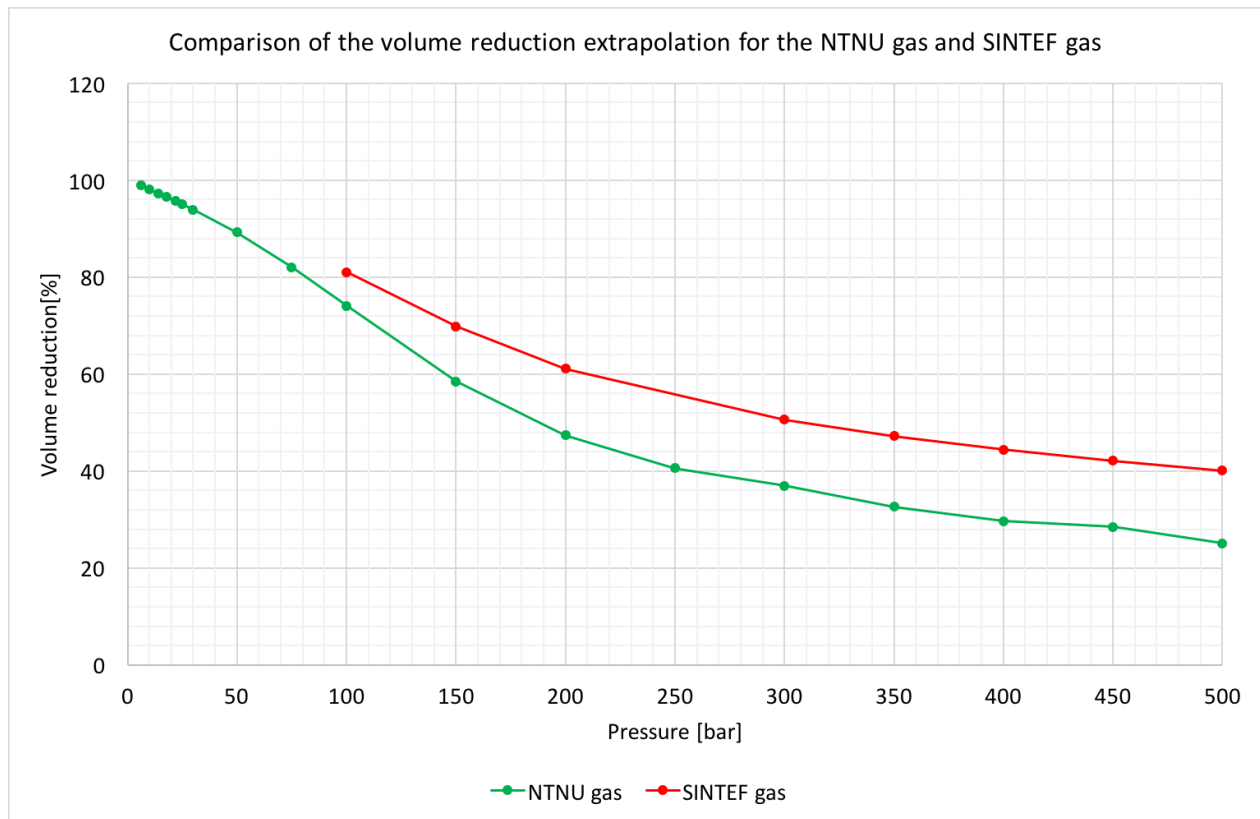


Figure 4.21: Volume reduction extrapolation for the NTNU and SINTEF gas (in-between case).

4.4 Hydrate Formation in a Barents Sea Well

The part of the well where hydrate formation is possible, can be determined if the pressure and temperature conditions, gas composition and mud composition are known. The temperature model described in Section 2.4, can be used to determine the well interval located inside the hydrate area at various times after shut-in. This is obtained by plotting the hydrate equilibrium curve together with the temperature model. Figure 4.22 shows the hydrate curve for the NTNU and SINTEF gas as a function of depth.

The green and red curve represent the hydrate equilibrium curve for the NTNU and SINTEF gas. A drilling fluid density of 1000 kg/m^3 was used to convert the hydrate formation pressure into a hydrostatic column height, by using Equation B.28, in order to plot the hydrate equilibrium curve as a function of depth.

The green and red arrows show the depth where the well conditions enter the hydrate area at shut-in. Because the SINTEF gas has the same composition as the reservoir gas from the Barents Sea well, this will be the main focus. The gas kick enters the hydrate area at 1177 mRKB, i.e. 1177 m below the rig floor, and exits the hydrate area when the gas reach 157 mRKB. Hydrates can form inside the well, at this depth interval.

When considering hydrate formation in the well, the worst case scenario should be considered. According to the temperature model, the worst-case in terms of hydrate formation depth is immediately after shut-in, while in terms of subcooling, the worst case is after a long shut-in time near the wellhead.

In order to fully prevent hydrate formation in the Barents Sea well, inhibitors have to be dissolved into the pure water phase until the hydrate equilibrium curve for the SINTEF gas overlaps the yellow curve in Figure 4.22. Meaning that salt must be added until the hydrate formation temperature is depressed with $\Delta T_h = 3.88^\circ\text{C} - 13.95^\circ\text{C} = -10.07^\circ\text{C}$. The yellow curve represents a fully inhibited water phase, because no part of the system is inside the hydrate area at any time after shut-in.

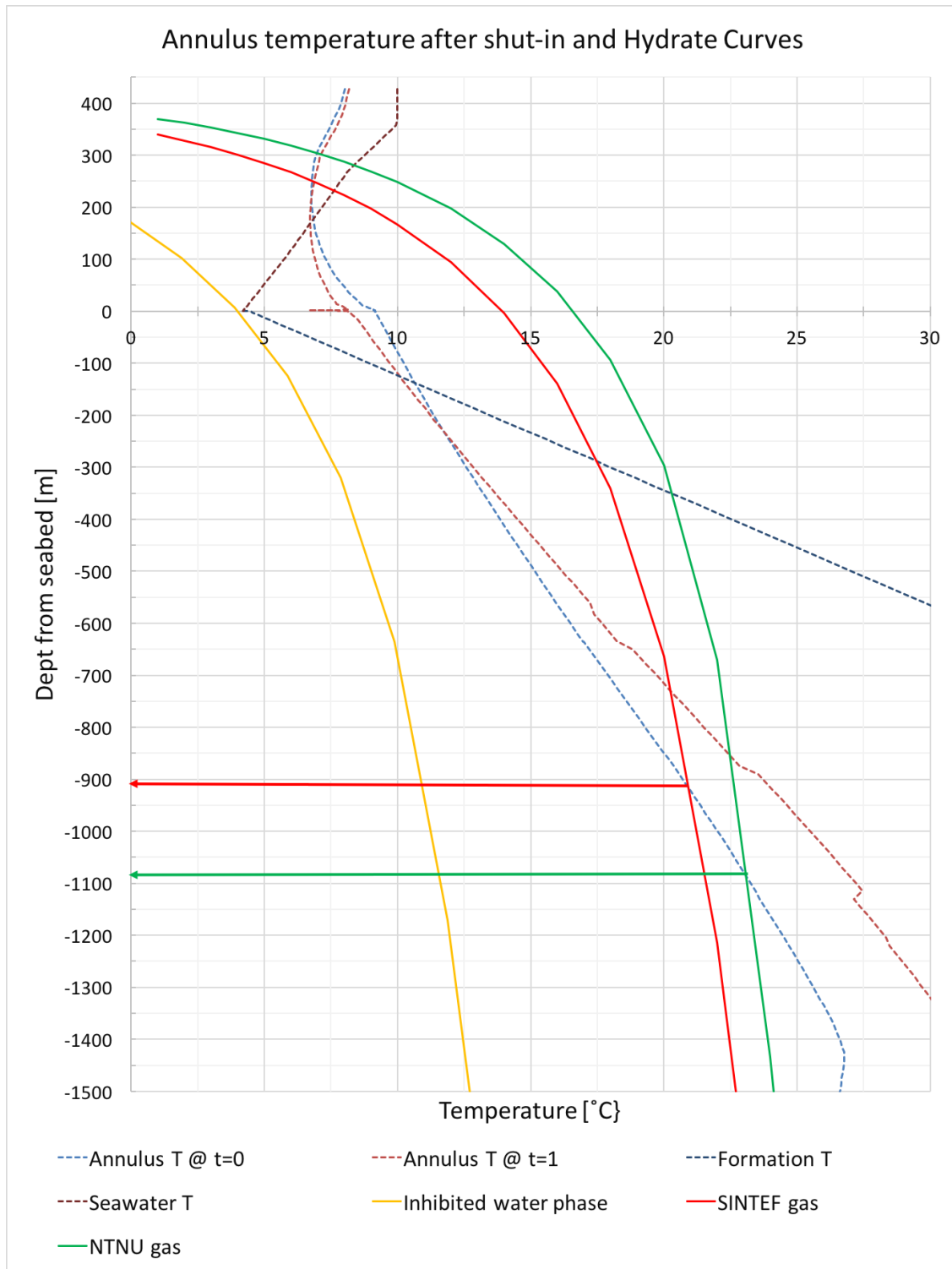


Figure 4.22: The hydrate equilibrium curve as a function of dept, and the well temperature model. A fluid density of 1000 kg/m^3 is used to convert the hydrate equilibrium pressures into depth. The arrows shows the depth, where the well conditions enters the hydrate formation area.

By using the equations presented in Section 2.1.5.1, the amount needed to inhibit the water phase can be calculated by solving the equations with respect to X_a . The wt% was found by solving Equation 2.9 and 2.12 numerically in Excel. If a gas kick with a similar composition as the SINTEF gas entered the well, the calculations show that at least 14.23 wt% of NaCl or 16.74 wt% of CaCl_2 or 18.61 wt% of KHCOO need to be added to the water phase of the drilling fluid. This amount would be enough to inhibit the water phase of the drilling fluid used in the Barents Sea well.

The SINTEF gas hydrate equilibrium curve in Figure 4.23 represents a system with pure water and the SINTEF gas. When salt is added to the water phase to inhibit the drilling fluid, the density increases, which increases the pressure in the well. Therefore, more salt needs to be added, in order to prevent hydrate formation.

The new temperature depression needs to be $\Delta T_h = 3.88^\circ\text{C} - 14.55^\circ\text{C} = -10.67^\circ\text{C}$, in order to inhibit the water phase after the density increase. By solving Equation 2.12 with respect to the X_a one more time, the amount of CaCl_2 needed in the water phase is 18.60wt%, i.e. almost 2wt% more than original calculated. This further increases the fluid density to 1115 kg/m^3 , which make the well pressure increase slightly more, which again means that more salt needs to be added to the water phase.

By iterating until $\Delta T_h(n-1) = \Delta T_h(n)$, the exact amount of salt needed to inhibit the water phase is determined, thus ensuring prevention of hydrate formation in the well. Note that this is the minimum salt needed to avoid hydrate formation under normal conditions, where the well pressure at every depth is equivalent to the hydrostatic pressure of the saline solution. If a kick occurs, and the well is shut-in, the well pressure will most likely increase, which could make new parts of the well enter the hydrate area. Therefore, the salt calculation should be based upon the worst-case pressure scenario in the well.

The black and light blue curve in Figure 4.23 illustrates the hydrate formation depth in a drilling fluid with a density of 1400 and 1800 kg/m^3 respectively, with no inhibitor in the water phase. By increasing the drilling fluid density, the well interval where hydrates may form becomes larger.

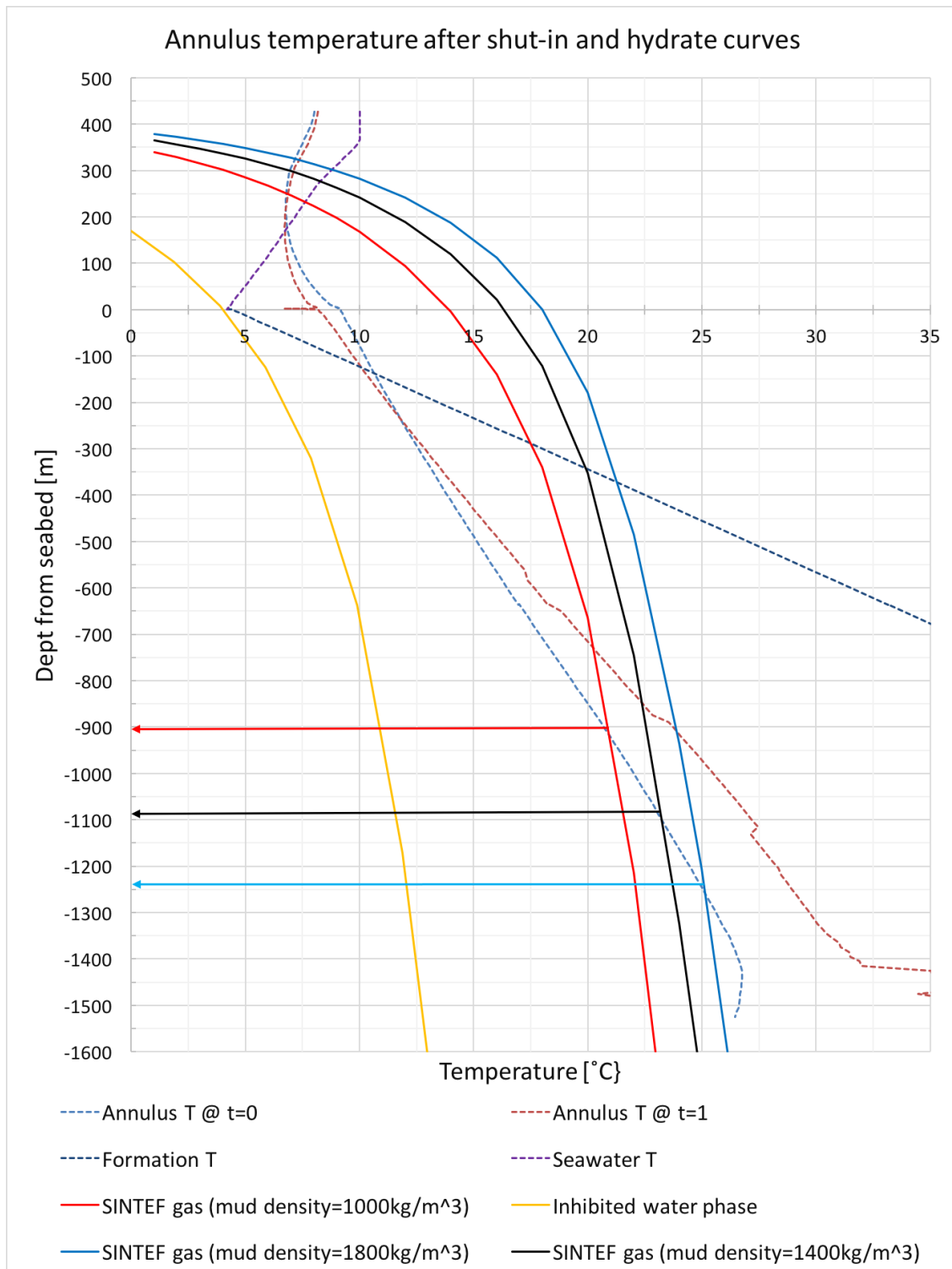


Figure 4.23: The well temperature model and the hydrate equilibrium curve for SINTEF gas, at various drilling fluid densities. The yellow curve represents a fully inhibited water phase. The arrows shows the depth, where the well conditions enters the hydrate formation area.

This is because the pressure at all depths increases, making the hydrate equilibrium temperature increase at the corresponding depth.

If the uninhibited drilling fluid has a density of 1800 kg/m^3 , hydrate formation can occur approximately 1250m below the seabed immediately after shut-in. At the wellhead, the subcooling is -14.12°C when the well has been shut-in for a long period. In this case, 18.01 wt% of NaCl or 21.99 wt% of CaCl_2 or 24.27wt% of KHCOOO have to be added to the water phase of the drilling fluid in order to prevent hydrate formation.

Gas migration velocity can vary from 0.085 m/s up to 0.55 m/s, depending on the gas void fraction, i.e. the fraction of the cross-section area occupied by the gas phase. If a large kick with a void fraction above 10% occurs, the velocity will be in the upper part of the velocity range (Johnson et al., 1995). Thus, a large gas kick could migrate up to 33 meters per minute. Considering the Barents Sea well, a gas kick could travel the 775 m from the bit (1952mRKB) to the hydrate area in the well interval (1177mRKB) in 23.5 minutes. Assuming that the gas temperature has the equivalent temperature as the surrounding mud, hydrate formation could start occurring in less than 25 minutes after the gas kick entered the well.

If a high-density mud without inhibitor was used when drilling, like the 1800 kg/m^3 drilling fluid in Figure 4.23, hydrates could start forming 8.3 minutes after the gas entered the well. If the well is not shut-in immediately after the kick, the gas can enter the hydrate area even faster because the kick could migrate with the mud flow rate, and the well temperature will be lower for a longer period.

Chapter 5

Conclusion

Drilling operations have moved to higher latitudes and deeper waters. In these extreme environments, the industry is forced to face numerous, previously foreign, challenges. One significant hazard that becomes a concern is the potential for natural gas hydrate formation in the drilling fluid. Based on this study, the conclusions are as follows;

- The hydrate equilibrium represents the minimum pressure-temperature conditions required to form hydrates.
- Hydrate nucleation are difficult to predict, especially at low driving forces, since it is a stochastic phenomenon.
- According to the real gas law, the final pressure in experiment 5 should be 23.86 bar. However, the final pressure of the experiment was recorded as 19.48 bar. Similar drops in final pressure were observed in the NTNU experiments and the SINTEF Test. This pressure difference could be explained as a result of hydrate formation.
- Impurities in the solution may cause a hydrate slurry to form and may increase the growth rate.
- Hydrate chunks might form in solutions containing few impurities.
- The volume reduction is dependent on the ratio between the gas and water volume used

to form hydrates and the volume of hydrates. Other factors affecting hydrate formation and volume reduction are salinity, impurity in the aqueous phase, number of cavities filled in the hydrate structure, pressure, temperature, initial gas and water volume and area of gas-water interface.

- The SINTEF Test 2 experiment reached equilibrium at 12°C and 104 bar. Theoretically, hydrate formation should have continued until system pressure was 40 bar. Hydrates preventing communication between the water and gas interface, is believed to be the main reason why the formation of hydrates stopped early in both the SINTEF and in many of the NTNU experiments.
- The volume reduction decreases with increasing pressure, and with a greater hydration number.
- The calculated volume reduction for the “in-between case” in all the NTNU experiments are similar, ranging from 92.8% to 96.3%.
- In the SINTEF Test, the volume reduction at 100 bar is 81.0% for the in-between case, whereas at 200 bar the volume reduction is 61.1%. If the hydration number increases from 6.071 to 10.968 at 100 bar, the volume reduction decrease from 81.0% to 78.8% .
- NaCl is the best hydrate inhibitor among the various additives tested.
- Barite and bentonite have no inhibiting effect based on the NTNU experiments, but the impurities might act as nucleation sites.
- Several new experiments should be conducted in order to be conclusive about the effect of the various additives.
- Hydrate formation inside the wellbore may occur at deeper depths compared to hydrates naturally occurring in the sediments. Analysis of a well in the Barents Sea shows that hydrates may form in the well interval between 1250 meters below seabed and 300 meters above seabed just after shut-in, in a 1800 kg/m³, non-inhibited drilling mud consisting of pure water. If drilling at 1525m, hydrates could start to grow 8.3 minutes after the kick

entered the well.

- To fully prevent hydrate formation in the Barent sea well, the hydrate equilibrium curve must be shifted -14.12°C , requiring 18.01wt% NaCl, 21.99wt% CaCl_2 or 24.27wt% of KCHOO to be added to the water phase of the drilling fluid.
- A volume decrease in the mud pit might be a result of hydrate formation and not loss of circulation. If a 4 m^3 kick enters the well at 181 bar, the volume change observed could be 3.03 m^3 , if all the gas are converted into hydrates. This volume change will decrease the mud column height by 114 m, if drilling with a 5" drillpipe, where a 9 5/8" casing is used in the previous section, resulting in a bottomhole pressure drop of more than 11 bar.

Chapter 6

Further Work

6.1 Further Work - NTNU Experiments

Conducting the experiments once more. By comparing the new experiments to the ones conducted the spring of 2017, it would be possible to compare the growth rate and determine if leakages occurred during some of the experiments. The experiments should run for at least 48 hours in order to determine if the system has reached steady state or is leaking.

New experiments with other chemicals added to the aqueous phase. By testing a tap water and barite solution, effect of the barite particles as nucleation sites can be observed. Also, a new 10wt% NaCl experiment and 10wt% CaCl₂ experiment should be performed. In addition, several bentonite experiments would have been interesting to perform in order to determine the effect of viscosity, and see if both hydrate chunks and hydrate slurry can be formed. The effect of chemicals like xantan gum, lignosulfonate and barium sulfate on hydrate formation would also be of interest. A broader range of tested chemicals makes it possible to determine which combination of additives prevent, and which combination initiate hydrate formation.

The effect of the additives should be tested in OBM. Then, it will be possible to see how different mud bases affect hydrate formation, and to see if the same additives have the same effect in

both drilling fluid bases.

Conduct the experiments by using a more realistic gas composition. The gas mixture used in the NTNU experiments is not representative for reservoir gases. Thus, by using a representative gas composition the results obtained would be of more value and could give an insight to what one might expect in a drilling environment.

A new pressure cell with different dimensions and a sapphire glass window should be used. If the experiments were conducted once more, the cross section area of the pressure cell should be larger. Several of the experiments stopped before reaching the hydrate equilibrium curve, meaning that further growth was prevented. It is believed that this occurred because the hydrate layer on top of the water phase became too thick, creating a physical boundary between the two phases. Thus, by creating a larger cross section area, the hydrate layer may never be thick enough to prevent further hydrate growth. A window into the pressure cell would make it possible to observe hydrate formation visually.

The temperature sensor was probably not calibrated properly and recorded a higher temperature than the actual temperature in the refrigerator. Correction of the temperature logs and the temperature calculations should therefore be done.

Calculating the exact hydrate density based on the hydration number for all scenarios. The hydrate density should be estimated based on the molecular distribution in the small and large cavities, using a software.

6.2 Further Work - SINTEF Test

Conducting the SINTEF Test once more. Make sure to monitor how much gas was injected into the wheel, as this was a large uncertainty in SINTEF Test 2. Also, the gas should be injected into the wheel until the pressure reaches 250 bar. At such pressures, the experiment will be more similar to a kick occurring in a deepwater well.

Ensure that enough gas is available in order to fill the wheel to the wanted pressure. In the SINTEF Test, pure methane had to be injected in order to achieve a system pressure of 140 bar. This changed the mud composition of the gas, making hydrate formation more difficult.

Increase the diameter and modify the wheel flow loop. By increasing the internal diameter of the wheel flow loop, and for instance insert a steel pipe, the experiment will more accurately simulate the annulus.

The temperature model could be used to determine the temperature changes over time. Thus, by changing the experimental temperature according to the temperature model, a more accurate kick scenario could be simulated.

6.3 Further Work - Temperature Model

The hydrate equilibrium curve for various mud compositions could be compared to the temperature model.

Making a temperature model for several other wells, drilled at various depths and locations could be interesting to analyze.

Appendix A

Figures

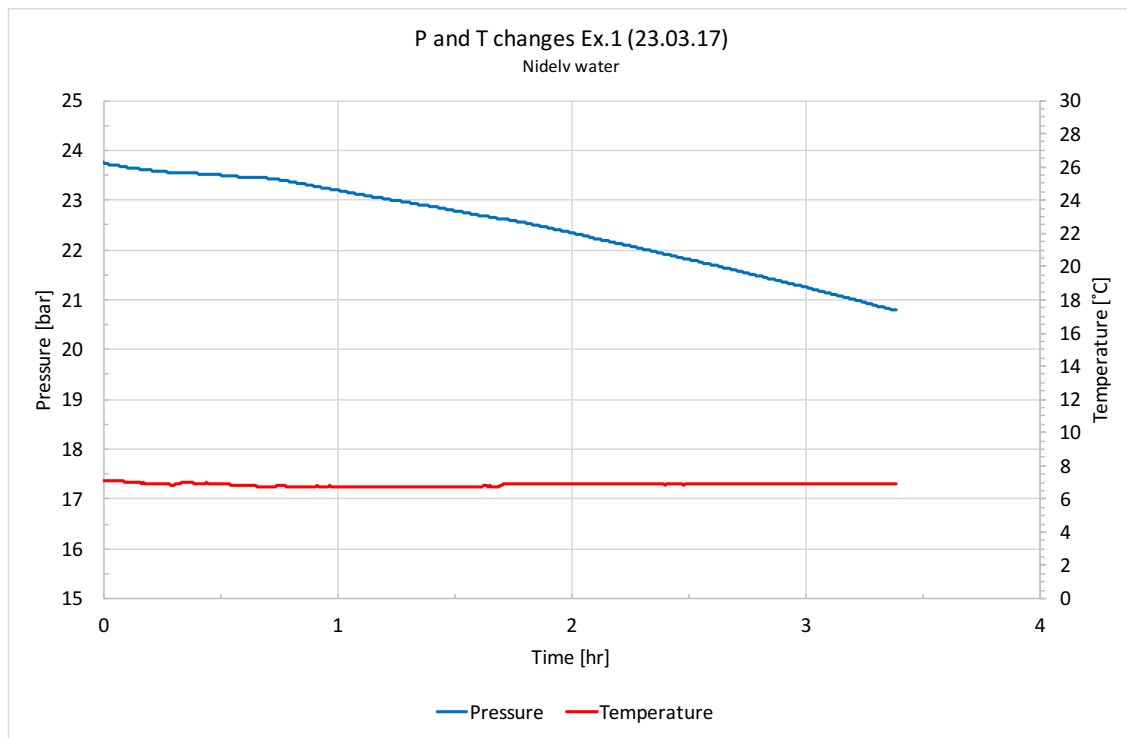


Figure A.1: Pressure and temperature changes in Experiment 1. This experiment was aborted after 3.4 hours because a leakage was believed to have occurred. The pressure cell was cooled down inside the refrigerator before starting to log the temperature and pressure. The leakage was not verified visually and the pressure decrease could have occurred because of hydrate formation.

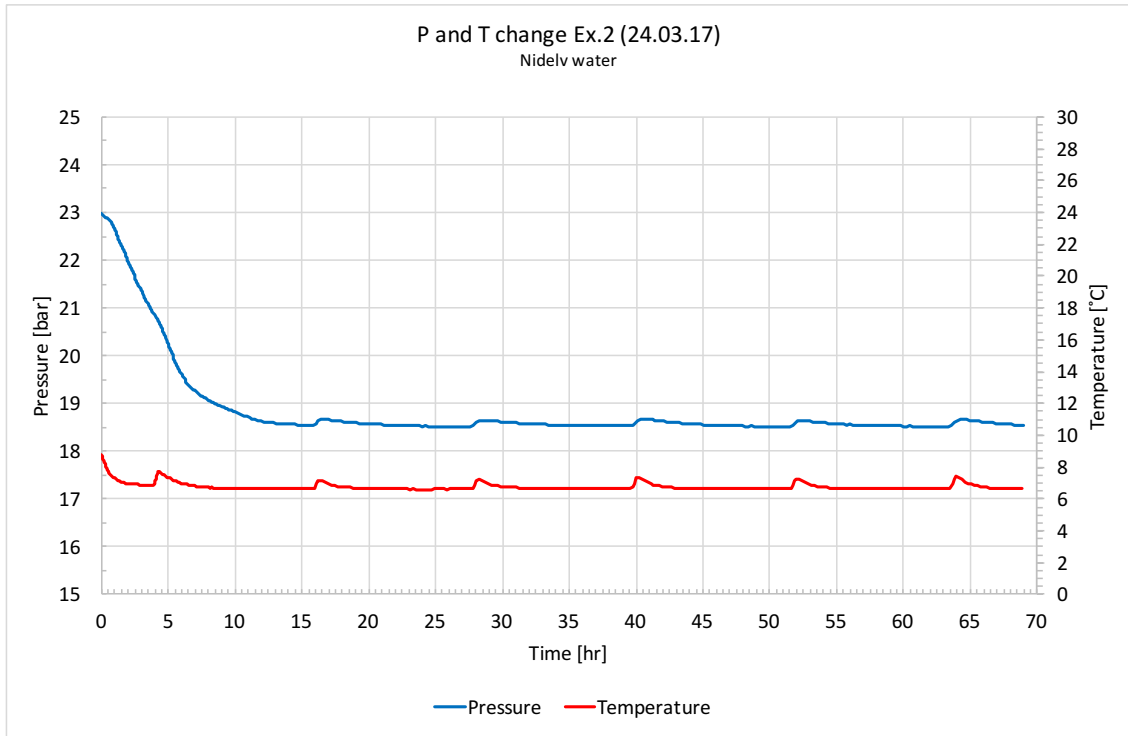


Figure A.2: Pressure and temperature changes in Experiment 2.

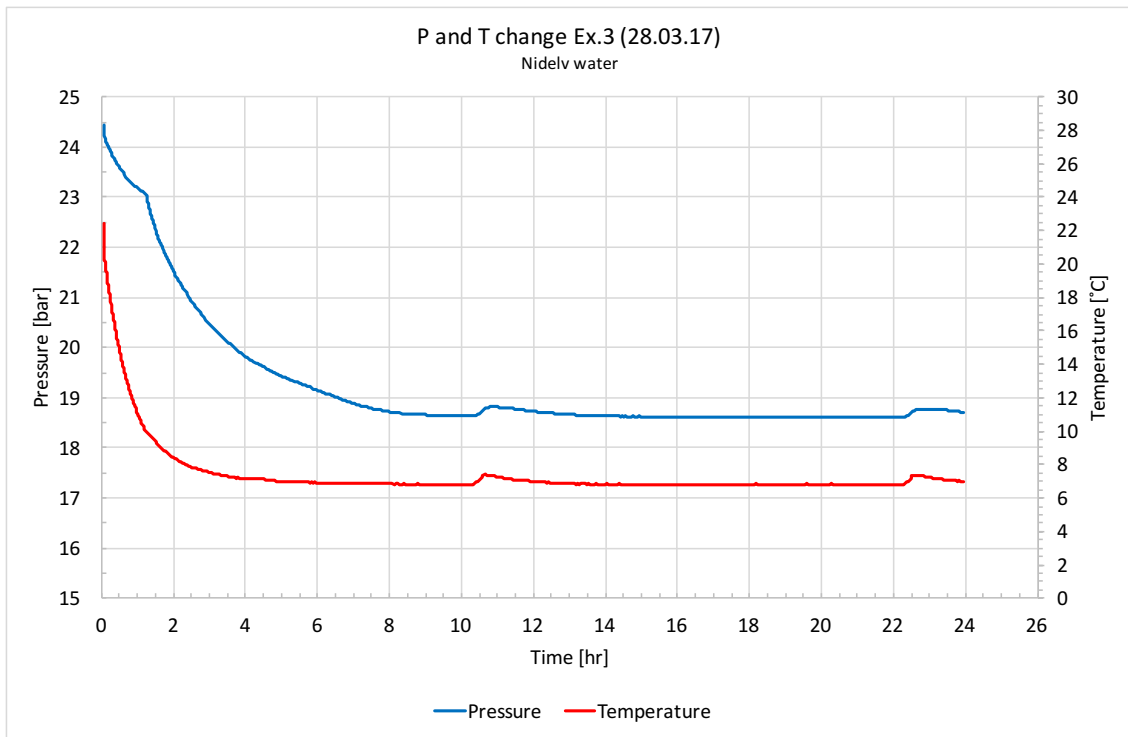


Figure A.3: Pressure and temperature changes in Experiment 3.

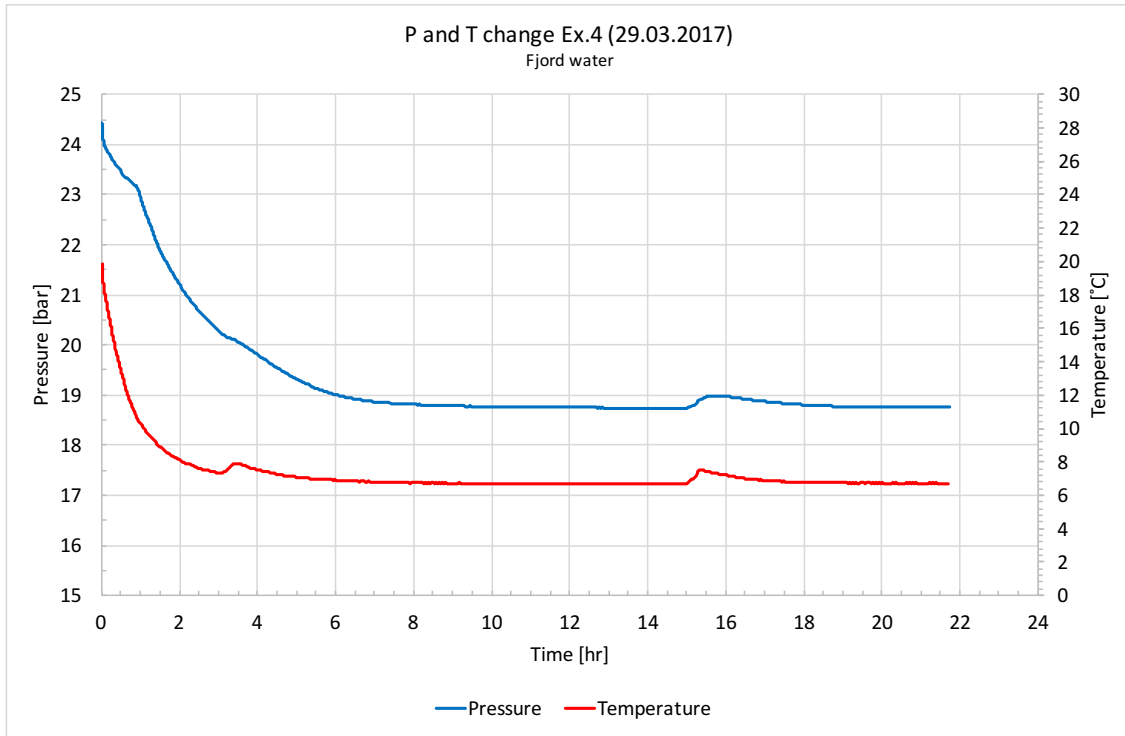


Figure A.4: Pressure and temperature changes in Experiment 4.

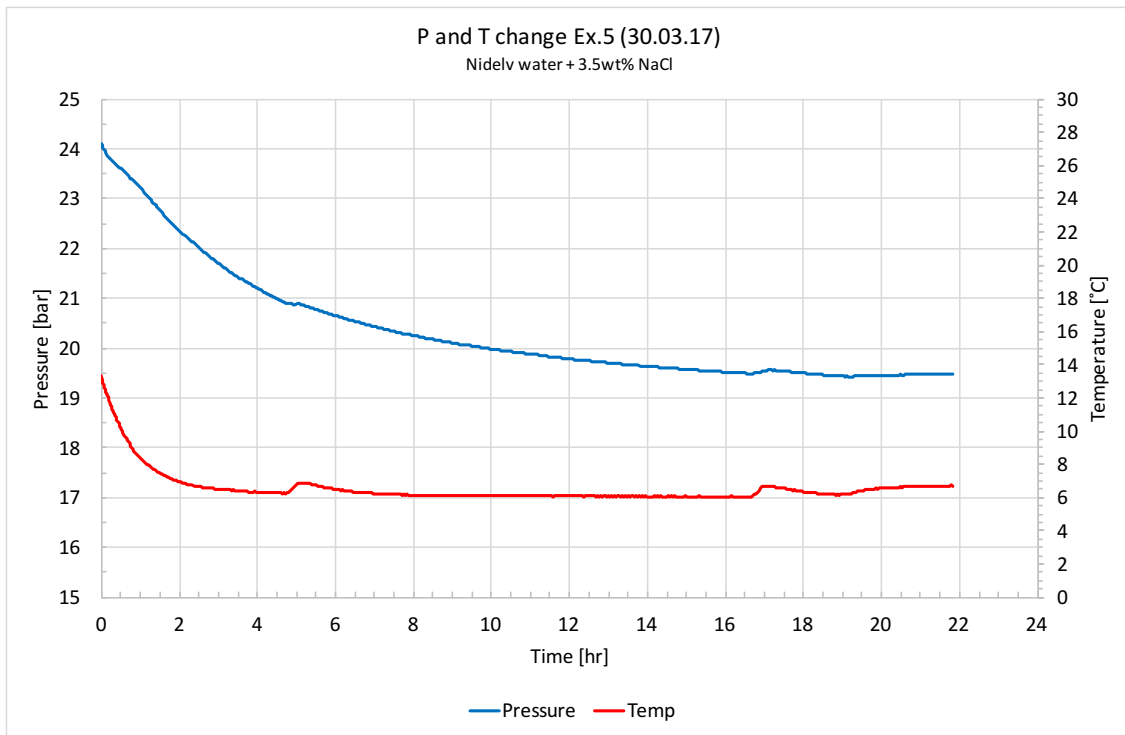


Figure A.5: Pressure and temperature changes in Experiment 5.

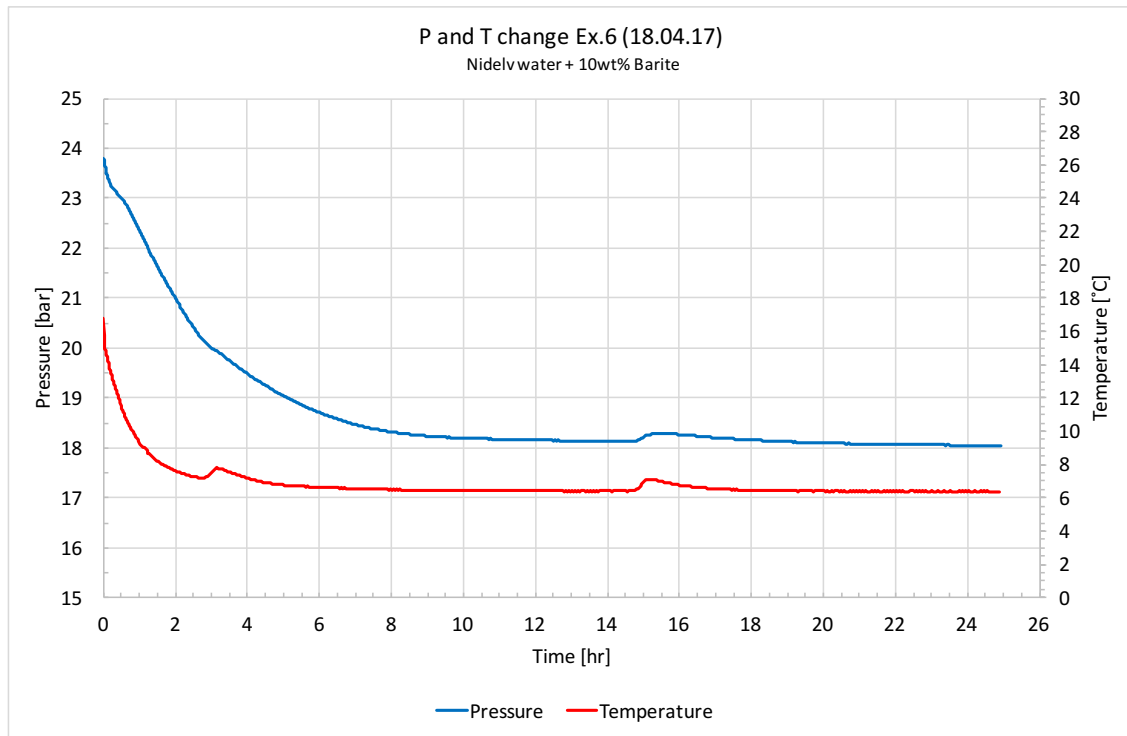


Figure A.6: Pressure and temperature changes in Experiment 6.

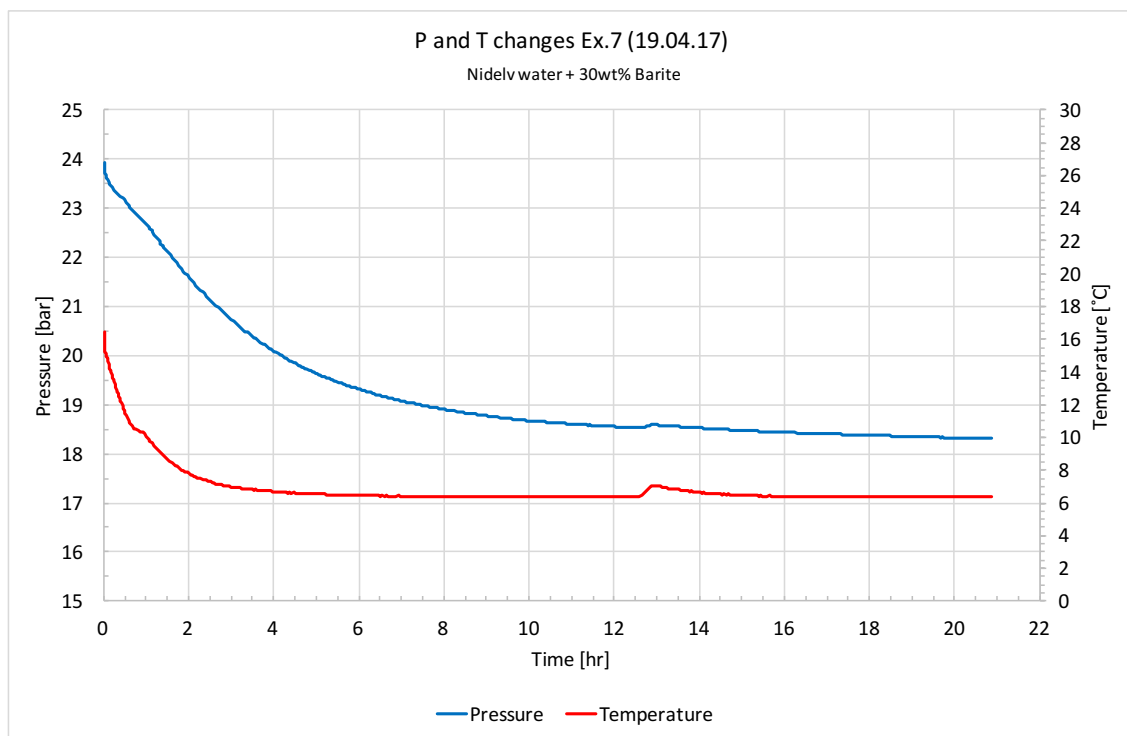


Figure A.7: Pressure and temperature changes in Experiment 7.

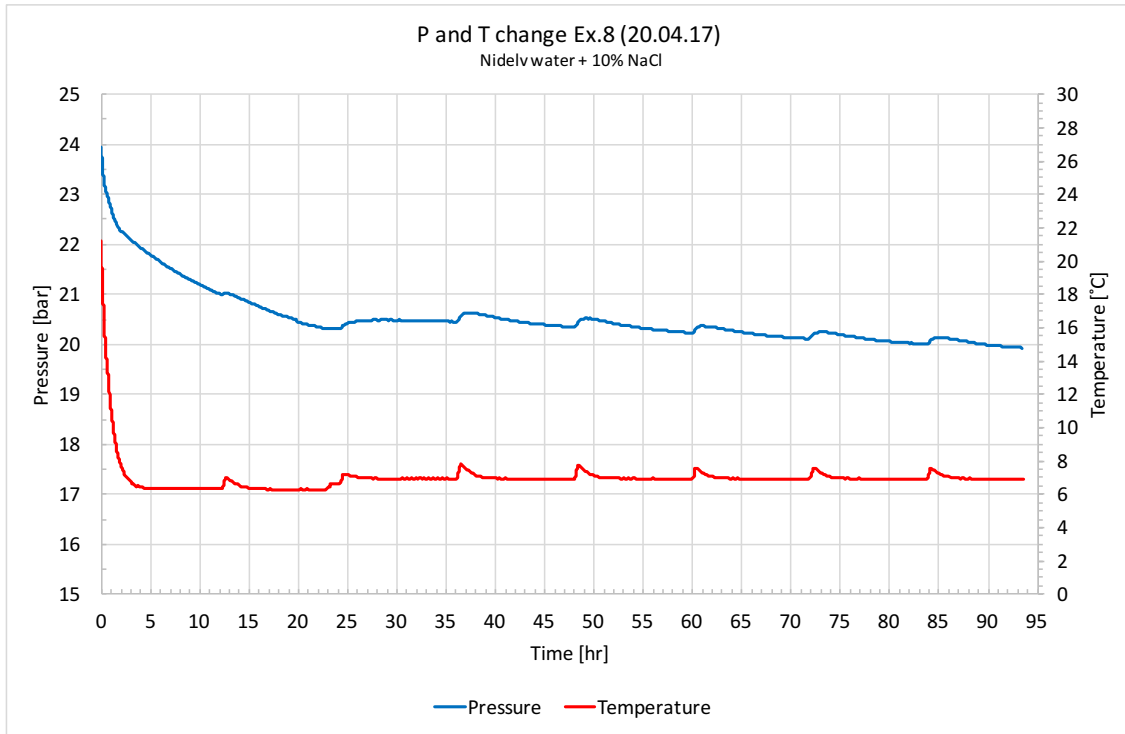


Figure A.8: Pressure and temperature changes in Experiment 8.

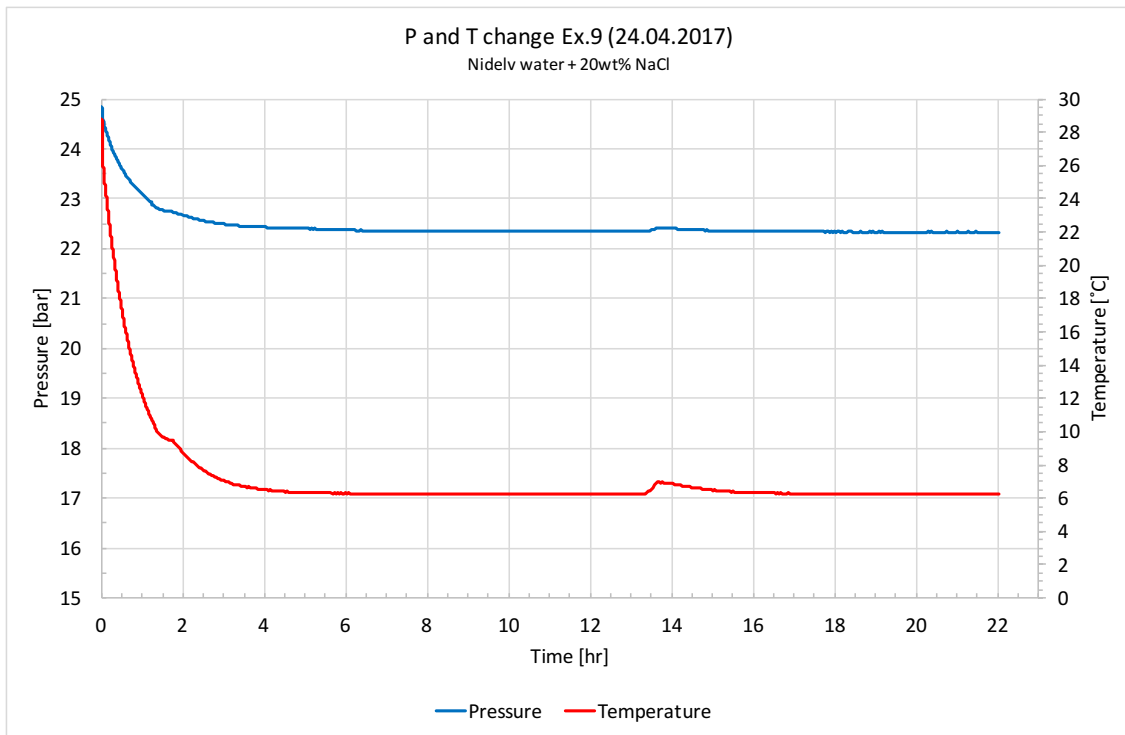


Figure A.9: Pressure and temperature changes in Experiment 9.

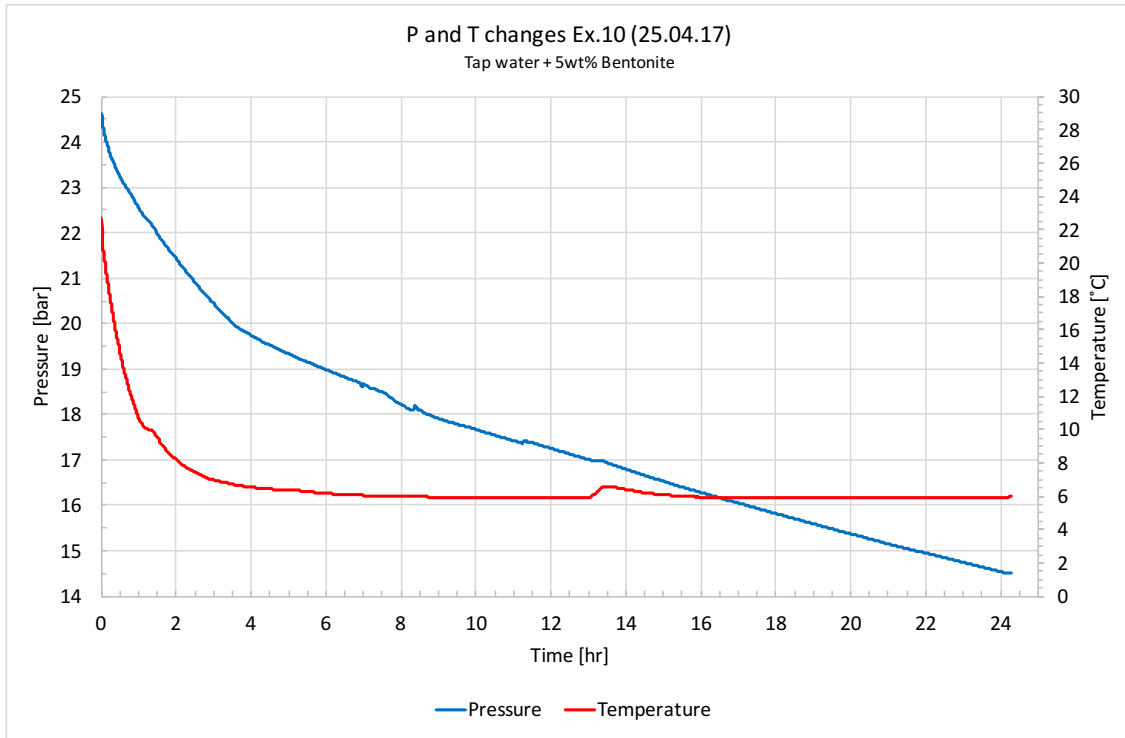


Figure A.10: Pressure and temperature changes in Experiment 10. Leakage verified.

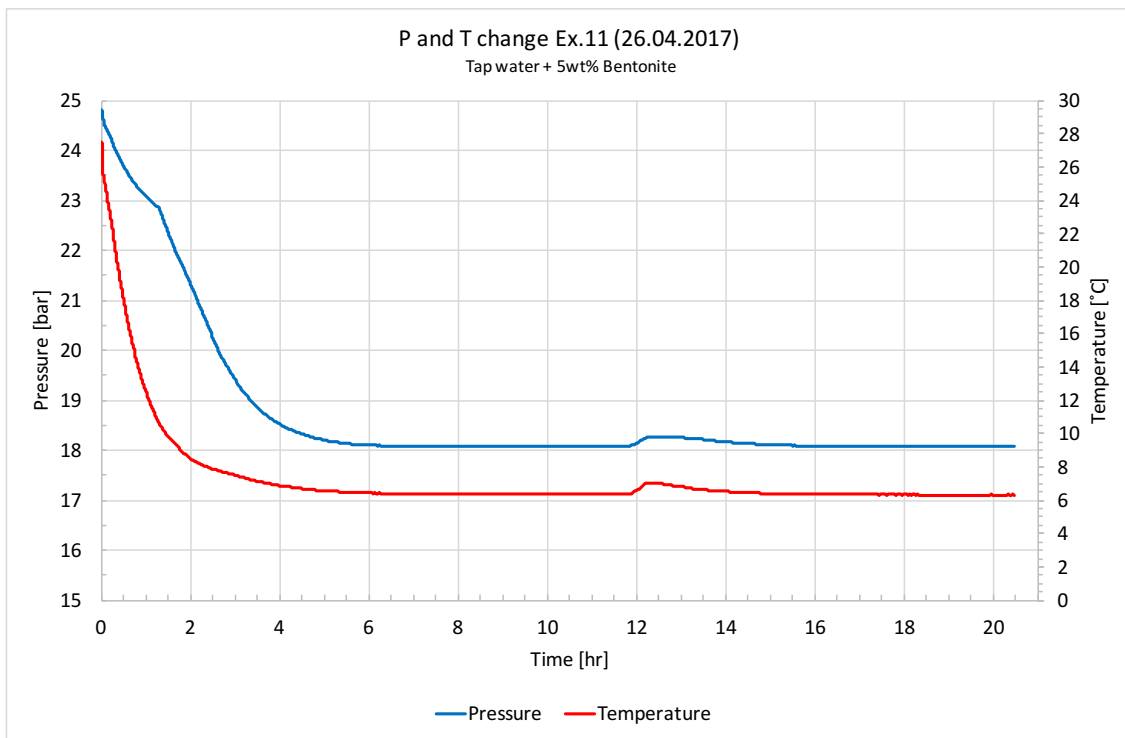


Figure A.11: Pressure and temperature changes in Experiment 11.

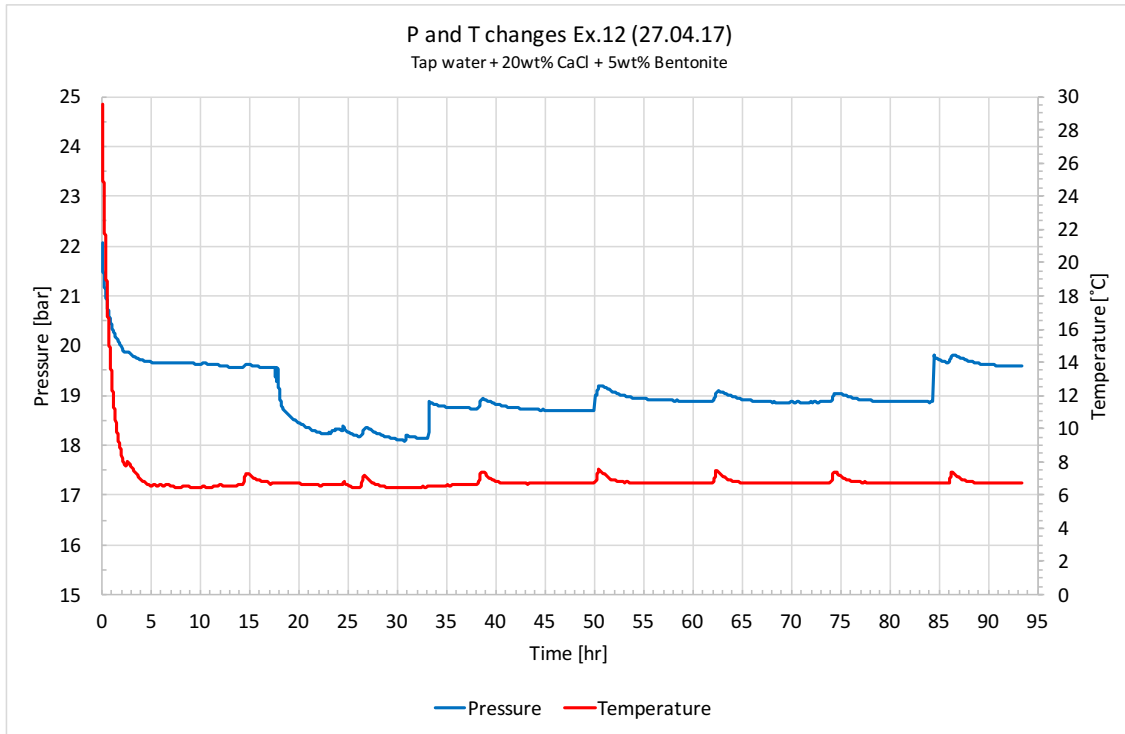


Figure A.12: Pressure and temperature changes in Experiment 12.

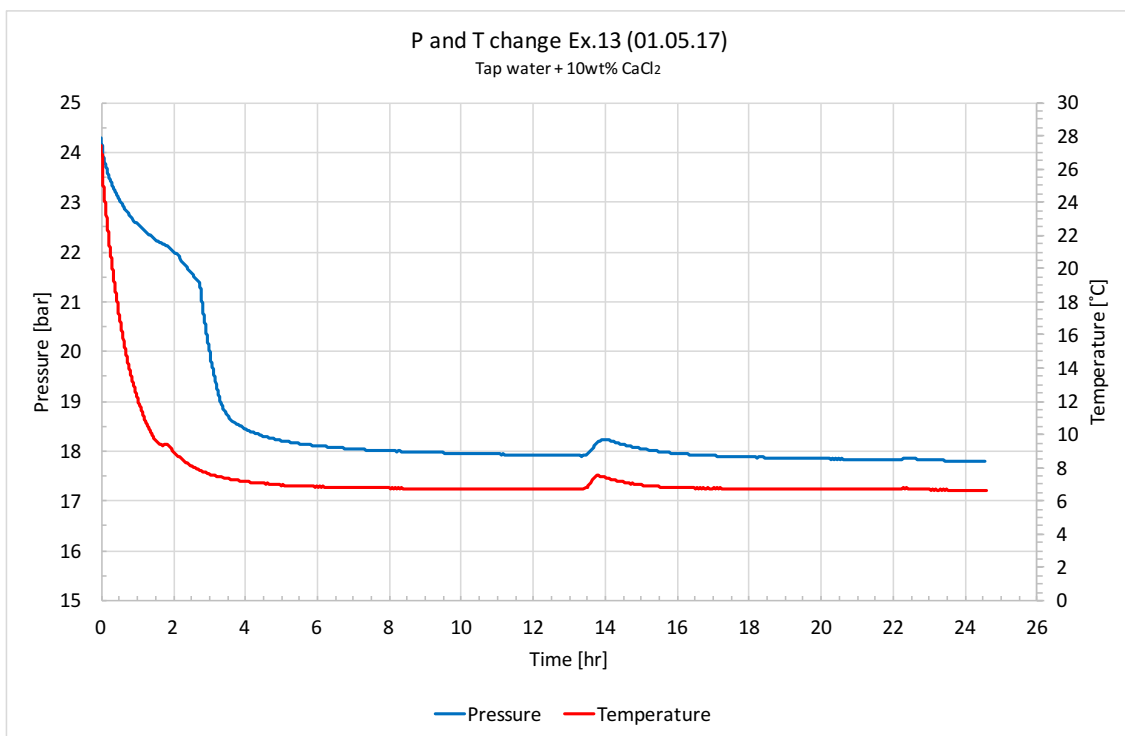


Figure A.13: Pressure and temperature changes in Experiment 13.

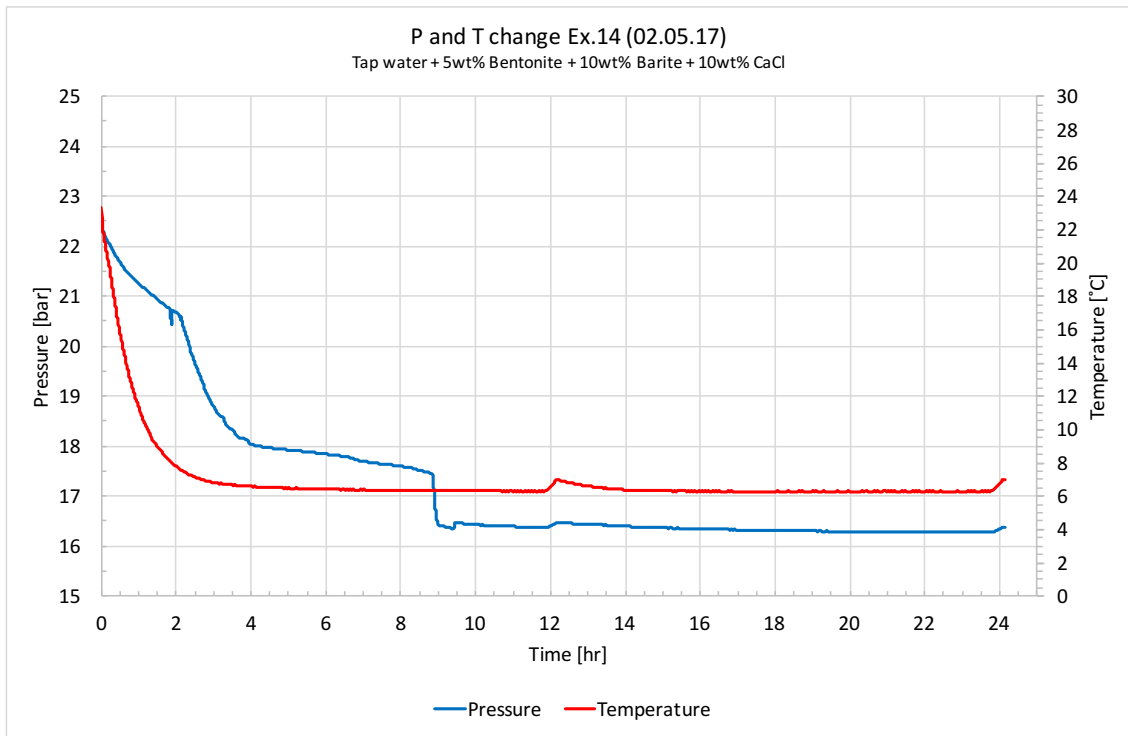


Figure A.14: Pressure and temperature changes in Experiment 14.

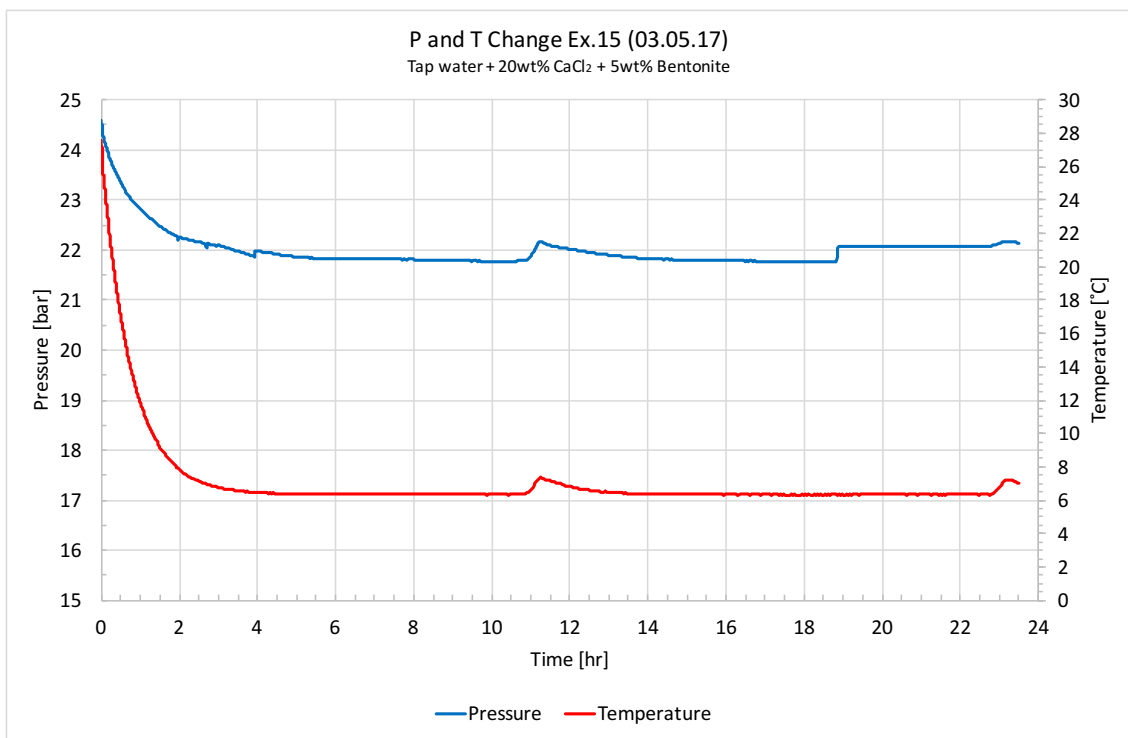


Figure A.15: Pressure and temperature changes in Experiment 15.

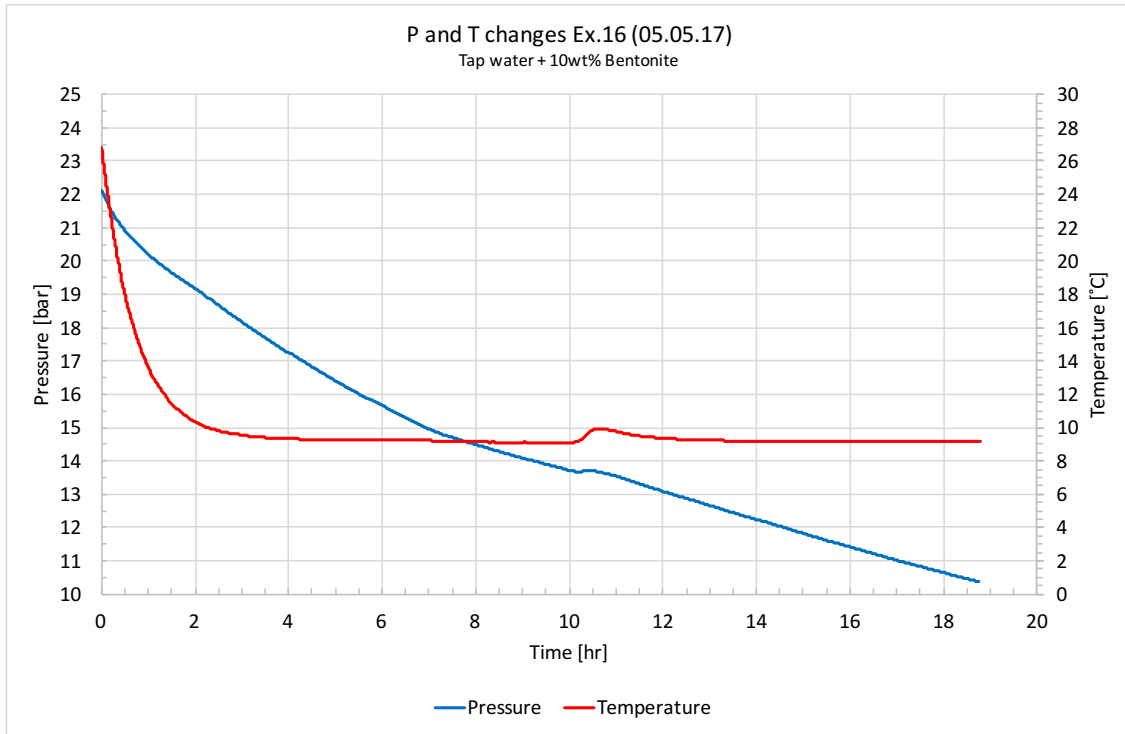


Figure A.16: Pressure and temperature changes in Experiment 16. Leakage verified.

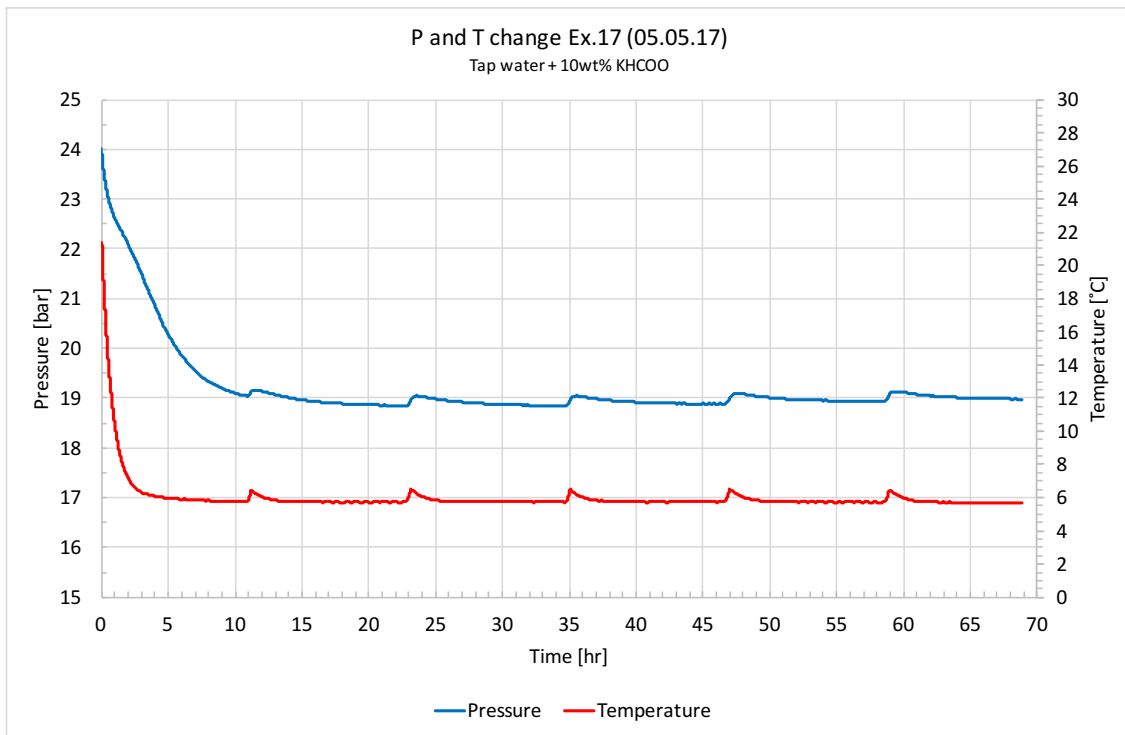


Figure A.17: Pressure and temperature changes in Experiment 17.

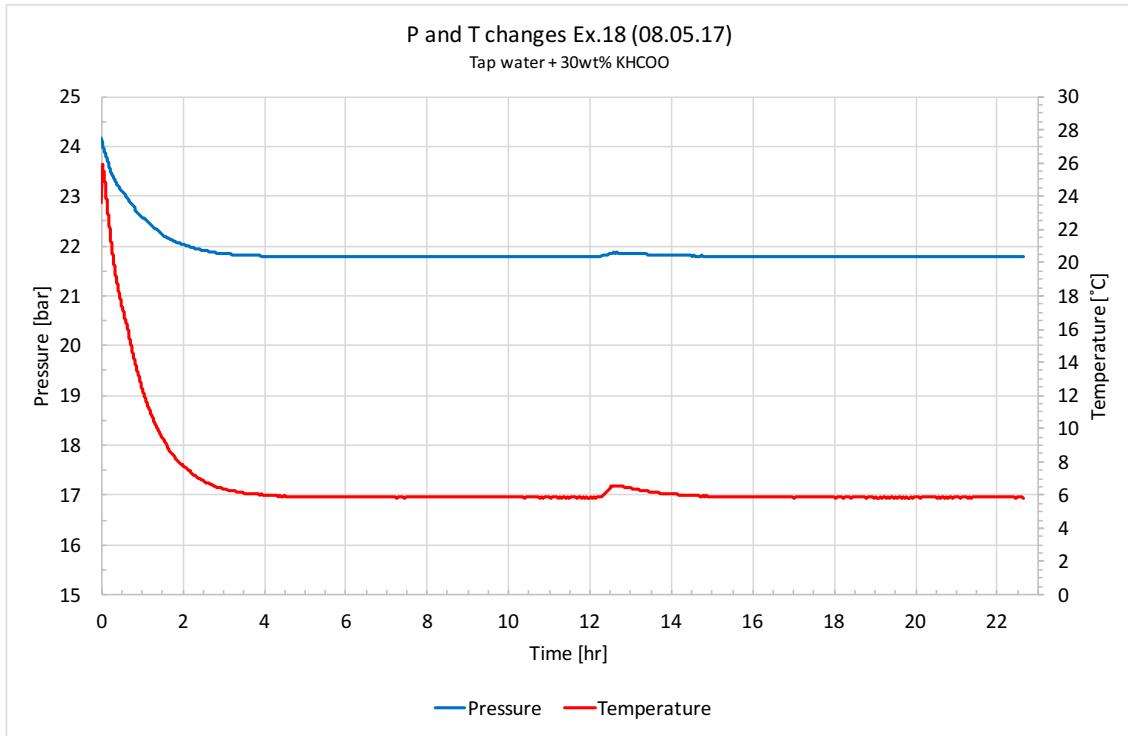


Figure A.18: Pressure and temperature changes in Experiment 18.

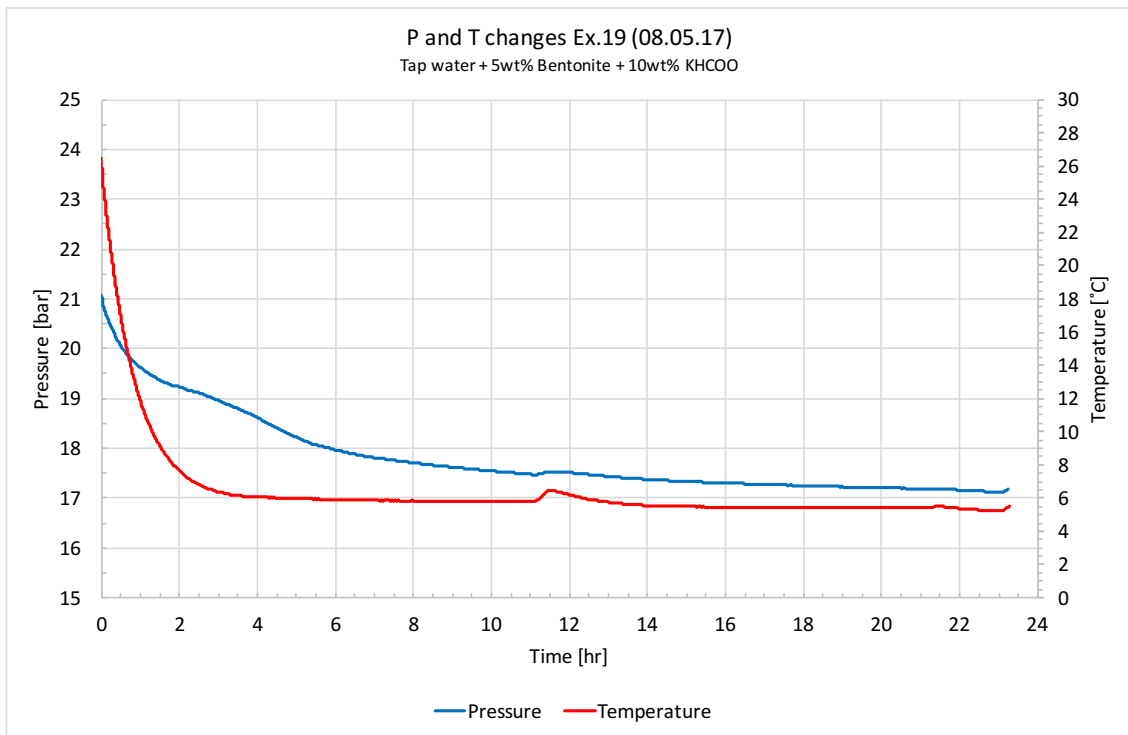


Figure A.19: Pressure and temperature changes in Experiment 19.

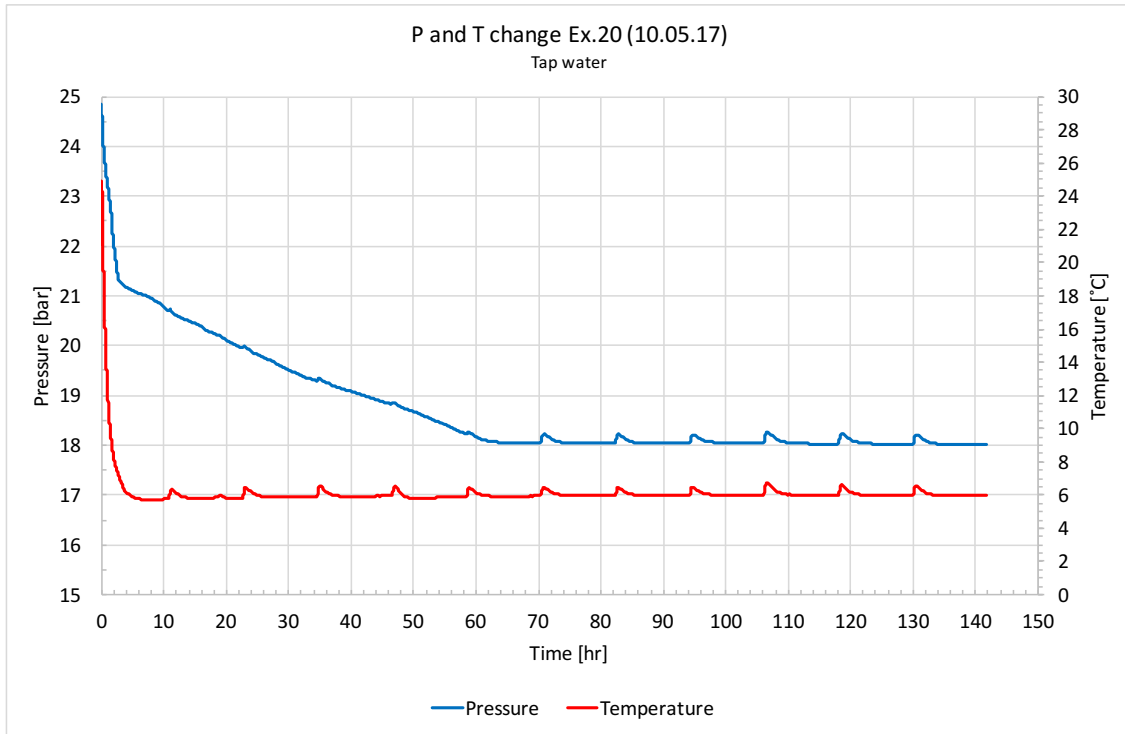


Figure A.20: Pressure and temperature changes in Experiment 20.

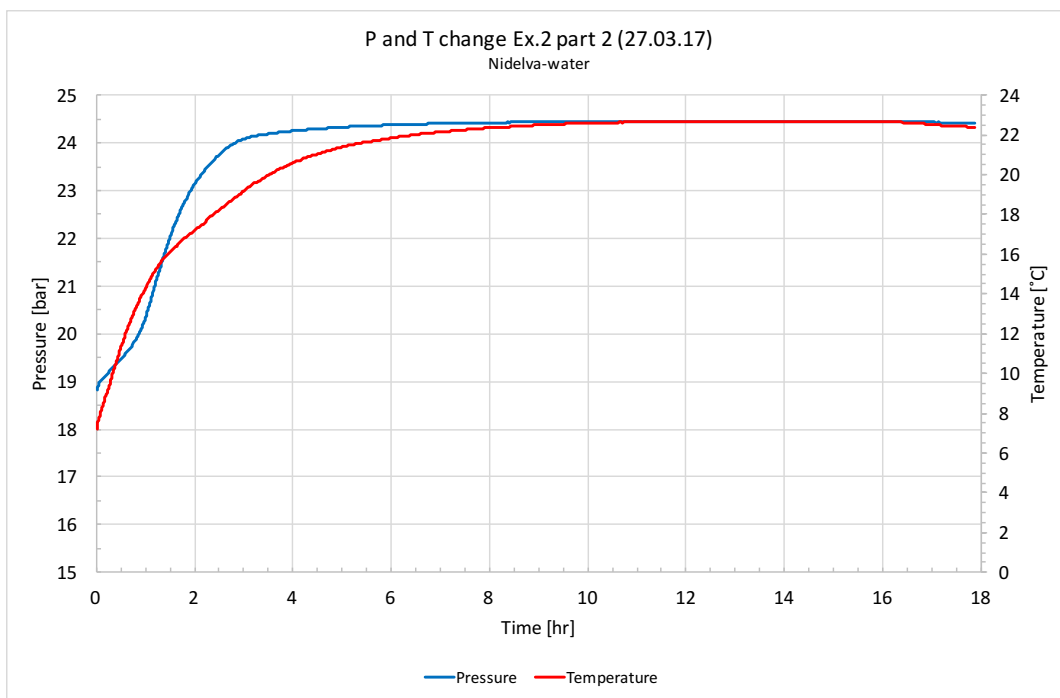


Figure A.21: Pressure and temperature changes in Experiment 2.2, dissociation of hydrates.

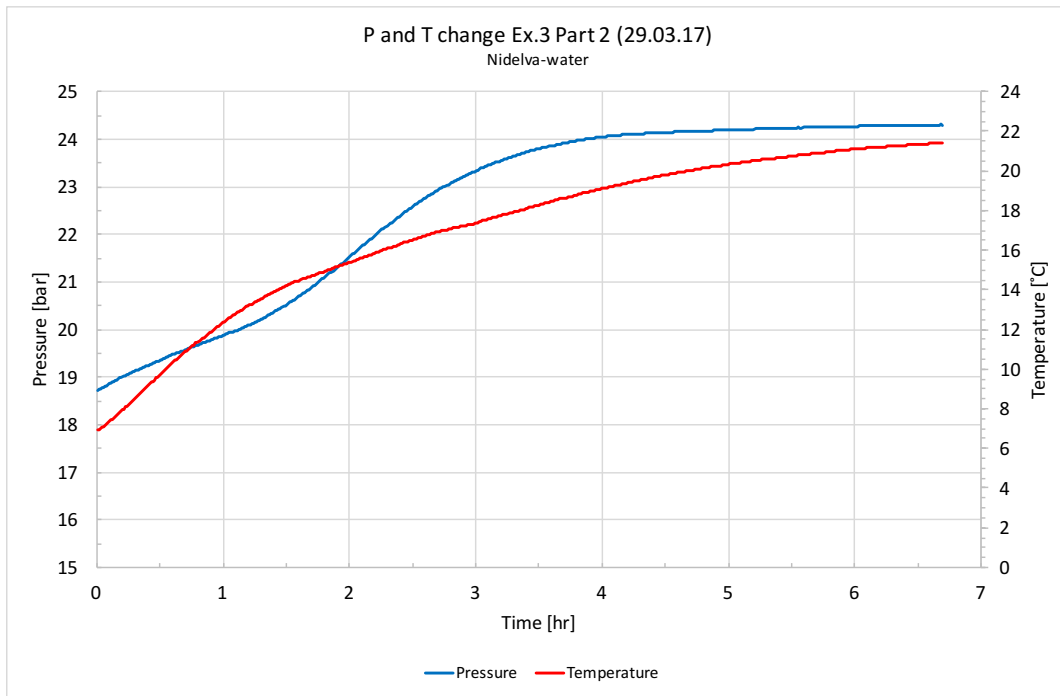


Figure A.22: Pressure and temperature changes in Experiment 3.2, dissociation of hydrates.

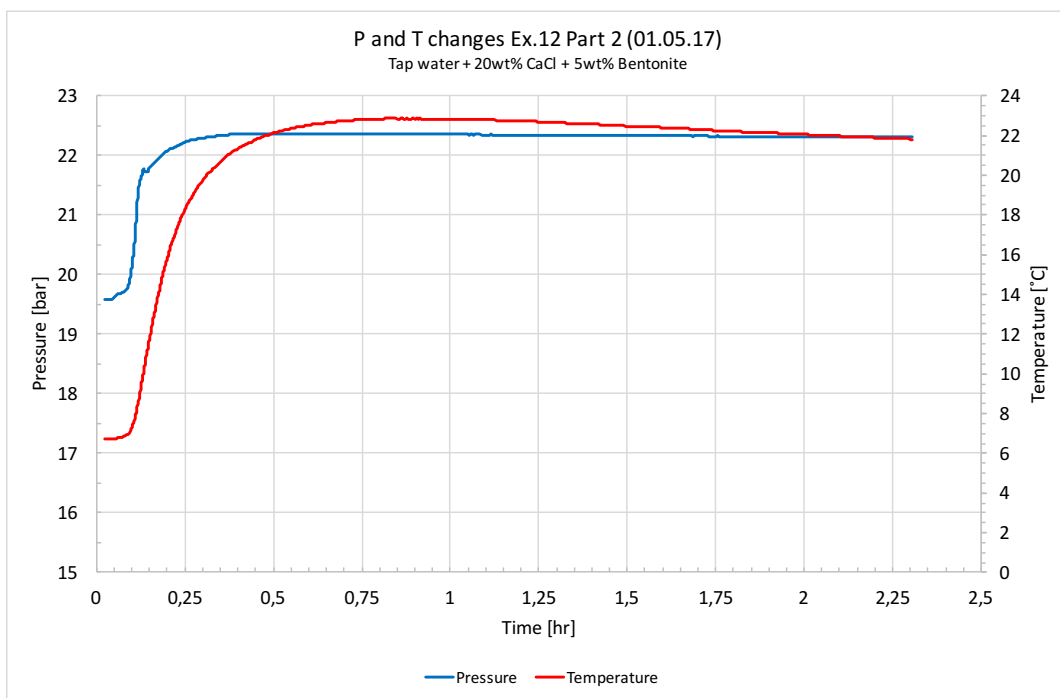


Figure A.23: Pressure and temperature changes in Experiment 12.2, dissociation of hydrates.

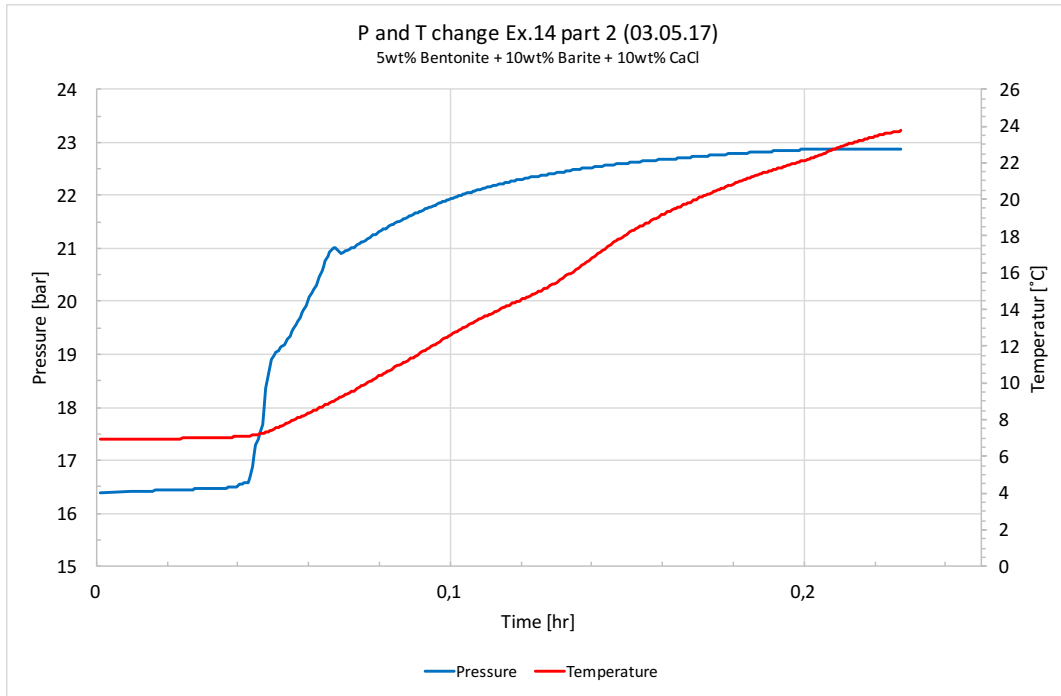


Figure A.24: Pressure and temperature changes in Experiment 14.2, dissociation of hydrates.

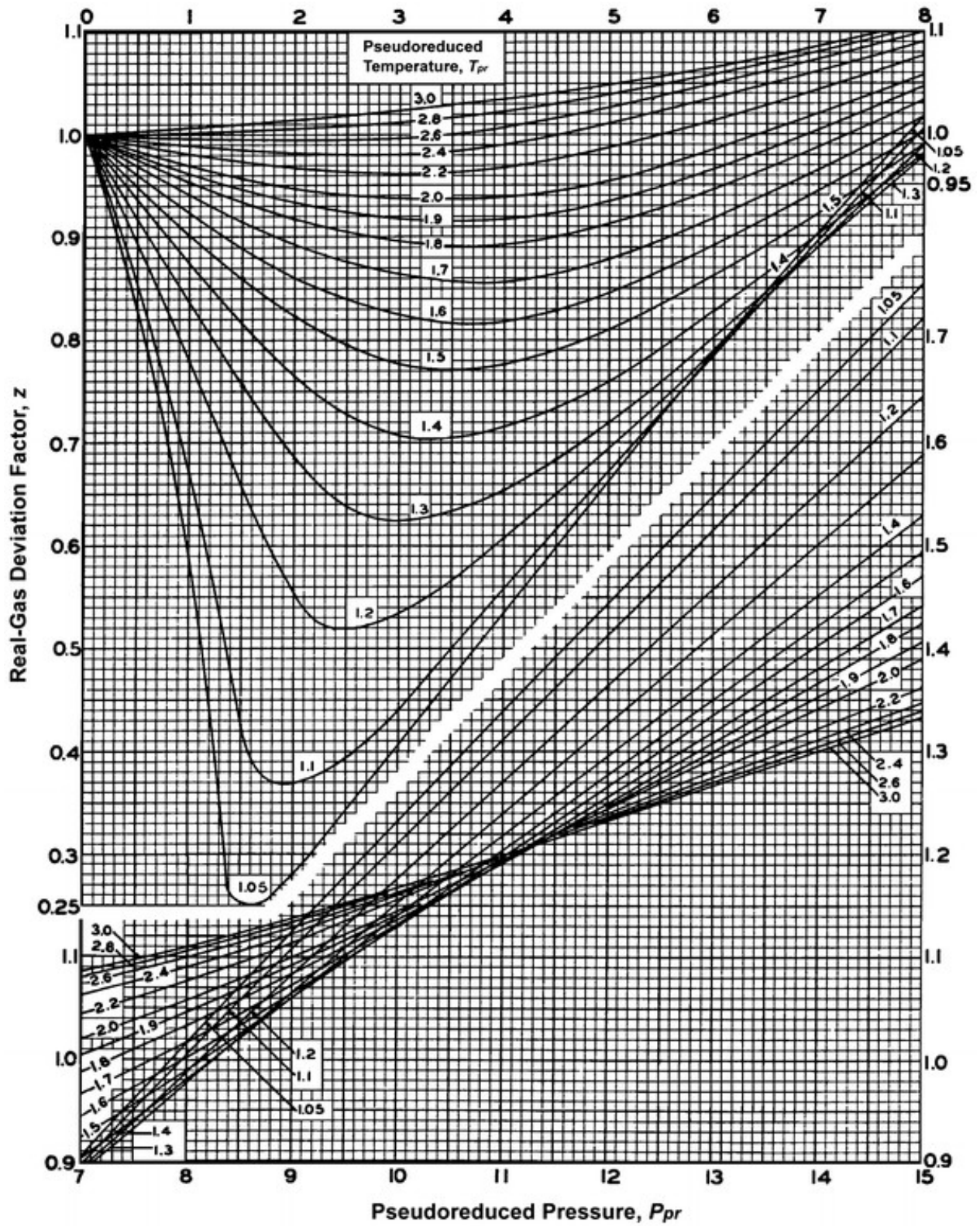


Figure A.25: Standing and Katz chart (DrillingFormulas.com, 2016)

Appendix B

Calculations

B.1 Aqueous Solution Weight Fraction Calculations

The total volume of the aqueous phase is decided to be 150mL. When the total volume is known, together with the density and weight fraction of all the additives, the total mass can be calculated. The different calculation steps are given below.

$$V_{tot} = V_w + \sum_{i=1}^N V_{a_i} = \frac{m_w}{\rho_w} + \sum_{i=1}^N \frac{m_{a_i}}{\rho_{a_i}} \quad (\text{B.1})$$

$$m_{tot} = m_w + \sum_{i=1}^N m_{a_i} \quad (\text{B.2})$$

If the weight fraction of additive is expressed as x_a , the mass of additives and water can be written as in Equation B.3.

$$m_a = x_a * m_{tot} \quad (\text{B.3})$$

$$m_w = (1 - \sum_{i=1}^N x_{a_i}) * m_{tot} \quad (\text{B.4})$$

By inserting into Equation B.1 and solving for m_{tot} , the total mass of the fluid can be expressed as

$$m_{tot} = \frac{V_{tot}}{\left(\frac{1 - \sum_{i=1}^N x_a}{\rho_w} + \sum_{i=1}^N \frac{x_a}{\rho_{a_i}} \right)} \quad (\text{B.5})$$

Since V_{tot} is known, the mass of the fluid phase can be calculated. By using Equation B.3 and B.4, the weight of water and additive which should be in the fluid phase is obtained.

B.2 Determining the Apparatus Volume

NTNU experiment

1. Temperature sleeve

$$h_{Temp_1} = 13.6 \text{ cm}$$

$$D_{Temp_1} = 0.7 \text{ cm}$$

$$\rightarrow V_{Temp_1} = \frac{\pi}{4} D_{Temp_1}^2 * h_{Temp_1} = 5.23 \text{ cm}^3$$

$$h_{Temp_2} = 1.83 \text{ cm}$$

$$D_{Temp_2} = 1.4 \text{ cm}$$

$$\rightarrow V_{Temp_2} = \frac{\pi}{4} D_{Temp_2}^2 * h_{Temp_2} = 2.82 \text{ cm}^3$$

2. Valve

$$h_{Valve_3} = 4.6 \text{ cm}$$

$$D_{Valve_3} = 0.99 \text{ cm}$$

$$\rightarrow V_{Valve_3} = \frac{\pi}{4} D_{Valve_3}^2 * h_{Valve_3} = 3.54 cm^3$$

$$h_{Valve_4} = 5.1 cm$$

$$D_{Valve_4} = 0.99 cm$$

$$\rightarrow V_{Valve_4} = \frac{\pi}{4} D_{Valve_4}^2 * h_{Valve_4} = 3.93 cm^3$$

3. Pressure sensor

$$h_{Pres_5} = 2.65 cm$$

$$D_{Pres_5} = 0.35 cm$$

$$\rightarrow V_{Pres_5} = \frac{\pi}{4} D_{Pres_5}^2 * h_{Pres_5} = 0.25 cm^3$$

4. Steel cylinder

$$h_{Cylinder_6} = 13.0 cm$$

$$D_{Cylinder_6} = 7.0 cm$$

$$\rightarrow V_{Cylinder_6} = \frac{\pi}{4} D_{Cylinder_6}^2 * h_{Cylinder_6} = 500.30 cm^3$$

5. Magnetic stirrer

$$V_{magnet_7} = 1.9 cm^3$$

6. Total internal volume of pressure cell

$$V_{tot} = V_{Cylinder_6} + V_{Pres_5} + V_{Valve_4} + V_{Valve_3} + V_{Temp_2} - V_{Temp_1} - V_{magnet_7} = 503.70 cm^3$$

B.3 Hydrate Volume and Volume Change Calculations

NTNU Experiments

1. Find the volume of the cell, volume of initial water and initial gas volume. The volume of the cell has been measured as stated in Section B.2 together with the given measures from drawings of the cell made by Noralf Vedvik at NTNU Workshop. The volume of water/mud was determined by using a scale. It was decided to have a water/mud volume of 150mL to more precisely compare the volume change and hydrate volume. In all experiments except from number 17 and 18 is the water volume close to 150mL. The exact amount of initial water volume is given in Table E.7. The initial gas volume was then found by subtracting initial water volume from the total cell volume (Equation B.6).

$$V_{gas,initial} = V_{cell} - V_{water,initial} \quad (B.6)$$

2. Find the molecular weight of the gas using Equation B.7

$$M_{gas} = \sum_{i=1}^n x_i M_i \quad (B.7)$$

3. Find the Z-factor used in the real gas law by using a Standing-Katz chart. To do this, the critical temperature and pressure to the gas components need to be found in order to find the pseudoreduced pressure and temperature which is required to be able to obtain the Z-factor from the Standing-Katz chart.

The pseudocritical pressure and temperature are calculated using Equation B.8-B.9

$$p_{pc} = \sum_{i=1}^n x_i p_{ci} \quad (B.8)$$

$$T_{pc} = \sum_{i=1}^n x_i T_{ci} \quad (\text{B.9})$$

Then, the pseudoreduced pressure and temperature can be found with Equation B.10-B.11

$$p_{pr} = \frac{p_{initial}}{p_{pc}} \quad (\text{B.10})$$

$$T_{pr} = \frac{T_{initial}}{T_{pc}} \quad (\text{B.11})$$

4. Now, the initial amount of mole gas can be found by using the real gas law given in Equation B.12

$$n_{gas,initial} = \frac{p_{initial} V_{gas,initial}}{ZRT_{initial}} \quad (\text{B.12})$$

5. The first thing that needs to be established before one can find the amount of gas moles used to create hydrates is to find the new Z factor at the final pressure and temperature which have been registered during the whole experiment. It is obtained in the same way as for the initial Z-factor by using Equation B.8-B.11.
6. The new gas density can be found using Equations B.13-B.14

$$p_{final} V = Z_{final} n R T_{final}$$

$$n = \frac{m}{M} = \frac{\rho V}{M} \quad (\text{B.13})$$

$$\rightarrow \frac{n}{V} = \frac{\rho}{M}$$

$$\rightarrow p_{final} = Z_{final} \frac{\rho_{final}}{M} RT_{final}$$

$$\Rightarrow \rho_{final} = \frac{p_{final} M}{Z_{final} RT_{final}} \quad (B.14)$$

7. The hydration number is found from Equation B.15 for sII unit cells. Three different cases with different number of filled cavities have been chosen in this thesis. $N=8.718$, $N=6.071$ and $N=10.968$ are the hydration numbers taken into consideration. The amount of hydrates formed affect the hydration number.

$$N = \frac{136}{X * 8 + Y * 16} \quad (B.15)$$

8. The molecular weight of the hydrate is given by Equation B.16.

$$M_{hyd} = M_{gas} + N * M_{water} \quad (B.16)$$

9. Set an initial hydrate volume. To be able to find out how many mole gas that has been used to form hydrates one has to start with a hydrate volume, which later will be iterated to match the pressure and temperature conditions registered on the computer from the pressure and temperature measurements.
10. When a hydrate volume has been guessed, the gas volume used to form the hydrates can be found using Equation B.17. The density of gas used in this equation is the average of the initial and final gas density, since the gas density will change continuously during the hydrate formation process.

$$V_{gas,used} = V_{hyd} \frac{\rho_{hyd}}{M_{hyd}} \frac{M_{gas}}{\rho_{gas}} \quad (B.17)$$

11. The mass of the gas used to form hydrates can be found by multiplying the gas density

and the volume of gas used.

$$m_{gas,used} = \rho_{final} * V_{gas,used} \quad (B.18)$$

Then, the amount of mole gas used can be determined by using Equation B.19

$$n_{gas,used} = \frac{m_{gas,used}}{M_{gas}} \quad (B.19)$$

12. To find the volume of water used to create hydrates one need to find the amount of mole water used and the mass of water used first. The amount of mole water used to form hydrates is found from Equation B.20, whereas the mass is obtained from Equation B.21

$$n_{water,used} = N * n_{gas,used} \quad (B.20)$$

$$m_{water,used} = n_{water,used} * M_{water} \quad (B.21)$$

Then the volume of water used can be found by dividing the mass with the density of the water, which is showed in Equation B.22

$$V_{water,used} = \frac{m_{water,used}}{\rho_{water}} \quad (B.22)$$

13. Next step is to find how much water and how much gas is left in the cell when a certain amount of hydrates have been formed. Volume of water left is given in Equation B.23 and the volume of gas is retrieved from Equation B.24. The volume of hydrates is still the guessed volume.

$$V_{water,left} = V_{water,initial} - V_{water,used} \quad (B.23)$$

$$V_{gas,left} = V_{cell} - V_{hyd} - V_{water,left} \quad (B.24)$$

14. The amount of mole gas left in the cell is calculated by subtracting the mole of gas used from the initial amount of gas moles in the cell.

$$n_{gas,left} = n_{gas,initial} - n_{gas,used} \quad (B.25)$$

15. Finally, one has to compare the calculated pressure obtained by using the volume and moles of gas left in the cell to the pressure measured from the real experiment at the temperature measured at the experiment. If they match, the guessed hydrate volume is the correct volume of hydrates formed assuming that the hydration number is correct. If the pressures differ from one another, one have to iterate the volume of gas until the pressures equals each other. This has been done my using Microsoft excel goalseeker function, by saying that the pressure obtained by using the volume and mole of gas left shall equal the final pressure conducted from the experiment by changing the hydrate volume.

The pressure obtained by using the volume and moles of gas left is found by using the real gas law.

16. The volume change is found using Equation [B.26](#).

$$Gas\ volume\ reduction = \frac{V_{gas,used} - V_{hyd} + V_{w,used}}{V_{gas,used}} \quad (B.26)$$

SINTEF Test

1. Find the seawater density by using a pycnometer.

$$m_{pycnometer} = 31.454\ g$$

$$m_{pycnometer\ w/\ water} = 83.456\ g$$

$$V_{\text{pycnometer}} = 50.655 \text{ mL}$$

$$\begin{aligned} \rightarrow \rho_{\text{water}} &= \frac{m_{\text{pycnometer w/ water}} - m_{\text{pycnometer}}}{V_{\text{pycnometer}}} \\ &= \frac{83.456 - 31.454}{50.655} = 1.02659 \text{ g/c}^3 \end{aligned}$$

2. Calculate volume of wheel

$$ID = 5.251 \text{ cm}$$

$$L = 2\pi$$

$$\begin{aligned} V_{\text{wheel}_1} &= \frac{\pi}{4} ID^2 L \\ &= \frac{\pi}{4} 5.251^2 * 2\pi = 13.607 \text{ L} \end{aligned}$$

3. Calculate volume of wheel filled with seawater, determined by weight

$$m_{\text{wheel}} = 218.634 \text{ kg}$$

$$m_{\text{wheel w/ water}} = 232.206 \text{ kg}$$

$$\begin{aligned} m_{\text{water inside wheel}} &= m_{\text{wheel w/ water}} - m_{\text{wheel}} \\ &= 232.206 - 218.634 = 13.573 \text{ kg} \end{aligned}$$

$$\begin{aligned} \rightarrow V_{\text{wheel}} &= \frac{m_{\text{water inside wheel}}}{\rho_{\text{water}}} \\ &= \frac{13.573}{1.02659} = 13.221 \text{ L} \end{aligned}$$

The two wheel volume calculations differs from each other because an air gap is formed at the top of the wheel due to the design where the inlet is on the inside of the wheel (Fossen, 2017a).

4. Drain approximately three litres of seawater out of the wheel, and refill with gas

$$m_{\text{wheel drained}} = 229.093 \text{ kg}$$

To find the exact volume of water and gas remaining inside the wheel it is essential to find the weight of the water that has been drained from the wheel.

$$\begin{aligned}
 m_{\text{drained seawater}} &= m_{\text{wheel w/seawater}} - m_{\text{wheel drained}} \\
 &= 232.206 - 229.093 = 3.113 \text{ kg}
 \end{aligned}$$

$$\begin{aligned}
 V_{\text{drained water}} &= \frac{m_{\text{drained water}}}{\rho_{\text{water}}} \\
 &= \frac{3.113}{1.02659} = 3.032 \text{ L}
 \end{aligned}$$

$$\begin{aligned}
 \rightarrow V_{\text{water inside wheel}} &= V_{\text{wheel}} - V_{\text{drained water}} \\
 &= 13.221 - 3.032 = 10.189 \text{ L}
 \end{aligned}$$

The volume of gas in the wheel is:

$$\begin{aligned}
 V_{\text{gas in wheel}} &= V_{\text{wheel}_1} - V_{\text{water inside wheel}} \\
 &= 13.607 - 10.189 = 3.418 \text{ L}
 \end{aligned}$$

5. The weight of gas injected was determined using the same scale as previously. The accuracy is $\pm 5\text{g}$. When this is known, both the initial gas density and the amount of initial moles injected into the wheel can be found.
6. The next steps are similar to step 7-16 for the NTNU experiment procedure (see Subsection [4.1.11](#))

B.4 Conversion of Hydrate Equilibrium Pressure into Depth

Equation [B.27](#) describes the pressure as a function of density and height. Solving for h one yield the height of a fluid column of density ρ which creates this pressure.

$$P = \rho gh \tag{B.27}$$

$$h = \frac{P}{g\rho} \tag{B.28}$$

By inserting the mud density in the well and the hydrate equilibrium pressure at a given temperature into Equation [B.28](#), the hydrate equilibrium curve can be plotted as a function of depth.

Appendix C

Procedures

C.1 Shut-in Procedure

Table C.1: Example procedure for shut-in while drilling (retrieved from [Robinson \(2015\)](#)).

Step	Action
1	Immediately raise the drillstring until the bit is off bottom and place the string at a proper shut-in location when a primary warning sign of a kick is being observed.
2	Stop rotation. Stop the mud pumps and check for flow. Ensure that the riser boost valve is closed.
3	Close the selected BOP.
4	Once the BOP is closed, ensure that the choke manifold is lined up properly (closed) and open the selected subsea choke- and kill line valves.
5	Monitor for flow in the riser.
6	Check for surface leaks. Alert supervisor.
7	Read and record SIDPP and SICP. Read and record SICP on both choke- and kill lines and pit gain. Monitor and record this data periodically.
8	If hang-off is desired, it can be initiated now.

According to ([Brechan, 2015](#)) it should be noted that

1. Only raise the drillstring if time permits. This operation should be carried out as fast as practically possible in critical or extreme circumstances.

2. On surface BOP, closing the ram locks are optional.
3. On subsea BOP, certain ram locks activate in any position along the piston stroke. It is an integral part of the operating system.
4. Make sure that the valve upstream of the choke is closed when monitoring the casing pressure.
5. If a float valve is present in the string, the drill pipe pressure might be zero.
6. If unable to install FOSV due to strong flow:
 - With top drive: Lower, stab and make up the top drive
 - Without a drop drive: Consider closing the shear rams or drop the string (provided there is no tool joint opposite the shear rams)

C.2 Well Control Methods

Driller's Method

Table C.2: Well control procedure for the first circulation in Driller's Method ([Brechan \(2015\)](#); [WildWellControl \(2016\)](#); [Welltrain \(2008\)](#)).

Step	Action
1	Open the choke. Bring the pump rate up to desired kill speed while containing a constant casing pressure. Start circulating the original drilling fluid simultaneously at the selected kill rate.
2	Adjust the choke opening until the choke pressure equals the SICP while reaching and maintaining kill rate. Record the choke pressure throughout the circulation.
3	Read standpipe pressure. It should be equal to the normal pre-kick pump test circulation pressure at the selected pump speed plus the SIDPP. If observed standpipe pressure disagrees with the calculated value, the observed pressure should be considered correct. Investigate.
4	Maintain a constant standpipe pressure and pump rate whilst circulating out the gas influx.
5	Stop the pump and close in the well when all gas influx is circulated out. Check the SIDPP and SICP. SICP must be equal to the original SIDPP. Note: The well is controlled, not killed.
6	Weight up kill mud to required density and prepare for the second circulation.

Table C.3: Well control procedure for the second circulation in Driller's Method ([WildWellControl \(2016\)](#); [Welltrain \(2008\)](#); [Samuel \(2010\)](#)).

Step	Action
1	Circulate heavy kill mud with a total volume, equal to the drill string volume capacity. Keep the choke pressure equivalent to, original SIDPP.
2	Maintain constant choke pressure until mud reach the bit. At the bit, the CDPP should drop from CDPPi to CDPPf.
3	Continue circulation until all original mud, in the annulus is displaced.
4	Close the choke. Read SIDPP and SICP. Note: Pressures should be equal to zero. If not, continue well control procedure.
5	Open the well and resume drilling operations.

Weight & Wait MethodTable C.4: Well control procedure for the Wait & Weight Method ([WildWellControl \(2016\)](#); [Well-train \(2008\)](#)).

Step	Action
1	Open choke. Start circulating kill fluid. Bring pump up to kill rate while maintaining constant SICP.
2	Follow drill pipe pressure schedule as kill fluid is pumped down to bit (Drill pipe pressure vs Pump strokes schedule).
3	At the bit, the CDPP should drop from CDPPi to CDPPe.
4	Maintain constant CDPPF until annulus is filled with kill fluid.
5	Stop pump. Check for flow.
6	Close choke. Check pressures. Note: Pressures should be equal to zero. If not, continue well control procedure.
7	Open the well and resume drilling operations.

Appendix D

Risk Assessment

NTNU		Risk assessment		Prepared by	Number	Date
				HSE section	HMSRV2603E	04.02.2011
HSE/IKS				Approved by		Replaces
				The Rector		01.12.2006




Unit: Department of Geoscience and Petroleum

Line manager:

Date: 06.06.2017

Participants in the identification process: Roger Overå (Staff Engineer, responsible for chemicals at the laboratory), Bendik Helgestad (M.Sc. Student) and Michaela Gunhildrud (M.Sc. Student)

Short description of the main activity/main process: Master project for students Bendik Helgestad and Michaela Gunhildrud. Project title. Drilling Fluid Volume Change due to Hydrate Formation and its Impact on Well Control

Signatures: Responsible supervisor: 

Bendik Helgestad
Michaela Gunhildrud
 Student: *Michaela Gunhildrud*

Activity from the identification process form	Potential undesirable incident/strain	Likelihood (1-5)	Consequence:			Risk Value (human)	Comments/status Suggested measures
			Human (A-E)	Environment (A-E)	Economy/material (A-E)		
Accidents and injuries related to unpredicted burst of pressure cell due to overpressure	Injury to personnel caused by debris and damage to equipment	1	B	A	A	1A	Safety factors will be applied to all calculations. Apparatus was pressure tested to 50 bar, while maximum pressure of the gas flask was 30 bar. A safety valve was mounted on the pressure cell.
Fire	Personnel could suffer from smoke inhalation and burns.	1	B	B	A	1B	Good housekeeping. Clear work area of all combustibles. Fire extinguisher and fire blanket available at the work area. Comply with site hot work permits/rules. Always be two or more people inside the laboratory.
Gas leakage	High methane concentration in the area	2	B	A	A	2A	Follow gas filling procedure. Ensure regulator and gas flask valve are closed. Use fume hood when depressurizing.

NTNU		Risk assessment		Number		Date	
				HMSRV/2603E		04.02.2011	
HSE/KS						Replaces 01.12.2006	



Falling objects hitting body	Serious foot and other injuries to workers, other on site.	2	A	A	A	2A	Always use both hands when carrying the pressure cell. Use protective foot wear.
Eye and skin irritation	Spilling of chemicals	2	A	A	A	2A	Use protective clothing and eye protection at all time. Use protective gloves when handling chemicals.

Likelihood, e.g.:
 1. Minimal
 2. Low
 3. Medium
 4. High
 5. Very high

Consequence, e.g.:
 A. Safe
 B. Relatively safe
 C. Dangerous
 D. Critical
 E. Very critical

Risk value (each one to be estimated separately):
 Human = Likelihood x Human Consequence
 Environmental = Likelihood x Environmental consequence
 Financial/material = Likelihood x Consequence for Economy/material

NTNU		Risk assessment		Prepared by	Number	Date
HSE/KS				HSE section	HMSRV2603E	04.02.2011
				Approved by		Replaces
				The Rector		01.12.2006



Potential undesirable incident/strain

Identify possible incidents and conditions that may lead to situations that pose a hazard to people, the environment and any materiel/equipment involved.

Criteria for the assessment of likelihood and consequence in relation to fieldwork

Each activity is assessed according to a worst-case scenario. Likelihood and consequence are to be assessed separately for each potential undesirable incident. Before starting on the quantification, the participants should agree what they understand by the assessment criteria:

Likelihood

Minimal 1	Low 2	Medium 3	High 4	Very high 5
Once every 50 years or less	Once every 10 years or less	Once a year or less	Once a month or less	Once a week

Consequence

Grading	Human	Environment	Financial/material
E Very critical	May produce fatality/ies	Very prolonged, non-reversible damage	Shutdown of work >1 year.
D Critical	Permanent injury, may produce serious serious health damage/sickness	Prolonged damage. Long recovery time.	Shutdown of work 0.5-1 year.
C Dangerous	Serious personal injury	Minor damage. Long recovery time	Shutdown of work < 1 month
B Relatively safe	Injury that requires medical treatment	Minor damage. Short recovery time	Shutdown of work < 1week
A Safe	Injury that requires first aid	Insignificant damage. Short recovery time	Shutdown of work < 1day

The unit makes its own decision as to whether opting to fill in or not consequences for economy/materiel, for example if the unit is going to use particularly valuable equipment. It is up to the individual unit to choose the assessment criteria for this column.

Risk = Likelihood x Consequence

Please calculate the risk value for "Human", "Environment" and, if chosen, "Economy/materiel", separately.

About the column "Comments/status, suggested preventative and corrective measures":

Measures can impact on both likelihood and consequences. Prioritise measures that can prevent the incident from occurring; in other words, likelihood-reducing measures are to be prioritised above greater emergency preparedness, i.e. consequence-reducing measures.

Appendix E

Tables and Lists

E.1 Technical Description of Equipment Used in the NTNU Experiments

Table E.1: Technical description of the equipment used in the NTNU experiments.

Type of Equipment	Producer	Operating Conditions
3-vay valve	Swagelok	
Steel cap	NTNU workshop	
Bottom steel container	NTNU workshop	
Temperature gauge	S+S Regeltechnik GmbH	+150°C
Immerson Sleeve	S+S Regeltechnik GmbH	
Pressure gauge	Gems	0-25 bar
Magnetic-Stirrer	Heidolph MR Hei-Standard	100-1.400 rpm
High-P Prop. Relief Valve	Swagelok	10-400 bar
Stir Bar	Bel-art	

E.2 Van't Hoff Factor and Molar Mass for NaCl, CaCl₂ and KCHOO

Table E.2: Van't Hoff factor and molar mass for various solutes used in used in Equation 2.12.

	NaCl	CaCl ₂	KCHOO
i	2	3	2
M_a [$\frac{kg}{mol}$]	0.0584	0.1110	0.0841

E.3 Effect of MEG, MeOH and NaCl as Hydrate Inhibitors

Table E.3: The temperature depressing effect of different inhibitors, in various concentrations, on the hydrate equilibrium. Calculated using Equations in (KAMATH and PATIL, 1994).

Inhibitor	MEG	MeOH	NaCl
[wt%]	ΔT_h [°C]	ΔT_h [°C]	ΔT_h [°C]
5	-0.97	-1.98	-2.61
10	-2.17	-4.00	-6.22
15	-3.59	-6.05	-10.85
20	-5.23	-8.12	-16.48
25	-7.09	-10.23	-23.13
30	-9.18	-12.37	-30.78
35	-11.49	-14.54	-39.45
40	-14.03	-16.74	-
45	-16.79	-18.97	-
50	-19.77	-21.23	-
55	-22.98	-23.52	-
60	-26.40	-25.85	-

E.4 Hydrate Equilibrium Pressure and Temperature

Input values for the hydrate equilibrium curve, 100% methane, 97% methane and 3% propane, NTNU gas, 85% methane and 15% propane

Table E.4: Hydrate equilibrium pressures at various temperatures, for different gas compositions. Data obtained from AspenHYSYS simulations.

Temperature [°C]	Hydrate Formation Pressures [bar]			
	100 % C ₁	97% C ₁ +3% C ₃	90% C ₁ +10% C ₃	85% C ₁ +15% C ₃
1	29.33	9.73	5.60	4.60
2	32.43	10.98	6.38	5.27
3	35.86	12.39	7.26	6.03
4	39.71	13.97	8.25	6.88
5	44.03	15.75	9.37	7.84
6	48.88	17.77	10.63	8.93
7	54.35	20.04	12.05	10.16
8	60.55	22.63	13.65	11.54
9	67.61	25.58	15.47	13.11
10	75.67	28.95	17.53	14.89
12	95.70	37.31	22.56	19.21
14	122.88	48.72	29.19	24.88
16	160.68	65.08	38.19	32.50
18	213.86	90.44	51.01	43.14
20	288.06	133.84	70.94	59.16
22	389.27	206.14	107.70	87.31
24	523.77	305.04	182.54	148.26
25	605.70	363.16	233.59	193.86

Input values for the hydrate equilibrium curve, SINTEF gas

Table E.5: Input values retrieved for the hydrate equilibrium curve for the SINTEF gas using Aspen HYSYS software.

Hydrate formation pressure [bar]	Hydrate formation temp.	
	Freshwater [°C]	Seawater (3.5wt% NaCl) [°C]
8.59	1.00	-0.717
9.70	2.00	0.28
10.95	3.00	1.28
12.36	4.00	2.28
13.93	5.00	3.28
15.71	6.00	4.28
17.72	7.00	5.28
19.98	8.00	6.28
22.55	9.00	7.28
25.47	10.00	8.28
32.65	12.00	10.28
42.25	14.00	12.28
55.60	16.00	14.28
75.29	18.00	16.28
107.04	20.00	18.28
160.96	22.00	20.28
240.42	24.00	22.28
287.99	25.00	23.28
596.75	30.00	28.28
1524.79	40.00	38.28
2684.71	50.00	48.28
3906.29	60.00	58.28

E.5 General Information About the Different Experiments Performed at NTNU

E.5.1 Notes From the NTNU Experiments

Ex. 1 Ended the experiment because the pressure cell was suspected to leak. No leak was observed visually.

Ex. 2 No notes.

Ex. 2 Part 2: Started heating the pressure cell 12:20pm 27.03.17. The experiment was heated over night. Observed that it takes approximately 6.7 hours to get the pressure back to original pressure when heating in room temperature.

Ex.3 Used the same fluid as in Experiment 2. Temperature change after 4.4 hours, could be due to leakage spray. No leak observed.

Ex.3 Part 2: No notes.

Ex.4 Systematic stirring 400rpm. Opened the pressure cell. Observed hydrates.

Ex.5 Systematic stirring 400rpm. Increased the stirring speed after 18 hours. Did not see a difference in pressure.

Ex.6 Systematic stirring 300rpm.

Ex.7 Used the same fluid as in Experiment 3 but added more barite. Calculated how much barite was needed to be removed in order to give 30wt% barite.

Ex.8 Systematic stirring 300rpm. increased the stirring speed after 22.9 hours.

Ex.9 Removed 9.22g fluid from Experiment 8 and added 18.76g NaCl to the fluid.

Ex.10 Proved leakage by using leakage spray, and by submerging the cell into water.

Ex.11 Opened the experiment and found two hydrate chunks. The biggest chunk melted after 20 minutes. Random stirring 500rpm.

Ex.12 Random stirring 500rpm.

Ex.12 Part 2: No notes.

Ex.13 Random stirring 500rpm. Stopped the experiment either before the hydrate formation was done, or leakage occurred. Could not find a leakage with the leakage spray.

Ex.14 Random stirring 500rpm.

Ex.14 Part 2: Placed the pressure cell in a bucket of water. The water temperature was 30°C, removed the pressure cell from the bucket once the temperature reached 22°C.

Ex.15 Added 174.54g of the fluid mixture, resulting in a volume of 150.6ml

Ex.16 Increased rotation from 750 to 1400rpm, could not hear any rotation. Maybe too viscous fluid. Leakage observed.

Ex.17 Uncertain whether 10wt% or 15wt% of KCHOO was added to the fluid phase

Ex.17 Part 2: No notes.

Ex.18 Random stirring 500rpm.

Ex.19 Checked for leakage with leakage spray, no leakage found.

Ex.20 Checked for leakage with leakage spray, no leakage found.

E.5.2 Composition and Initial Volume of the Aqueous Phase

Composition of the aqueous phase

Table E.6: Composition of the aqueous phase in each experiment.

Experiment	Tap water [wt%]	Nidelva water [wt%]	Fjord water [wt%]	NaCl [wt%]	CaCl ₂ [wt%]	KHCOO [wt%]	Bentonite [wt%]	Barite [wt%]
1		100						
2		100						
3.1		100						
4			100					
5			98.5	1.5				
6		90						10
7		70						30
8		90		10				
9		80		20				
10	95						5	
11	95						5	
12.1	75				20		5	
13	90				10			
14.1	75				10		5	10
15	75				20		5	
16	90						10	
17	90					10		
18	70					30		
19	85					10	5	
20	100							

Initial Volume of the Aqueous Phase

Table E.7: Initial volume of the aqueous phase in each experiment.

Experiment	$V_{water, initial}$ [mL]
1*	
2	150.0
3	150.0
4	150.0
5	150.0
6	150.1
7	150.0
8	149.9
9	150.0
10*	
11	149.3
12	150.8
13	150.0
14	150.7
15	150.6
16*	
17	155.8
18	163.7
19	150.7
20	150.0
* Leakage	

E.5.3 Volume Change and Amount of Hydrate Volume Formed

In-Between Case

Table E.8: Total amount of hydrates formed and the volume reduction obtained in the experiments conducted at the NTNU laboratory with the NTNU gas (in-between case).

Experiment	In-between case				
	$V_{gas,used}$ [mL]	$V_{water,used}$ [mL]	$V_{tot,used}$ [mL]	V_{hyd} [mL]	Volume reduction [%]
1*					
2	80.93	12.06	93.00	15.09	96.3
3	79.46	11.91	91.37	14.89	96.2
4	81.22	12.17	93.39	15.31	96.1
5	74.28	11.24	85.52	14.36	95.8
6	93.73	12.78	106.52	17.33	95.2
7	90.19	10.35	100.54	16.86	92.8
8	46.65	6.75	53.40	8.92	95.4
9**	8.68	1.26	9.94	1.77	94.2
10*					
11	89.47	12.84	102.31	16.48	95.9
12**	13.28	1.64	14.93	2.37	94.5
13	87.52	12.02	99.54	15.80	95.7
14	98.00	11.06	109.07	16.41	94.5
15**	9.21	1.29	10.50	1.86	93.8
16*					
17	64.07	9.21	73.27	12.03	95.6
18**	11.06	1.53	12.59	2.22	93.8
19	62.34	7.74	70.08	10.44	95.7
20	99.40	14.94	114.34	18.58	96.3

* Leakage in the pressure cell.

** Assumed not possible to form hydrates.

Best Case

Table E.9: Total amount of hydrates formed and the volume reduction obtained in the experiments conducted at the NTNU laboratory with the NTNU gas (best case).

Experiment	Best case				
	$V_{gas, used}$ [mL]	$V_{water, used}$ [mL]	$V_{tot, used}$ [mL]	V_{hyd} [mL]	Volume reduction [%]
1*					
2	80.54	8.36	88.90	10.94	96.8
3	79.07	8.25	87.33	10.80	96.8
4	80.80	8.43	89.24	11.10	96.7
5	73.84	7.78	81.62	10.40	96.4
6	93.00	8.83	101.83	12.53	96.0
7	88.86	7.10	95.96	12.11	94.4
8	46.29	4.67	50.96	6.45	96.1
9**	8.57	0.87	9.44	1.27	95.3
10*					
11	88.96	8.89	97.85	11.94	96.6
12**	13.14	1.13	14.27	1.71	95.6
13	86.94	8.31	95.26	11.44	96.4
14	97.02	7.63	104.65	11.84	95.7
15**	9.10	0.89	9.98	1.34	95.0
16*					
17	63.63	6.37	69.99	8.71	96.3
18**	10.92	1.05	11.97	1.60	95.0
19	61.88	5.35	67.24	7.56	96.4
20	98.95	10.36	109.31	13.49	96.8

* Leakage in the pressure cell

** Assumed not possible to form hydrates in this system.

Worst Case

Table E.10: Total amount of hydrates formed and the volume reduction obtained in the experiments conducted at the NTNU laboratory with the NTNU gas (worst case).

Experiment	Worst case				
	$V_{gas, used}$ [mL]	$V_{water, used}$ [mL]	$V_{tot, used}$ [mL]	V_{hyd} [mL]	Volume reduction [%]
1*					
2	81.27	15.24	96.51	18.64	95.8
3	79.79	15.05	94.84	18.40	95.8
4	84.68	15.97	100.65	19.64	95.7
5	74.67	14.21	88.88	17.76	95.3
6	94.37	16.19	110.56	21.47	94.4
7	91.35	13.18	104.53	21.02	91.4
8	46.96	8.55	55.51	11.05	94.7
9	8.76	1.60	10.37	2.19	93.2
10*					
11	89.91	16.24	106.15	20.37	95.4
12	13.41	2.09	15.50	2.94	93.6
13	88.02	15.21	103.22	19.55	95.1
14	98.85	14.04	112.89	20.37	93.6
15	9.31	1.64	10.96	2.32	92.8
16*					
17	64.44	11.65	76.10	14.89	95.0
18	11.19	1.94	13.13	2.76	92.7
19	62.73	9.80	72.53	12.93	95.0
20	99.78	18.86	118.65	22.96	96.0

* Leakage in the pressure cell

** Assumed not possible to form hydrates in this system.

Bibliography

- Barker, J. W. and Gomez, R. K. (1989a). Formation of hydrates during deepwater drilling operations. *SPE-16130-PA*, 10.2118/16130-PA.
- Barker, J. W. and Gomez, R. K. (1989b). Formation of hydrates during deepwater drilling operations. *Journal of Petroleum Technology*, 41(03):297–301.
- Behseresht, J. and Bryant, S. L. (2012). Sedimentological control on saturation distribution in arctic gas-hydrate-bearing sands. *Earth and Planetary Science Letters*, 341–344:114–127.
- Bleier, R. (1990). Selecting a drilling fluid. *SPE-20986-PA*, 10.2118/20986-PA.
- Botrel, T. (2001). Hydrates prevention and removal in ultra-deepwater drilling systems. *OTC-12962-MS*, (10.4043/12962-MS).
- Brandee A Elieff, J. J. S. (2006). Replacing ‘pump and dump’ with a rdg system.
- Brechan, B. A. (2015). Drilling, completion, intervention and p&a - design and operations.
- Bybee, K. (2001). Hydrate prevention and removal in ultradeepwater drilling systems. *SPE-0701-0040-JPT*, (10.2118/0701-0040-JPT).
- Bysveen, J., Fossli, B., Stenshorne, P. C., Skärgård, G., and Hollman, L. (2017). Planning of an mpd and controlled mud cap drilling cmcd operation in the barents sea using the cml technology. *IADC/SPE Managed Pressure Drilling & Underbalanced Operations Conference & Exhibition*, 28-29 March, Rio de Janeiro, Brazil.

Carlsen, Liv A. Nygaard, G. G. J. E. N. M. S. J. (2008). Performing the dynamic shut-in procedure because of a kick incident when using automatic coordinated control of pump rates and choke-valve opening. Society of Petroleum Engineers.

Chemtotal (2012). Additives for drilling fluid. Retrieved 27.05.2017 from <http://www.chemtotal.com/drilling-mud-components.html>.

Chernov, A. A., Pil'nik, A. A., Elistratov, D. S., Mezentsev, I. V., Meleshkin, A. V., Bartashevich, M. V., and Vlasenko, M. G. (2017). New hydrate formation methods in a liquid-gas medium. 7:40809 EP –.

David L. Nelson, M. M. C. (2012). *Lehninger Principles of Biochemistry*. Lehninger Principles of Biochemistry. W.H. Freeman, 6 edition edition.

DrillingFormulas.com (2011). Well ballooning (wellbore breating or micro fracture). Retrieved 02.05.2017 from <http://www.drillingformulas.com/well-ballooning-wellbore-breathing-or-micro-fracture/>.

DrillingFormulas.com (2016). Determine compressibility of gases. Retrieved 06.06.2017 from <http://www.drillingformulas.com/determine-compressibility-of-gases/>.

Duan, Z. and Mao, S. (2006). A thermodynamic model for calculating methane solubility, density and gas phase composition of methane-bearing aqueous fluids from 273 to 523k and from 1 to 2000bar. *Geochimica et Cosmochimica Acta*, 70(13):3369–3386.

E. Dendy Sloan, C. A. K. (2008). *Clathrate Hydrates of Natural Gases*, volume 3, book section 1-4, pages 1–252.

Ebeltoft, H., Yousif, M., and Soergaard, E. (1997). Hydrate control during deep water drilling: Overview and new drilling fluids formulations. *SPE-38567-MS*.

Fjellvåg, H. (2009). Polar kovalent binding. In *Store Norske Leksikon*. Retrieved 04.11.2016 from https://snl.no/polar_kovalent_binding.

- Fossen, M. (2017a). Futurewellcontrol - hydrate formation in wheel flow loop. Technical Report 7021129/01/17, SINTEF.
- Fossen, M. (2017b). Video of hydrate formation through a sapphire optical section of the pipe. Video retrieved from the video camera filming through the sapphire optical section.
- Fossil, B. and Sangesland, S. (2004). Managed pressure drilling for subsea applications; well control challenges in deep waters.
- Gabalton, O., Culen, M., and Brand, P. (2014). Enhancing well control through managed pressure drilling.
- Gautier, D. L., Bird, K. J., Charpentier, R. R., Grantz, A., Houseknecht, D. W., Klett, T. R., Moore, T. E., Pitman, J. K., Schenk, C. J., Schuenemeyer, J. H., Sørensen, K., Tennyson, M. E., Valin, Z. C., and Wandrey, C. J. (2009). Assessment of undiscovered oil and gas in the arctic. *Science*, 324(5931):1175–1179.
- GeoDF (2010). Petrodrill oil based mud systems. In *Geo Drilling Fluids Technical Data*. Retrieved 09.05.2017 from <http://www.geodf.com/index.cfm/fuseaction/Pages.Page/id/551>.
- Grigg, R. B. and Lynes, G. L. (1992). Oil-based drilling mud as a gas-hydrates inhibitor. *SPE-19560-PA*, 7:32–38.
- Gunhildrud, M. (2016). Hydrate formation and its impact on well control.
- Hannegan, D. M. (2005). Managed pressure drilling in marine environments - case studies.
- Helgestad, B. (2016). Natural gas hydrates in drilling fluids.
- Heriot-WattUniversity (2016). What are gas hydrates? Retrieved 18.11.2016 from http://www.pet.hw.ac.uk/research/hydrate/hydrates_what.cfm.
- Hilts, B. (2013). Managed pressure drilling.
- HMDB (2017). Metabocard for propane. In *Human Metabolome Database*. Retrieved 05.06.2017 from <http://www.hmdb.ca/metabolites/HMDB31630>.

- Ji, G., Wang, H., Wang, L., and Cui, M. (2013). Current situation and development trend of arctic drilling equipment. *The Twenty-third International Offshore and Polar Engineering Conference, 30 June-5 July, Anchorage, Alaska.*
- Johnson, A., Rezmer-Cooper, I., Bailey, T., and McCann, D. (1995). Gas migration: Fast, slow or stopped. *SPE-29342-MS.*
- KAMATH, V. A. and PATIL, S. L. (1994). Analogy between effect of inhibitors on hydrate equilibrium thermodynamics and hydrate decomposition kinetics. *Annals of the New York Academy of Sciences*, 715(1):463–467.
- Khabibullin, T., Falcone, G., and Teodoriu, C. (2011). Drilling through gas-hydrate sediments: Managing wellbore-stability risks. *SPE Drilling and Completion*, 26(02):287–294.
- Kotkoskie, T. S., Al-Ubaidi, B., Wildeman, T. R., and Sloan, E. D. (1992). Inhibition of gas hydrates in water-based drilling muds. *SPE Drilling Engineering*, 7(02):130–136.
- Lai, D. T. and Dzialowski, A. K. (1989). Investigation of natural gas hydrates in various drilling fluids. *SPE-18637-MS, 10.2118/18637-MS.*
- Lake, L. W. and Mitchell, R. F. (2006). *Petroleum Engineering Handbook*, volume 2, book section 4, pages 187–192. Society of Petroleum Engineers, Richardson, US.
- Larsen, R. (2015). Thermodynamic inhibitors. In *A Chemical War...* Retrieved 20.12.2016 from http://www.betong.net/ikbViewer/Content/745662/Chemical_War%20RL.pdf.
- Larsen, R. (2017). Personal communication. Personal Communication in the spring of 2017.
- Lasse Amundsen, M. L. and Reichel, T. (2013). Gas hydrates part iv: Where are gas hydrates found? In *GEOExPro*. Retrieved 19.12.2016 from <http://www.geoexpro.com/articles/2013/05/gas-hydrates-part-iv-where-are-gas-hydrates-found>.
- LeTran, D. (2017). The ideal gas law. Retrieved 25.04.2017 from https://chem.libretexts.org/Core/Physical_and_Theoretical_Chemistry/Physical_Properties_of_Matter/States_of_Matter/Properties_of_Gases/Gas_Laws/The_Ideal_Gas_Law.

- Manning, M. (2016). Offshore oil production in deepwater and ultra-deepwater is increasing. *eia, U.S Energy Information Administration.*
- Neff, J. M. (2005). Composition, environmental fates and biological effect of water based drilling muds and cutting discharges to the marine environment. Petroleum Environmental Research Forum (PERF) and American Petroleum Institute.
- Nimblett, J. N., S. R. C. S. F (2005). Gas hydrate as a drilling hazard: Examples from global deepwater settings. Houston, Texas. Offshore Technology Conference.
- NORSOK (2013). Well integrity in drilling and well operations.
- Onan, D. and Brake, B. (1996). Combating lost circulation during the drilling of wells. US Patent 5,501,277.
- Østergaard, K. K., Tohidi, B., Danesh, A., and Todd, A. C. (2000). Gas hydrates and offshore drilling: Predicting the hydrate free zone. *Annals of the New York Academy of Sciences*, 912(1):411–419.
- Pakulski, M., Qu, Q., and Percy, R. (2005). Gulf of Mexico deepwater well completion with hydrate inhibitors. *SPE-92971-MS*, 10.2118/92971-MS.
- PetroWiki (2013). Ballooning. In *Glossary Balloning*. Retrieved 02.05.2017 from <http://petrowiki.org/Glossary:Ballooning>.
- PetroWiki (2015). Functions of drilling fluid. Retrieved 27.05.2017 from http://petrowiki.org/Functions_of_drilling_fluid.
- Pinho, S. P. and Macedo, E. A. (2005). Solubility of NaCl, NaBr, and KCl in water, methanol, ethanol, and their mixed solvents. *Journal of Chemical & Engineering Data*, 50(1):29–32.
- Purdue (2017). Freezing point depression. In *Purdue Science - Department of Chemistry*. Retrieved 25.05.2017 from <https://www.chem.purdue.edu/gchelp/solutions/freeze.html>.

- Robinson, E. (2015). *Well Control Procedures*, volume 2, book section 4, pages 93–115. International Association of Drilling Contractors (IADC), 2nd edition.
- Samuel, G. R. (2010). *Well Control*, book section 9, pages 301–316. John Wiley & Sons, Inc.
- Schlumberger (2017a). calcium chloride. In *Oilfield Glossary*. Retrieved 29.04.2016 from http://www.glossary.oilfield.slb.com/Terms/c/calcium_chloride.aspx.
- Schlumberger (2017b). Product sheet: Potassium formate (dry). In *Schlumberger Resources*. Retrieved 09.05.2017 from http://www.slb.com/resources/other_resources/product_sheets/miswaco/potassium_formate_dry.aspx.
- SchlumbergerOilfieldGlossary. Barite. Retrieved 03.05.2017 from <http://www.glossary.oilfield.slb.com/Terms/b/barite.aspx>.
- SchlumbergerOilfieldGlossary. Bentonite. Retrieved 03.05.2017 from <http://www.glossary.oilfield.slb.com/Terms/b/bentonite.aspx>.
- Schubert, J. J., Juvkam-Wold, H. C., and Choe, J. (2003). Well control procedures for dual gradient drilling as compared to conventional riser drilling. *SPE/IADC Drilling Conference, 19-21 February, Amsterdam, Netherlands*.
- Sevillano, L. C. (2017). *Wellbore Temperature Model*. PhD thesis, NTNU.
- Sloan, E. and Koh, C. (2007). *Clathrate Hydrates of Natural Gases, Third Edition*. Chemical Industries. CRC Press.
- Sloan, E. D, J. (1991). Natural gas hydrates. *Journal of Petroleum Technology*, 43(12):1414–1417.
- Soghondikolaee, M. P. G. A. S. H. T. (2014). Hydrate-related drilling hazards and their remedies. Semnan University. 2nd National Iranian Conference on Gas Hydrate (NICGH).
- Sowa, B. and Maeda, N. (2015). Statistical study of the memory effect in model natural gas hydrate systems. *The Journal of Physical Chemistry A*, 119(44):10784–10790.

- SPE, I. (2015). Drilling fluid types. Retrieved from http://petrowiki.org/Drilling_fluid_types.
- SPEinternational (2015a). Drilling fluid types. Retrieved 26.10.2016 from http://petrowiki.org/Drilling_fluid_types.
- SPEinternational (2015b). Shut-in procedures for well control. volume 2016. Retrieved from http://petrowiki.org/index.php?title=Shut-in_procedures_for_well_control&oldid=48147.
- Unitrove (2017). Natural gas density calculator. Retrieved 05.05.17 from <http://unitrove.com/engineering/tools/gas/natural-gas-density>.
- V. Løvø, A. Elverhøy, P. A. A. S. G. B. O. G. O. L. (1990). *Submarine permafrost and gas hydrates in the northern Barents Sea*, volume 56. Norsk Polarinstitut.
- Vedvik, N. (2017). Pressure cell sketch. Blueprint of pressure cell.
- Weisene, A. T. (2014). Well control during extended reach drilling - conventional drilling compared to reelwell drilling method. Master's thesis, University of Stavanger.
- Vieira, P., Arnone, M. A., Torres, F., and Barragan, F. (2009). Roles of managed pressure drilling technique in kick detection and wellcontrol—the beginning of the new conventional drilling way.
- Watkins, T. (2016). Euler's theorem concerning polyhedra composed of pentagons and hexagons. Retrieved 08.11.2016 from <http://www.sjsu.edu/faculty/watkins/eulergem.htm>.
- Weatherford (2010). Potassium formate. In *Drilling fluids*. Retrieved 09.05.2017 from <http://www.weatherford.com/doc/wft137414>.
- Weems, M., Moore, D., and Leach, C. (2016). Managed pressure drilling as well control in deep-water gom: Challenges to current modes of thinking.

- Welltrain (2008). Kill procedure. Retrieved from [https://www.welltrain.com.au/repository/download/18.Kill%\\$%20Procedures%\\$%20-%\\$%20Summary.pdf](https://www.welltrain.com.au/repository/download/18.Kill%$%20Procedures%$%20-%$%20Summary.pdf).
- WildWellControl (2016). Well control methods. Retrieved from <http://www.wildwell.com/literature-on-demand/literature/well-control-methods.pdf>.
- Williams, J. (2017). What is hydrophobic? - definition and interactions. In *Study.com*. Retrieved 26.05.2017 from <http://study.com/academy/lesson/what-is-hydrophobic-definition-interactions-quiz.html>.
- Yakushev, V. S. Collett, T. S. (1992). Gas hydrates in arctic regions: Risk to drilling and production. International Society of Offshore and Polar Engineers.
- Yousif, M. H. Dunayevsky, V. A. H. A. H. (1997). Hydrate plug remediation: Options and applications for deep water drilling operations. Society of Petroleum Engineers.